FLOW-INDUCED, IN-LINE VIBRATIONS OF A CIRCULAR CYLINDER

by

Jorge E. Aguirre Romano, BSc, MSc, DIC

Thesis submitted to the University of London
for the degree of Doctor of Philosophy

Civil Engineering Department
Imperial College of Science and Technology
London SW7

September 1977

Flow-Induced, In-Line Vibrations of a Circular Cylinder

by

Jorge E. Aguirre Romano, BSc, MSc, DIC

ABSTRACT

An investigation has been conducted on the flow-induced, in-line vibrations of circular cylinders. Two-dimensional cylinders immersed in a one-dimensional water stream were tested in the laboratory.

Detailed observation of cylinder and flow behaviour revealed some novel characteristics of this type of excitation, such as a new type of wake, variations of the mean drag coefficient and frequency variations which reduced a variable mass coefficient to zero.

A new "non-dimensional frequency parameter" was obtained which unlike the commonly used "reduced velocity", unified the results of previous researches and provided a precise definition of the instability regions; this allowed the avoidance of instability in engineering problems at the design stage.

In contrast with aerodynamic practice, it was here concluded that density and damping should be considered separately. Density was found to determine the frequency response. Damping was divided into hydrodynamic (included in the total hydrodynamic force) and external (structural); the latter was represented by a modified "stability parameter" which is independent of cylinder density and which was found to determine the amplitude response.

The identification and definition of the independent rôles played by density and external damping, led to correlations which allowed the prediction of the amplitude and frequency response and of the instability regions, for any two-dimensional cylinder-flow arrangement.

The hydrodynamic exciting, damping and added mass forces were analysed leading to a theoretical model which represents the excitation in terms of force coefficients and a phase angle; these parameters were found to represent the hydrodynamic processes.

Frequency variations were attributed to a constant mass coefficient and variable drag forces; this led to a marked simplification of the theoretical model in the second instability region, and to the prediction of the force coefficients and the phase angle from knowledge of flow characteristics and cylinder motion and geometry.

Good agreement was also found between the predictions of the model and the results of full-scale three-dimensional experiments.

CONTENTS

		Page
ABSTRACT		2
ACKNOWLEDGEMENTS		8
LIST OF SYMBOLS		9
1	INTRODUCTION	13
1.1	Engineering Considerations	13
1.2	In-line Vibration Induced by a Steady Flow	13
1.3	Previous Studies of In-line Vibration	15
1.3.1	Cylinder-flow arrangements	15
1.3.2	Flow pattern	16
1.3.3	Mechanisms of excitation	16
1.3.4	Velocity and frequency parameters	17
1.3.5	Influence of damping	18
1.3.6	Exciting forces	18
1.4	Aims and Scope	19
2	EXPERIMENTAL APPROACH	21
2.1	Alternative Experimental Configurations	21
2.1.1	Two or three dimensional	21
2.1.2	Restricted in-line or free	22
2.1.3	Choice of fluid	23
2.1.4	Cross section and position of the cylinder	23
2.1.5	Externally driven or flow induced	24
2.1.6	Measurement of forces	24
2.2	The Experimental Set-Up	25
2.3	Experimental Procedure	26
3	KINEMATIC BEHAVIOUR OF CYLINDER AND FLOW	28
3.1	Introduction	28
3.2	First Instability Region	29
3.2.1	General observations and description	29
3.2.2	Splitter plate results	30
3.2.3	Rearrangement section	31
3.2.4	Lock-in section	32
3.2.5	Double harmonic excitation section	34

Page

3.3 Second Instability Region 36
3.3.1 Introduction 36
3.3.2 The wake 36
3.3.3 Cylinder behaviour 37
3.3.4 Growth of the instability 38
3.4 Region between First and Second Instability Regions 39
3.5 A Note on Flow Pattern Correlation 40
3.6 Summary and Conclusions 41
3.6.1 Interacting mechanisms in the first instability region 42
3.6.2 The wake of the second instability region 42
3.6.3 Cylinder behaviour 43
3.6.4 The reduced velocity (V/ND) 44

4 THE NON-DIMENSIONAL FREQUENCY PARAMETER 45

4.1 An Alternative Form of the Reduced Velocity 45
4.2 Derivation of the New Parameter 46
4.3 Analysis of the Parameter 48
4.3.1 Definition of the instability regions 49
4.3.2 Contributions of f_s/f to the explanation of phenomena 49
4.3.3 Practical considerations 50

5 ANALYSIS OF VARIABLES 53

5.1 Cylinder Behaviour 53
5.2 Cylinder Characteristics 54
5.3 Hydrodynamic Forces and f_s 56
5.4 Non-dimensional Groups 59

6 DENSITY AND DAMPING 61

6.1 Density 61
6.1.1 Frequency ranges 62
6.1.2 Flow velocity ranges 63
6.1.3 Frequency response in the first instability region 64
6.1.4 Frequency response in the second instability region 65

Page

6.2 Damping 66
6.2.1 The separate roles of density and damping 66
6.2.2 Definition of damping 68
6.2.3 Damping parameter 69
6.2.4 Vibration amplitudes 73
6.2.5 Instability regions 75
6.3 Discussion of Results 77
6.3.1 Efficiency of the excitation forces 77
6.3.2 Comparison of results 78
6.3.3 Practical considerations 79

7 HYDRODYNAMIC FORCES 81

7.1 Analysis of Forces 81
7.2 Added Mass 83
7.2.1 The coefficient of added mass 83
7.2.2 A variable mass coefficient 85
7.2.3 A constant mass coefficient 86
7.3 Hydrodynamic Damping 88
7.3.1 Still water damping 88
7.3.2 Flowing water damping 89
7.4 Excitation Forces 90
7.4.1 A theoretical model of the excitation 90
7.4.2 The pairs mechanism 94
7.4 3 The transverse flow mechanism 95

8 EXCITATION MECHANISMS 98

8.1 Second Instability Region 98
8.1.1 Phase relationships 98
8.1.2 $\overline{C}_F$ and hydrodynamic damping 100
8.1.3 C'_F and the excitation forces 101
8.1.4 A two-dimensional model 102
8.1.5 Prediction of cylinder behaviour 103
8.2 First Instability Region 109
8.2.1 The "pairs mechanism" 109
8.2.2 Rearrangement and lock-in sections 114
8.2.3 Double harmonic excitation section 116

Page

9 THREE-DIMENSIONAL CONSIDERATIONS 119

9.1 Influence of Three-Dimensional Effects on the Results of the Present Research 119

9.1.1 Damping forces 120

9.1.2 Excitation forces 122

9.1.3 Phase angle 123

9.2 Engineering Applications of the Results of the Present Research 124

9.2.1 Avoidance of the instability regions 124

9.2.2 Prediction of cylinder behaviour 126

10 SUMMARY AND CONCLUSIONS 132

10.1 The Non-dimensional frequency parameter 132

10.2 Density and Damping 134

10.3 Hydrodynamic Forces 136

10.4 Practical Applications and Conclusions 139

APPENDIX I APPARATUS AND EQUIPMENT DETAILS 141

APPENDIX II EXPERIMENTAL DATA 142

II-1 Table of data (1st set of tests) 143

II-2 Table of data (2nd set of tests) 144

APPENDIX III ADDED MASS, DENSITY AND STIFFNESS 145

APPENDIX IV MEASUREMENT OF S AND C_{DO} 149

APPENDIX V DAMPING 150

V-1 Structural damping 150

V-2 Damping mechanism 151

V-3 Aerodynamic damping 151

V-4 End gaps 152

V-5 Supporting arms 153

V-6 Splitter plate 155

V-7 Total damping 156

			Page
APPENDIX VI	BLOCKAGE EFFECTS		157
APPENDIX VII	DEDUCTION OF EQUATIONS		163
	VII-1	Equations 7.4 & 7.5	163
	VII-2	Equation 7.15a	164
	VII-3	Equations 7.16/17	165
	VII-4	Equations 7.26/7/8	166
	VII-5	Equations 7.31/2/3/4	167
	VII-6	Equations 7.39/40/41	169
	VII-7	Equation 8.2	170
REFERENCES			171
PLATES 1 to 8			174
FIGURES 1 to 89			182

ACKNOWLEDGEMENTS

This research was made possible by all kinds of help and support from my wife, Marta, who also helped me with the drawings of this thesis.

The author wishes to express his gratitude to his supervisor, Dr J.D. Hardwick, for his guidance, encouragement and advice throughout the project.

Special thanks are due to Geoff Thomas, the other members of the technical staff of the Hydraulics section and to Joyce Gurr (Photography) for their advice and technical assistance.

Thanks are also due to Professor J.R.D. Francis and the other members of the academic staff for their advice.

This research was partially financed by the Science Research Council of Great Britain and the Consejo Nacional de Ciencia y Tecnología of México.

LIST OF SYMBOLS

a = vibration double amplitude ($2x_o$)

c = viscous damping constant or damping force coefficient

C_{DA} = apparent drag coefficient

C_{DO} = drag coefficient for a stationary cylinder

C_f = a force coefficient (undefined)

C_F = variable force coefficient

$\overline{C}_F$ = mean component of C_F

C'_F = amplitude of the fluctuating component of C_F

C_I = inertial coefficient [= $(N/f)^2(\rho_r + 1) - \rho_r$]

C_M = mass coefficient

C_{MS} = mass coefficient in still water

C_{MV} = variable mass coefficient

d = water depth (or distance as defined in text)

D = diameter

E_p = energy ratio [= $C_{DA}\ f_s/C_{DO}\ f$]

E_w = energy ratio [= $C_{DA}\ f_s/C_{DO}\ f_e$]

f = vibration frequency

f_e = frequency of eddies in the distant wake

f_s = value of "f_e" for a stationary cylinder [= $2SV/D$]

f_w = frequency of the wake behind a stationary cylinder [= $f_s/2$]

F = total drag force

$\overline{F}$ = mean hydrodynamic (drag) force

F' = fluctuating drag force

F'_o = amplitude of fluctuating drag force

F'_I = inertial, fluctuating hydrodynamic force

F_T = total hydrodynamic force

F'_T = fluctuating component of F_T

F'_{To} = amplitude of F'_T

g = acceleration of gravity

G = hysteretic damping parameter

k = stiffness

k'_e = equivalent stiffness per unit length

k_s = stability parameter [$= c/\rho_f D^2 Lf$]

k'_s = stability parameter for constant frequency [$= 2M\delta/\rho_f D^2 L$]

k'_{so} = k_s for f = N and (a/D) = 0.055

ℓ = length (as defined in text)

L = total length of cylinder

L' = equivalent active length

L_I = logarithmic increment

m = slope of curve

M = mass

M_a = added mass

M_{as} = added mass in still water (or when $C_M = 1$)

M'_{as} = added mass per unit length ($C_M = 1$)

M_c = effective mass of cylinder

M'_{ce} = equivalent mass of cylinder per unit length

M_T = total mass ($= M_c + M_a$)

M_{TS} = total mass in still water or when $C_M = 1$ ($= M_c + M_{as}$)

N = natural frequency in still water

N_{air} = natural frequency in air

N_v = natural frequency in vacuo

P_d = total damping force

P_e = hydrodynamic excitation force

P_{hd} = hydrodynamic damping force

R_e = Reynolds number [$= VD/\nu$]

S = Strouhal number [$= f_w D/V$]

t = time

V = flow velocity

V_r = cylinder/flow, velocity ratio [$= \omega x_o/V$]

x = cylinder displacement

$\bar{x}$ = mean cylinder displacement

x' = fluctuating cylinder displacement

x_o = amplitude of x'

$\dot{x}$ and $\ddot{x}$ = first and second derivatives of x with respect to t

α = phase angle of C_F' or P_e with respect to x_o'

β = blockage correction factor for V

δ = logarithmic decrement

ζ = phase angle of F_T' with respect to x_o'

ϕ = phase angle of F' with respect to x_o'

μ_f = fluid's dynamic viscosity

ν = fluid's kinematic viscosity

ε = negative damping parameter

ρ_c = effective density of cylinder

ρ'_{ce} = equivalent density of cylinder

ρ_f = density of fluid

ρ_r = density ratio [$= \rho_c/\rho_f$]

ω = vibration's circular frequency [$= 2\pi f$]

ω_n = natural circular frequency in still water [$= 2\pi N$]

ψ $= (1 + 0.25V_r^2)/(1 + 0.75V_r^2)$

Other variables as defined in text.

CHAPTER 1

INTRODUCTION

1.1 Engineering Considerations

Flow induced vibrations are a problem of growing engineering concern as structures exposed to fluid flow grow in size, number and variety. Moreoever, as the design of these structures becomes more refined, economic considerations demand that safety-margins be reduced and consequently much of the material regarded as excessive for *static* stability is being eliminated. The *dynamic* stability often suffers as a result of these economies through a reduction of both damping and the natural frequencies of the structure. Moreover, as the numbers of marine and estuarine works multiply, more structures are exposed to hydrodynamic action which in comparison with aerodynamic action is associated with larger inertial forces and larger exciting forces relative to the structural damping.

It is clear from these trends not only that more refined and reliable engineering knowledge and methods should be developed, but also that new types of vibration phenomena previously unknown or neglected are assuming greater importance to the designer. One such new source of flow-induced vibration is described below.

1.2 In-Line Vibrations Induced by a Steady Flow

In what follows only steady flows approaching structural members will be considered although the results will be applicable to those unsteady flows with scales and frequencies of unsteadiness which are greatly different from the structure's scale and natural frequency, i.e. small scale turbulence on the one hand and tidal flows on the other.

Except for cases such as "galloping" and "flutter" the most important flow-induced excitations are associated with the periodic shedding of eddies in the wake of a bluff body. This wake has normally been thought to be of the Von Kàrmàn type (Fig. 1), where in addition to a steady drag force, the flow exerts a periodic force upon the body with the same frequency as that of alternate eddies shed into the wake.

If the body is at rest this wake frequency, f_w, is related to the velocity of the flow, V, and the dimensions of the body in this case its diameter, D, by the Strouhal number, S, i.e.:

$$S = \frac{f_w D}{V}$$

In practical situations these periodic forces become significant when the vibration amplitudes are dynamically magnified by a resonance phenomenon when the forcing frequency coincides with a natural frequency of the body. Thus for a given structural member there correspond critical values of the flow velocity, given by the Strouhal relationship and the natural frequencies of the member,at which a resonance could occur.

In some situations the vibration of the body is so large that it interferes with and can even control the flow pattern. Under such circumstances the fluid dynamic forces themselves can be magnified and so through some interactive process the vibration of the body can be increased still further. In this type of largely "self-excited" vibration the dynamic characteristics of the body cause the frequency of the wake to diverge from that predicted by the Strouhal relationship (a phenomenon sometimes termed "frequency lock-in") and so the range of flow velocity over which vibration will be important is extended.

The forces associated with eddy shedding can produce vibrations in the direction of the flow (in-line), or at right angles to it (cross-flow). Research has so far been concentrated in studying the latter, and until recently the weaker, in-line vibrations have not been detected or have been ignored. In the last decade however, the structural design trends mentioned above have brought to light examples of in-line vibration which have necessitated expensive remedial work. Auger reports the in-line vibrations caused by a steady wind of the members of an aluminium, tubular space-frame built for "Expo 68", which was designed to avoid cross-flow vibration only. Vibrations absorbers had to be installed on every member of the structure.

During the construction of a jetty at Immingham in 1967 (see Sainsbury and King, Wootton et al), severe in-line vibrations occurred in circular cross section piles subject to tidal currents. The excitation occurred here at flow velocities both inside *and outside* the

then known critical ranges. Moreoever,there was evidence that some of the vibrations were associated with the shedding of a pair of *simultaneous* eddies for each cycle of motion of the pile, rather than with the usual alternate shedding of eddies (Fig. 2 and 4).

The experience of Immingham is important because it demonstrated that excitation could occur at a considerably lower flow velocity than was previously thought possible and that unforeseen combinations of in-line and cross-flow motion can occur; in practical terms a designer must now consider raising the lowest natural frequency of a lightly-damped piled structure, by a factor of perhaps 3 over the value formerly believed to be safe (see Chapter 6). The cost of the necessary stiffening to achieve this increase can be high, and so there is clearly a need for greater understanding of in-line vibration if the demand continues for berthing facilities in deeper and faster flowing water.

1.3 Previous Studies of In-Line Vibration

The Immingham vibration problem stimulated a series of investigations into flow-induced, in-line vibrations of cylinders. Wootton et al conducted a full-scale research at Immingham in the site where the original problem arose and identified the type of vibration. Hardwick and Wootton reproduced the same type of excitation using small-scale two-dimensional cylinders in the laboratory and analysed excitation mechanisms and flow patterns. Clark studied the amplitude and frequency response of a small two-dimensional cylinder and investigated the possibility of suppressing the motion with flow "spoilers". King has conducted several series of experiments mainly with cantilevered model piles in the laboratory, has developed matrix methods for the representation of three-dimensional cylinder-flow arrangements and has analysed in-line and cross-flow excitation. Dickens has studied flow patterns and excitation mechanisms of the first instability region of two-dimensional cylinders in various fluids. From these researches, the following description of flow-induced, in-line vibration has emerged.

1.3.1 Cylinder-flow arrangements

Qualitatively similar characteristics have been identified in the different modes of vibration of differing cylinder-flow arrangements such as: encastré-pinned pile in three-dimensional flow (Wootton et al), cantilevered from the bed in one-dimensional flow (king),

two-dimensional motion with one dimensional flow (e.g. Clark) etc. (see also Hardwick and Wootton). As can be appreciated in Fig. 3 and as will be shown later however, there are also marked differences for example in the flow velocity and frequency response ranges, which cannot be attributed merely to Reynolds number effects, and which differences limit the applicability of the research results.

1.3.2 Flow patterns

Two main instability regions for in-line motion have been identified in all the studies; the first region is associated with the simultaneous shedding of a pair of eddies per vibration cycle and the second with eddies alternately shed from each side of the cylinder at the rate of one per vibration cycle (see Fig. 2).

There has however been difficulty in relating the flow patterns to the mechanisms of excitation when, for example, the simultaneous shedding appears to change to alternate shedding near the end of the first instability region (e.g. Dickens[2]). Hardwick and Wootton moreover have observed a rearrangement of the wake of the first instability region into one of the Von Kàrmàn type, and King reports an influence of the Strouhal frequency throughout the first instability region.

1.3.3 Mechanism of excitation

Two explanations for the excitation of the cylinder have been postulated: in the first instability region, Hardwick and Wootton suggested that the narrowing and widening of the wake as the cylinder crosses its central possition on its forward and backward strokes respectively (fig. 4), indicated a force in phase with the cylinder's velocity which does work on the cylinder and so overcomes the system's damping.

In the second instability region, the fluctuating forces associated with the alternate shedding of eddies can conveniently be resolved into two components (Fig. 4): the larger is perpendicular to the flow direction and with the frequency of the wake, f_w (the cross-flow component), and the smaller acts in the direction and sense of the flow (the in-line component) which when considered as a fluctuating force, acts with twice the frequency of the cross-flow component.

No satisfactory explanations have yet been put forward to account for the beginning and the end of either instability region.

1.3.4 Velocity and frequency parameters

The "reduced velocity" (V/ND), has been used generally as a base parameter for plotting amplitudes of vibration, although in some cases the actual frequency of the vibration, f, has been used instead of the natural frequency, N.

In-line vibration has been reported for reduced velocities ranging from 0.8 to 3.8 but disagreement over the precise ranges for the two instability regions (see Fig. 3) has complicated the interpretation of the phenomena and reduces the usefulness and reliability of the available information.

If the mechanism of excitation for the second instability region given above is correct it should follow that an in-line resonance will occur at a flow velocity, V, for which single eddies are shed with the same frequency, f_s, as the natural frequency of the cylinder, N, i.e. at:

$$f_s = N \qquad \text{or} \quad \frac{V}{ND} = \frac{1}{2S} \simeq 2.5$$

$$\text{since} \qquad S = \frac{f_w D}{V} = \frac{f_s D}{2V} \simeq 0.2$$

But Fig. 3 indicates that precisely at (V/ND) = 2.5 large self-excited amplitudes of motion have in some cases been suppressed and no satisfactory explanation for this apparent contradiction has yet been put forward.

Although in-line vibrations with similar characteristics have been reported in the ranges of Reynolds number, ($R_e = VD/\nu$), 10^4 to 10^6 for prototype studies and 10^3 to 10^4 for laboratory experiments, there also are unexplained differences between the two situations (see Fig. 3) and the precise role played by the Reynolds number is not known.

For two-dimensional in-line motion, Clark and Dickens[2] have reported a divergence of the vibration frequency, f, from the natural frequency of the cylinder in still water, N, which is similar to that

observed in cross-flow vibrations; for cantilevered or pinned cylinders however, vibration frequencies have either been assumed constant or, the very slight frequency variations observed have been attributed to secondary factors specific to the particular situation studied (see e.g. King).

1.3.5 Influence of damping

The amplitudes of vibration are limited by damping processes which dissipate the vibrational energy of a system. Maximum double amplitudes, a, have been predicted as 0.22 D (Hardwick and Wootton) or about 0.2 D (Dickens) for two-dimensional flow situations in the first instability region. King reports maximum amplitudes of up to 0.3 D at the free end of cantilevered piles. Maximum amplitudes for the second instability region have not been previously predicted.

Damping has been treated in various ways in previous studies. To facilitate model scaling, and following aerodynamic experience, "structural" and "fluid dynamic" damping expressed by logarithmic decrements, δ, have been combined with the mass of the cylinder, M, and density of the fluid, ρ_f, into a "stability parameter", $\frac{2M\delta}{\rho_f D^2 L}$ where L is the cylinder's length. This combination rests on the assumptions that the frequency is constant, that the density has no independent influence on the phenomenon and that damping is not affected by vibration amplitude (see King, Vickery and Watkins). The form of the stability parameter has been accepted by most research workers but there is disagreement over the appropriate damping to be used. Hydrodynamic damping has sometimes been extrapolated from still to running water situations in spite of the radically different flow patterns associated with the two cases (e.g. Dickens[2]). In other cases damping has been attributed to the drag forces (e.g. King) arising from the relative motion of fluid and cylinder, but in this case the damping cannot strictly be included in the stability parameter because the latter would not then represent the energy output of the system (see Chapter 6).

1.3.6 Excitation forces

King obtained fluctuating drag coefficients based on the excitation mechanism suggested by Hardwick and Wootton and on the assumptions

that the frequencies did not change and that the forces were in phase with the velocity of the cylinder. Frequency variations of as much as 20% have nevertheless been reported by Clark, and Dickens[2] reports a phase shift of the flow pattern (supposedly associated with the forces) with respect to the cylinder motion, for different amplitudes of vibration or reduced velocities.

1.4 Aims and Scope

The researches described above leave many questions unanswered and the results of some appear to conflict with others. The results of these researches moreover, tend to be applicable to specific situations only, e.g.: prototype or laboratory; two or three-dimensional; restricted in-line or free; circular cylinder or other cross section; in water or air; etc.

In view of this, the aims of the present project can be summarised as follows: (a) to improve the understanding and definition of in-line, flow-induced vibration; (b) to clear some of the contradictions apparently arising from the different types of research previously conducted; and (c) to incorporate all the previous experiences in this field with those of the present research into a general model of widest applicability. Such a general model should represent all the basic characteristics of this type of vibration which are common to all situations, but the model should be adaptable to represent also specific cases. It is moreoever intended that such an approach will permit a reinterpretation of the previously reported behaviour of both prototypes and laboratory models, so as to improve their agreement and thus to increase the reliability and usefulness of modelling techniques for this type of vibration problem.

More specifically, it is intended here to: (a) arrive at an improved qualitative definition of flow-induced in-line vibration; (b) find appropriate parameters to define the excitation; (c) correlate cylinder behaviour with flow and cylinder densities, structural damping, flow velocity, etc. leading to the prediction of instabilities from data easily available to designers; (d) find limits in general to the ranges of the excitation; and (e) investigate forces and phase relationships that would contribute to the explanation for the occurrence and characteristics of the vibration.

It is intended moreover that the results to be presented will facilitate the solution of similar vibration problems (e.g. cross-flow vibration) and will also lead to a greater understanding of interactions between fluids and solids in general.

In the next chapter a discussion of the selected approach to the problem is followed by a description of the experimental equipment and method.

Chapter 3 is concerned with a correlation between flow patterns and observed vibration response. On the basis of this correlation, a parameter is described in Chapter 4 which appears to unify several sets of independent experimental results, in addition to helping with the organization and understanding of the data.

Chapter 5 presents a dimensional analysis and a study of most of the main parameters which influence the excitation. The two most important ones, density and damping however, are dealt with separately in Chapter 6, leading to prediction of cylinder behaviour from characteristics of cylinder and flow.

Chapter 7 arrives at a theoretical model of the excitation after an analysis of added mass, hydrodynamic damping and the excitation forces. The excitation mechanisms are analysed in more detail in Chapter 8, allowing simplifications of the theoretical model and further predictions of cylinder behaviour.

The subject of Chapter 9 is the consideration of the three-dimensional factors which affected the results of the present research, and the applicability of such results to prototype three-dimensional situations. The thesis is concluded in Chapter 10.

CHAPTER 2

Experimental Approach

The aims of this research as stated in the previous chapter, together with practical and economic considerations dictated a laboratory investigation of flow-induced, in-line vibration of cylinders, which when compared with prototype studies presents the advantages of flexibility, independent control of variables and the possibility of a less specific research of wider applicability.

The first section of this chapter (2.1) analyses different alternative types of cylinder-flow arrangements previously used for similar laboratory researches; this leads to a description in 2.2 of the arrangement adopted for the present research. Section 2.3 presents a brief description of the experiments and their sequence.

2.1 Alternative Experimental Configurations

2.1.1 Two or three-dimensional

In the typical three-dimensional cylinder-flow arrangements encountered in civil engineering practice, the characteristics of the approaching flow change with location, and the amplitudes of vibration of the cylinder change along its length according to different modal deflection curves which are particular to every cylinder configuration.

Previous researchers (e.g. Hardwick and Wootton, Dickens) have achieved a significant degree of similarity when reproducing such three-dimensional situations in the laboratory, with rigid,two-dimensional cylinder arrangements immersed in basically one-dimensional approaching streams (see Fig. 3).

These experimental outcomes indicate that any flow-induced, in-line vibration has basic chracteristics which are common to all situations; it should therefore be possible to represent any such excitation by a simplified model as described above with the additional and separate consideration of the particular three-dimensional characteristics involved. More specifically, a three-dimensional situation can be assumed to be made up of a series of two-dimensional components;

consequently if the characteristics of a two-dimensional excitation are known it is only necessary to know the interaction patterns of the different two-dimensional components in order to obtain a three-dimensional representation.

In contrast to this, the laboratory modelling of one specific cylinder-flow arrangement would not only be incompatible with widening the applicability of the experimental outcome, but it would also introduce three-dimensional patterns which would obscure the more basic and general characteristics of the excitation.

It was therefore decided to approximate as far as possible the case of a rigid two-dimensional cylinder immersed in a one-dimensional approaching stream.

2.1.2 Restricted in-line or free

Apart from torsional vibrations which are not important from a fluidelastic point of view, the motion of a two-dimensional rigid cylinder can be represented by two degrees of freedom namely, in-line and cross-flow motion. The resonant character of the type of excitation here dealt with moreover, implies that the control of the two natural frequencies of vibration of the cylinder leads to the propitiation or suppression of excitation in the corresponding direction.

In practice vibration can occur in both directions simultaneously or worse, as cross-flow forces tend to be considerably larger, in-line vibration is often but a detail of the mainly cross-flow motion. For these reasons designers normally increase the cross-flow natural frequency as far above the flow exciting frequency as is possible, in order to restrict motion in that direction, but often neglect the possibility of in-line vibration which in some cases occurred (see 1.2).

Hardwick and Wootton, Dickens and Clark have adopted a similar measure in order not only to reproduce in the laboratory the prototype vibration problem but also to maximise the possibility of in-line vibration for its study and to minimise any cross-flow interference which would obscure the character of the in-line excitation. These researchers have achieved a reasonably good degree of similarity in reproducing the prototype excitation and have provided basic information which was not reported in the studies of more complex situations.

King, who studied the behaviour of cylinders with equal natural

frequencies in the two directions moreover, reports for the case of light cylinders that the second instability region of in-line vibration was severely distorted by cross-flow excitation, and that cross-flow forced vibration could be detected in the first instability region of in-line motion.

It was therefore decided to isolate in this case the in-line excitation process for its study by allowing the cylinder to vibrate in that direction alone.

2.1.3 Choice of fluid

Dickens has shown that flow-induced in-line vibration can occur in water, air or even in a polyvinyl alcohol solution. Significant in-line vibration problems in civil engineering structures however, have only been reported occurring in water. This is because the fluid dynamic excitation forces are proportional to the density of the fluid, and consequently the structural damping of the cylinder is more effective in suppressing the vibration the lighter the fluid is.

The present objective of maximising in-line excitation for its study thus favours the use of a heavier fluid, i.e., water instead of air. The choice of water as the fluid to be used moreover,increased the experimental flexibility and range by decreasing the lower limit of the attainable ranges of both the cylinder/fluid density ratio, ρ_r, and the stability parameter, k_s.

2.1.4 Cross-section and position of the cylinder

Clark has shown that circular as well as several non-circular, cross section cylinders can be induced to vibrate in-line by steady flows. A circular cross-section cylinder was chosen for the present research however, because (a) it is most widely used due to structural and economic advantages, (b) the cylinders of any practical in-line vibration problem thus far reported had that shape, and (c) more practical and theoretical information exists for such cylinders than for any other.

Previous researchers have shown that in-line excitation with similar characteristics can be obtained with both vertical and horizontal cylinders. For this research however, the cylinder was placed horizontally to simplify its rigging and operation, and to avoid the

specific problems caused by the flume's bottom boundary layer and by the air water interface..

2.1.5 Externally driven or flow induced

Some research workers (e.g. Bishop and Hassan, Toebes and Ramamurthy) have contributed to the understanding of cross-flow excitation by forcing cylinders to oscillate in this direction and studying the flow response to given cylinder motion characteristics.

This experimental method allows prediction of flow induced behaviour but not its direct study. The method is consequently more useful and practicable once a reasonable description of flow induced behaviour exists, which allows confirmation and interpretation of results and which reduces an otherwise extremely wide experimental range to limited areas of interest. A research based on externally driven cylinders moreover, requires complex apparatus and equipment, including a two-degree-of-freedom transducer, and a considerably more elaborate interpretation of results, all of which imply additional economic and time expenditure.

Bearing in mind (a) the early stage of development of knowledge of in-line excitation when compared with the cross-flow case and (b) the complexities and lack of understanding arising from the various types of in-line excitation and their interactions, it was decided to study the flow induced behaviour by devising a cylinder, that would as far as possible be acted upon by fluid forces alone, exception made of the cylinder's mass, stiffness and structural damping forces whose influence on the vibration is an integral part of the research.

An exception to the above decision was made for a short set of preliminary tests involving an externally driven cylinder. Although these tests showed some qualitative characteristics of the wake for various flow and motion conditions, they also revealed a multiplicity of flow patterns which reinforced the above decision.

2.1.6 Measurement of forces

Bishop and Hassan, Toebes and Ramamurthy and others, have used two-degree-of-freedom systems to measure the flow forces on their externally driven, cross-flow vibrating cylinders. Except in the case of pressure transducers (see e.g. Small) whose use would severely limit

the experimental range of the present research, in a flow induced, steady state vibration it is only possible to measure the resultant of all the fluid forces. This force can also be inferred from the motion of the cylinder itself, if the latter is rigged as a transducer.

For analytical purposes and to facilitate useful correlations such a force is usually divided by analytical methods into the added mass and the excitation force components. In the case of cross-flow vibration the order of magnitude of these two components can be the same; not so for in-line vibration however, where the added mass forces are typically two orders of magnitude higher than the excitation or the damping forces. Consequently the accuracy needed, complexity and cost of the equipment needed are that much higher in the case of in-line vibration than in the cross-flow case.

For these reasons and to avoid complications which would limit the flexibility and range of the research, it was decided to infer the flow forces from: (a) the cylinder motion, which was detected by strain gauges attached to its supports and (b) the mass, stiffness and damping of the cylinder which were measured in additional simple tests.

2.2 The Experimental Set-Up

The considerations outlined above led to the following experimental arrangement (see Figs. 5, 6 & 7 and Appendix 1).

The variable density cylinders used were held horizontally and perpendicular to the approaching stream by two long supporting arms of variable stiffness and damping, so as to allow the cylinders to swing in a quasi-linear motion in the direction of the flow only.

Two 33 cm long cylinders were used, one 3.38 cm diameter (durapipe) and the other 2.5 cm diameter (aluminium). They were placed in a glass walled flume 56 cm wide and 35 cm deep, between two large stationary and transparent end plates which isolated the cylinders from the large boundary layers of the flume's walls.

External damping could be controlled by a vertical plate attached to the cylinder's supporting arms, which oscillated on its own plane and immersed in different depths of a variable solution of syrup in water. Density of the cylinders was varied by filling them with different substances. Stiffness was controlled by adjusting the length of

cantilevered spring leafs at the top end of the supporting arms. The arrangement also permitted adjustment of cylinder submergence depth and of the gaps which separated the cylinder from the end plates.

Other additions included a dye injection probe for flow visualisation, a splitter plate (see Chapter 3), a displacement calibration device, additive weights, etc.

The flexibility of the arrangement can be appreciated in Table 2.1, which gives the main variable's ranges covered during the experiments.

Variable	Dimensions	Range	Notes
V	cm/s	5-50	within the instability regions
R_e	-	1700-17000	
D	cm	2.5-3.38	
N	Hertz	1.5-2.8	
ρ_r	-	0.5-4.5	
k_s	-	.005-2.0	external damping, see Chapter 6

Table 2.1 Flexibility of the experimental arrangement

The motion of the cylinder was detected by four wire strain gauges attached to the springs of the supporting arms and connected to form a four active arm Wheatstone bridge. The signal was amplified and recorded in ultra-violet, light-sensitive paper by a recorder which provided marks on the paper at fixed time intervals. The traces obtained provided information of amplitudes and frequencies of vibration and of mean displacement of the cylinder.

Flow velocities were measured with a propeller meter and pulse counter. Wake frequencies were obtained by counting the eddies in the wake and with a stopwatch.

2.3 Experimental procedure

The experimental work consisted of a series of tests to investi-

gate the response to different flow conditions, of cylinders with different characteristics.

In a typical test, values of the natural frequency, N, of the density, ρ_r, and of the damping parameter, k'_{so}, were fixed. The cylinder was then induced to oscillate by between 20 and 70 different steady flow velocities covering the expected ranges of instability. For each flow velocity flow patterns were observed by injecting dye in the wake of the cylinder and measurements were made of amplitude and frequency of vibration, mean cylinder displacement, wake frequency and flow velocity.

Two sets of tests were conducted (see Appendix 2). In the first set of (10) tests the 3.38 diameter cylinder was used to investigate the influence on the excitation of the natural frequency, N, stiffness, k, cylinder density, ρ_c, reduced velocity, (V/ND) and Reynolds Number, R_e; these parameters were systematically varied from test to test. For the second set of (22) tests conducted with the 2.5 cm diameter cylinder, external damping was controlled with a viscous damper and the natural frequency of the cylinder was approximately the same for all the tests; more attention was concentrated during the second set of tests on the mean displacement of the cylinder, the wake frequency and external damping; the tests differed from one another in the values of density and damping.

Two of the tests of the first set and nine of the second were conducted with the splitter plate shown in Fig. 6; to eliminate the influence of the alternate wake (see Chapter 3).

Before and after each test, transient oscillations of the cylinder were produced and recorded both in air and in water, as well as with additional weights attached to the cylinder; from these, natural frequencies, density and damping were measured. The transducer was also calibrated before and after each test by comparing known displacements of the cylinder with the recorded traces.

Besides the two main sets of tests, additional experiments were conducted (Appendix III toV): (a) to measure the drag coefficient and the Strouhal number for a stationary cylinder, (b) to verify the measurements of k and ρ_r, (c) to investigate the influence on damping of amplitude and frequency of vibration, end gaps, supporting arms etc., (d) to investigate the effects of flume's bottom, free water surface, etc.

CHAPTER 3

KINEMATIC BEHAVIOUR OF CYLINDER AND FLOW

3.1 Introduction

The results of observations of flow patterns and of recordings of cylinder behaviour made throughout the tests described in the previous chapter are presented here and a first attempt is made to correlate them. This correlation will serve to identify initially qualitatively the characteristics of in-line vibration which will later be incorporated in a general theoretical model.

Flow patterns are described from visualization of the wake behind the cylinder, while cylinder behaviour is described in terms of the following non-dimensional groups of recorded variables (see Fig. 8): (a) double amplitude of vibration (a/D), (b) frequency of vibration (f/N), (c) frequency with which single eddies in the distant wake pass a fixed position in the flume (f_e/N), and (d) mean apparent drag coefficient (C_{DA}/C_{DO}), given by:

$$C_{DA} = \frac{k\bar{x}}{\frac{1}{2}\rho_f DLV^2} \qquad (3.1)$$

where, k is the stiffness (see Appendix III), ρ_f is the density of the fluid and $\bar{x}$ is the mean displacement of the cylinder with respect to its position when V = 0 (i.e. still water); C_{DO} is the "stationary cylinder equivalent" value that C_{DA} would adopt at the same flow velocity in the absence of vibration.

For want of a better alternative at this stage and following current practice the "reduced velocity" (V/ND), where N is the (constant) natural frequency of the cylinder oscillating in still water, will be used as a base parameter, both for plotting the variables and for the sequence of the data presentation.

It is then argued that the reduced velocity is an unsatisfactory parameter, and so only a qualitative description of the excitation can be presented at this stage. In later chapters, chiefly 4 and 6, a quantitative description will be given.

In accordance with previous researches reported, two main and distinct instability regions are identified and are dealt with separately in 3.2 and 3.3. Although some characteristics are common to both instability regions, emphasis is given to the *uncommon* features in 3.4 in an attempt to interpret the cylinder behaviour where the two regions overlap.

After a brief note on the three-dimensional characteristics of the flow patterns in 3.5, the most important observations of the chapter are discussed in 3.6.

3.2 First Instability Region

3.2.1 General observation and description

In accordance with the conclusions of previous researches the first instability region was associated with the shedding of a pair of simultaneous eddies, one from each side of the cylinder, per cycle of vibration.

There was a hint of a change of phase angle but essentially, a pair of eddies first appeared as the cylinder approached its furthest upstream position (see Fig. 9 and plate No 1); then onwards the eddies grew drawing fluid from the wake; when the cylinder was near its mean position in the downstream stroke, the eddies began to move towards the rear of the cylinder, and were finally detached as the cylinder decelerated towards the end of this stroke; as the eddies moved downstream into the wake, the free shear layers joining them with the cylinder came closer together consequently narrowing the wake; this trend continued approximately until the new pair of eddies appeared.

As the eddies entered the "near" wake they appeared to undergo a process of coalescence and reorganization (see Hardwick and Wootton, Dickens) in which many lost their identity; those that emerged to enter the "distant" wake had the staggered form associated with the wake from a stationary cylinder. The length of the near wake shrunk with increasing reduced velocity from a maximum of about 4D; for the highest (V/ND) values the reorganization was nearly instantaneous and the cylinder appeared to shed staggered eddies rather than pairs.

The interaction between the free shear layers on opposite sides of the wake and subsequently the mutual influence of velocity fields

of the resulting eddies are essential to the stability of a staggered wake; a "splitter plate" (see Fig. 6) prevents this interaction (Bearman, Clark) and was used in the present study to eliminate the feed-back from the staggered wake, so that the process associated with pairs of eddies could be isolated. The results of experiments using this technique are presented below in Section 3.2.2.

On the basis of the rearrangement of the wake mentioned above, three different sections of the instability region were identified (see Fig. 10): (a) a central "rearrangement section" where the cylinder sheds pairs of simultaneous eddies which were eventually rearranged into a staggered wake, (b) "locked-in section" where the rearranged staggered wake formed immediately behind the cylinder and its eddies had the same frequency as the motion of the cylinder and (c) a "double harmonic excitation section" where the frequency of the eddies in the rearranged wake was equal to half the vibration frequency of the cylinder. These sections are described in detail below in 3.2.3/4/5 respectively.

3.2.2 Splitter plate results

The use of a splitter plate eliminated the feed-back process in which the distant wake influenced the excitation.

In agreement with the results of Clark, only one instability region was identified in these experiments (see Fig. 11). In the (V/ND) range between the beginning of the instability region and the point of maximum amplitude of vibration, the wake presented the characteristics described in Fig. 9, with laminar eddies (see plate 2a). As the reduced velocity was increased from the onset of motion, an increase also was observed of (a) the size and strength of the eddies, (b) of the widening and narrowing of the wake during each cycle, and (c) the distance travelled by the points where the boundary layers separated from the cylinder wall.

The amplitudes and frequencies of the cylinder's vibration increased with increasing reduced velocity as shown in Fig. 11; the vibration was highly regular as can be seen in Fig. 12a. The apparent drag coefficient, C_{DA} (see 3.1) increased with an increase in (a/D), when compared with its stationary cylinder value, C_{DO}; the latter was in turn slightly lower than the equivalent value for a cylinder without the splitter plate (see Appendix IV).

As the reduced velocity was further increased and amplitudes approached their peak values the eddies in the wake increasingly showed signs of turbulence and their size and apparent strength changed from cycle to cycle; at the same time the average amplitudes of vibration decreased as shown in Fig. 11, while the amplitude-time traces became increasingly irregular (Fig. 12b).

This situation continued until at some critical value of the reduced velocity the amplitudes of vibration were abruptly reduced by approximately 60%, the level of turbulence in the wake increased markedly and the separation points on the cylinder moved towards the rear of the cylinder and oscillated comparatively less during each cycle (see plate 2c,d). The value of R_e at which this abrupt change of flow pattern was observed to occur ranged between 3500 and 9500.

For further increases of the reduced velocity the vibration amplitudes, which in this section were more regular (see Fig. 12c), continued to decrease until they were so small that they could not be distinguished from those resulting from turbulence in the oncoming stream. For this reason it was impossible to identify the end of the region of self-excitation.

Vibration frequencies increased throughout the instability region independently of the amplitude of vibration or the characteristics of the wake (see Fig. 11). C_{DA} increased above its value for an equivalent static cylinder by an amount roughly proportional to a/D (see Fig. 11).

The above observations describe cylinder and flow behaviour very similar to those observed in the first instability region, which allows the conclusion that the "pairs mechanism" is not seriously disrupted by the addition of a splitter plate. On the other hand the differences between the two situations clearly suggest the division of the total phenomenon into two component ones, the first associated with the patterns just described and the second with the staggered wake arrangement observed.

In the light of the above observations the behaviour of the cylinder on its own is described below.

3.2.3 Rearrangement section

The flow patterns in the "near" wake for (V/ND) values falling

in the central section of the first instability region (Fig. 10), were similar to those of the splitter plate case. The amplitude and frequency responses of the cylinder with and without splitter plate were also similar. In addition the C_{DA} values were in this case also slightly higher than the corresponding stationary cylinder value, C_{DO} (see Fig. 13).

Further downstream from the cylinder however, the symmetrical wake produced by the shedding of pairs of simultaneous eddies rearranged itself into a staggered wake resembling that of Fig. 1 (see plate 6). The distance from the cylinder to the beginning of the rearranged wake was variable and in general shrank as (V/ND) increased. The eddies of the rearranged wake had a diffuse appearance and it was sometimes difficult to establish their frequency, f_e, but apart from certain exceptions f_e diverged from the Strouhal frequency, f_s for an equivalent non-vibrating cylinder, typically by not more than 5%. An exception occurred for example when $f_e \simeq \frac{2}{3} f$, i.e. where for every three eddies shed from one side of the cylinder there corresponded one eddy of the same rotational sense in the staggered rearranged wake. Such divergence has also been reported by King who, for a cylinder free to oscillate in both the in-line and the cross-flow directions, observed f_e increasing in discrete steps according to "preferred" values of the ratio$(2N/f_e)$ such as 4, 3.5, 3, 2.5 and 2.

3.2.4 Lock-in section

As the reduced velocity was increased beyond the limits of the previous section (see Fig. 10) the length of the early wake wherein the rearrangement was effected, shrank and from time to time there were bursts of distinctive, vigorous transverse flow across the wake immediately downstream of the cylinder. This transverse flow was associated with pairs of eddies of unequal strength where the stronger member of the pair was immediately integrated in the staggered wake, and the weaker member was swept inwards and either vanished or it was absorbed by the next large eddy of the corresponding rotational sense (see Fig. 15 and plate 3). In the next cycle of cylinder vibration the positions of the stronger and the weaker eddies on opposite sides of the wake as well as the sense of the transverse flow were reversed. These bursts of transverse flow although short in duration were

associated with staggered eddies of obviously greater strength than the diffuse "rearranged" eddies of the previous section.

As the reduced velocity was increased further, these bursts of transverse flow occurred more often and lasted longer until they dominated the flow pattern near the cylinder with only short bursts of pairs of large eddies of equal strength. The resulting staggered wake (see plate 7a) had all the appearances of the theoretical model described by Von Kàrmàn (see Fig. 16) and was wider, stronger, clearer and more regular than either the wake from a stationary cylinder or a rearranged wake for the same boundary conditions. (See plates 6).

As the rearrangement process was superseded by the strong transverse motion in the early wake (see Fig. 13), the frequency of the eddies in the wake, f_e, which had a value approximately equal to f_s (or 0.666 f, see 3.2.3), increased very rapidly with increasing reduced velocity, to match the vibration frequency, f. The resulting common frequency of cylinder and eddies, $f = f_e$, was neither equal to the cylinder's natural frequency, N, nor to the Strouhal frequency, f_s, being higher than both and apparently controlled by the cylinder's motion. This behaviour, known as "frequency lock-in", persisted to the end of the instability region, and the slope of the frequency response curve with respect to (V/ND), was steepest in this locked-in condition.

The amplitude response for the locked-in condition is indicated in Figs. 13 and 14b. Where the slope of the curve is negative instabilities in the wake were observed accompanied by irregularities in the amplitude vs time traces which became more obvious as the reduced velocity was increased. The apparent drag coefficient, C_{DA}, increased markedly when the lock-in phenomenon appeared, after which it roughly followed the trends of (a/D) vs (V/ND). (See Fig. 13).

As (V/ND) was increased further a point was reached where (a/D) fell abruptly in a similar way to that observed for a cylinder fitted with a splitter plate (see Fig. 13). The wake after this point and to the end of the instability region, still adopted the staggered shape immediately behind the cylinder, although it was narrower and weaker and with smaller eddies of more turbulent appearance (see plate 7b) whose frequency, f_e, was still equal to the vibration frequency, f. A hysteresis loop was also observed for this instability (see Fig. 10).

Further increases of V/ND were accompanied by decreasing amplitudes of vibration which eventually vanished among either those caused by random flow instabilities or those due to the second instability region. This fact made it impossible to establish the end of the first instability region in terms of the reduced velocity and of vibration amplitude observations.

In this last part of the instability region the (a/D) vs time traces were more regular than those obtained before the abrupt drop of (a/D) (see Fig. 14). The synchronized frequencies of the eddies and of the cylinder continued to increase in the direction of the corresponding value of the Strouhal frequency, f_s, for that velocity of flow (fig. 13). C_{DA} continued to decrease roughly following the trends of a/D as shown in Fig. 13 and finally approaching the corresponding value of the drag coefficient for a static cylinder, C_{DO}. For further details of the end of the first instability region see 3.4.

In this locked-in section of the instability region values of amplitude, frequency and drag coefficient reached the maximum recorded values of (a/D) = 0.248, f/N = 1.191 and (C_{DA}/C_{DO}) = 1.46. The values were averaged from records lasting one minute each or approximately 100-200 cycles of cylinder vibration and they were higher than any previously reported for this instability.

3.2.5 Double harmonic excitation section

For the lowest range of (V/ND) in the instability region and especially with light cylinders, a third type of cylinder-wake interaction gave rise to a local maximum of the amplitude response (Fig. 13). Analysis of the corresponding (a/D) vs time traces (Fig. 17a) revealed a non-sinusoidal motion (Fig. 18a) where two essential components could be identified with frequencies in the ratio 2:1 (Fig. 18b and c).

Flow visualization revealed that a pair of eddies of apparently equal strength was generated during every cycle of cylinder vibration with period T (Fig. 18b). In addition, a process was observed in the wake immediately behind the cylinder in which four consecutive eddies of the same rotational sense coalesced to form one of the dominant eddies of the distant wake (plate 4 and Fig. 19). The period of these dominant eddies was 2T (Fig. 18c) indicating that the distant wake did not conform to the Strouhal relationship but it was instead controlled by

the motion of the cylinder according to: $f = 2f_e$. A fluctuating transverse flow was observed at the back of the cylinder in association with the larger dominant eddies, although this flow appeared much weaker than that observed in the lock-in section of the instability region. The resulting distant wake presented characteristics similar to those of the wake observed in the second instability region (see 3.3 and plates 8a and 8b).

It was concluded (see Chapter 8) that the vibration in this section resulted from the combination of two excitation mechanisms, one associated with pairs of simultaneous eddies and the other with the transverse flow and the distant wake, which mechanisms acted on the two harmonic components of the cylinder's motion (b and c respectively in figure 18). This interpretation of the excitation thus suggests that the vibration should start when $2f_s = N$, i.e. when $(V/ND) = (1/4S)$.

It should be noted that this type of excitation extends the first instability region beyond the minimum (V/ND) values of the splitter plate instability, and that high values of both cylinder's density or damping reduced or totally suppressed this type of instability. The minimum recorded values of (V/ND) for the commencement of the instability region thus ranged between 1.15 and 1.6.

As the motion started (see Fig. 20) the average amplitudes of vibration increased rapidly towards a maximum accompanied by a sharp increase of C_{DA}. f/N decreased only slightly while f_e remained equal to $f/2$.

As (V/ND) was increased further a point was reached where the rearranged wake moved away from the cylinder during intervals of a few cycles only. During these intervals, the wake was like that described in 3.2.3, with pairs of simultaneous eddies being shed and preserved in the wake near the cylinder. The corresponding a/D vs time traces (Fig. 17b) showed regular constant amplitudes which were smaller than the average amplitudes obtained with the double harmonic excitation. Vibration frequencies increased nearer to N, and C_{DA} decreased nearer to C_{DO}. The frequency of the eddies of the distant rearranged wake, f_e, seemed to be equal to f_s, although it was difficult to measure it due to the short time available for eddy counting, combined with weak and confusing flow patterns. These intervals were longer and occurred more often as (V/ND) was increased further until the central

"rearrangement section" was reached.

This harmonic excitation phenomenon explains the "hump" at the beginning of the (a/D) vs (V/ND) diagram observed by other researchers (e.g. Wootton et al) and it also offers an explanation for the initiation of motion of lightly damped cylinders at (V/ND) ≈ (1/4S).

3.3 Second Instability Region

3.3.1 Introduction

The second instability region was characterized by the shedding of alternately clockwise and anticlockwise eddies in the wake of the cylinder, at the rate of one per cycle of motion of the cylinder, in agreement with all previous reported observations.

The ranges of the reduced velocity V/ND over which the second instability region extended were highly variable from test to test and in some cases values of (V/ND) as high as 6.3 were recorded. This is considerably higher than the (≈ 3.5) limiting values previously reported (King, Clark) and therefore the flow velocity ranges over which vibration can occur were extended significantly. It will be seen in Chapter 6 however, that although it is theoretically possible to obtain in-line excitation with even higher (V/ND) values than those achieved in the present laboratory research, practical considerations make this unlikely at full scale.

Some novel flow patterns were observed in the wake, as shown in 3.3.2, and the cylinder behaviour observed, as reported in 3.3.3, contrasted markedly with some previous reports (e.g. King, Clark). The growth of the vibration at the beginning of the instability region is discussed separately in 3.3.4 to facilitate the presentation.

3.3.2 The wake

Previous researchers have regarded the wake in the second instability region as being similar to that here described in connection with the "lock-in section" of the first instability region (see 3.2.4), i.e. a wake of the Von Kàrmàn type commencing immediately downstream of the cylinder, with eddies of frequency, f_e, locked-in to the vibration frequency. The wakes observed in the second instability region during the present research however, while commencing in the same area and

having the same lock-in frequency relationship with the cylinder, clearly did not resemble the Von Kàrmàn model.

The eddies in the wake over a distance of up to 15 diameters downstream from the cylinder, were all aligned in a single row (see plate 8b and Fig. 21), instead of being aligned in the two usual separate rows, according to their sense of rotation (see plate 6a and Fig. 1). It was impossible to say however if the wake would eventually rearrange itself far downstream from the cylinder into a staggered one according to the Von Kàrmàn model, because the flow patterns become indistinct in the region of 15 diameters from the cylinders.

The eddy shedding process that characterised the second instability region can be described as follows (see Fig. 22 and Plate 5):

(a) When the oscillating cylinder crossed its mean position in the upstream stroke, the interacting velocity fields of the cylinder and of the eddy formed during the previous cycle appeared to induce a transverse flow between the eddy and the cylinder, which deflected outwards the shear layer on which the eddy was formed and drew the opposite shear layer towards the centreline of the wake.

(b) When the cylinder reached its furthest upstream position, the drawn-in shear layer began to roll up to form a new eddy in the lee of the cylinder; the transverse flow appeared to have gained in strength at that point.

(c) As the cylinder crossed its mean position in the downstream stroke, the new eddy had grown in strength and diameter and had taken up a position 180^{o} from the frontal stagnation point in the cylinder. The transverse flow seemed now to have weakened but by this time it appeared to have so distorted the longer of the two shear layers as to interrupt the flow of vorticity to the old eddy.

(d) As the cylinder reached its furthest downstream position there was still an obvious transverse flow between the two eddies, but as yet no evidence of a transverse flow in the opposite direction between the new eddy and the cylinder. Immediately after this point the new eddy began to move downstream along the wake's centreline.

3.3.3 Cylinder behaviour

In contrast to previous observations of the second instability

region (e.g. Clark) where the a/D vs V/ND diagram had a peaked shape, the observations of the present research showed approximately constant amplitudes of vibration throughout the instability region (Fig. 23) except for a steeply rising limb (see 3.3.4). The corresponding a/D vs time traces were fairly regular (Fig. 24 a).

The frequency of the eddies in the wake was locked-in to the frequency of vibration and the common frequency, $f = f_e$, increased with (V/ND) above the value of the natural frequency,N,but remained below the value of the Strouhal frequency, f_s (Fig. 23).

Contrary to the observations of previous research workers who observed only slight variations of frequency, the vibration frequencies observed in the present research, especially for light cylinders exceeded the natural frequency of the cylinder by as much as 75%.

Another important observation concerned the behaviour of the apparent mean drag coefficient, C_{DA}, which was here observed to increase markedly, reaching values up to 90% higher than the corresponding C_{DO}, at the beginning of the flat top of the amplitude response curve. For higher (V/ND) values, C_{DA} decreased to a value only 40% or 50% higher than C_{DO} at the end of the instability region (Fig. 23).

Towards the end of the instability region (a/D) decreased slightly with increases of (V/ND) until a point was reached where the (a/D) vs (V/ND) curve fell abruptly. This was associated with a large hysteresis loop as shown in Fig. 23.

After the cylinder had ceased to vibrate the wake recovered its usual staggered shape, commencing some 1.5 diameters downstream of the cylinder beyond the formation region; the eddies in the wake adopted the Strouhal frequency, f_s, and C_{DA} took on its static cylinder value C_{DO}; vibration frequencies were difficult to measure at this point owing to the random character of the resulting vibration (see Fig. 24c). At this point, if the cylinder was forced to oscillate and then was released, the rate of decay of the resulting transient was relatively low (Fig. 25a); but as (V/ND) was increased further, the decay rate could be so high that only 2 to 3 cycles of the transient were oberved (Fig. 25b).

3.3.4 Growth of the instability

Self-excitation commenced for the second instability region in

the range $2.3 < (V/ND) < 3$. Just after the commencement of self-excitation where (a/D) values were still small the frequencies f, N, f_e and f_s were all nearly identical and $C_{DA} \simeq C_{DO}$ (see Figs. 23 and 26).

As (V/ND) was increased beating forms of vibration appeared (Fig. 24b), whose average amplitude increased with (V/ND) as shown in Fig. 26. The vibration frequency, f, was only slightly different from f_e, and both these frequencies were greater than N, but less than f_s. The mean displacement, $\bar{x}$, and consequently C_{DA}, increased by an amount roughly proportional to (a/D) as can be seen in Figs. 24b and 26.

The corresponding flow patterns fluctuated between the Von Kàrmàn type of wake and the one described in 3.3.2, being at times indistinct and badly correlated along the cylinder's length. (See plate 7b).

As (V/ND) was increased further the beating motion gradually diminished and eventually disappeared as the flat top of the amplitude response curve was reached. The flow pattern thereafter became stable as described in 3.3.2.

3.4 Region Between First and Second Instability Regions

For values of the reduced velocity between 2 and 3, it was often difficult to know exactly in which instability region a vibration belonged and so it was difficult to establish the limits of the two regions.

This was because: (a) previous reports are inprecise and contradicting in this area (see Fig. 3), (b) the ranges and values of (V/ND) in the present research were also found to vary from case to case, (c) the flow patterns in the wake at the end of the first instability region and at the beginning of the second were very similar as can be seen in Plates 7a, 7b & 8b, and (d) at the very low values of (a/D) found in this region, the correlation of the flow patterns along the cylinder's length was very poor (see 3.5); as a result of poor correlation visualization of flow patterns was more difficult, and the behaviour of the cylinder was erratic and difficult to analyse.

However, with the aid of the knowledge of the behaviour of (f/N) and C_{DA} described in 3.2 and 3.3 it was possible to make certain observations as described below.

Fig. 27 presents an example of a selected portion of a long vibration record of a/D vs time obtained with (V/ND) = 2.59. It can be seen from the trace in Fig. 27 that the maximum amplitudes are only 6.5 % of the cylinder diameter, are irregular and show evidence of beats. However, significant differences can be identified between the various beating forms as follows:

In parts (1) and (2) of Fig. 27b the frequencies of vibration are significantly higher than the natural frequency, N, and also higher than those in parts (3) and (4); the frequencies of (3) and (4) however are only *slightly higher* than N. Moreover, in (1) and (2) the average displacement of the trace during one cycle with respect to a fixed reference point, $\bar{x}$, is approximately constant, while in (3) and (4) $\bar{x}$ seems to grow proportionally with (a/D).

As can be seen in Figs. 13 and 26 the frequencies at the end of the first instability region are higher than N, while at the beginning of the second they are near the value of N. Figs. 13 and 26 also show the values of C_{DA} and consequently of $\bar{x}$ decreasing towards the static cylinder values at the end of the first instability region, while at the beginning of the second, these values increased sharply, roughly in propotion to the increasing (a/D). It was thus concluded that (1) and (2) represented vibration typical of the first instability region while (3) and (4) represented the second.

A possible explanation of this observation could be that the instability regions overlap and the form of the excitation can fluctuate between the first and the second types of instability at the same value of (V/ND). Alternately, or possibly in addition to the above, it could be that the self-excitation is highly sensitive to the unsteadiness which is inevitable in the approaching flow.

Quantitative considerations of the variables involved and comparison of different experimental results described in later chapters led to the conclusion that the instability regions did overlap and thus furnished another reason to question the value of using (V/ND) as the base parameter.

3.5 A Note on Flow Pattern Correlation

During the tests conducted in this research it was observed that

reductions of vibration amplitude and frequency could occur associated with desynchronization or lack of correlation of the flow patterns in the wake along the length of the cylinder.

When the cylinder remained stationary events of the eddy shedding process did not in general occur simultaneously in all parts of the wake along the cylinder, although it was often observed that these events were synchronized over half the length of the cylinder or more.

When the cylinder vibrated shedding pairs of simultaneous eddies, the dependence of the shedding process on the motion of the cylinder and the symmetry of the wake ensured a perfect correlation along the entire length of the cylinder in the near wake, although desynchronized events were often apparent in the distant reorganized wake.

The symmetry of the wake in the second instability region combined with the dependence of the shedding process on the motion of the cylinder, permitted either (a) a perfect correlation of the wake along the entire length of the cylinder, or (b) half-cycle desynchronization of events in different points along the cylinder's length, i.e. when an eddy was being shed from one side of the cylinder along some portion of its length, another counter-rotating eddy could be shed from the opposite side of the cylinder in another portion of its length, with a wake discontinuity in between. Up to two of these discontinuities were observed in a given vibration condition; the discontinuities could move along the cylinder's length but they neither disappeared nor did additional ones appear once a steady state vibration was set in the second instability region.

Similar discontinuities were also observed in the lock-in and double harmonic excitation sections of the first instability region. The correlation of the wake in the lock-in section was very variable due to the bursts of pairs of simultaneous eddies and consequently a perfectly correlated wake in this section was very difficult to achieve.

3.6 Summary and Conclusions

In accordance with previous research reports, two different instability regions were identified in the experiments here conducted, although some further observations which in general were neglected in previous researches deserve special attention.

3.6.1 Interacting mechanisms in the first instability region

Interpretations of the first instability region and predictions of the corresponding cylinder behaviour have been made previously (e.g. Dickens, King) on the basis of the one excitation mechanism characterized by the shedding of pairs of simultaneous eddies. The present work and especially the experiments with the splitter plate have shown however that the excitation of this instability region is a complex one and embraces in addition to the pairs mechanism one associated with an interaction between free shear layers leading to a more stable staggered wake. Therefore, any improvement in such interpretations or predictions should include these two mechanisms and their interaction. Two clear cases in point are the ranges of (V/ND) over which the instability region extends and the variations of C_{DA}, both of which appear to be markedly influenced by interaction. Another important consequence of this interaction is the double harmonic excitation at the beginning of the instability which explains the local maximum of the (a/D) vs (V/ND) curve reported by previous researchers in this region. This type of excitation moreover, could be responsible for the initiation of the vibration, which should occur approximately when $f_s = \frac{1}{2}N$, i.e. at (V/ND) = 1/4S, although other factors such as damping and flow instabilities have to be considered. (See Chapters 6 and 9).

On the other hand, the marked similarities between the cylinder behaviour in the first instability region and that observed when using a splitter plate, such as the shape of the (a/D) vs (V/ND) curve with the abrupt drop of (a/D) and the trends of (f/N), show the dominant influence of the "pairs mechanism". This is reinforced by the observation of pairs of simultaneous eddies throughout the instability region even when a strong transverse flow occurs. Another consequence of this is that the abrupt decrease of (a/D) cannot be explained solely in terms of the presence of the second instability region as others have suggested.

3.6.2 The wake of the second instability region

The second instability region has previously been associated with a wake of the Von Kàrmàn type, similar to that observed at the end of the first instability region; this has complicated the differentiation between the two types of instability. The present research showed

however, that when the cylinder was restricted to in-line motion only, the wake of the second instability region alone had charcteristics markedly different from those of a Von Kàrmàn wake. These observations, besides showing a new and interesting type of wake, have provided a means for distinguishing between the two instability regions and their corresponding types of excitation.

The difference between the two locked-in wakes of the two instability regions was attributed to a variation in the timing of the shedding of the eddies, with respect to the events in the wake represented by the transverse flow which sweeps the back of the cylinder. This suggested that in order to arrive at a better explanation of the phenomena involved, great importance should be attached to the phase relationships between the wake and the cylinder motion.

3.6.3 Cylinder behaviour

The careful and combined analysis of the variables that expressed the behaviour of the cylinder showed novel characteristics that even at this early stage have contributed significantly to the understanding of the phenomenon.

The approximately constant value of the amplitudes of vibration observed in the second instability region differed from previous reports and, as will be seen in later chapters, facilitated the theoretical analysis of the phenomenon.

In contrast with previous research reports, frequencies of vibration were neither constant nor approximately constant; instead they increased with reduced velocity, reaching maxima of $(f/N) = 1.19$ and $(f/N) = 1.76$ in the first and second instability regions respectively. Although these variations are less marked in practical situations (see Chapter 6), they eliminated the possibility of assuming constant frequencies and thus complicated the mathematical interpretation which is to follow. A study of frequency variations however has already shown valuable details such as the increases of (f/N) in the first instability being independent of (a/D), which suggests a trend progressing undisturbed as (V/ND) increases in spite of amplitude collapse. Knowledge of frequency variations also contributed to the distinction of the two instability regions from recorded vibration traces as shown in 3.4.

Analysis of the frequency of the eddies in the wake together with the frequency of vibration showed three areas of "frequency lock-in", namely, at the beginning and at the end of the first instability region and throughout the second, which confirmed the strong interaction between the flow behaviour in the wake and the cylinder vibration. This analysis also contributed to the identification and understanding of the "double harmonic excitation" of the first instability region.

The variations of the apparent mean drag coefficient, C_{DA}, here observed in both instability regions also contrasted with previous research reports in which it has been regarded as a constant (e.g. King). C_{DA} increased sharply whenever transverse flow was observed sweeping the back of the cylinder in both instability regions, and it reached values up to 90% higher than C_{DO}. As is the case for the frequencies, the study of the behaviour of C_{DA} has already been fruitful, as for example in the first instability region where it contributed to the understanding of the interaction of the different excitation mechanisms, and in the area between the two regions where it allowed a better distinction of the two different phenomena involved.

3.6.4 The reduced velocity (V/ND)

The (V/ND) ranges over which the two instability regions occurred overlapped considerably, and they varied widely from test to test. Thus in the first region motion could commence in the range $1.1 < (V/ND) < 1.7$, and the sudden drop of (a/D) occurred at $2.2 < (V/ND) < 3$, while the (V/ND) value corresponding to the end of the instability could rarely be identified. The second region commenced and terminated in the ranges $2.3 < (V/ND) < 3$ and $3.3 < (V/ND) < 6.3$ respectively. This lack of definition was even more marked when comparing the present results with previous reports as shown in Fig 3. This uncertainty in the ranges of the base parameter complicated the comparison of different results and made it impossible to study accurately the influence of other factors such as density and damping.

CHAPTER 4

A NEW BASE PARAMETER

In the last chapter it was found that all the experimental results in the present and previous studies of in-line vibration showed similar trends. It was also found that the reduced velocity (V/ND), failed to provide a satisfactory quantitative comparison of the results of widely differing experiments.

It is intended in this chapter to present a more satisfactory base parameter which: (a) unified the results of different experiments into a general model which incorporates the underlying trends and characteristics of in-line vibration, (b) defines more precisely the instability regions, (c) helps to explain certain features of the excitation and (d) leads to further quantitative analysis of in-line vibration.

Some previous authors have adopted an alternative form of the reduced velocity: this is analysed in 4.1 leading to the presentation in 4.2 of the new parameter whose characteristics and advantages are discussed in 4.3

4.1 An Alternative Form of the Reduced Velocity

Some previous researchers (e.g. Dickens) have used an alternative form of the reduced velocity, namely (V/fD) where f is the actual vibration frequency instead of, as was the case in Chapter 3, the natural frequency in still water, N. Although (V/fD) is not directly proportional to V alone and is therefore not directly representative of flow velocity variations, it is more practical in situations such as the present one where f is not a constant. Arguments in support of this last statement and leading to a discussion of the theoretical implications of the use of (V/fD) as a base parameter are presented below.

Figure 28 shows vibration amplitudes and frequencies plotted against (V/ND), recorded from three tests conducted with the same cylinder, in the same flume, with similar values of N and for similar flow velocity ranges, but with the cylinder loaded with different masses and with the

stiffness of the supporting arms adjusted to provide the same N. It is clear from the figure that when there was a large variation of f/N in the self excited range there was a corresponding wide variation of V/ND. This suggested that the (V/ND) range was influenced to some extent by f, and so any improved base parameter ought to contain information about the vibration frequency.

The reduced velocity can be interpreted as the distance travelled by the flow per cycle of motion of the cylinder, expressed in cylinder diameters. In the cases when f is not a constant this interpretation is valid only for (V/fD) and not for (V/ND), and (V/fD) is then proportional to the distance, ℓ (see Fig. 1) in the direction of the flow, between consecutive eddies in the wake near the cylinder (or throughout the wake in the cases of lock-in). The distance between eddies has been shown by Von Kàrmàn to be related to the stability of a staggered wake; and as was shown in Chapter 3, the staggered wake plays an important part in the excitation. Moreover as will be seen in Chapter 8, the distance between consecutive pairs of simultaneous eddies may be a factor which determines the magnitude and timing of the exciting forces. Thus the interpretation of the reduced velocity as a distance ratio also suggests the use of (V/fD) instead of (V/ND). Indeed, when the results of Fig. 28 were plotted using (V/fD) as the abscissa (Fig. 29), the amplitude response curves coincided approximately, and it was concluded that (V/fD) was a better parameter than (V/ND) for unifying and comparing different experimental results. The use of V/fD as a base parameter was less successful when the results of the present and previous researches were compared, as can be seen in Fig. 30.

4.2 Derivation of the New Parameter

The problems then arise of how to explain the differences between the curves of Fig. 30 and of how to account for these differences in an improved base parameter.

It is clear from Fig. 29 that (V/fD) is a satisfactory base parameter for any one series of observations involving similar geometrical and dynamic conditions. The difficulty seems to arise when there are differences in these conditions such as Reynolds number, turbulence of the main stream, blockage and boundary effects, cylinder's surface roughness and measurement techniques and accuracy. Clearly

an improved base parameter would have to reflect these conditions to reduce the divergence of Fig. 30.

Bishop and Hassan report that for each flow velocity, when a certain forced frequency of cross-flow oscillation of their externally driven cylinder was reached, a sudden decrease of the exciting force would occur accompanied by an equally abrupt shift of the phase angle between the force and the motion. They suggested the existence of one characteristic frequency of the flow corresponding to each flow velocity. In Chapter 3 it was shown that the tendency of the staggered wake to adopt the frequency for a constant Strouhal number was an important factor influencing the vibration and in particular the reduced velocity ranges.* Information about this frequency should therefore be considered for its inclusion in the base parameter.

Moreover, the fact that the Strouhal number, S, is influenced by the same flow and cylinder characteristics mentioned above, namely: R_e (see Fig. 31), flow turbulence and cylinder surface roughness (see Fage & Warsap) blockage (see Richter), measurement techniques, etc., suggested that both S and the excitation might have features in common. If this were indeed correct, the inclusion of the Strouhal number in the base parameter could not only account for the Strouhal wake frequency of the flow but would also reflect the characteristics of cylinder and flow as mentioned above.

The expression for the inverse of twice S:

$$\frac{1}{2S} = \frac{V}{f_s D}$$

suggested a direct ratio with the reduced velocity, thus:

$$\frac{V/fD}{V/f_s D} = 2S\frac{V}{fD} = \frac{f_s}{f}$$

where (f_s/f) is a new non-dimensional frequency parameter.

This parameter is proportional to the reduced velocity (V/fD) if S is constant, which for a given situation and for the range $10^3 < R_e < 3 \times 10^5$, is approximately the case (see Fig. 31); if the

* For exqmple in the first instability region this tendency was associated with the onset of motion, with the rearrangement of the wake, with the lock-in phenomena and with the sudden drop of the (a/D) vs (V/ND) curve which occurred earlier when compared with the case of the splitter plate; while in the second instability region f_s appears to control the onset of motion.

frequency variations are not large moreover, (f_s/f) is approximately proportional to (V/ND). Curves of amplitude and frequency response with (f_s/f) as abscissa should therefore be similar to those using the reduced velocity.

The experiments represented in Fig. 29 were conducted with the same cylinder and with similar flow characteristics; therefore it can be said that the S vs R_e relationship was the same for all three tests, and hence the good agreement between the curves. Curves 2 and 3 of Fig. 30, represent tests conducted with different cylinders and flows (see Appendix II); the disagreement between the curves moreover corresponds to the variation of S for the two cases (see Fig. 33). It thus seemed reasonable to conclude that the disagreement in the reduced velocity ranges of the various research reports is mainly due to the differences in the characteristics of the flow-cylinder system mentioned above, which, within the R_e ranges here covered, appear to affect both S and the vibration phenomenon in a similar manner.

Figure 32 presents the data of Fig. 30, plotted this time against (f_s/f) instead of (V/fD) and it shows a significant improvement in the collapse of the data from the various sources especially if compared with Fig. 3. Curve 1 of Fig. 32 moreover, shows good agreement with the other curves in spite of the relatively much higher R_e values involved.

On the strength of Fig. 32 it was argued that f_s/f allowed a direct comparison of different and hitherto incompatible experimental results, provided that f_s is appropriate to the particular situation under consideration, rather than obtained from a S vs R_e relationship intended for general application. The unified diagram thus obtained shows the common characteristics of the excitation in a manner suitable for a generalised quantitative analysis.

Further refinement of the various curves of Fig. 32 will be made in Chapter 6 and 9, where density, damping and three-dimensional factors are considered. The remainder of this chapter is concerned with the assessment of (f_s/f) as a base parameter and with the analysis of its main characteristics.

4.3 Analysis of the Parameter

The non-dimensional frequency parameter evidently provides a

basis for comparing different experimental results. It remains now to see if it is satisfactory for a quantitative definition of the instability regions and to discuss the practical implications of its use.

4.3.1 Definition of the instability regions

In comparison with Figs. 3 and 30 in which the reduced velocity is used as base parameter, Fig. 32 shows with far greater precision the trends and limits of the instability regions according to whether f_s/f is less or greater than unity; i.e. the first instability is characterised by vibration frequencies which are higher than the eddy frequency, f_s, of a "Strouhal wake", while in the second instability, vibration frequencies are lower than f_s.

Fig. 32 also shows that no vibration occurs for: (a) f_s/f values smaller than 0.5 (except for curve 1, see Shapter 9), that is when

$$\frac{V}{ND} = \frac{1}{4S} \qquad \text{if } f = N$$

as observed in 3.2.5; and (b) for f_s/f values above $\sqrt{2}$, the significance of which will be discussed in Chapter 8. Thus the parameter f_s/f defines quantitatively the two instability regions as follows:

$$\text{1st instability for} \quad \tfrac{1}{2} < \frac{f_s}{f} < 1$$

$$\text{2nd instability for} \quad 1 < \frac{f_s}{f} < \sqrt{2}$$

4.3.2 Contributions of f_s/f to the explanation of the phenomenon

The interpretation of f_s as a flow characteristic or natural frequency suggests that a resonance should occur when $(f_s/f) = 1.0$, but this is clearly not the case (see Fig. 32). Considering however that when (a/D) has a non-zero value the cylinder's motion interferes with the flow patterns, it can be then expected that the flow's "natural" frequency will change accordingly, and therefore f_s can only be said to be the "flow's natural frequency" when (a/D) = 0. This is in agreement with Bishop and Hassan who reported different characteristic flow frequencies corresponding to different amplitudes of vibration.

At the point where f_s passes from less than f to greater than f however, (a/D) is small and this interpretation of f_s suggests a change of phase lead, i.e. in the first instability the motion of the cylinder in some way leads that of the wake, while in the second the converse occurs. This is reinforced by the observations of Chapter 3, where a comparison of the eddy shedding process of the lock-in section of the first instability with that of the second instability, show a difference in the timing of the transverse flow that sweeps the back of the cylinder(which seems to depend on events of the wake) with respect to the shedding of the eddies(which can be associated with the motion of the cylinder)(see Figs. 15 and 22).

A change of phase lead between the events in the wake and the motion of the cylinder may thus be associated with: (a) differences between the two instabilities; (b) the absence of significant vibrations for $(f_s/f) = 1$ and (c) the decrease of (a/D) at the end of the first instability region on the one hand and the increase of (a/D) at the beginning of the second instability on the other, in spite of a similar type of wake having been observed in both situations.

One of the advantages of identifying the threshold of instability by $(f_s/f) > 0.5$ rather than by some fixed limiting value of (V/ND) is evident for conditions when $R_e < 10^3$; in this range where S is decreasing with decreasing R_e (Fig. 31), f_s decreases more rapidly than V, and so the limiting (V/ND) at the threshold of vibration cannot be a constant and must increase somewhat with decreasing R_e. Another advantage of linking the characteristics of cylinder and wake through (f_s/f) suggests itself when attempting to explain the absence of in-line vibration reported by King when $R_e < 1000$ and by Dickens when $R_e < 750$. Although no specific experiments were conducted in the present study to confirm these values it seems likely that some disorganization of the distant wake, which is presumably responsible for the scattered Strouhal numbers when $R_e \simeq 10^3$ (Fig. 31), is also responsible for inhibiting the self-excitation process.

4.3.3 Practical considerations

Figure 32 on its own does not provide a designer with information about flow velocity and vibration frequency in the self-excited ranges, because the figure does not show the relationship between (f/N) and

either (f_s/f) or (V/fD). The behaviour of (f/N) will be discussed in Chapter 6. The designer would also require a relationship between f_s and V for the boundaries and conditions of flow under consideration. Figure 31 is an example of such a relationship which might be adequate for a preliminary estimate, but since the figure is applicable to smooth cylinders in wide, one-dimensional, low turbulence approach flows, a correction to Fig. 31 may be necessary to account for the practical conditions of the design.

In this respect it should be noted that the parameter (f_s/f) permits the designer to arrive at more accurate predictions than is the case with the reduced velocities; this is because besides S vs. R_e relationships there is some information available in the literature on the influence that the other factors involved have upon the value of S, while to the knowledge of the author, no method exists to assess the influence that any of these factors have upon the reduced velocity ranges.

As an illustration of the discrepancy between values of "S" shown in Fig. 31, and observed Strouhal numbers for flows more representative of practical situations, it is appropriate to cite the observations of the present study where an accurate estimate of S was essential.

During the test programme it was found that the observed S and that predicted from Fig. 31 differed considerably (see Fig. 33) and it was concluded that the effect of blockage, three-dimensional effects and the difficulties of measuring low velocities were responsible for the discrepancies. Blockage corrections were complex and unreliable (see Appendix VI) and they alone were insufficient to overcome the discrepancy; so it was decided that since f_s for a stationary cylinder could be measured with greater confidence than the *effective* V, an empirical relationship between f_s and a respresentative V was obtained.

The use of (f_s/f) rather than the reduced velocity and the direct calibration of the flow meter with the actual value of f_s thus avoided additional complications due to: (a) accurate measurement of the "true" value of V at the meter's location, involving independent calibration of the meter, and assessment of the flow characteristics at that point in relation to the flow in which the meter was calibrated; (b) knowledge of the relationship between this true value and a significant

one from the point of view of the excitation; (c) blockage corrections. In this case moreover, if it is assumed that the output of the flow meter is not significantly affected by the vibration of the cylinder and that it reasonably reflects the flow behaviour, accuracy depends then only on the repeatability of the combined behaviour of the flow and of the meter and on the technique used to measure the frequency of the eddies, independently of the accuracy of the meter to detect the "true" value of V.

CHAPTER 5

ANALYSIS OF VARIABLES

Before proceeding to a more detailed analysis of in-line vibration it is opportune in this chapter to identify and briefly discuss certain variables which have a significant although indirect or secondary influence. The analysis of the variables will be based on the following considerations: (a) influence of the variable on the excitation, (b) likely range of the variable, (c) control, suppresion or avoidance of vibration and (d) economic and other practical considerations. Point (c) above embraces the three main methods of solving a flow-induced vibration problem, namely: (i) avoiding the instability regions, (ii) increasing damping (energy dissipation) and (iii) modifying the cylinder's shape or the flow patterns.

For convenience the chapter will be divided into sections containing groups of variables relating to: cylinder behaviour (5.1), cylinder characteristics (5.2) and hydrodynamic forces and f_s (5.3). The analysis ends with the identification (in 5.4) of the most important non-dimensional groups for use in subsequent chapters.

5.1 Cylinder Behaviour

The behaviour of the cylinder can be represented by its displacement, x, consisting of a mean, $\bar{x}$, and a fluctuating component, x'. Assuming sinusoidal motion moreover (see Chapter 7), x' can be said to be a function of the maximum fluctuating displacement, x'_o, the freqency, f, and the time, t, thus:

$$x = \text{function of } (\bar{x}, x'_o, f, t) \qquad (5.1)$$

Of these four variables, x'_o is perhaps the most important because it is an index of the magnitude of the strain reversals experienced by the structural member, and because it is often the largest contribution to the total strains.

In contrast to cross-flow vibration the maximum total displacements (and hence the maximum total strains) of an in-line vibrating

cylinder are obtained by the arithmetic sum of $\bar{x}$ and x'_o and hence the importance of $\bar{x}$. In Chapter 3 it was shown moreover that the mean drag force can be up to 90% higher for a vibrating cylinder than for a static one, and as will be shown later (see Chapter 8) in most practical cases, and especially with light cylinder, $\bar{x}$ can be equal to or larger than x'_o.

Besides determining the flow velocity ranges when vibration can occur, the vibration frequency, f, determines the possibilities of resonance with other members of the structure and, together with x'_o, it determines the local fatigue stresses of the structure.

The time, t, is not an important variable if all fluctuating variables are sinusoidal, but phase angles will be introduced (Chapters 7 & 8) to relate motions, flow pattern and forces in time.

5.2 Cylinder Characteristics

Newton's Second Law can be used to represent the motion of a solid induced by fluid forces (see e.g. Den Hartog) thus:

$$F_T = M_c \ddot{x} + c \dot{x} + k x$$

In this equation F_T represents all the fluid forces; M_c is the mass of the cylinder given by its density, ρ_c, and its dimensions D and L; k and c, are respectively the structural stiffness and damping of a cylinder in flexure or of the supports of a rigid one; and $\dot{x}$ and $\ddot{x}$ are the 1st and 2nd derivatives of x with respect to time. Thus:

$$F_T = \text{function of } (D, L, \rho_c, k, c, x) \qquad (5.2)$$

or conversely:

$$(x) = \text{function of } (D, L, \rho_c, k, c, F_T) \qquad (5.3)$$

where D, L, ρ_c, k and c are cylinder characteristics.

The three variables k, D and L together with ρ_c and ρ_f (the fluid density) determine the value of the natural frequency N, i.e.

$$N = \frac{1}{2\pi} \sqrt{\frac{k}{M_{TS}}} \qquad (5.4)$$

where $M_{TS} = \frac{\pi}{4} D^2 L(\rho_c + \rho_f)$ (see Chapter 7)

Although an independent correlation between N and the cylinder motion was not identified, N is important because it is a major factor in determining f, and consequently, through f_s/f, it determines whether or not vibration will occur. In practical situations a vibration problem can be avoided more often by a modification of such structural variables as D, L, ρ_c and k than by enforcing some change of the flow's characteristics. For example through a decrease of f_s or an increase of f (or both) it is possible to ensure that (f_s/f) is always so low that it never crosses the threshold of instability. On the other hand it is usually not prudent to design for a high value of (f_s/f) outside the instability regions (see 4.3) because, among other considerations, of the possibility of exciting cross-flow motion or higher harmonics of in-line motion.

A designer wishing to achieve low (f_s/f) must consider many interelated factors.

To decrease f_s at constant V and S, the cylinder diameter should be increased with the consequent higher costs and also higher forces acting on the cylinder's supports which may further increase the costs. There is a second advantage in an increase of diameter through the consequent increase of f (through k and N); this increase of f leads to a further reduction of (f_s/f). An additional increase of f can sometimes be achieved through increased cylinder wall thickness or a stiffening of the supports, but these measures entail higher costs. Another method of increasing stiffness is through a decrease of cylinder's length although this is rarely practical. It should be noted that in contrast to increasing the damping, increasing stiffness reduces the mean deflection of piles which can be an important design factor.

In the case of hollow piles full of water, ρ_c is difficult to modify owing to the large weight of the water inside the pile; the "added mass" moreoever, (see Chapter 7) makes it even more difficult to modify f via changes in ρ_c; for example if it were intended to increase N by decreasing ρ_c with thinner cylinder walls, the resulting lowering of k would probably overrule the decrease of $(\rho_c + \rho_f)$ and consequently N would decrease instead of increasing.

In the cases of cylinders vibrating in air or hollow empty cylinders vibrating in water however, the absence of the water inside the pile and, in the first case, the relatively negligible density of the

"added mass" make the modification of ρ_c more significant. For example if the diameter of the cylinder were increased and the thicknesses were kept constant, ρ_c would be reduced significantly; as explained above moreover,increasing D would reduce f_s and k, and consequently reductions of (f_s/f) would result from three different sources. A more detailed analysis of both density and damping is presented in the next chapter.

It has sometimes been possible to reduce or eliminate self-excitation, especially in aerodynamic situations, by intentionally altering the geometry of the cylinder by means of strakes, wires, grids, etc. (see Clark, Walshe & Wootton). In a marine environment however, the use of such devices is likely to increase risks and costs significantly owing to the growth of shell-fish, etc. Consequently this method of eliminating vibration may be satisfactory as a temporary measure only; in the long term, the avoidance of the instability regions appears to be the only practical solution.

5.3 Variables Influencing f_s and the Hydrodynamic Forces

To complete the analysis of the variables which determine the motion of the cylinder, the flow forces, F, of equation 5.3 have to be considered. These forces are influenced by characteristics of the flow such as its velocity, V, its density, ρ_f, and its dynamic viscosity, μ_f, which in engineering practice, are often environmental characteristics determined by such factors as local temperature and geography and are therefore difficult and expensive to modify. In laboratory situations however, their modification is often an essential feature in the test procedure.

The importance of the flow velocity, V, has been discussed in Chapter 3 and 4 in connection with the reduced velocity and the parameter (f_s/f), although it should also be noted that in most cases, the fluid forces are functions of V^2 (see Chapter 7). The fluid density, ρ_f, also contributes to the determination of the fluid forces, including those of the added mass and of hydrodynamic damping (see Chapter 8). In the next chapter it will be shown moreover that ρ_f, when combined with ρ_c and c, forms two fundamental parameters for the determination of the phenomenon.

The fluid forces do not however arise from those flow characteristics alone but from their interaction with the cylinder's shape and motion;

thus the drag force acting on a static cylinder depends on V and ρ_f as well as on D, L and C_{DO}, in the expression:

$$\text{Drag} = \tfrac{1}{2}\rho_f V^2 D L C_{DO} \qquad (5.5)$$

Other fluid forces can similarly be expressed in terms of force coefficients, C_F, and consequently:

$$F = \text{function of } (V, \rho_f, D, L, C_F) \qquad (5.6)$$

where C_F is a function of flow characteristics and of the cylinder's shape and motion.

The variables, V, ρ_f and μ_f, when combined with the diameter of the cylinder, affect the phenomenon through the Reynolds Number, $R_e = VD\rho_f/\mu_f$ this in turn, when combined with the shape of the cylinder, determines the values of the Strouhal Number, S, and of the drag coefficient, C_{DO}, and consequently it determines f_s and the mean drag force of a static cylinder.

Owing to the impossibility of scaling both R_e and the dominant parameter f_s/f, most laboratory experiments on in-line vibration of cylinders immersed in water flows, are conducted in the R_e range 10^3- 10^5, where the values of C_{DO} and S are approximately constant (see Fig. 31 and 55) and consequently the importance of their relationship to R_e is not critical.

For R_e values below 10^3 both S and C_{DO} change significantly and, as explained in Chapter 4, this marked variation may be the cause of the absence of vibration reported by previous authors at low R_e values.

For R_e values greater than about 3×10^5 commonly found in prototype situations, Walshe and Wootton have reported values of $S \simeq 0.45$ for static cylinders but $S \simeq 0.2$ for cylinders vibrating across the flow direction, and Wootton et al report $S \simeq 0.22$ for cylinders vibrating in-line with the flow. As can be seen in Fig. 32 moreover, very similar cylinder responses can be obtained for R_e values as far apart as 3×10^3 and 6×10^5. Thus it can be assumed that as far as the in-line vibration phenomenon is concerned, there appears to be no significant difference between laboratory and prototype observations due to R_e.

To the knowledge of the author there are no reports available on the behaviour of the mean drag coefficient of a cylinder vibrating in-line for $R_e > 3 \times 10^5$. The similarities of the curves of Fig. 32 and the marked resemblance of the flow patterns observed in the wake of models and prototype cylinders suggest that the force coefficients are also insensitive to R_e in the range $10^5 < R_e < 10^6$. See also Chapter 8.

As explained in Chapter 4 there are other secondary factors such as blockage effects, velocity profiles, boundary layers, turbulence, etc. which also affect the values of S, although their effects are relatively minor; this also applies to the drag coefficient C_{DO}, so that: (see Chapter 9).

$$S \text{ and } C_{DO} = \text{function of } (R_e, \text{ secondary factors}) \quad (5.7)$$

These secondary factors arise mainly from the differences existing between a two-dimensional cylinder immersed in a one-dimensional approaching flow, and the three-dimensional situations encountered in practice; thus they are most relevant (a) when attempting to predict prototype behaviour from one or two-dimensional considerations, or (b) as in the present case, when trying to study the basic characteristics of in-line excitation from the observed behaviour of cylinder-flow arrangements which, even when intended to be two-dimensional, they present inevitable three-dimensional charactersitics. In general thtc modification or elimination of these secondary factors is very limited, difficult and expensive.

In previous chapters it was shown that the force coefficient C_{DA} was affected both by the parameter f_s/f and by the cylinder motion, x; thus for a vibrating cylinder:

$$C_F = \text{function of } (f_s, x, R_e, \text{ secondary factors}) \quad (5.8)$$

In the last chapter it was also shown that the complicated and often inaccurate mathematical consideration of R_e and the secondary factors, could sometimes be avoided if it were possible to measure directly the value of f_s, and to correlate it with the output of the flow velocity meter used. This direct calibration method can also be

used to obtain the values of C_{DO}, which in turn, as is the case with f_s, can be included in non-dimensional groups of variables, in this case representing flow forces, such that

$$C_F = \text{function of } (f_s, C_{DO}, x) \qquad (5.9)$$

Reynolds number effects and the influence of the other secondary factors are thus accounted for in equation 5.9 through C_{DO}. This simplification however, is not always applicable as for example (a) when comparing the excitation forces with the inertial forces of the added mass, the second of which are not affected by R_e or the secondary factors, or (b) at the design stage when a direct calibration as described above is impossible. Consequently from equations 5.6/8/9:

$$F = \text{function of } (V,\rho_f,D,L,C_{DO},x,R_e,\text{secondary factors}) \qquad (5.10)$$

5.4 Non-Dimensional Groups

Combining equations 5.1, 5.3 and 5.10 an expression is obtained which contains all the identified variables:

$$\bar{x},x_o',f,t = \text{function of } (D,L,\rho_c,k,c,V,\rho_f,R_e,S,C_{DO},\text{secondary factors}) \qquad (5.11)$$

On the basis of both previously reported experience and the observations of Chapters 3 and 4, it is possible to advantageously identify the following non-dimensional groups:

(a) $$\frac{a}{D} = \frac{2x_o'}{D}$$

(b) $$\frac{C_{DA}}{C_{DO}} = \frac{k\,\bar{x}}{\frac{1}{2}\rho_f V^2 D\,L\,C_{DO}}$$

(c) $$\frac{f}{N} = 2\pi f\sqrt{\frac{M_{TS}}{k}} = 2\pi f\sqrt{\frac{\frac{\pi}{4}D^2L(\rho_f+\rho_c)}{k}}$$

(d) $$\rho_r = \rho_c/\rho_f$$

(e) $k_s = \frac{c}{\rho_f D^2 L f}$

(f) $R_e = V D \rho_f / \mu_f$

(g) $\frac{f_s}{f} = 2S \frac{V}{fD}$

Parameters a, b and c can describe the cylinder's motion as shown in Chapter 3. If R_e is included with the remaining secondary factors, the following expression is obtained:

$$\text{Cylinder motion} = \text{function of } \left(\frac{a}{D}, \frac{f}{N}, \frac{C_{DA}}{C_{DO}}\right) = \text{function of } \left(\rho_r, k_s, \frac{f_s}{f}, \text{ Secondary factors}\right) \quad (5.12)$$

(f_s/f) was the subject of the previous chapter, ρ_r and k_s are the subject of Chapter 6.

CHAPTER 6

DENSITY AND DAMPING

In this chapter two important parameters, density and damping, are dealt with in detail. The role of density in determining ranges of vibration frequency, and consequently the (V/ND) ranges for instability, is presented first and then correlations and predictions of these frequencies are put forward.

After a brief consideration of the influence of damping on both (f/N) and (a/D), it is concluded that density and damping, in contrast with aerodynamic practice, should here be considered separately. There follows a discussion of the various ways previously used to deal with damping which concludes with a definition of a parameter to describe the external damping of the cylinder. External damping is then correlated with both (a/D) and the (f_s/f) ranges, thus rendering possible their prediction for two-dimensional cases. A general discussion closes the chapter.

6.1 Density

During the tests conducted with the larger cylinder (D = 3.38 cm) it was observed that the ranges of variation of both (f/N) and V were modified by changes of the cylinder density (see Fig. 28) and so it was decided to conduct a systematic study of the influence that the density of the cylinder exerted upon its motion. For this purpose the two cylinders used were provided with removable ends so that they could be variously weighted internally so as to change their density. Tests were conducted with a total of seven different densities ranging from $\rho_r \simeq 0.5$ to $\rho_r \simeq 4.4$, where ρ_r is the ratio of the effective mass of the vibrating system (or of its effective density, ρ_c) to the mass displaced by the cylinder (or the fluid density, ρ_f), i.e. $\rho_r = \rho_c/\rho_f$. The values of ρ_r were calculated before and after each test from repeated transients of the cylinder alone or with known additional weights, in air and in water; additional factors such as gravity and buoyancy forces, mass and added mass of the supports, the influence of gaps between cylinder and end plates, etc., were taken into consideration. (See Appendix III).

6.1.1 Frequency ranges

Fig. 34 presents vibration frequency variations with (f_s/f) for the tests of Fig. 28 which were conducted with three different values of ρ_r. The most important features of this figure are firstly that all the curves have similar shape, with the lighter cylinders reaching higher frequencies (f/N), and secondly that the maximum values of f, which occur at the end of the second instability region tend towards the value of the natural frequency of the same cylinder when oscillating in vacuo (N_v).

The implications of the first observation are that (f/N) is a function of f_s/f and either ρ_c or ρ_r and that, owing to the similarity of the various curves, it should be possible to represent them all by a single function. To make the implications of the second observation more explicit, the frequency N_v, in its non-dimensional form N_v/N, can be expressed in terms of stiffness and densities as follows: (see Chapter 7)

$$\left.\frac{f}{N}\right|_{1im} \rightarrow \frac{N_v}{N} = \frac{\frac{1}{2\pi}\sqrt{\frac{k}{\rho_c \ \text{Volume}}}}{\frac{1}{2\pi}\sqrt{\frac{k}{(\rho_c+\rho_f)\ \text{Volume}}}} = \sqrt{\frac{\rho_c + \rho_f}{\rho_c}}$$

$$= \sqrt{\frac{\rho_r + 1}{\rho_r}} \qquad (6.1)$$

i.e. (N_v/N) is a function of ρ_r alone.

This conclusion is compatible with the first observation mentioned above provided (f/N) is a function of ρ_r rather than ρ_c. The absence of the parameter (f_s/f) in Equation 6.1 can be explained by the fact that these limiting frequency values were reached at the end of the second instability region only when they all tended towards a constant value of $(f_s/f) = \sqrt{2}$ (see Chapter 4).

Equation 6.1 moreover suggests an explanation for the very slight and often neglected frequency variations reported in aerodynamic researches on oscillating cylinders where ρ_r is relatively much larger owing to the comparatively small air density.

It was shown in Chapter 3 that the frequency, f, was larger than or equal to the frequency, N, in the two instability regions,

except for the "double harmonic excitation section" of the first instability region where the slight variations of f, below the value of N, were negligible; the limits of frequency variation can therefore be set as:

$$1 \lesssim \frac{f}{N} < \sqrt{\frac{\rho_r + 1}{\rho_r}}$$

On this basis Fig. 35 was plotted in terms of the upper limiting values of (f/N) achieved by cylinders of varying ρ_r. It appears from the small scatter of Fig. 35 that $f/N\Big|_{lim}$ is indeed uniquely determined by ρ_r.

The figure also shows that although only negligible frequency variations can be expected in most aerodynamic situations (say <5%, for $\rho_r > 10$), in water and especially under laboratory conditions, very large frequency variations can be achieved (i.e. $1 < f/N < 2$, for $\rho_r = 0.33$); in practical hydrodynamic engineering situations, ρ_r values between 2 and 1 and frequency variations between $1 < f/N < 1.2$ and $1 < f/N < 1.4$ would be typical.

6.1.2 Flow velocity ranges

When the instability regions have been defined in terms of f_s/f (see Chapter 4), the ranges of frequency variation permit the definition of such regions in terms of the flow velocity, because

$$\frac{f_s}{f} \times \frac{f}{N} = \frac{f_s}{N} = 2S \frac{V}{ND} \qquad (6.1a)$$

On the basis of equation 6.1 and on the assumptions that $f > N$, and that $0.5 < f_s/f < \sqrt{2}$ (see Chapter 4), Fig. 36 thus presents the maximum flow velocity ranges where vibration can occur in the form $(f_s/N) = (2S\,V/ND)$ and as a function of ρ_r alone. If the relationship between f_s and V (or S and R_e) is known, the stability diagram of Fig. 36 gives the ranges of V.

The upper limit of the instability region of in-line vibration shown in Fig. 36 is evidently a function of ρ_r and it should be noted that for neutrally buoyant or lighter cylinders and when the natural frequencies in-line and cross-flow are similar, a mixed type of motion in the two directions is possible. This provides an explanation for

the previously reported extension of the cross-flow instability region below (V/ND) = 5 for light cylinders (see e.g. King). For the heavier cylinders it can be seen in the figure that the upper limit of (f_s/N) tends towards $\sqrt{2}$.

Even though Fig. 36 is modified somewhat by damping and other factors as will be shown later, it should nevertheless be helpful to designers because it shows that self-excited vibration can be avoided if

$$\frac{f_s}{N} = 2S\frac{V}{ND} < 0.5$$

i.e. the still water natural frequency, N, of a pile should be designed such that:

$$N > 4\frac{SV}{D}$$

When damping or other factors reduce the instability regions of (f_s/f), a detailed relationship between (f/N) and (f_s/f) is necessary in order to determine the precise instability regions in terms of (f_s/N) or V.

6.1.3 Frequency response in the first instability region

The frequency response in the first instability region is illustrated in Figs. 34 and 37.

Figure 34 shows higher (f/N) values corresponding to lower ρ_r for a given (f_s/f); this explains the increased overlap of the two instability regions of in-line vibration for lighter cylinders shown in Fig. 3. (See equation 6.1a).

Fig. 37 represents several tests conducted with the same values of ρ_r but with different levels of external damping; in this figure the curves in the first instability region do not collapse on a single curve as successfully as those for the second instability region. It seems likely that the trends shown in the figure, which appear to reflect the changing vibration amplitude as the structural damping is varied, are the result of the complex mechanism of excitation discussed

in Chapter 3. This conclusion is prompted by the observation that corresponding plots of frequency collapsed more successfully when the cylinder was fitted with a splitter plate to eliminate one source of excitation (see Fig. 38).

6.1.4 Frequency response in the second instability region

The (f/N) vs (f_s/f) relationship of the second instability region shown in Fig. 34 appears to be a family of straight lines with a common origin at (f/N) = (f_s/f) = 1.0, and this, together with equation 6.1 suggests the following expression:

$$\frac{f}{N} = m\frac{f_s}{f} - (m - 1) \qquad (6.2)$$

where

$$m = \frac{\sqrt{\frac{\rho_r+1}{\rho_r}} - 1}{\left(\frac{f_s}{f}\right)_{maximum} - 1}$$

Assuming:

$$(f_s/f)_{maximum} = \sqrt{2}$$

$$m = \frac{\sqrt{\frac{\rho_r+1}{\rho_r}} - 1}{\sqrt{2} - 1} \qquad (6.3)$$

If, for example, $\rho_r = 1$, Eqn. 6.3 suggests that m = 1 and (f/N) = (f_s/f), i.e.: the departure of f from N is equal to its departure from f_s, as shown in Fig. 40.

It should be noted that in the second instability region the cylinder and the eddies of the wake have a common locked-in frequency $f = f_e$, which reaches a compromise between the "natural frequencies" of both cylinder (N) and wake (f_s) when the densities of cylinder and fluid are equal; otherwise this common frequency $f = f_e$ will approach N for the heavier cylinders ($m < 1$) and f_s for the lighter cylinders ($m > 1$). The case where $m = 1, (\rho_r = 1)$ can thus be regarded as a special or "natural" case.

Fig. 39 presents experimental frequency variations from tests on the two cylinders with varying ρ_r in comparison with equations 6.2 and 6.3

Although the agreement is in general satisfactory extrapolation to maxima of (f/N) results in values slightly smaller than those of equation 6.1; this shortfall was probably due to a reduction of the exciting forces caused by boundary layers and other factors. (See 6.3 and Chapter 9). The greatest deviation of the experimental results from equation 6.2 occurs near the commencement of the second instability region just beyond $(f_s/f) = 1.0$. The discrepancy here can perhaps be attributed to the practical difficulties of measuring small frequency variations and amplitudes of motion when beats are present and when the unsteadyness of the incoming flow is important. This wider scatter however does not modify the ranges of f/N or the upper limit of the instability region and it can therefore be said that the semiempirical relationship of equation 6.2 constitutes a satisfactory description of the frequency response in the second instability region for practical purposes. In Chapter 8 however, an improvement to the relationship of equation 6.2 will be made after considering the hydrodynamic forces.

6.2 Damping

6.2.1 The separate roles of density and damping

Following aerodynamic practice and mainly to facilitate the modelling process the influences of density and damping have been treated in combination by previous researchers (e.g. King) and represented by the combined stability parameter:

$$k'_s = \frac{2M\delta}{\rho_f D^2 L}$$

where M is the vibrating mass and δ is the logarithmic decrement of the transient vibration of M due to damping. Kolkman (see King) suggests moreover that the correct *separate* scaling of density and damping is not important provided that the discrepancy for each is not more than 200% and provided that the combined parameter is correctly scaled.

This approach seems to be incompatible with the observations of the previous section of this chapter, where it has been argued that ρ_r is the only parameter besides (f_s/f) which determines the frequency response, and consequently there may be any number of different

frequency responses corresponding to the same value of the combined parameter k'_s. It follows from this that density and damping must affect the behaviour of the cylinder in different and separate ways.

The most likely explanation for this divergence between aerodynamic and hydrodynamic treatment is the very large difference that exists between the densities of air and of water, and the consequently negligible frequency variations observed for the former in comparison with the latter.

In order to confirm the independent role played by the two variables density and damping, it was decided to conduct experiments where each variable was changed systematically and independently. For this purpose a viscous damping mechanism was devised, as shown in Fig. 5, for purposes of increasing the external damping of the cylinders.

The variations of (f/N) with respect to (f_s/f) observed in these systematic tests are presented in Figs. 37 and 38. In Fig. 37a, ρ_r was held constant at an approximate value of 1.2 for five different levels of damping while Fig. 38a presents similar test results for the cylinder when fitted with a splitter plate. For the results shown in Figs. 37b and 38b the conditions were approximately the same except for an increased density $\rho_r \simeq 4.4$.

These figures show that the variations of frequency are not appreciably affected by changes in the external damping either in the second instability region or when the cylinder is fitted with a splitter plate, i.e. when either of the two main excitation mechanisms acts on its own. Although some slight frequency variations can be identified in the first instability region, corresponding to changes of damping, these variations can be attributed to the complex interaction between the two prevailing excitation mechanisms and the behaviour of the cylinder, and should therefore be considered separately (see Chapter 8).

Previous researches (e.g. King, Dickens) have shown that the amplitude of flow induced in-line vibrations decreases with increasing levels of damping. This is confirmed by Figs. 41 and 42 which show the amplitude response for different levels of external damping corresponding to the tests of Figs. 37 and 38 respectively. Fig. 43 moreover reproduces curve 3 of Fig. 41a and curve 2 of Fig. 41b and thus provides a comparison of vibration amplitudes of two cylinders with

similar external damping but with considerably different densities; it is clear from this figure that ρ_r has no significant influence on the vibration amplitudes.

It was concluded therefore that density and damping have different and independent effects on the motion of the cylinder, the former primarily affecting its frequency and the latter primarily affecting its amplitude, and that density and damping should henceforth be considered separately.

6.2.2 Definition of damping

Because of the many types and sources of damping involved in the field of flow-induced vibrations of structures, a precise and appropriate definition of damping is necessary to avoid incompatibilities and apparent contradictions with previously published data and also to facilitate useful comparisons.

Damping forces are here understood to be those through which the vibrating cylinder dissipates energy, i.e. those forces acting in antiphase with the cylinder's oscillating velocity, $\dot{x}$.

Damping can be classified according to sources as follows:

(a) Structural damping of the supports of the cylinder or of the cylinder itself in flexure under fluid action.

(b) Damping provided by artificial or mechanical dampers.

(c) Hydrodynamic damping of the supporting arms, end plates, etc. and in the gaps between cylinder and end plates.

(d) Hydrodynamic normal and shear forces.

(e) Inefficiency of the excitation flow forces, due to boundary layers, turbulence, uncorrelated flow patterns, etc.

In a steady state vibration the addition of the damping forces arising from all these sources must necessarily be equal and opposite to the excitation forces. For a self-excited cylinder it is impossible to measure either the excitation forces or the hydrodynamic damping forces directly, because the cylinder experiences only the net force. The only damping which can be estimated with any certitude is therefore the damping from external sources (e.g. structural) which can be measured in independent experiments.

It is intended in the present research moreover to study the characteristics of a *generalised* model of flow-induced in-line vibrations, which can then be adapted to specific situations.

It was therefore necessary to separate the measurable damping arising from the "external" sources which can vary from case to case (a,b,c & e, above) from the "internal" hydrodynamic damping (d, above) which was an integral part of the excitation mechanisms studied and which could not be directly measured.

The similarities presented by reports of widely differing cases of in-line vibration, and curves such as those of Figs. 41 and 42 suggest a self-regulating excitation process with invariant basic characteristics, which is influenced by the amount of energy extracted by external sources of damping.

What follows is a more detailed study of the influence of external damping on such an excitation process as reflected by the cylinder behaviour.

6.2.3 Damping parameter

It is intended in this section to find a suitable parameter for the representation of external damping which is independent of the relative density, ρ_r.

The four parameters most commonly used to represent damping are: (a) the viscous damping constant, c; (b) the hysteretic damping parameter G; (c) the logarithmic decrement, δ; and (d) the stability parameter, k_s'. Any of these parameters can have constant values when (f/N), (a/D), the stiffness, k, and the total mass of the cylinder, M_T (including the added mass), remain sensibly constant. This is not so in the present case however, and consequently each parameter will be discussed in turn.

(a) The viscous damping constant, c, is the simplest mathematical representation of damping. It expresses the damping forces per unit velocity, $\dot{x}$, and consequently it has the disadvantage of being dimensional; c is a constant for viscous damping only, as is the case with the damping mechanism devised for the present research, but structural damping on the other hand is a function of the frequency and amplitude of vibration together with structural stiffness, and

consequently c would have to be a variable to represent damping in this case. It should be noted however that c contains no information about the fluid or the cylinder's geometry and it is therefore not suitable for a generalized representation of this interactive process.

(b) The hysteretic damping parameter, G, is non-dimensional and more appropriate to represent structural damping although it is mathematically more complicated. The parameter G represents the ratio of the damping forces to the stiffness forces, i.e., it is a structural parameter containing no information about the fluid and is therefore inappropriate for the present purposes.

In cases where $f \simeq N \simeq$ constant (i.e. heavy cylinders) the stiffness forces are approximately equal in magnitude to the inertial forces of both cylinder and added mass, and consequently, if the variations of G with (a/D) can also be neglected and if most of the external damping is structural, this parameter can remain nearly constant and can therefore be useful.

In the present research however, G was observed to vary both with (f/N) and (a/D) (see Appendix V), and it was clearly unsuitable to represent the additional viscous damping applied by the damping device.

(c) The logarithmic decrement, δ, is defined as the natural logarithm of the ratio of the amplitudes of two consecutive cycles of a decaying transient.

When the vibration frequency is equal to the natural frequency of the system, δ represents the ratio of the damping forces to the inertial forces (including the added mass if any), i.e.

$$\delta = \pi \frac{c\omega_n x_o}{M_{TS}\omega_n^2 x_o} = \frac{2}{\pi} \frac{c}{\rho_f D^2 L N (\rho_r + 1)} \qquad (6.4)$$

Although δ includes information of the fluid, it also includes the parameter ρ_r, and is therefore unsuitable for the representation of damping independent of relative density.

The non-dimensional parameter, δ, is easy to measure and consequently widely used.

In the present research δ could not be estimated from transients

in still water because of the difficulties of either deducing the hydrodynamic damping of flowing water measurements (see Chapter 7), or accurately estimating the still water damping to calculate the structural damping.

Values of δ obtained from transients in air on the other hand can be used provided that aerodynamic damping be estimated and discounted from the total and provided also that (i) f is a constant, or (ii) c is a constant, or (iii) damping is hysteretic and there are no excitation forces which can modify the frequency (i.e. (f/N) = 1). In cases where as in the present research none of the requirements (i) to (iii) above are met, values of δ measured from transients in air can only be used to calculate c, G or k_s.

(d) The non-dimensional stability parameter, k_s', has been widely used in previous work concerned with flow induced vibrations in both air and water, to correlate damping with vibration amplitudes and to determine instability regions.

Vickery and Watkins present the stability parameter:

$$k_s' = \frac{2M\delta}{\rho_f D^2 L} \qquad (6.5)$$

as a combination of two parameters namely, a mass ratio $(M/\rho_f D^2 L)$, and a damping parameter, δ.

This interpretation of k_s' suggests that heavier cylinders should have a higher value of k_s' and consequently they should vibrate with lower amplitudes (see e.g. King).

If k_s' is expressed in terms of c rather than δ however, from $\delta = c/2MN$ it follows that:

$$k_s' = \frac{c}{\rho_f D^2 L N} \qquad (6.6)$$

i.e. k_s' is *independent* of the density of the cylinder. Fig. 43 moreover shows approximately equal values of (a/D) corresponding to cylinders with equal values of the stability parameter but for widely differing cylinder densities.

The stability parameter expressed in terms of c can therefore

be seen not as a combination of a mass ratio and a damping parameter, but rather as the ratio (multiplied by $\pi^2/2$) of the external damping forces ($c\omega x_o$) to the inertial forces of the *added mass alone* ($M_{as}\omega^2 x_o$). It should be noted that this definition is only valid if the "mass coefficient" is constant and equal to one (see Chapter 7), and if the frequency N of Eqn. 6.6 is replaced by f to account for frequency variations. The stability parameter k_s, results thus:

$$k_s = k_s' \frac{N}{f} = \frac{c}{\rho_f D^2 L f} \qquad (6.7)$$

The parameter k_s will be adopted here because (a) it is non-dimensional, (b) it is independent of ρ_r and (c) it relates external damping to characteristics of the flow.

Although it can be seen in equation 6.7 that k_s is independent of ρ_r, it should be noted that in specific cases the density of the cylinder can affect k_s *indirectly*. This occurs when frequency variations are significant because ρ_r influences (f/N) which in turn, and depending on the value of N, influences: (a) the value of f and consequently from equation 6.7 the value of k_s, or (b) the value of c and consequently k_s when the hysteretic damping is important. Confusion can arise moreover if changes of k_s are attributed to ρ_r when the mass of the cylinder is increased but N is kep constant or increased; in this specific case the increases of k_s arise from the increase of c that accompanies the necessary stiffening of the supports of the cylinder; this increase of c however as well as the value of N and the hysteretic nature of damping mentioned in (a) and (b) above, are all dependent on *structual* characteristics of a *specific* cylinder arrangement, and are not *directly* related to the *general* characteristics of the interaction between cylinder and flow which are the concern of this work. Thus it was felt that k_s was most appropriate for a general representation of the independent influence of external damping on the excitation process.

It should be noted that k_s' is constant only when c is a constant (viscous damping), and that for k_s to be constant, the ratio c/f has to be invariant rather than the more usual hysteretic condition where cf is constant.

The parameter k_s can also be expressed in terms of G; in the

present case however, it was expressed in terms of c owing to the complex nature of the damping used and to avoid further mathematical complications.

Although the viscous part of c could be maintained constant for a given test, the structural part of c was observed to vary with both (f/N) and (a/D), and several additional experiments had to be conducted to investigate these variations for each cylinder arrangement and for each test as follows: (see also Appendix V).

For a given test the length of the cantilevered springs of the cylinder supports were fixed and the viscous damping device was adjusted as needed; the cylinder was then made to oscillate in air with various additional known masses attached to it so as to cover the frequency range expected for that test; damping was measured for various amplitudes of vibration from the decay of the resulting recorded transients, and correlations were obtained of c against (a/D) and (f/N). Aerodynamic damping and damping due to the supporting arms, gaps, etc. were also taken into account (see Appendix V). In this manner, values of k_s were calculated for every vibration condition from knowledge of the appropriate values of (a/D) and (f/N).

To simplify the presentation and analysis of data a standardized, constant value of k'_s was also obtained for each test, for (a/D) = 0.055 and for f = N, which is here denominated k'_{so}. The variations of k_s with respect to k'_{so} occurring in a typical test are plotted against (f_s/f) in Fig. 44.

6.2.4 Vibration amplitude

Vibration amplitude reductions corresponding to increases of k'_{so} are shown in Figs. 41 and 42. Fig. 44 shows however that (k_s/k'_{so}) can vary as much as 27%*, and consequently the plots of Figs. 41 and 42 are not constant damping curves. The use of k_s instead of a constant stability parameter allowed important observations and conclusions as indicated below:

Variations of (a/D) with respect to k_s, for various values of (f_s/f) in the first and second instability regions are presented in Figs. 45a and 45b respectively; the data correspond to the five tests of Figs. 37a and 41a conducted with approximately the same ρ_r value but for five different levels of external damping.

---

* Fig. 44 refers to a cylinder with $\rho_r \simeq 1.2$; variations of more than 50% were calculated for the lightest cylinders tested.

Fig. 45b shows a distinct trend in the second instability region, towards a common maximum value of (a/D) as k_s tends to zero, for all values of f_s/f. This indicates that in the undamped condition the amplitude response curve for the second instability region has a flat top; slight deviations from this occurring as k_s increases.

It should be noted that this trend was deduced previously from observation of the amplitude response curves presented in Chapter 3, although a slight increase of (a/D) was also observed as (f_s/f) increased (see e.g. Figs. 28 and 29); this slight increase of (a/D) however can be attributed to decreases of k_s which are due to increasing (f/N). These observations permitted the approximate assumption that (a/D) is invariant in the second instability region when k_s is constant, which assumption greatly simplifies the mathematical representation of the excitation process, as will be shown in Chapter 8.

Although the common trend shown in Fig. 45b is not apparent from the curves of Fig. 45a for the first instability region, the curves of this figure appear to have similar shapes. Indeed if the data of figure 45a are replotted (Fig. 46) as a propotion of the maxima obtained from Fig. 45a by extrapolation to $k_s = 0$, a common trend *is* apparent in the response of (a/D) to k_s for most values of (f_s/f).

These trends permit an extrapolation to the undamped condition ($k_s = 0$), to predict maximum vibration amplitudes for each value of f_s/f in the first instability region or for all values of (f_s/f) in the second. Such maxima are plotted in Fig. 47 as a function of f_s/f and they represent the amplitude response of an undamped cylinder.

It was then concluded from Figs. 45b and 46 that the vibration amplitudes for a given (f_s/f) value in either instability region, decreased from their maxima corresponding to the undamped condition (Fig. 47) according to a function of k_s alone; this function was approximately the same for all (f_s/f) values in each instability region.

From the above observations and conclusion it follows that the maximum amplitude of vibration in the first instability region should occur at a fixed value of (f_s/f), if the cylinder were subjected to a constant external damping k_s; Fig. 41 suggests moreover that this value is about 0.9, although this is only a limited approximation because such maxima are slightly displaced along the f_s/f axis by the variations

of k_s along each curve, by the instabilities of the excitation and by the hysteresis phenomena.

If the maxima of (a/D) in the first instability region for different tests are nevertheless assumed to occur when (f_s/f) has the same value, the trends of (a/D) vs k_s referred to above are further confirmed by Figs. 48a and 48b; these figures are plots of the maximum amplitudes recorded for each of the two instability regions and they include all the tests for which damping data were available.

Exceptions to these common trends of (a/D) vs k_s can be seen in Figs. 45 to occur at the extremes of both instability regions where double harmonic excitation, beats or hysteresis occur.

In agreement with reports by King the reductions of (a/D) due to damping here observed were different in the two instability regions, especially if amplitudes (a/D) smaller than 5% were considered. Although the (a/D) vs k_s curves in both instability regions showed a discontinuity for $k_s \simeq 0.6$ (Fig. 45), for higher levels of damping (k_s) the values of (a/D) in the first instability region could be as high as 4% while those in the second were negligible. Nevertheless, if vibration amplitudes smaller than 4% can be neglected, the common value of $k_s \simeq 0.6$ where the said discontinuities occur indicates an approximate practical threshold for in-line instability.

No systematic tests were conducted for k_s values higher than 0.7, because it was felt that the corresponding vibrations with amplitudes (a/D) < 4% were not very important. It should be noted however, that when conducting auxiliary tests to investigate S and C_{DO}, (a/D) was smaller than 1% for values of $k_s > 1.2$.

Finally it should be noted that the expression of k_s in terms of c (Eqn. 6.7) rather than δ (Eqn. 6.5), together with the threshold value of k_s identified above, clearly indicate that in-line vibrations in practice are more likely to arise from hydrodynamic excitation, when the large ρ_f yields a low k_s, rather than from aerodynamic excitation.

6.2.5 Instability regions

Figure 41 shows reductions of the ranges of (f_s/f) in which instability occurs, corresponding to increases of the external damping parameter k'_{so}.

As explained in 6.2.4 these plots are not constant damping curves because of the variations of (k_s/k'_{so}) with (f_s/f) (e.g. Fig. 44), and are therefore unsuitable for further quantitative analysis. Fig. 49 however, presents these (f_s/f) instability ranges as a function of k_s; the figure was obtained by calculating the k_s values corresponding to the maximum and minimum values of (f_s/f) for which vibration was recorded, in each instability region and for each one of the tests of Figs. 37 and 41 as well as for two additional tests (see Table II-2).

At the threshold of instability in Fig. 49 values of k_s of about 0.6 and 0.65 can be identified for the first and the second instability regions respectively, if amplitudes smaller than 0.05 can be ignored. The instability regions shrink with increasing external damping, about their respective "central" values of (f_s/f) in an approximately symmetrical shape. An exception to this occurs for the lowest values of (f_s/f) where the double harmonic excitation mechanism is operative. A slight trend of the instability regions of the heavier cylinders to be narrower can also be seen in this figure; this narrowing arises perhaps because it is more difficult for a heavier cylinder to respond to the excitation at the extremes of the instability regions where hysteresis effects occur and where the excitation mechanism tends to break down.

Figure 49 together with the relationships between (f/N) and (f_s/f) (equation 6.2) and between f_s and V (e.g. Fig. 31) determine the ranges of flow velocity for which instability occurs. Such velocity ranges are influenced by both ρ_r and k_s, although in different ways, i.e. ρ_r affects the (f/N) ranges but not the (f_s/f) ranges, while the converse applies to k_s. As explained in 6.2.3 however, in cases where frequency variations are significant, ρ_r can affect the (f_s/f) ranges indirectly via modifying f, which not only changes k_s directly but it can also affect c and consequently k_s and the (f_s/f) ranges.

In contrast with aerodynamic situations where the flow velocity ranges for instability often depend on the stability parameter alone, Table 6.1 below shows that in hydrodynamic situations a higher maximum value of (V/ND) can be reached with a lighter cylinder (lower ρ_r), in spite of its higher value of the stability parameter (k'_{so} or k_s), although it can be seen in the same table that the maximum value of f_s/f for this lighter cylinder is in fact lower than that for the heavier cylinder.

It was thus concluded that the *possibility* of vibration is

Run No.	maximum values of: V/ND	f_s/f	f/N	ρ_r	k_s approx.	k'_{so}
80	3.59	1.367	1.083	4.22	0.26	0.275
102	4.08	1.346	1.254	1.21	0.49	0.502

Table 6.1 Comparison of Experimental Results

determined by the stability parameter k_s, while the *flow velocity ranges* in which instability can occur are also influenced by ρ_r. On the other hand the stability parameter k_s determines the vibration amplitudes while ρ_r determines the frequency variations. These dependence relationships and the indirect influences of ρ_r on k_s referred to in 6.2.3 are illustrated in Fig. 50.

6.3 Discussion of Results

6.3.1 Efficiency of excitation forces

The hydrodynamic damping and excitation forces can be reduced by factors such as boundary layers, badly correlated flow patterns along the cylinder's length and turbulence. This provides an explanation for the differences existing between the maximum values of (f/N) and (f_s/f) obtained from an extrapolation of the recorded data to the undamped condition on the one hand, and the respective theoretical values $[\sqrt{(\rho_r+1)/\rho_r}]$ and $\sqrt{2}$ on the other. (Figs. 39 and 49).

The vibration amplitudes are determined by the balance between hydrodynamic excitation forces and the (predominantly hydrodynamic) damping forces (see Chapter 7) and consequently are also affected by the boundary layers etc. as mentioned above. Because of the influence of these factors on both excitation and damping it is not feasible merely to apply some increment to k_s to obtain a representative damping parameter and it is therefore more difficult to estimate maximum amplitudes.

A case illustrating the influence of the factors mentioned above is shown in Fig. 41b where the (a/D) curves 1 and 3 overlap with curves 2 and 4 in the second instability region; this overlapping occurs because

of discontinuities seen in the flow patterns of the wake (see 3.5) for the tests of curves 1 and 3. This situation should be compared with the uniformly spaced curves of Fig. 41a, where special care was taken in the tests to maintain well correlated flow patterns in the wake, throughout the second instability region.

A comparison of Fig. 41b with Fig. 37b shows moreover, that the relatively lower points of the (f/N) vs (f_s/f) curves correspond to the relatively low amplitudes occurring in association with the observed discontinuities in the wake.

6.3.2 Comparison of results

The possibilities of quantitatively comparing the results of the present research with previously published data are severely limited by complexity and differences in presentation, incomplete data and diversity of situations. Qualitative comparisons however are possible as shown below.

Frequency variations have been reported by Clark, Dickens and Wootton[2] for two and three-dimensional situations. From the data of Dickens it is clear moreover that higher (f/N) values correspond to lower ρ_r values, although this information is limited to the first instability region and often strongly influenced by hydrodynamic damping. King neglects the frequency variations of his cantilvered cylinders, although his Fig.9.8(b) shows (f/N) vs (V/ND) trends which are similar to those here observed. The frequency variations reported by Wootton[2] are more significant because they occurred in a full-scale three-dimensional situation.

Although similar vibration amplitude curves have been presented in all in-line vibration reports, little information on damping has been presented. King and Dickens extrapolate hydrodynamic damping from still water transients to flowing water steady-state conditions. The values of "k_s" so obtained by King moreover, do not always correlate with the amplitudes (presented as bending moments) of his cantilevered cylinders oscillating in-line.

Dickens bases his analysis and complex stability parameters on hydrodynamic damping, which is here not considered part of external damping. The (a/D) vs k_s curves here presented however, resemble

those obtained by Wootton from tests of free-ended model stacks oscillating across the flow in a wind tunnel; the similarities of the curves in spite of the great disimilarities of the two situations can be attributed to the negligible effects of both the aerodynamic damping and the added mass of air, relative to the respective structural damping and cylinder mass. These conditions in this aerodynamic case made the constant k_s extrapolated from still air tests, more appropriate to represent the stability of the system.

In addition to the need for damping data, a comparison of (f_s/f) ranges is possible only if either precise S or f_s are known. Dickens and Clark do not report their S values; while King, Hardwick and Wootton, and Wootton et al do not provide sufficient damping data for a more meaningful comparison of the (f_s/f) ranges than that of the curves of Fig. 32. The base bending moment vs (V/ND) curves presented by King however, show a general reduction of the (f_s/f) ranges corresponding to decreasing bending moment responses, and thus presumably corresponding also to decreasing vibration amplitudes; his work is thus in agreement with the trends presented in Figs. 41. It should be noted moreoever that the comparison of (f_s/f) ranges of different cylinder-flow arrangements is complicated by the vibration amplitudes which, in three-dimensional situations, change with the cylinder's length, and which when combined with hysteresis phenomena, beats or double harmonic excitation, may further modify the limiting values of f_s/f for the two instability regions.

6.3.3 Practical considerations

The analysis presented in this chapter suggests that it should be possible to predict the dynamic behaviour of a cylinder in a two-dimensional arrangement oscillating in the direction of the flow in terms of (a/D), (f/N) and (f_s/f) from knowledge of ρ_r and k_s.

The parameters ρ_r and k_s as interpreted here could be more readily determined at the design stage than the "combined stability parameter" which depends on hydrodynamic damping and which does not provide reliable predictions of (a/D), (f/N) or of the ranges of (f_s/f).

When damping data are to be obtained from transients in still or in slowly flowing water $(f_s/f < \frac{1}{2})$ however, it becomes necessary to calculate the appropriate hydrodynamic damping. For still water

situations, the researches of Bramley and of King provide useful information. For slowly running water there is, to the knowledge of the author, no reliable method to calculate the hydrodynamic damping which depends not only on the reduced velocity but it also depends markedly on vibration amplitudes (see Chapter 8).

When dealing with the three-dimensional situations more often encountered in practice, the data here presented cannot in general be used directly, although the curves of Fig. 32 and the data of the full-scale tests at Immingham provided by Wootton[2] indicate that very similar variations of (f/N) and ranges of (f_s/f) result in both two and three-dimensional situations. Prediction of the variable amplitudes of a three-dimensional cylinder can only be made after considering flow forces and energy exchanges along the cylinder's length. (See remaining chapters).

Nevertheless, the analysis here conducted for two-dimensional situations identifies causes of cylinder behaviour and results in successful correlations of this behaviour with flow and cylinder parameters; this approach could perhaps be adapted to the more practical three-dimensional situations.

Especially important from a practical point of view is the confirmation of ($f_s/f = \frac{1}{2}$) as a lower limit for excitation, which arises from the following observations: (a) no vibrations in-line have been reported for (f_s/f) < 0.5 *; (b) increases of both ρ_r and k_s tend to increase this threshold value; (c) this limiting value has been approached only by extremely light and lightly damped cylinders which are not common in practice; (d) suppression of the double harmonic excitation increases this limit; and (e) although f values have been recorded which are slightly smaller than N and which reduce the flow velocity threshold value below (f_s/N) = $\frac{1}{2}$, these departures are not considered to be of practical importance.

* This assumes that curve 1 of Fig. 32 represents average values of a variable f_s/f (see Chapter 9).

CHAPTER 7

HYDRODYNAMIC FORCES

A simple theoretical model is presented in section 7.1 which permits the analysis of the hydrodynamic forces of the added mass and damping in sections 7.2 and 7.3 respectively. A constant mass coefficient is adopted and it is concluded that hydrodynamic damping cannot be extrapolated from still water tests because it depends on the mean drag forces of flowing water.

Section 7.4.1 then considers all the hydrodynamic forces leading to a theoretical model of the excitation. Sections 7.4.2 and 7.4.3 support the validity of this model to represent the two main excitation mechanisms, with a brief analysis of the flow patterns observed in association with the hydrodynamic forces predicted by the model.

7.1 Analysis of Forces

Newton's Second Law can be used to relate the total hydrodynamic forces, F_T, to the cylinder's characteristics and motion (see Chapter 5), thus:

$$F_T = M_c \ddot{x} + c \dot{x} + k x \qquad (7.1)$$

where M_c, c and k represent respectively mass, external damping and stiffness of the cylinder and its supports and x, $\dot{x}$ and $\ddot{x}$ represent respectively the displacement, velocity and acceleration of the cylinder with respect to its supports. Most of the ultra-violet recorder traces of the cylinder's displacement, x, were sinusoidal and consequently the cylinder's motion can be represented by:

$$x = \bar{x} + x_o \sin \omega t \qquad (7.2)$$

where $\bar{x}$ is the mean displacement, $\omega = 2\pi f$, and x_o is the amplitude of the vibration. The sinusoidal motion of the cylinder indicates that the excitation forces are either very small or are themselves

sinusoidal functions. It was observed in Chapter 3 moreover that events in the wake near the cylinder occurred periodically with the same frequency, f, of the vibration. Thus the total hydrodynamic forces can be represented by:

$$F_T = \overline{F} + F'_{To} \sin(\omega t + \zeta) \tag{7.3}$$

where $$\overline{F} = k\overline{x} \tag{7.3a}$$

is the mean force; F'_{To} is the amplitude of the fluctuating component, F'_T; and ζ is the phase angle between F'_{To} and x_o. Equations 7.2 and 7.3 represent a solution for equation 7.1 (see Den Hartog) which then describes the motion of a cylinder oscillating in vacuo and acted upon by the addition of all the hydrodynamic forces, F_T. Figure 51 illustrates the forces of Eqn. 7.1 vectorially; it can be shown from a resolution of the forces parallel and at right angles to x_o that: (see Appendix VII)

$$F'_{To} = k\, x_o \sqrt{\left[1 - \left(\frac{f}{N_v}\right)^2\right]^2 + \left[\frac{c}{2\pi M_c N_v}\left(\frac{f}{N_v}\right)\right]^2} \tag{7.4}$$

$$\tan \zeta = \frac{c\,\frac{f}{N_v}}{2\pi M_c N_v\left[1 - \left(\frac{f}{N_v}\right)^2\right]} \tag{7.5}$$

where N_v is the natural frequency of the cylinder oscillating in vacuo, i.e.:

$$N_v = \frac{1}{2\pi}\sqrt{\frac{k}{M_c}} \tag{7.6}$$

It was observed in Chapter 5 that the hydrodynamic forces depended not only on flow characteristics, but also on an interaction between the motion of the cylinder and the flow patterns which result in self excited vibration. In Chapter 6 it was shown that the excitation mechanisms responded to changes of both ρ_r and k_s; while both external damping and cylinder density are indeed characteristics of the cylinder, it should be noted that they influenced excitation indirectly through their influence on cylinder motion which in turn

modified the flow pattern.

The present chapter is concerned with the hydrodynamic features of the excitation which are applicable to all in-line vibration situations; it is therefore intended to identify parameters which represent the purely hydrodynamic features of the excitation and which are independent of cylinder characteristics such as density, stiffness or damping.

F_T' is the only directly measurable fluctuating hydrodynamic force, but if obtained from equations 7.4 and 7.5, it depends on M_c, k and c and is consequently inappropriate for the present purposes. Theoretically however, F_T' can be divided into components which can be related to those variables associated with the flow and cylinder motion only. These components are discussed in the following sections.

7.2 Added Mass

7.2.1 The coefficient of added mass

It is common practice to analyse fluctuating forces into: (a) those associated with the relative acceleration of the cylinder and flow (inertia forces), and (b) those associated with the relative velocity of the cylinder and flow (drag forces), so that:

$$F_T' = F_I' + F' \tag{7.7}$$

This division is convenient for still water situations when forces are predominantly inertial or in moving water at high Reynolds numbers when drag forces predominate. In still water moreover, the hydrodynamic inertial forces, like the inertial forces of the cylinder's own mass, are proportional to the acceleration, $\ddot{x}$.

It is a mathematical advantage to represent the inertial forces in terms of an "added mass", M_a, thus

$$F_I' = M_a \ddot{x} \tag{7.8}$$

such that the mass, M_a, can be added directly to the cylinder's own mass, M_c, to form a "total mass", M_T. It is then possible to represent the vibration of a cylinder of mass M_T excited solely by drag forces F' by

$$F' = M_T \ddot{x} + c\dot{x} + kx' \qquad (7.9)$$

and $$F' = F'_o \sin(\omega t + \phi) \qquad (7.10)$$

where F'_o is the amplitude of the fluctuating drag force and ϕ is the phase angle with respect to the cylinder's displacement, x_o, as shown in the phase diagrams of Fig. 52. The natural frequency of such vibrating system will then depend on the value of M_a.

The added mass can be related to the mass of fluid displaced by the cylinder, so that:

$$M_a = \frac{\pi}{4} D^2 L \rho_f C_M \qquad (7.11)$$

where C_M is usually termed the "mass coefficient".

Potential flow theory (see e.g. Lamb) indicates that for an infinitely long circular cylinder oscillating in an inviscid and otherwise still fluid:

$$C_{MS} = 1$$

and (7.12)

$$M_{as} = \frac{\pi}{4} D^2 L \rho_f$$

where the subscript "s" indicates "still water". The practical experiments in still water reported in Appendix III as well as numerous research reports (e.g. King, Bramley) confirm this theoretical prediction of C_{MS}. In still water the natural frequency, N, of the cylinder is given by:

$$N = \frac{1}{2\pi} \sqrt{\frac{k}{M_c + M_{as}}} = N_v \sqrt{\frac{\rho_r}{\rho_r + 1}} \qquad (7.13)$$

For the conditions of flowing water on the other hand the appropriate coefficient for added mass is not obvious. Even if the hydrodynamic force on a cylinder could be reliably measured it would not be possible to separate the inertia force of the added mass from other forces. To make progress therefore it is necessary to assign, somewhat arbitrarily, a value or values to C_M; in the following two subsections alternative methods of treating added mass are discussed.

7.2.2 A variable mass coefficient

It would not be unreasonable to attribute variations of vibration frequency solely to variations of the inertial forces of the added mass. If such a variable mass is assumed it follows that the excitation force, F_o', will have a constant phase angle $\phi = 90^o$, and a magnitude, $c\omega x_o$, i.e. F' represents only the forces providing the necessary energy to sustain the vibration (see Fig. 52a).

The resulting variable mass coefficient, C_{MV}, can be obtained by expressing the vibration frequency, f, in terms of a variable mass such that:

$$\frac{f}{N} = \frac{\frac{1}{2\pi}\sqrt{\frac{k}{\frac{\pi}{4}D^2L\rho_f(\rho_r+C_{MV})}}}{\frac{1}{2\pi}\sqrt{\frac{k}{\frac{\pi}{4}D^2L\rho_f(\rho_r+1)}}} = \sqrt{\frac{\rho_r+1}{\rho_r+C_{MV}}} \qquad (7.14)$$

and consequently:

$$C_{MV} = \left(\frac{N}{f}\right)^2(\rho_r+1) - \rho_r \qquad (7.15)$$

It should be noted that (f/N) is a function of (f_s/f) and ρ_r only (see Chapter 6) and consequently C_{MV} is independent of k_s. Equations 7.15 and 6.1 in addition to the assumption (see Chapter 6) that:

$$\frac{N_v}{N} \gtrsim \frac{f}{N} \gtrsim 1$$

indicates that: $0 \lesssim C_{MV} \lesssim 1$. This can be seen in Fig. 53, which presents the results of several tests with various values of ρ_r and k_s; the values of C_{MV} were deduced from equation 7.15. It should be noted that the values of C_{MV} slightly higher than one correspond to the double harmonic excitation section of the first instability region where f was slightly lower than N (e.g. see Fig. 20). Figure 53 shows in addition that C_{MV} varies little with ρ_r and appears to be independent of k_s; the scatter of the experimental data moreover can be attributed

to three-dimensional considerations and secondary factors (see Chapter 9). At first sight it would appear that a variable C_{MV} could be helpful in determining the exciting forces and the frequency variations in instability regions for two-dimensional situations.

It is difficult however to explain the physical behaviour of C_{MV}, especially when $C_{MV} = 0$, i.e. absence of inertial forces, or to explain the constancy of the angle $\phi = 90^{o}$; calculations using this model moreover are complicated by a variable value of the natural frequency.

For the reasons just given (see the next subsection) the variable mass coefficient C_{MV} was not adopted for this analysis of the excitation.

The characteristics of Fig. 7.2 however suggested that C_{MV} was a useful parameter to represent frequency varitaions. It should be noted moreover that equation 7.15 also represents the vectorial addition of the stiffness and inertial forces of the cylinder alone, divided by the inertial forces of the added mass in still water (see Appendix VII), i.e.

$$\left(\frac{N}{f}\right)^2(\rho_r+1) - \rho_r = \frac{k\,x_o - M_c\omega^2 x_o}{M_{as}\omega^2 x_o} \qquad (7.15a)$$

It will be clear later in the thesis that this force ratio is very useful not only to represent frequency variations but also to simplify analysis and calculations in general. For these reasons and to avoid future confusion this force ratio will be henceforth referred to as the "inertial coefficient", C_I, i.e.

$$C_I = \left(\frac{N}{f}\right)^2(\rho_r + 1) - \rho_r \qquad (7.15b)$$

where $0 < C_I \leq 1$, and is approximately independent of ρ_r and k_s (see Fig. 53).

7.2.3 A constant mass coefficient

An alternative way to treat C_M is to assume that its still water value of 1.0 is applicable to flowing water situations and is unaffected by variations of flow pattern. This implies that the acceleration of the cylinder, $\ddot{x}$, will always be opposed by a force which is proportional

both to the acceleration and to the mass of fluid displaced by the cylinder. A value of $C_M = 1$ seemed appropriate for the following reasons:

(a) A value of $C_M = 1$ was observed in slowly flowing water, i.e. when $(f_s/f) < 0.5$ (see Appendix III). When $(f_s/f) > \sqrt{2}$, strong fluctuating drag forces (see 7.3) made any independent measurement of C_M impossible.

(b) It was argued that $C_M = 1$ from a process of superposition of component flow patterns and a consideration of their respective effects on the cylinder. Fundamental to this argument is the assumption that the basic potential flow pattern which leads to $C_{MS} = 1$ in still water persists in flowing water and still depends on the acceleration $\ddot{x}$, in spite of other patterns being superimposed on it.

(c) If it is assumed that $C_M = 1$, ϕ must be variable and the fluctuating drag force, F', is responsible for the variations of (f/N) (see Fig. 52b). In the previous section where a variable C_{MV} was postulated, there was difficulty in providing a physical explanation for $C_M \to 0$, as $(f_s/f) \to \sqrt{2}$. Here, where C_M is assumed constant it seemed more reasonable to argue that as $(f_s/f) \to \sqrt{2}$, $\phi \to 180^o$ and the fluctuating drag force approached the value of the inertial forces of the added mass (see Fig. 52b); in the limit the only hydrodynamic loading on the cylinder would be two equal and opposite forces and consequently the vibration frquency would tend to the in-vacuo natural frequency, N_v.

(d) The fact that the excitation frequency, f, is different from the characteristic or natural frequencies of both the cylinder (N) and the flow (f_s), suggests that there should be phase variations as (f_s/N) changes, rather than a constant $\phi = 90^o$.

(e) If $C_M = 1$, the stability parameter, k_s, then represents the ratio of the external damping forces to the inertial forces of the added mass in both still and flowing water (see Chapter 6). Similarly by the adoption of $C_M = 1$, the inertial coefficient, C_I (see 7.2.2) then becomes the vectorial addition of the stiffness and inertial forces of

the cylinder alone divided by the inertial forces of the added mass, both in still and in flowing water.

(f) By the adoption of $C_M = 1$, the natural frequency of the cylinder then remains constant and equal to its still water value, N; measurement and calculations are thereby facilitated.

The above arguments indicated many advantages in adopting a constant $C_M = 1$, and consequently this will be assumed henceforth in this thesis.

A resolution of the forces of Fig.52b for $C_M = 1$, and the inclusion of the parameters C_I and k_s result in the equations: (see Appendix VII)

$$F_o' = M_{as}\omega^2 X_o \sqrt{(C_I - 1)^2 + (\frac{2}{\pi^2} k_s)^2} \qquad (7.16$$

and

$$\tan \phi = \frac{2 k_s}{\pi^2 (C_I - 1)} \qquad (7.17)$$

where $90^o \leq \phi < 180^o$, if $1 \geq C_I > 0$.

7.3 Hydrodynamic Damping

7.3.1 Still water damping

The rate of decay of transients obtained outside the instability regions (see Figs. 25 and 54) indicates the presence of *hydrodynamic* damping forces which are considerably larger than the forces due to external damping.

Previous authors (e.g. Dickens, King) have measured hydrodynamic damping from transients in still water and have then extrapolated such measurements to steady state vibrations in flowing water. This procedure will not be adopted in the present research for the following reasons:

(a) In slowly flowing water, i.e. $0 < (f_s/f) < 0.5$, the value of the logarithmic decrement, δ, of transients was observed to increase with f_s/f for large amplitudes of vibration, and to decrease with f_s/f for small vibration amplitudes (see Fig. 54).

(b) Transients recorded for $f_s/f > \sqrt{2}$ show much larger δ values than those obtained in still water (see Fig. 25).

(c) The flow patterns are very different in still and flowing water; in still water the relative velocity of the flow with respect to the cylinder, $(V - \dot{x})$, alternately changes from positive to negative, while in flowing water, the maximum predicted and recorded values of the velocity ratio $V_r = (\omega x_o/V)$ of about 0.35, ensure that $(V - \dot{x})$ is always positive.

(d) In still water, and especially with the small "size numbers" (ND^2/ν) of the present research (see e.g. Bramley), the hydrodynamic damping forces are mainly due to viscous friction, i.e. proportional to the velocity, while in flowing water situations and assuming $R_e > 10^3$ (see Chapter 5), the viscous friction forces represent only a small fraction (< 12%) of the total forces, which are predominantly pressure forces, i.e. proportional to the square of the velocity. Figure 55 illustrates the small influence of viscous friction at the higher Reynolds numbers for a *stationary* circular cylinder; at least in terms of orders of magnitude, the diagram is probably applicable to *vibrating* cylinders.

7.3.2 Flowing water damping

If it is assumed that the hydrodynamic damping and the excitation forces were predominantly pressure forces, these could be represented by:

$$F = \tfrac{1}{2}\rho_f DLV^2(1 - V_r \cos \omega t)^2 C_f \qquad (7.18)$$

where $$V_r = \frac{\omega \ddot{x}_o}{V}$$

$V(1 - V_r \cos\omega t)$ is the relative velocity of the flow with respect to the cylinder and C_f is a force coefficient.

Three components can be identified in this equation when it is expanded, i.e.:

(a) $$F_{mean} = \tfrac{1}{2}\rho_f DLV^2 C_f(1 + \tfrac{1}{2}V_r^2) \qquad (7.19)$$

is the mean drag force.

(b) $$F_{variable} = -\tfrac{1}{2}\rho_f DLV^2 C_f(2V_r\cos\omega t) \qquad (7.20)$$

is clearly a damping force in antiphase with $\dot{x}$ and is intended to include both pressure and friction hydrodynamic damping forces; and

(c) $$F_{2\omega} = \tfrac{1}{2}\rho_f DLV^2 C_f[\tfrac{1}{2}V_r^2\cos(2\omega t)] \qquad (7.21)$$

has twice the frequency of the vibration and consequently does not work on the system. This force in the experiments moreoever, never exceeded 9% of $F_{variable}$ and is thus neglected.

If the second term of equation 7.19 is neglected, equation 7.20 can be written:

$$F_{variable} \simeq -F_{mean}(2V_r\cos\omega t) \qquad (7.22)$$

From this approximate relationship it can be seen that $F_{variable}$ is of the same order of magnitude as the mean drag force(and is considerably larger than the external damping forces $c\omega x_o$) and would thus account for the strong damping forces observed for $(f_s/f) > \sqrt{2}$. $F_{variable}$ moreoever, increases with V_r and consequently with x_o. In addition it has been shown (Chapter 3) that F_{mean} also increases with x_o and so

$$F_{variable} \propto (x_o)^a$$

where $a > 1$. The heavy damping represented by this power law could be an important factor in imposing an upper limit to the maximum vibration amplitude even when $c\omega x_o \to 0$.

7.4 Excitation Forces

7.4.1 A theoretical model of the excitation

To sustain a steady state vibration a strong exciting force is required to counter the hydrodynamic damping of equation 7.18 in which the force coefficient is as yet undefined.

The flow patterns observed in the two instability regions suggested that the force coefficient undergoes variations with the same frequency as the motion of the cylinder; the sinusoidal character of this motion suggested moreover that all the forcing functions were also sinusoidal. Consequently the force coefficient could be expressed by:

$$C_F = \bar{C}_F + C_F' \sin(\omega t + \alpha) \tag{7.23}$$

where $\bar{C}_F$ and C_F' are the mean and fluctuating parts of C_F respectively and α is the phase angle of C_F' with respect to x_o. This expression of C_F can be substitued for C_f in equation 7.18, which then becomes:

$$F = \tfrac{1}{2}\rho_f DLV^2(1 - V_r\cos\omega t)^2[\bar{C}_F + C_F'\sin(\omega t+\alpha)] \tag{7.24}$$

Equations 7.23 and 7.24 represent the excitation in terms of C_F. These equations can be solved for the components of F, which are given by:

$$F = \bar{F} + F' \tag{7.25}$$

where from equation 7.10, $F' = F_o'\sin(\omega t + \phi)$; solving thus: (see Appendix VII)

$$\bar{F} = \tfrac{1}{2}\rho_f DLV^2[(1 + \tfrac{1}{2}V_r^2)\,\bar{C}_F - V_r C_F'\sin\alpha] \tag{7.26}$$

and

$$F_o'\cos\phi = \frac{1}{2}\rho_f DLV^2(1 + \frac{1}{4}V_r^2)C_F'\cos\alpha \tag{7.27}$$

$$F_o'\sin\phi = \frac{1}{2}\rho_f DLV^2(1 + \frac{1}{4}V_r^2)C_F'\sin\alpha - \frac{1}{2}\rho_f DLV^2(1 - \frac{1}{4}V_r\frac{C_F'}{\bar{C}_F}\sin\alpha)2V_r\bar{C}_F \tag{7.28}$$

It should be noted that the second term of the R.H.S. of equation 7.28 is always negative because both V_r and $\bar{C}_F$ are always positive and because the negative term inside the parenthesis is always smaller than 0.1; the second term of equation 7.28 thus opposes $F_o'\sin\phi$, which in turn is

in antiphase with the external damping force, $c\omega x_o$; (see Fig. 52a), it then follows that this term of equation 7.28 represents a hydrodynamic damping force, P_{hd}, which is in antiphase with the velocity $\dot{x}$, i.e.

$$P_{hd}\cos\omega t = -\frac{1}{2}\rho_f DLV^2\left(1 - \frac{1}{4}V_r\frac{C_F'}{\bar{C}_F}\sin\alpha\right)2V_r\bar{C}_F\cos\omega t \qquad (7.29)$$

The first term of equation 7.28 and equation 7.27 clearly represent the two components of an excitation force, P_e, which is in phase with the fluctuating force coefficient, C_F', i.e.

$$P_e\sin(\omega t+\alpha) = \frac{1}{2}\rho_f DLV^2\left(1 + \frac{1}{4}V_r^2\right)C_F'\sin(\omega t+\alpha) \qquad (7.30)$$

$F_o'\sin\phi$ must be positive (in phase with $\dot{x}$) to sustain the vibration and $F_o'\cos\phi$ must be negative (in antiphase with x) if $f \gtrsim N$ (see Fig. 52b); it then follows from equation 7.27 and 7.28 that $\sin\alpha$ must be positive while, $\cos\alpha$ must be negative, i.e. P_e must be in the 2nd quadrant of the phase diagram. This can be seen in Fig. 56 where the hydrodynamic forces P_e, P_{hd} and $M_{as}\omega^2 x_o$ and their phase relationships are shown together with the cylinder inertial, stiffness and external damping forces.

The excitation process is thus expressed in terms of forces which are functions of C_F, flow characteristics, cylinder motion and geometry; it is now necessary to correlate C_F with the above parameters in order to confirm that P_e and P_{hd} are indeed hydrodynamic parameters, and that they are independent of cylinder characteristics such as ρ_r and k_s. This will be attempted in the next chapter.

To obtain such correlations however, $\bar{C}_F$, C_F' and α must be calculated from the measurable characteristics and behaviour of the cylinder and flow. From a resolution of the forces of Fig. 56 and from equations 7.3a, 7.9 and 7.26 to 7.30 (see Appendix VII), thus:

$$\bar{C}_F = \frac{C_{DA} + V_r C_F'\sin\alpha}{1 + \frac{1}{2}V_r^2} \qquad (7.31)$$

$$C_F' = \frac{\pi^2 V_r}{\frac{V}{fD}\left(1 + \frac{1}{4}V_r^2\right)}\sqrt{(C_I - 1)^2 + \left[\frac{2\psi}{\pi^2}\left(\bar{C}_F\frac{V}{fD} + k_s\right)\right]^2} \qquad (7.32)$$

$$\tan \alpha = \frac{2\psi}{\pi^2} \frac{\overline{C}_F \frac{V}{fD} + k_s}{C_I - 1} \qquad (7.33)$$

where

$$\psi = \frac{1 + \frac{1}{4} V_r^2}{1 + \frac{3}{4} V_r^2} \leq 1 \qquad (7.34)$$

It should be noted (equation 7.31) that the mean force coefficient $\overline{C}_F$ is different from C_{DA} and hence the latter's name, "apparent drag coefficient".

The theoretical model just developed shows the hydrodynamic forces and energies to be significantly larger than those due to external damping. The excitation thus appears to depend on a delicate balance between relatively large forces which tolerates only small energy outputs.

In contrast with the model of Fig. 52a and equations 7.16 and 7.17, the model of Fig. 56 does not neglect the influence of C_{DA} on the excitation process and in this way it opens an additional source of available data.

As will be shown later, the maximum ϕ variation of 90^o (Eqn. 7.17) corresponds to only 45^o of α variation, which indicates that the excitation is also very sensitive to phase angle variations. Bearing in mind the self-excited character of the vibration, this sensitivity is more obvious if α is not only regarded as indicating the phase angle between force and cylinder motion, but also as an indicator of the phase relation between the cyclic power supply to the wake near the cylinder and the motion of the wake itself.

Before proceeding to a detailed analysis (in Chapter 8) of the excitation mechanisms, it is opportune here to make a preliminary assessment of the validity of the model just described to represent the excitation. This assessment is presented in the next two subsections, in the form of a brief analysis of the patterns of behaviour of cylinder and flow, which have been observed to occur in association with the variations of the forces predicted by the model.

7.4.2 The pairs mechanism

The excitation in the first instability region which occurred in association with pairs of simultaneous eddies ("pairs mechanism") was first assessed by Hardwick and Wootton. They suggested that when the wake was narrowest as the cylinder moved upstream through its central position (see Fig. 9), the flow pattern resembled the wake behind a stationary cylinder when $R_e > 5 \times 10^5$, for which case $C_{DO} = 0.35$ only (see Figs. 9 & 55); and consequently a lower value of the force coefficient of the vibrating cylinder should occur at this moment. When the cylinder moved downstream through its central position, the wake was widest and resembled that occurring behind a stationary flat plate placed perpendicular to the flow, for which case $C_{DO} \simeq 2.05$; an increase of the force coefficient of the vibrating cylinder was likely at this stage. The two conditions were represented thus:

$$\overline{F} + F' = \tfrac{1}{2}\rho_f DL(\overline{C}_F + C_F')(V - \omega x_o)^2 \quad \text{(downstream stroke)}$$

$$\overline{F} - F' = \tfrac{1}{2}\rho_f DL(\overline{C}_F - C_F')(V + \omega x_o)^2 \quad \text{(upstream stroke)}$$

Subtracting:

$$\frac{F'}{\tfrac{1}{2}\rho_f DLV^2} = C_F'(1 + V_r^2) - 2\overline{C}_F V_r \qquad (7.35)$$

where the first term in the right hand side is the excitation force and the second is the hydrodynamic damping.

With the aid of this model Hardwick and Wootton predicted a maximum amplitude for the first instability region.

This model implies that the excitation forces are always in phase with the cylinder's vibration velocity, $\dot{x}$, but it was argued in section 7.2 that this can only be true when $f = N$, or if C_M is assumed to vary, none of which criteria is here applicable. There is an additional deficiency in that both Hardwick and Wootton and later King using the same model, have assumed $\overline{C}_F$ to be constant and equal to its stationary cylinder value, C_{DO}; but it was shown in Chapter 3 that C_{DA} was variable, especially when the two excitation mechanisms there identified were observed to interact.

In the present study an attempt was made to improve Hardwick and Wootton's model by incorporating a variable phase angle, α, between the fluctuating force coefficient C_F' and the cylinder displacement, x_o, and introducing also a variable mean force coefficient, $\overline{C}_F$. This led to equations 7.23 and 7.24.

7.4.3 The "transverse flow mechanism"

In the second instability region (and in the lock-in sections of the first) the excitation can be associated with the strong periodic transverse flow observed in the wake near the cylinder (see Chapter 3) rather than with a widening and narrowing of the wake.

It was suggested in Chapter 3 that this transverse flow was associated with the velocity field of the strong eddy just downstream of the cylinder, as shown schematically in Fig. 57. It was evident from flow visualization that the major part of the transverse flow was supplied by water flowing in a streamtube of some width, b (Fig. 57), which is turned through 90^o from the original direction of the approaching flow to the transverse direction. What follows is an attempt to express the force required to turn the flow in this streamtube and thus change its momentum.

The flow velocity (relative to the cylinder) in the streamtube of width b will be somewhat larger than V because of the constriction imposed by the cylinder and could thus be represented by:

$$\gamma(V - \dot{x})$$

where γ is a coefficient whose value is likely to be in the range 1.0-2.0.

The mass flow rate through the streamtube of width b and length parallel to the cylinder axis L, will be:

$$\rho_f b L \gamma (V - \dot{x}) \qquad (7.36)$$

As the transverse flow velocity fluctuates in each cycle between some maximum and zero, the horizontal (Fig. 57) component of the velocity of the flow in the streamtube, immediately downstream of the cylinder, fluctuates between zero and $\gamma(V - \dot{x})$. Assuming a sinusoidal variation, the horizontal velocity component can be represented by:

$$\gamma(V - \dot{x})\,\tfrac{1}{2}\,[1 + \sin(\omega t + \xi)] \qquad (7.37)$$

where ξ is the phase angle between this component and x_o.

A periodic force acting on the cylinder in the direction of the flow can thus be associated with the loss of momentum in that direction experienced by the flow in the streamtube. This force is given by equations 7.36, 7.37 and the momentum equation, i.e.

$$F = [\rho_f bL\gamma(V-\dot{x})][\gamma(v-\dot{x})\,\tfrac{1}{2}\,\{1 + \sin(\omega t + \alpha)\}] \qquad (7.38)$$

where the first factor in the right hand side represents the mass flow rate through the stream tube, and the second represents the variation of the *loss* of velocity in the direction of the main stream experienced by such flow; it should be noted that instead of changing the sign of $\sin(\omega t + \xi)$, the angle ξ has been replaced by

$$\alpha = \xi + 180^o$$

which is the phase angle between F and x_o.

If it is now assumed that:

$$\frac{b}{D}\,\gamma^2 = C_F'$$

an expansion of equation 7.38 results in three components, namely: (see Appendix VII)

(1) $$F_1 = \tfrac{1}{2}\,\rho_f DLV^2 C_F'(1 + \tfrac{1}{2}V_r^2 - V_r \sin\alpha) \qquad (7.39)$$

is a constant force which indicates that in this type of excitation an increase of the mean force occurs which is of the same order of magnitude as the excitation force; this is in agreement with the observed behaviour of C_{DA} in the second instability region (see Chapter 3).

(2) $$F_2 = -\tfrac{1}{2}\,\rho_f DLV^2 C_F'(1 - \tfrac{1}{4}V_r \sin\alpha)2V_r \cos\omega t \qquad (7.40)$$

is a damping force in antiphase with $\dot{x}$, and

(3) $$F_3 = \tfrac{1}{2}\rho_f DLV^2 C_F'(1 + \tfrac{1}{4}V_r^2)\sin(\omega t + \alpha) \qquad (7.41)$$

is an excitation force of amplitude P_e. (See equation 7.30).

It should be noted moreoever that if the equality:

$$\overline{C}_F = C_f + C_F' \qquad (7.42)$$

is assumed, the force $\overline{F}$ of equation 7.26 results from the addition of the forces F_1 of equation 7.39 and F_{mean} of equation 7.19; similarly the force P_{hd} of equation 7.29 results from the addition of the amplitudes of the forces F_2 of equation 7.40 and $F_{variable}$ of equation 7.20.

The addition of the forces obtained from this model and those obtained from the model developed in 7.3 in connection with hydrodynamic damping thus result in the same forces $\overline{F}$, P_e and P_{hd} of 7.4.1 and 7.4.2.

It can then be concluded that the model presented in 7.4.1 can represent the two main excitation mechanisms.

CHAPTER 8

EXCITATION MECHANISMS

In this chapter the excitation mechanisms of the two instability regions are considered separately and with the help of the models developed in Chapter 7.

An analysis of the second instability region leads to a simplification of the model of the excitation which permits predictions of cylinder behaviour.

The same success is not achieved for the first instability region owing to the complex nature of the excitation. Some insight into the excitation is gained however from a qualitative analysis of the predominant "pairs excitation mechanism" and of its influence in the various sections of the first instability region.

8.1 The Second Instability Region

8.1.1 Phase relationships

The behaviour of the phase angle α can be predicted qualitatively from consideration of the flow patterns in the following way. The variations of the hydrodynamic force coefficient in the second instability region were associated in 7.4.3 with periodic variations of the transverse flow at the back of the cylinder which constituted an integral part of the kinetic field of a newly shed eddy (see Fig. 58a). The variation with time of the kinetic field of such eddies has been investigated by Schaefer & Eskinazi for the staggered wake behind a stationary cylinder and can be represented by the curves of Fig. 58b. The figure shows the tangential velocity, v, at a point in the field as a function of the distance between this point and the centre of the eddy; ν is the kinematic viscosity and t is the time. The curves suggest that eddies behave as free vortices, except for a core which behaves as a forced vortex. The figure shows moreover that the maximum velocity at any instant occurs at increasing radius, say r_1, as t increases.

If the eddies in the wake of the second instability region follow the trends of Fig. 58b, the maximum value of v which can probably be associated with the maximum of the fluctuating force, will occur at the back of the cylinder when the eddy is at a distance, r_1, from that point (see Fig. 58a). Fig. 58b indicates that this distance is likely to decrease with increasing frequency (i.e. decreasing νt). It follows that even if the distance away from the cylinder travelled by an eddy in a given portion of a cycle were independent of frequency, the distance, r_1, should then be reached by an eddy somewhat earlier in a cycle, the higher the frequency. Consequently and bearing in mind that frequency increases with f_s/f , the leading phase angle, α, of the excitation force should not decrease as f_s/f increases, but if anything, α should in this case increase with f_s/f.

Owing to the symmetry of the wake however it is likely that the translatory velocity of the eddies will eventually reach the flow's velocity, V, and consequently, the distance between consecutive eddies in the distant wake will be equal to (V/fD). Observations of the wake about three diameters downstream of the cylinder moreover, showed increases of the distance between eddies roughly proportional to (V/fD). It is therefore also likely that the distance away from the cylinder travelled by an eddy in a given portion of a cycle, will be proportional to (V/fD) and therefore to (f_s/f), since $(f_s/f) = (SV/fD)$. Like the argument of the previous paragraph, these observations also suggest that the distance, r_1, will be reached by an eddy earlier in the cycle the larger (f_s/f), and consequently they suggest that α should increase with (f_s/f).

This trend of α is also suggested by the interpretation of f_s as a natural or characteristic frequency at which events in the wake tend to occur (see Chapters 4 & 6). It should be noted that the above arguments assumed that the eddies were released at a fixed point in the cycle. The above interpretation of f_s suggests however that as f_s increases above and apart from f (i.e. as f_s/f increases) events in the shedding process should tend to occur faster or earlier in a cycle and consequently α should tend to increase with (f_s/f).

Increases of α with (f_s/f) can be seen in Fig. 59 which presents results from several experiments with different values of k_s and ρ_r; the values of α were obtained from the recorded behaviour of the

cylinder and flow and with the aid of equation 7.33. This figure also shows that, unlike the phase angle ϕ, (see equation 7.17 and Fig. 52b) the angle α is not significantly affected by either ρ_r or k_s, and it was considered satisfactory as a generalized hydrodynamic parameter of the excitation applicable to any cylinder in two-dimensional flow.

A general trend of α increasing from 90^o towards approximately 130^o for, $(f_s/f) = \sqrt{2}$ can also be seen in this figure. It will be shown in Chapter 9 moreoever that consideration of boundary layers, flow pattern correlation, etc., modifies this trend towards 135^o when $(f_s/f) = \sqrt{2}$ for an ideal two-dimensional case.

8.1.2 $\overline{C}_F$ and hydrodynamic damping

The above observations suggest tan $\alpha = -1$ when $(f_s/f) = \sqrt{2}$, for the ideal two-dimensional situation; under these circumstances moreover, $C_I = 0$, and from equation 7.33:

$$\frac{2}{\pi^2} \psi \left[\overline{C}_F \frac{V}{fD} + k_s\right] = \text{constant} = 1 \qquad (8.1)$$

for all values of ρ_r and k_s; and (V/fD) is constant since $(f_s/f) = \sqrt{2}$.

In Chapter 6 it was argued that in the second instability region, for every value of k_s there corresponded a unique value of (a/D) (see Fig. 45). If $\overline{C}_F$ is assumed to be a hydrodynamic parameter which is independent of ρ_r and k_s, it then follows that $\overline{C}_F$ should be a function of (a/D). (Since ψ in equation 8.1 is approximately constant).

Fig. 60 presents values of $(\overline{C}_F/C_{DO})$ calculated with the aid of equations 7.31/2/3, from a series of tests with various values of k'_{so}, and plotted against (f_s/f); the figure shows for $1 < (f_s/f) < \sqrt{2}$, that $\overline{C}_F$ decreases both with decreasing (a/D) or with increasing (f_s/f) which suggests that the product $(\overline{C}_F \frac{V}{fD})$ is a function of (a/D). This product is thus plotted in the form: $(\frac{\overline{C}_F}{C_{DO}} \frac{f_s}{f})$ against (a/D) in Fig. 61 for all values of (f_s/f) in the second instability region; the data are the result of tests with different values of ρ_r and k_s. It is clear from this figure that that product and consequently also $(\overline{C}_F \frac{V}{fD})$ are functions of (a/D) only.

It was confirmed in Chapter 6 moreover that for a given value of k_s, the vibration amplitudes were constant in most of the second

instability region, i.e. there was a flat top to the (a/D) vs (f_s/f) diagram. Therefore, if equation 8.1 is valid when $f_s/f = \sqrt{2}$ and for any value of k_s, the same equality should also apply for any value of (f_s/f) within the flat top of the (a/D) vs (f_s/f) diagram.

Equation 8.1 can also be written as follows: (see Appendix VII).

$$\frac{P_{hd} + c\omega x_o}{M_{as}\omega^2 x_o} = \frac{P_d}{M_{as}\omega^2 x_o} = \text{constant} = 1 \qquad (8.2)$$

where P_d is the total damping force. This equation indicates that independently of cylinder characteristics or motion, the total damping forces are equal in magnitude to the inertial forces of the added mass throughout the flat top of the second instability region.

8.1.3 C_F' and the excitation forces

Equation (8.2) suggests that $M_{as}\omega^2 x_o$ could be valuable as a common denominator for all the forces involved. The ratio of the excitation forces to the inertial forces of the added mass results thus in absolute terms:

$$\frac{P_e}{M_{as}\omega^2 x_o} = \frac{C_F'(1 + \frac{1}{4}V_r^2)}{2\pi^2 S V_r}\left(\frac{f_s}{f}\right) \qquad (8.3)$$

The velocity ratio V_r is directly related to the magnitude and time distribution of the vorticity generated at the cylinder's wall, and it is therefore also related to the strength of the eddies, whose kinetic field constitutes the transverse flow associated with the fluctuating force. Fig. 62 shows moreover that in the second instability region C_F' decreases with decreasing (a/D) or with increasing values of (f_s/f), i.e., it behaves similarly to V_r, since $V_r = \pi S(a/D)(f_s/f)^{-1}$. Therefore C_F' should be a function of V_r. Fig. 63 presents values of C_F' plotted against $2\pi^2 SV_r/(1 + 0.25V_r^2)$, from several tests with various values of k'_{so}. It can be seen in this figure that in the flat top of the (a/D) vs (f_s/f) diagram, the data approximately follow the relationship:

$$C_F' = 2\,\frac{\pi^2 S\, V_r}{1 + \frac{1}{4}V_r^2} \qquad (8.4)$$

8.1.4 A two-dimensional model

Equations 8.1 and 7.33 lead to:

$$\tan \alpha = \frac{1}{C_I - 1} \tag{8.5}$$

or

$$\operatorname{cosec} \alpha = \sqrt{1 + (C_I - 1)^2} \tag{8.6}$$

i.e. α is independent of ρ_r and k_s. Experimental results (see Fig. 64), show only a slight disagreement with equation 8.6 which will be discussed in Chapter 9, in connection with three-dimensional and other secondary factors.

In contrast with equations 7.31, 7.32 and 7.33, equations 8.4 and 8.5 together with figures 53 and 61 provide relationships between $\bar{C}_F$, C_F' and α, on the one hand and flow and cylinder motion parameters only on the other, thus confirming that C_F can represent the excitation independently of the cylinder characteristics, ρ_r and k_s.

The experimental confirmation of Eqn. 8.4 shown in Fig. 63, indicated that the excitation force, P_e (Eqn. 7.30) in common with the force, P_{hd} (Eqn. 7.29) and all other time varying forces on the cylinder (see Fig. 56), was proportional to (a/D); it was argued therefore that the model could be simplified through the elimination of (a/D), by dividing all forces by $M_{as}\omega^2 x_o$. Thus from equations 8.3 and 8.4:

$$\frac{P_e}{M_{as}\omega^2 x_o} = \frac{f_s}{f} \tag{8.7}$$

This equation together with 7.15a, 7.15b and 8.2 provide the force ratios resulting from the simplification. The corresponding phase diagram is shown in Fig. 65.

It should be noted that when any one of the following three conditions are met, namely (a) $N < f < N_v$ i.e. $0 < C_I < 1$; (b) $1 < (f_s/f) < \sqrt{2}$ and (c) $90^o < \alpha < 135^o$; the model then predicts the other two.

From the diagram of Fig. 65, moreover

$$\operatorname{cosec} \alpha = \frac{f_s}{f} \tag{8.8}$$

This equation is compared with experimental data in Fig. 64.

It was concluded that in an ideal, two-dimensional situation, the phase angle of the excitation forces depends only on the ratio of the excitation frequency, f, to the characteristic or "natural" frequency of the flow, f_s, thus indicating that, as Bishop and Hassan have suggested, the excitation can be treated as a dynamic system with its own independent characteristics.

8.1.5 Prediction of cylinder behaviour

(a) Vibration frequencies

It can be seen from the diagram of Fig. 65 that for the ideal two-dimensional case C_I is a function of (f_s/f) only, i.e.

$$C_I = 1 - \sqrt{(f_s/f)^2 - 1} \qquad (8.9)$$

C_I values obtained from this equation are compared in Fig. 66 with data from several experiments conducted with different values of ρ_r and k_s. It should be noted that because of the good agreement between the frequency responses of cylinders having the same ρ_r but different k_s (see Fig. 37), only representative average values of C_I are plotted in Fig. 66 for these cases

Equation 8.9 when combined with 7.15b, results in the expression:

$$\frac{f}{N} = \left[1 - \frac{[(f_s/f)^2 - 1]^{\frac{1}{2}}}{\rho_r + 1}\right]^{-\frac{1}{2}} \qquad (8.10)$$

which gives the frequency response from knowledge of ρ_r and (f_s/f). When compared with the linear relationship 6.2, equation 8.10 improves the agreement between predicted and experimental data, for the lower values of f_s/f (see Figs. 37 & 67).

~~It should be noted that because of the good agreement between the frequency responses of cylinders having the same ρ_r but different k_s (see Fig. 37), only representative average values of (f/N) are plotted in Fig. 67 for these cases.~~

The disagreement between predicted and experimental data which can be observed in Figs. 66 and 67 for the higher (f_s/f) values, can be attributed to three-dimensional and other secondary factors (see Chapter 9).

(b) Vibration amplitudes

An approximate interpolation of the data of Fig. 61 lead to the following expression:

$$\frac{\bar{C}_F}{C_{DO}} \frac{f_s}{f} = 1 + 2.5(a/D)^{\frac{1}{2}} \qquad (8.11)$$

this relationship when combined with Eqn. (8.1) results in:

$$\frac{\psi C_{DO}}{\pi^2 S} \left[\frac{2S}{C_{DO}} k_s + 1 + 2.5(a/D)^{\frac{1}{2}}\right] = 1 \qquad (8.12)$$

which gives (a/D) as a function of k_s alone, if C_{DO}, S and ψ are constant. Given the marked difference between the magnitudes of k_s and $(\bar{C}_F \frac{V}{fD})$ however, the values of (a/D) obtained from this equation will be very sensitive to variations of C_{DO}, S and ψ. A first approximation can be made nevertheless, assuming the average value of (C_{DO}/S) for the whole instability region and the minimum value of ψ, i.e.

$$\psi_{min} = \frac{1}{1 + 0.83(a/D)^2} \qquad (8.13)$$

where f_s/f is assumed to be constant and equal to one, in order to obtain the maximum values of (a/D). Fig. 68 shows that the (a/D) values obtained from equations 8.12 and 8.13 present some similarities with the corresponding experimental data from Fig. 45b, both quantitatively and qualitatively. The marked influence of C_{DO}, S and ψ indicates however, that in order to obtain more accurate predictions of (a/D), by this method, the following is needed: (1) a very high accuracy of measurement, (2) very close resemblance to the ideal two-dimensional case and (3) a more accurate relationship that that of equation 8.11.

The small scatter of the data of Fig. 61 indicates however that for the present research, $(\frac{\bar{C}_F}{C_{DO}} \frac{f_s}{f})$ depends on a/D only, in spite of the slight three-dimensional and other secondary factors involved; consequently, if the values of C_{DO}, S and ψ can be fixed for a given situation, an estimated value of the maximum amplitudes (a/D) for the case when $k_s = 0$ (e.g. Fig. 47) would lead to a value of the right hand side of equation 8.12 different from one, which would in turn allow an improved prediction of the (a/D) v k_s variation.

(c) Speculation concerning the ranges of (f_s/f)

The model of Fig. 65 does not indicate any limit to (f_s/f), (f/N) or α that would predict the end of the instability region, although it shows the coincidence of the conditions $(f_s/f) = \sqrt{2}$; $f = N_v$ and $\alpha = 135^o$. The reason for the breakdown of the excitation as $(f_s/f) \to \sqrt{2}$ may be related to the following processes:

(i) The phase *lead* of the angle, α, can also be thought to represent the phase *lag* of the periodic supply of vorticity or power to the wake (associated with V_r and thus with the cylinder's motion), with respect to the periodic fluctuations of the kinetic or pressure fields of the wake (associated with the force, P_e). This interpretation suggests that the wake or the excitation mechanism are very sensitive to phase changes, tolerating only 45^o variations of α. It is therefore likely moreover, that as (f_s/f) tends towards either one or $\sqrt{2}$, the excitation becomes less stable and tolerates progressively smaller extractions of energy (external damping). The above then constitutes a possible explanation for the reduction of the ranges of (f_s/f) as k_s increases from zero.

(ii) The end of the instability region can also be attributed to decreasing values of V_r as (f_s/f) increases (since $V_r = \pi S(a/D)f/f_s$), which not only reduced the supply of vorticity to the wake, but also make such supply more uniform; the vorticity in the wake consequently becomes more diffuse and the eddies are weakened.

(iii) It should be noted that the same type of wake as that obtained for $(f_s/f)=\sqrt{2}$, with the same geometrical proportions and frequency and for the same velocity of flow, could also be produced with a cylinder of diameter, $D' = \sqrt{2}D$; this larger diameter would decrease the value of f_s to $(f_s/\sqrt{2})$ and consequently $(f_s/f)'$ would be equal to one. If the power supply to the wake per cycle is proportional to the drag force multiplied times (V/f), then the power supply of the larger cylinder would be twice as much as that of the smaller. This is because the power is proportional to D and C_{DA}, and $C_{DA} = \sqrt{2}$ for the smaller cylinder while $C_{DA} = 2$ for the larger one. The increased power supply can be explained by the larger bluffness, wall surface and velocity ratio, V_r, in the case of the larger cylinder, which would result in an

increased and more markedly periodic vorticity supply to the wake. The 2:1 ratio of power supply between the two cases then suggests a likely range within which this type of wake can be produced, and consequently a possible reason for the end of the instability region when $(f_s/f) = \sqrt{2}$. It should finally be noted that the above argument is also compatible with the observed reductions of the limiting value of $(f_s/f) = \sqrt{2}$, which occurred in association with power outputs, i.e. when $k_s \neq 0$.

It is more difficult to explain the *onset* of the instability. The traces of the beating vibrations indicate however, that the frequency of the excitation is different from the vibration frequency, f, which itself varied even though the flow velocity was constant. The values of $(f_s/f) > 1$ also suggest that the frequency of P_e is larger than f and consequently the phase angle α is constantly increasing, so that when, $0 < \alpha < 180^o$, the vibration grows, and it decays when $180^o < \alpha < 360^o$.

It can therefore be assumed that the delay in terms of (f_s/f) of the start of the instability depends on the force ratio:

$$L_I = \pi \frac{P_e \sin\alpha - (P_d + c\omega x_o)}{M_{TS}\omega^2 x_o + P_e \cos\alpha}$$

i.e. the "logarithmic increment" of the beating vibration. Assuming $P_e \cos\alpha$ to be negligible when $\alpha \simeq 90^o$ and dividing both the numerator and the denominator by $M_{as}\omega^2 x_o$, L_I becomes:

$$L_I = \pi \frac{\frac{f_s}{f}\sin\alpha - \frac{2}{\pi^2}[\bar{C}_F \frac{V}{fD} + k_s]}{\rho_r + 1}$$

For unsteady conditions, the second term in the numerator is not constant but $(\bar{C}_F \frac{V}{fD})$ depends on (a/D) according to Fig. (8.5). Therefore L_I will increase with f_s/f or decrease with increases of ρ_r, k_s or (a/D).

It should be noted however that for a given value of L_I, the number of cycles needed for the cylinder to reach its final amplitude and thus a steady state vibration, should not exceed the number of cycles taken by α to move from 0^o to its final value, α_f, as given by Equation 8.8. If the frequency of P_e is assumed to be approximately

equal to f_s, when $(a/D) \simeq 0$, this number of cycles is likely to be proportional to:

$$\frac{\alpha_f}{\frac{f_s - f}{f}}$$

Although α_f can be assumed to be proportional to (f_s/f) (see Fig. 64), it should be noted that the few cycles gained or lost through variations of α_f caused by f_s/f changes, are the most important because $\alpha_f \simeq 90^o$ and $\sin \alpha$ is near its maximum; consequently the number of cycles mentioned above is likely to be proportional to:

$$\frac{(f_s/f)^n}{\frac{f_s - f}{f}} = \frac{(f_s/f)^{n-1}}{1 - \frac{f}{f_s}}$$

where $n > 1$. Therefore as the value of (f_s/f) increases, the number of cycles available for the vibration to grow to its final steady state amplitude will increase, and the corresponding necessary value of L_I will decrease.

The above argument thus indicates that the lower the ρ_r and k_s, the lower the (f_s/f) is required to achieve a given amplitude of steady state vibration. These trends are shown by the experimental data of Fig. 49.

(d) Mean amplitude and energy output

Although not vital to the arguments of these subsection, it is interesting and oportune to consider the mean displacement of the cylinder and the energy extracted by it from the stream.

If the cyclinder were to be dragged through still water, the ratio of the energy per cycle of the wake needed to drag a vibrating cylinder to that needed to drag a non-vibrating one, is given by:

$$E_w = \frac{C_{DA}}{C_{DO}} \frac{f_s}{f_e} \qquad (8.14)$$

The non-vibrating cylinder has been chosen as a reference point because in this case the same type of wake persists through a very wide range

of R_e; consequently this wake can be regarded as a characteristic or "natural" flow pattern for given values of V and D.

E_w, like the similar parameter involving $\bar{C}_F$ (see Fig. 61) also appears to depend on (a/D) only, as shown in Fig. 69, which is a plot of E_w against (a/D) in the second instability region, for various values of k'_{so}. This figure shows that $E_w \to \simeq 2$ when (a/D) $\simeq$ 0.2 and that the slope of the curve flattens for (a/D) > 0.13, i.e. for the amplitudes observed in the second instability region. Consequently it is not unreasonable to assume: $E_w = 2$, i.e. the energy per cycle of the wake needed to drag a vibrating cylinder in the second instability region is approximately twice the amount needed to drag a non-vibrating one. This can also be seen in Fig. 70, which plots E_w against f_s/f in the two instability regions, from the results of the tests of Fig. 69.

The approximation $E_w \simeq 2$ greatly simplifies the prediction of the maximum values of $\bar{x}$, as follows: from equation 3. 1, 7.12 and 7.13:

$$\bar{x} = \frac{\frac{1}{2}\rho_f DLV^2 C_{DA}}{k} \frac{M_c + M_{as}}{M_c + M_{as}} = \frac{C_{DA}}{8S^2\pi^3(\rho_r+1)} \left(\frac{f}{N}\right)^2 \left(\frac{f_s}{f}\right)^2$$

if the maximum of $\bar{x}$ occurs when $(f_s/f) = \sqrt{2}$, i.e. when

$$\frac{f}{N} = \sqrt{\frac{\rho_r + 1}{\rho_r}}$$

then:

$$\left(\frac{\bar{x}}{D}\right)_{max} = \frac{C_{DA}}{4\pi^3 S^2} \frac{1}{\rho_r}$$

Assuming: $E_w = 2$, $C_{DO} \simeq 1$; $S \simeq 0.2$ and $(f_s/f) = \sqrt{2}$:

$$\left(\frac{\bar{x}}{D}\right)_{max} \simeq \frac{0.28}{\rho_r} \qquad (8.15)$$

Equation 8.15 thus provides an estimate of the maximum value of $(\bar{x}/D)$ from knowledge of ρ_r alone. Further refinements can be made if the values of S and C_{DO} are known. This equation indicates moreover, that for a common steel pipe full of water where $\rho_r \simeq 1.5$, $(\bar{x}/D)$ can be as high as 0.18, i.e. approximately equal to the maximum double amplitude of vibration, (a/D), in the second instability region.

8.2 First Instability Region

8.2.1 The "pairs excitation mechanism"

(a) Influence of vibration amplitudes

When the excitation was characterised by the shedding of pairs of simultaneous eddies ("pairs mechanism"), both in the reorganization section of the first instability region and in the vibration of the cylinder with a splitter plate, the calculated fluctuating force coefficient, C_F', roughly followed the same trends as those exhibited by (a/D) (see Figs. 41,43,62 and 71. This dependence of C_F' on (a/D) is explained below.

For a given value of (f_s/f), the velocity ratio of cylinder and flow, V_r, is determined by (a/D).

The vorticity generated in the boundary layer of the cylinder in the upstream stroke increases with increasing V_r. On the other hand the translational velocity of the small eddies generated in the boundary layers during the upstream stroke decreases as V_r increases. It would appear that the confirmation of these trends leads to improved organization of the small eddies within the large eddies which dominate the wake; the large eddies are thus strengthened as V_r increases. As shown in Chapter 3, the large eddies do not appear to roll up until the cylinder accelerates downstream (i.e. after its mean position in the upstream stroke) and the eddies, which are still growing, accelerate together with it. It is towards the end of this stage that the cylinder together with the large eddies, presents a "bluffer" shape to the uncoming flow, than is the case with a stationary cylinder; this results in a decrease of the base pressure and a consequent increase of the drag force with respect to the corresponding values for a stationary cylinder.

It should be noted that during the first half of the cylinder's downstream stroke, the higher the acceleration (which is proportional to a/D) the further upstream the eddies will be with respect to the cylinder, and consequently the bluffer the shape presented to the uncoming flow. This shape is also made bluffer by the upstream flow which results from the previous upstream motion of the cylinder and which is diverted towards the eddies by the back of the cylinder. This upstream flow tends to displace the eddies upstream and away from the

typical "Föppel vortices" arrangement (see Goldstein), which can be observed with non-periodic acceleration, or with very low R_e values.

The above arguments thus suggest that larger amplitudes of vibration should be accompanied by larger increases of the drag force in the downstream stroke of the cylinder.

As the cylinder decelerates in its downstream stroke, the fluid immediately behind the cylinder tends, by its own inertia, to maintain its downstream translation. The low pressure thus generated just downstream of the cylinder induces an onward flow from outside the wake which is apparent from the narrowing of the wake. In addition the separation points move towards the rear of the cylinder. The two effects promote a recovery of pressure in the wake and hence a reduced drag.

The downstream displacement of the separation points is thus associated with the relative downstream acceleration of the fluid in the boundary layers with respect to the upstream accelerating cylinder, which assists the fluid in the boundary layers to overcome the friction forces that cause the separation.

(b) Influence of (f_s/f)

The above description of the excitation also indicates a strong influence of (f_s/f), which determines the velocity ratio, V_r and the acceleration ratio.

This influence is clearly illustrated below the self-excited range i.e. $f_s/f \ll 0.5$ when for a given a/D, V_r is large (say V_r approaching unity). In this case there can be a periodic reversal of the flow in the boundary layers, leading to the formation of smaller eddies of the opposite rotational sense, similar to those observed when the cylinder oscillates in still water. The resulting wake disruption and the extremely low relative velocity of the flow in the downstream stroke, cause increases of the drag force which are too small to overcome the much larger hydrodynamic damping forces. This phenomenon was reflected in the increases of the logarithmic decrement of small amplitude transients, which were observed as f_s/f was decreased below the value 0.5.

The influence of f_s/f on the excitation is also illustrated by the ratio of the energy extracted from the stream by the vibrating

cylinder per pair of eddies shed, to the energy extracted from the same stream by the stationary cylinder per eddy shed. This ratio, E_p, is given by:

$$E_p = \frac{\frac{1}{2}\rho DLV^2 C_{DA}\left(\frac{V}{f}\right)}{\frac{1}{2}\rho DLV^2 C_{DO}\left(\frac{V}{f_s}\right)} = \frac{C_{DA}}{C_{DO}} \frac{f_s}{f} \qquad (8.15)$$

For given values of V, D and (a/D) therefore, lower (f_s/f) values indicate relatively shorter periods of the vibrating cylinder, and since C_{DA}/C_{DO} = constant it follows that less energy is given to the eddies and their strength is consequently limited.

The stationary cylinder case has been used as a reference point because the same type of wake with only secondary changes can be observed over a very wide range of flow velocities.

(c) Geometrical considerations

The understanding of the excitation can be advanced by considering geometrical parameters such as the distance between consecutively shed eddies, which, if expressed in cylinder diameters is proportional to (v/fD) or (f_s/f).

Consider for the sake of argument the extreme situation where this distance is very small (i.e. f_s/f is small). If it is assumed moreover that the furthest upstream position reached by the eddies on the cylinder wall is about 90^o from the frontal stagnation point (see Fig. 73a), the proximity of consecutive eddies and the wall of the cylinder would inhibit the expansion and contraction of the wake; in addition these wake fluctuations would not reach the back of the cylinder where pressure variations are most effective. If on the other hand the eddies were formed well downstream of the 90^o position so as to improve the effectiveness of the wake fluctuations (see Fig. 73b), the eddies would then be less effective in increasing the bluffness of the combined cylinder-eddies' shape. A small "distance" (V/fD) thus indicates low values of C_F', while the position of the eddies on the cylinder's wall indicates whether the increase of bluffness (and of C_F') with respect to the stationary cylinder case is larger than its reduction or vice versa.

It is interesting to note that the proximity of the values of

C_{DA} and C_{DO} recorded in the reorganization section of the first instability region suggest, that the average of the fluctuating bluffness (presumably associated with the fluctuating drag) is equal to the bluffness in the case of a stationary cylinder. This contrasts with the excitation mechanism of the second instability region, where practically the entire variations of the drag force occur above the value of the drag force for a stationary cylinder.

It should be noted moreover that the smaller the "distance" (V/fD), the lower the vibration amplitudes which will be possible without interference between consecutive eddies.

When (V/fD) is very large, the free shear layers joining the separation points with the previously shed eddies are very long, unstable, they tend to roll up to form additional large eddies, and, in the absence of a splitter plate, they as well as the members of a pair of eddies also tend to interact. These instabilities are aided by the higher values of (f_s/f) (equation 8.15).

These instabilities reflect themselves in the behaviour of the cylinder with the splitter plate (see Chapter 3) for large increasing values of (V/fD), when the shear layers and the eddies gradually become more turbulent. With further increases of (V/fD) beyond the point where (a/D) is suddenly reduced, the apparent separation points move somewhat to the rear of the cylinder, while the wake narrows and becomes completely turbulent. This transition thus resembles that of the wake behind a stationary cylinder for $R_e \simeq 3 \times 10^5$ (see Figs. 42 and 55).

These observations suggest that this transition is not determined solely by R_e criteria as in the case of a stationary cylinder; what appears to be the important criterion is the *fluctuating* ratio of the inertial to viscous forces in the flow which is strongly influenced by the fluctuating accelerations and velocities of the cylinder, especially in the boundary layers.

It is significant that for approximately constant k_s values, the experimental results suggest that the sudden drop of the (a/D) vs (f_s/f) curve was independent of R_e. This applied throughout the range covered by the experiments, i.e. $3500 < R_e < 9500$, at the (a/D) instability. The fact that a corresponding sharp fall of vibration amplitude was observed at Immingham with $R_e \simeq 10^6$ supports the argument that R_e is not an important factor.

Finally it should be noted that the larger (V/fD), the larger the distance travelled downstream by an eddy in a given portion of an oscillation period; or conversely, the smaller portion of the period taken by an eddy to occupy the same position relative to the cylinder. The narrowing of the wake is therefore likely to occur earlier in the cycle as V/fD increases and this would explain the increase of α with f_s/f shown in Figs. 59 & 72.

(d) Quantitative considerations

A quantitative analysis of the excitation is complicated by four identifiable types of instability associated with the "pairs mechanism": (a) the small amplitude vibration for high k_s or low (f_s/f); (b) the large amplitude vibration for low k_s and for (f_s/f) values before irregularities appear; (c) the unstable peak amplitude vibration leading to the sudden (a/D) drop; and (d) the turbulent wake, low amplitude vibrations occuring at the end of the instability region.

Another difficulty arises from the relatively small variations of (C_{DA}/C_{DO}) which as shown in equations 7.29 & 7.31 determines the balance of external and hydrodynamic damping. In the work with the splitter plate experimental problems such as the thickness, motion, drag and damping of the plate, and inaccuracies in obtaining the values of $\overline{x}$ caused by electronic equipment, also added to the difficulties mentioned above.

The main quantitative characteristics of this excitation mechanism however, can be summarised as follows:

Figure 74 presents values of $(\overline{C}_F/C_{DO})$ against (a/D) from a series of experiments using the splitter plate, with approximately equal ρ_r but with widely differing k_s values. An approximately linear relationship between $\overline{C}_F$ and (a/D) can be identified in the figure, if the results of one of the experiments are neglected. In contrast with the second instability region of the bare cylinder where ($\overline{C}_F$ V/fD) was a function of (a/D) only, in this case the identifiable relationship of Fig. 74 suggests a different k_s vs (a/D) relationship for every value of (V/fD) or (f_s/f).

Fig. 75, which presents the C_F' values corresponding to the tests of Fig. 74, shows an approximately linear relationship between C_F' and V_r, although the difficulties mentioned above did not permit

the identification of more consistent correlations. The maximum recorded value of C_F' for the splitter plate tests was equivalent to $0.75\ C_{DO}$.

Fig. 72 suggests that α is a function of (f_s/f) only, in spite of the wake transition referred to in (c) above.

8.2.2 Rearrangement and lock-in sections

The influence of the staggered wake in the first instability region, which is characterized by a strong transverse flow immediately behind the cylinder, can either reinforce the excitation due to the "pairs mechanism" and lead to the peak amplitudes of the instability, or it can oppose such excitation and promote a sudden drop of the vibration amplitude at a lower value of f_s/f in comparison with the results for the splitter plate.

As can be seen in the frequency diagram of Fig. 13b, the interaction of the excitation mechanisms is prompted by the mutual proximity of the values of f and f_s, which allows the staggered wake to modify its eddy frequency, $f_e \simeq f_s$, to match that of the vibrating cylinder, f, and thus to influence the excitation more significantly as the transverse flow reaches the back of the cylinder. The onset of this lock-in section appears more or less consistently when $f_s/f \simeq 0.85$.

In contrast to this, the sharp fall of (a/D) is not well defined in terms of (f_s/f). A probable reason for this is that the amplitude response curves are not only determined by the "distance" (V/fD), which as pointed out in 8.2.1c, increases the instability of the free shear layers; but as in the case of the splitter plate, the value of (f_s/f) where the mentioned (a/D) reduction occurs is also modified by (a/D) itself, which contributes to the organization and stability of the wake. Thus the abrupt reduction of (a/D) occurs earlier in terms of f_s/f, the smaller the values of (a/D) for given (f_s/f) values. (see Fig. 41). If k_s controls the vibration amplitudes moreover, this could explain the reduced (f_s/f) ranges of the instability region, corresponding to higher values of k_s (see Fig. 49).

The interaction of excitation mechanisms can be seen also in the behaviour of C_F', $\overline{C}_F$ and α.

Fig. 59 shows two different trends of α vs (f_s/f) according to

whether (a/D) is large (before the sharp fall) or small (after the sharp fall). The curve representing the latter case seems to be roughly proportional to f_s/f and tending towards $\alpha = 135^o$ for $f_s/f = 1$, while the other curve indicates slightly lower values of α and a less definite relation with f_s/f.

Fig. 62 shows the behaviour of C_F' vs (f_s/f) to be following approximately the trends exhibited by (a/D); a plot of C_F' vs (a/D), however did not lead to any clear correlation. The absence of a flat top in the (a/D) vs (f_s/f) curve of the first instability region which led to different (a/d) vs k_s correlations for every value of (f_s/f), (Fig. 45a), suggested the C_F' vs (a/D) plots of Fig. 76 for constant values of (f_s/f).

This figure shows: (a) similar shape for all the curves; (b) different numerical values for each curve, and (c) two different trends in every curve. Points (a) and (b) above, result from the different maximum amplitudes corresponding to different values of f_s/f, while point (c) reflects the changes in the excitation process.

It should be noted that because of the addition of the interacting excitation mechanisms, C_F' and (a/D) reached higher values in the first instability region than those observed in the splitter plate case. Thus C_F' can be higher than C_{DO} although it is always smaller than the mean force coefficient $\overline{C}_F$.

The mean force coefficient $\overline{C}_F$ is more noticeably affected by the type of excitation, as shown in Fig. 60. In general $\overline{C}_F$ follows the patterns of C_{DA} (see Fig. 13), increasing when the mechanism associated with the transverse flow dominates the excitation; under these circumstances, increases of $\overline{C}_F$ correspond to increases of (a/D). In the rearrangement section of the instability region however, larger (a/D) values indicate more stable pairs of eddies which tend to suppress the interaction of the excitation mechanisms and the consequent increase of $\overline{C}_F$; thus in this section $\overline{C}_F$ is often smaller for higher values of (a/D).

The interaction between the mechanisms of excitation can also be appreciated in Fig. 70 which shows the behaviour of E_w (see 8.1.5d) with respect to (f_s/f). A marked contrast in the scatter of the points in the two instability regions can be seen in the figure. In the second instability region the slight variations of E_w can be associated

with a/D (or k_s), variations. In the first instability region however, although E_w increases with (a/D) in the lock-in section, it decreases with higher (a/D) values in the rearrangement section where E_w remains at a value of one approximately for the two cases of highest amplitude.

8.2.3 Double harmonic excitation section

In this section of the first instability region the shedding frequency of pairs of eddies coincided with the vibration frequency. In addition, the amplitude of vibration was observed to increase in alternate cycles, i.e. with a frequency equal to that of the distant wake or the transverse flow just downstream of the cylinder. It was concluded from these observations that two mechanisms of excitation were again operating one associated with the pairs of eddies and one with the transverse flow.

Observation of the transient vibrations of the cylinder with a splitter plate, obtained with (f_s/f) values lower than those of the corresponding instability region, resulted in the curves of Fig. 54; the curves represent qualitatively the behaviour of the logarithmic decrement, δ, of the transients with respect to (a/D) and (f_s/f). It can be seen in the figure that as (f_s/f) increases from zero the slope of the curves increasess but the vertical axis intercepts decrease. This trend continued until at (f_s/f) values within the instability region δ became negative, i.e. excitation occurred. When the cylinder without a splitter plate was externally excited at low (a/D) and with $(f_s/f) \lesssim 0.5$, the flow patterns in the wake showed a marked similarity to those observed with the splitter plate for equivalent (a/D) and (f_s/f).

These observations suggested that the balance of hydrodynamic energy inputs and outputs associated with the "pairs mechanism", changes as (f_s/f) increases; for example, when $(f_s/f) = 0$ the excitation forces are absent, while when (f_s/f) reaches the instability region of the cylinder with a splitter plate, these excitation forces are large enough to oppose the hydrodynamic damping at low (a/D) and thus to sustain a vibration.

The double harmonic excitation section moreover, commenced with (f_s/f) values which were only slightly lower than those of the splitter plate instability region; this indicates that only a small energy input

is necessary, in addition to that due to the pairs mechanism, to overcome the damping and thus to cause the vibration.

The 2:1 ratio of the frequencies f and f_e maintained throughout this section of the instability region, further suggested that the additional energy required was provided by the excitation mechanism associated with the transverse flow and with the distant wake.

Since energy inputs can only be caused by forces acting in phase with the vibration velocity and consequently with the same vibration frequency, the resulting non-sinusoidal motion, x (Fig. 77) can thus be said to be produced by the double excitation of: (a) its second harmonic component, x_1, by a force F_1, of frequency f, associated with the shedding of pairs of eddies, and (b) of its fundamental component, x_2, by a force F_2, of frequency f_e, associated with the distant wake.

A factor that confirmed the influence of the transverse flow and the distant wake in this type of excitation, was a corresponding sharp increase of C_{DA}, similar to that observed in the lock-in section of 3.2.4 (see Fig. 13).

Since the frequencies of the excitation and of the cylinder's motion were synchronised, it would be possible to refer to a frequency lock-in if the former were controlled by the latter. That this was so was confirmed by the departure of the eddy frequency from the value f_s, which that frequency would have otherwise adopted.

From the above interpretation of the excitation it follows that the energy inputs due to the mechanism associated with the transverse flow, will increase with an increase of the amplitude x_2 (see Fig. 77). As the excitation frequency f_e is considerably smaller than N, there is practically no dynamic magnification in this component of the motion, and therefore:

$$\frac{F_2}{kx_2} \simeq \text{constant}$$

or, for a given size of cylinder:

$$x_2 \simeq \frac{F_2}{(\rho_r + 1)N} \times \text{constant}$$

i.e. for given values of F_2 and N, the amplitude x_2 will decrease as ρ_r

increases, consequently reducing the energy input via this excitation mechanism. This effect of ρ_r is reflected in: (a) the smaller values of (a/D) at the onset of the first instability region of curve 1 in Fig. 41b , when compared with curve 2 of Fig. 41a , in spite of a slightly higher value of k_s for the latter; or (b) in the slight reduction of the f_s/f ranges of the first instability region which correspond to higher values of ρ_r in Fig. 49.

It should be noted that the model described in equation 7.25 does not strictly apply in this section because the vibration is non-sinusoidal, but since the pairs mechanism predominates in the excitation, some qualitative observations are worth noting.

Curve 1 of Fig. 62 shows a peak of the value of C_F' in this section which is notably more marked than the smoother transition of the corresponding (a/D) vs (f_s/f) curve 1 of Fig. 41a. This is because the hydrodynamic damping forces in this section are larger than those of the adjacent reorganization section, as illustrated by the behaviour of $\overline{C}_F$ in Fig. 60. It should be noted however that the value of C_F' in the double harmonic excitation section of Fig. 62 is significantly higher than a value extrapolated from the adjacent reorganization section; the difference between the two values is not due to the energy input via the transverse flow mechanism alone, which was argued above to be weak. The pairs mechanism is predominantly responsible for the increase of (a/D), which is in turn associated with increases of C_F'. These observations clearly show the self-excited nature of the pairs mechanism and the amplitude controlling action of the mean drag force.

CHAPTER 9

THREE-DIMENSIONAL CONSIDERATIONS

The previous chapters have been primarily concerned with two-dimensional cylinders free to vibrate only in the flow-direction of a one-dimensional stream. For these situations, cylinder behaviour can be predicted from the empirical relationships of Chapter 6, or for the second instability region, from the theoretical model developed in Chapters 7 and 8.

The first part of this chapter is concerned with the discrepancies between truly two-dimensional flow-cylinder arrangements and the results of the present study where small three-dimensional effects were unavoidable.

In practical situations, three-dimensional effects are likely to be more pronounced than in the present study; the second part of this chapter is concerned with the applicability of the material of Chapter 4 & 6 to 8, to full-scale situations where the flow velocity and vibration amplitude are variable along the length of a pile for example.

9.1 Influence of Three-Dimensional Effects on the Results of the Present Research

Although the experiments of this research were designed to approximate the ideal case of a two-dimensional cylinder immersed in a one-dimensional stream, the unavoidable imperfections of the experimental models were responsible for a departure of the experimental results from the predictions based on two-dimensional models.

Except for the effects of "blockage" (see Appendix VI) the most important factor contributing to these discrepancies was the approaching flow's velocity distribution along the cylinder's length, especially in the boundary layers near the end plates where the magnitude and the correlation of the hydrodynamic forces, P_d and P_e were altered.

The irregularities of the approaching stream often resulted in flow patterns which were not correlated along the cylinder's length and

which caused reductions of (a/D) or (f/N), as shown in Chapter 6, presumably due to a weakening of the total excitation forces.

Reductions of these hydrodynamic forces could also be attributed to other factors (turbulence of the approaching stream, roughness of the cylinder's surface, etc.) but these reductions were small (say < 3%) and were not felt to be important.

It should be noted that the inertial forces of the added mass have been assumed to be a function of cylinder geometry and motion only and were therefore independent of the factors mentioned above. This assumption allows the use of $M_{as}\omega^2 x_o$ as a common denominator for the force analysis which follows.

Owing to the complexities and inaccuracies involved in the assessment of the three-dimensional factors here dealt with, this illustrative analysis will for convenience concentrate on the second instability region, and it will refer mainly to the results of run 99 (see Table II-2). For further details of this analysis please see Appendix VI.

9.1.1 Damping forces

The damping forces depend on the mean force coefficient, $\overline{C}_F$, which in the present research was affected by the additional drag forces caused by the supporting arms of the cylinder; these forces were not included in external damping for the reasons given in Appendix V. The consequent increase of $\overline{C}_F$ can be calculated by assuming a drag coefficient for the arms (see Appendix V) of say $C_D = 1.5$, and an average drag coefficient for the cylinder of say 1.5. Considering the reduced moment arm of the resultant force and the ratio of the areas presented to the flow by the cylinder and by its supports. The contribution of the supports to the total mean force results about 1.5%.

The ratio of the total damping forces to the inertial forces of the added mass (see Eqns. 8.1 & 8.2) was observed to depart from the value of one predicted by the two-dimensional model by an amount which appeared to be proportional to $\overline{C}_F$, i.e. 4% for $\overline{C}_F = 1.4$ to 7% for $\overline{C}_F \simeq 2$. This variation was probably due to blockage effects (see Appendix VI).

The measurements of velocity made for this research were not affected by blockage because they were made about six diameters upstream from the cylinder. If the effect of blockage is to increase the local

flow velocities and consequently the hydrodynamic forces above the values they would adopt in an infinite stream, it then follows that any hydrodynamic force coefficient calculated from the measured values of V will be overestimated accordingly.

It can be shown (see Appendix VI) that the product $(\overline{C}_F\ V/fD)$ which predominates in the numerator of Eqn. 8.1 is approximately proportional to $V^{-1.3}$. If $M_{as}\omega^2 x_o$ is assumed to be unaffected by blockage or three-dimensaionl effects and if β is the increase of V due to blockage effects, an approximate correction for P_d results:

$$\frac{(P_d)_m}{(P_d)_b} \simeq \frac{\left(\overline{C}_F \frac{V}{fD}\right)_m}{\left(\overline{C}_F \frac{V}{fD}\right)_b} \simeq 1 + 1.3\beta$$

where "m" indicates measured or calculated from the measured values of V, and "b" indicates calculated considering the increased values of V due to blockage. Combining this correction with a linear variation of $P_d/(M_{as}\omega^2 x_o)$ with respect to $\overline{C}_F$, based on the values given above, and assuming β to be small, the correction for the velocity due to blockage will be: (see Appendix VI).

$$\beta \simeq \frac{\overline{C}_F}{26}$$

When $\overline{C}_F = C_{DO}$ (i.e. stationary cylinder), this expression results in an 8% correction for the drag force, which is a not unreasonable value for the cylinder/flume area ratio of about 7%.

When $(f_s/f) = \sqrt{2}$, $\overline{C}_F \simeq 1.4$ and $\beta \simeq 5\%$; considering the additional drag due to the supporting arms:

$$\frac{(P_d)_m}{(P_d)_{b/cyl.}} \simeq 1.08$$

i.e. the actual value of $P_d/(M_{as}\omega^2 x_o)$ or $\overline{C}_F \frac{V}{fD}$ excluding the drag of the supports is about 8% lower than the corresponding measured value. When $(f_s/f) = \sqrt{2}$, the measured value of $P_d/(M_{as}\omega^2 x_o)$was $\simeq 1.04$, and consequently the actual total damping forces acting on the cylinder alone are about (8-4) = 4% below the model's prediction of one (Eqn. 8.2).

This can be attributed mainly to boundary layers, which result of a thickness of about 0.7 cm (2% of L), if considered as an equivalent step function of V^2 (see Fig. 78). This is not an unreasonable estimate considering the short length of the end plates upstream of the cylinder.

It should be noted that the factor $\frac{\overline{C}_F}{C_{DO}} \frac{f_s}{f}$ of Fig. 61, is affected neither by boundary layers nor by the additional drag of the supports because as explained in Chapter 5, both $\overline{C}_F$ and C_{DO} are affected equally by these factors. The product is nevertheless affected by blockage effects which influence $\overline{C}_F$, C_{DO} and f_s in slightly different ways. Consideration of these effects (see Appendix VI) suggests that this product may be overestimated by 3% to 7% (depending on the value of $\overline{C}_F$) with respect to the actual drag force acting on the cylinder alone.

9.1.2 Excitation forces

The excitation forces depend on C_F' which in turn is affected by blockage. It can be shown (Appendix VI) that:

$$\frac{(C_F')_m}{(C_F')_b} \simeq 1 + 3\beta$$

The ratio $P_e/(M_{as}\omega^2 x_o)$ (Eqn. 8.3) depends in addition on V^2 (Eqn. 7.30) which is affected by blockage; consideration of these effects when $(f_s/f) = \sqrt{2}$, and assuming $M_{as}\omega^2 x_o$ to be constant, leads to: (see Appendix VI)

$$\frac{(P_e)_m}{(P_e)_b} \simeq 1.045$$

i.e. the calculation of $P_e/(M_{as}\omega^2 x_o)$ overestimated it by about 4.5% when $(f_s/f) = \sqrt{2}$, due to blockage effects.

Extrapolation of C_I in Fig. 66 to $f_s/f = \sqrt{2}$, for the case here considered (Run 99), leads to $C_I \simeq 0.09$ instead of the predicted zero. This is illustrated in the phase diagram of Fig. 79 where all the hydrodynamic forces are shown divided by $M_{as}\omega^2 x_o$; three different vectors are drawn for each force, namely (1) the measured value, m, calculated from the measured values of V; (2) the actual value, b, corrected for

the effects of blockage; and the ideal value, 2-D, predicted by the two-dimensional model.

It can be seen in Fig. 79 that the ratio of the ideal (2-D) to the actual (b) values of the excitation force is approximately:

$$\frac{(P_e)_{2\text{-}D}}{(P_e)_b} \simeq \sqrt{(1.04)^2 + (1.09)^2} \simeq 1.07$$

i.e. the actual value of P_e is likely to be about 7% below the two-dimensional model prediction. It should be noted that this percentage is higher than the corresponding one for the damping forces, which can be explained by (1) the excitation forces being more sensitive than the mean drag force to disturbances in the correlation and timing of the flow patterns along the cylinder's length, and (2) by the additional disturbances of the wake caused by the supporting arms of the cylinder. Therefore if C_F' is more sensitive than $\overline{C}_F$ to three-dimensional and secondary effects, it follows that: (see Fig. 79)

$$(1 - C_I) < 1 \qquad \text{when } (f_s/f) = \sqrt{2}$$

It can then be concluded that three-dimensional and secondary effects are responsible for the failure of (f/N) and C_I to reach the values of (N_v/N) and zero respectively, predicted by the two-dimensional model.

Fig. 79 further shows that when $(f_s/f) = \sqrt{2}$ the *measured* value of C_F' is about $(7 - 4\frac{1}{2}) = 2\frac{1}{2}$ % below the ideal value predicted by the three-dimensional model. As (f_s/f) tends to one, the calculated value of C_F' depends increasingly on $\overline{C}_F(V/fD)$, which is itself progressively overestimated; consequently C_F' should also be progressively greater than $(2\pi^2 S V_r)/(1 + \frac{1}{4}V_r^2)$ as V_r increases, since $V_r = \pi S(a/D)(f_s/f)^{-1}$. This trend can be observed in Fig. 63.

9.1.3 Phase angle

Fig. 79 shows that although the prediction, $\csc\alpha = f_s/f$ (Eqn. 8.8), was approximated by the hydrodynamic model used for this research, it was not actually achieved. The proximity of the actual value of $(\alpha)_b$ to that predicted by the two-dimensional model suggests however, that in the central portion of the cylinder outside the boundary layers,

$\alpha = 135^{o}$. The total excitation force shown in Fig. 79 could then be divided into two components: (a) one with $\alpha = 135^{o}$ representing most of the excitation, and (b) the other (or a series of them) with a phase angle smaller than $(\alpha)_b$ and representing the smaller and lagging excitation in the boundary layers. It is however impossible to predict with any certainty from the results here presented, whether α would be determined by equation 8.8 in the case for example of a significantly sheared velocity profile. This question can only be answered by further research specifically concerned with this problem and which would probably require a more complex transducer and a controlled three-dimensional flow.

9.2 Engineering Applications of the Results of the Present Research

The typical flow-induced vibration problem encountered in engineering practice cannot strictly be represented by a two-dimensional model. The most important divergences between prototype structures and models of the type considered here, are: (a) the significant variations of flow velocity, flow direction and vibration amplitude along the length of a three-dimensional cylinder, and (b) the degrees of freedom in prototype structures which permit both in-line and cross-flow motion on the one hand and the excitation of higher harmonics on the other.

A potential vibration problem can sometimes be avoided at the design-stage by ensuring that the prototype never enters an instability region. If an instability region cannot be avoided a designer would attempt to predict the levels of excitation and if necessary modify the structural charactersitics to reduce the vibration. In the subsections which follows these two approaches are discussed in relation to the results of the present work.

9.2.1 Avoidance of the instability regions

Given the possibility in three-dimensional situations of cross-flow motion and excitation of higher harmonics, the avoidance of instability can only be achieved with (V/ND) values *below* those of the instability regions. The threshold of instability was identified as $(f_s/f) = 0.5$ (Chapter 4) and was shown to be influenced by ρ_r and k_s (Chapter 6); the effect of these factors however, was to increase the threshold value.

It was shown in previous chapters that the vibration in the fist instability region commenced with a double harmonic excitation which led to a local peak of the amplitude response, and which occurred for (f_s/f) values greater than 0.5. This local peak can be identified in most published amplitude response curves as shown in Fig. 32. The full-scale experiments conducted at Immingham (see Wootton et al) moreover, showed lissajous figures representing the vibration patterns in this section of the first instability region, which had a 4:1 ratio of the in-line to cross-flow vibration frequencies. Such evidence seems to be in accord with the description of the double harmonic excitation (see 8.2.3); the influence of the transverse flow associated in the present study with the distant wake, can be seen in the small amplitude cross-flow motion of the full-scale pile.

The results of the experiment at Immingham provided by Wootton [2] moreover, confirmed the observation of Chapter 6 that the vibration frequency is nearly equal to the natural frequency, N, at the onset of the first instability region.

Consequently the only condition necessary to avoid instability is:

$$\frac{V}{ND} < \frac{1}{4S} \qquad (9.1)$$

It should be noted that the curve representing the experiments conducted at Immingham in Fig. 32, commences with f_s/f values smaller than 0.5; this might be attributed to flow velocity variations along the cylinder's length, bearing in mind the small additional energy inputs which are necessary to sustain the self-excited vibration for these values of f_s/f (see 8.2.3). This interpretation also explains the gradual increase of that amplitude response curve in contrast with all the others which represent cases of uniform flow velocity profiles; the sharp (a/D) increase of these curves suggests an excess of energy, for (a/D) values below the steady state amplitude reached at that particular threshold value of (f_s/f).

Thus in order to ensure stability in cases of irregular flow velocity profiles, the maximum velocity should be considered in equation (9.1).

It should be noted that in-line vibration can in some cases

reduce the threshold values of (f_s/f), for *cross-flow* instability. This is because the excitation mechanisms associated with transverse flow and an alternate wake, induce forces in both directions (see Bishop and Hassan). Thus when ρ_r is small, the second instability region of in-line vibration can extend near to or within the instability region of cross-flow motion (see Chapter 6); this may result in considerable extensions of the cross-flow instability region towards the lower (V/ND) values. (See e.g. King).

The interaction of in-line and cross-flow excitation could be observed during the present research in the traces of vibration in the second instability region of the lightest cylinders; in one case, alternate increases of (a/D) of as much as 80% in every second cycle of oscillation were recorded. As shown in 8.1.5d the mean displacement of the cylinder, $\bar{x}$, is an approximate function of ρ_r only, consquently when ρ_r was lowest the supporting arms of the cylinder were not perpendicular to the flow direction because $(\bar{x} + x_o)$ was largest; this permitted a component of the cross-flow force to excite the cylinder. The supports of the arms had to be slightly turned to avoid this problem. The large increases of amplitude compared with the small component of the cross-flow force (slope of the arms about 1:20) indicated that in-line motion can cause large cross-flow forces, even for $(f_s/f) < \sqrt{2}$ instead of the commonly observed $(f_s/f) > 2$.

9.2.2 Prediction of cylinder behaviour

The two-dimensional models of Chapter 8 showed that all the hydrodynamic forces depend on (a/D) and/or (f_s/f). Consequently in cases where these two parameters vary along the cylinder's length, the coefficients $\bar{C}_F$ and C_F' and the angle α should vary accordingly.

For a typical flexible pile in a marine or estuarine environment moreover, the stiffness, structural damping and inertial forces of the cylinder itself act over the entire length of the cylinder; the inertial forces of the added mass however act only over that portion of the cylinder's length which is immersed in the fluid. The hydrodynamic damping and excitation forces, although acting over the entire immersed length of the pile can vary considerably with the changing flow velocity and with the variable flow patterns along the cylinder's length, especially in the quasi-static portions near the supports or

in the boundary layers.

To account for these variations in the prediction of cylinder behaviour a three-dimensional cylinder might be assumed to consist of a series of short two-dimensional cylinders, each subjected to hydrodynamic forces as predicted by the two-dimensional model from the local flow and cylinder motion characteristics. This assumption neglects the interaction between flow patterns corresponding to adjacent rings; the errors arising from this interaction are likely to diminish with decreasing gradients of either the displacement x, or the flow velocity V, with respect to the pile length L; i.e. for long piles vibrating in their first normal mode.

(a) Vibration amplitudes

A flexible pile with one or more fixed points of support can vibrate with amplitudes varying along its length from zero to some maximum value. For this reason it is necessary to know the relationship between the net excitation forces and (a/D), over the whole range of the latter in order to calculate the amplitude response of the pile.

The curves of Fig. 45 can be useful if the values of k_s are multiplied by $M_{as}\omega^2 x_o$, to give plots of the net excitation force, $\varepsilon\omega x_o = (-c\omega x_o)$ with (a/D), where ε is the net excitation or negative damping coefficient. Figure 80 presents such curves for various (f_s/f) values.

The steady-state self-excited experiments of the present research however, did not provide all the information required because of the discontinuous nature of the excitation mechanisms, hysteresis phenomena, beatings, etc. Observation of the unstable behaviour of the cylinder and analysis of Figs. 80 and 41 however, led to an approximate shape of the ($\varepsilon\omega x_o$ vs (a/D)) curves, as shown in Fig. 81 and to a tentative hysteresis diagram (Fig. 82).

The curves of Fig. 81 can be assumed to represent the variation of the excitation force along the length of a hypothetical "pinned-free" rigid cylinder immersed in a one-dimensional stream whose amplitudes of vibration are proportional to the distance from the pinned end. For such a simplified system, the curves can be replotted in the form: $(\varepsilon-c)\omega x_o$ vs (a/D) , (see Fig. 83); the resulting positive and negative

areas under the curve, which represent the energy input and output of the system respectively, should be equal in order to sustain a steady state vibration. It should thus be possible to estimate the vibration amplitudes of such a system.

Similar curves could be drawn for piles whose vibration amplitudes vary with length in a non-linear manner and interpolations could be made between the curves for the cases where f_s/f varies along the cylinder's length.

Although time did not permit the experimental confirmation of the above procedure, it should be noted that in general the portions of the cylinder whose vibration amplitude is small contribute little to the total energy exchange, since energy is in this case proportional to $(a/D)^2$. The trends of Figs. 82 and 83 thus provide a likely explanation for the partial suppression of the second instability region in the case of the "pinned-encastré" piles studied by Wootton et al (see Fig. 32); the piles' maximum (a/D) may have fallen inside the negative area ("a" in Fig 84) and the piles thus became sensitive to ε reductions occurring for lower (a/d) ("b" in Fig. 84) as f_s/f increased. In contrast are the cylinders investigated by King, which were cantilvered from the bottom of the flow channel; almost all the energy exchange in these cases took place near the water level where the maximum amplitudes occurred due to the type of deflection curve of the cylinders; consequently these were not very sensitive to ε reduction, for low (a/D) ("b" in Fig. 84) and the second instability region was extended beyond the limits of curve 1 of Fig. 32.

(b) Vibration frequencies

For the prediction of frequency response, the variations of (a/D) along the cylinder's length are not as important as in the case of amplitude response predictions; this is because when C_M is assumed equal to one, both the excitation forces and the inertial forces are in general proportional to (a/D) for a given value of (f_s/f). However, the interaction between different portions of a cylinder whose vibration amplitude changes along its length, depend on energy exchanges which are proportional to $(a/D)^2$.

One procedure for an approximate prediction of frequency response

is described below and is based on the assumptions of equations 8.2 and 8.8.

In a quarter of a vibration cycle the work done against the spring and the excitation force, $P_e\cos\alpha$, must be equal to the work done in the same quarter of a cycle by the inertial forces of the cylinder and the added mass, i.e.

$$\int_{L'} M'_{ce}\omega^2 x_o^2 dL + \int_{L'} M'_{as}\omega^2 x_o^2 dL = \int_{L'} k'_e x_o^2 dL + \int_{L'} P_e \cos\alpha x_o^2 dL \tag{9.2}$$

where M'_{ce}, M'_{as} and k'_e are the equivalent values of the mass, added mass and stiffness of the cylinder per unit length.

It should be noted that the active length of the pile, L', where the excitation forces are applied is not necessarily equal to either the full pile's length, L, or the immersed length, d; consequently the equivalent cylinder mass M'_{ce} can be given by:

$$M'_{ce} = \frac{\pi}{4} \frac{\int_L D^2 \rho_c x_o^2 dL + \int_d D^2 \rho_f x_o^2 dL - \int_{L'} D^2 \rho_f x_o^2 dL}{\int_{L'} x_o^2 dL} \tag{9.3}$$

i.e. M'_{ce} considers all the masses falling outside the active length, L', as if they were distributed within that length. The equivalent stiffness and added mass can be given by:

$$k'_e = \frac{\int_L k x_o^2 \, dL}{\int_{L'} x_o^2 \, dL} \tag{9.4}$$

$$M'_{as} = \frac{\pi}{4} D^2 \rho_f \tag{9.5}$$

where

$$k'_e = (2\pi N)^2 (M'_{ce} + M'_{as}) \tag{9.6}$$

and

$$\rho'_{r_e} = \frac{M'_{ce}}{M'_{as}} \tag{9.7}$$

Dividing equation 9.2 by $M'_{as}\omega^2$ and with the aid of equations 9.6 and 9.7, and Fig. 65:

$$\int_{L'} \rho'_{re} x_o^2 dL + \int_{L'} x_o^2 dL = \int_{L'} \frac{k'_e}{M'_{as}} \left(\frac{\rho'_{re} + 1}{\rho'_{re} + 1}\right) \frac{x_o^2}{\omega^2} \, dL +$$

$$\pm \int_{L'} \frac{P_e \cos\alpha}{M'_{as}\omega^2 x_o} \, x_o^2 \, dL$$

i.e.

$$(\rho'_{re} + 1) \int_{L'} x_o^2 dL - (\rho'_{re} + 1)\left(\frac{N}{f}\right)^2 \int_{L'} x_o^2 dL =$$

$$= \int_{L'} (1 - C_I) x_o^2 \, dL$$

hence:

$$1 - \left(\frac{N}{f}\right)^2 = \frac{\int_{L'} (1 - C_I) x_o^2 dL}{(\rho'_{re} + 1) \int_{L'} x_o^2 dL} \qquad (9.8)$$

If the flow velocity profile is known, (f_s/f) can be calculated or an initial value of it can be estimated for an iterative process; (f_s/f) together with the data of Fig. 53 or equation 8.9 give values of C_I for equation 9.8; knowledge or an estimate of the pile's deflection curve then leads to the frequency response.

The active length, L', should in general be equal to the immersed length of the pile, d, although in some cases it may be convenient to reduce it so as to consider only the portions of the pile which make the greatest contribution to the excitation; for example in cases when the flow velocity profile presents very marked three-dimensional characteristics, or when simplified estimates of the frequency response are needed.

Finally it should be noted that when the direction of the approaching stream varies along the cylinder's length, excitation in some portions of the cylinder may arise from a component of the cross-flow force (see 9.2.1).

Figure 85 shows a comparison of equation 8.9 with C_I values calculated from the data provided by Wootton[2] and corresponding to the full scale three-dimensional experiments conducted at Immingham. To calculate C_I, the variable values of (f_s/f) along the cylinder's length were averaged arithmetically; S was assumed equal to 0.23, and an equivalent mass of the pile was obtained with the aid of an equation similar to 9.3 (see Wootton et al[2]).

The figure shows that although the trend of the experimental data agrees with that of equation 8.9, there is a divergence similar to that observed in the data of the present research (Fig. 66) which was here attributed mainly to boundary layers and uncorrelated flow. In the case of Fig. 85 therefore, the divergence can be attributed mainly to (a) uncorrelated flow patterns; (b) turbulence; (c) piles surface roughness; (d) the arithmetic average value of (f_s/f) used, and (e) the variations of the direction of the flow along the pile's length which, as indicated in 9.2.1 can have a marked influence on the vibration, by allowing a mixed, cross-flow and in-line excitation.

CHAPTER 10

SUMMARY AND CONCLUSIONS

An experimental and analytical study has been conducted on the flow-induced, in-line vibration of a two-dimensional, circular cylinder in approximately one-dimensional flow.

10.1 The Non-Dimensional Frequency Parameter

In agreement with previous research reports, two instability regions and two different excitation mechanisms ("pairs" and "transverse flow") were here identified. It was observed however that the first instability region could not be associated with the pairs mechanism alone; the interacting patterns of the two excitation mechanisms led to the identification of three distinct sections in this instability region.

The commonly-used base parameter, (V/ND), was found unsatisfactory, both for a quantitative representation of the excitation and for comparing the reported behaviour of different cylinder-flow arrangements.

The large frequency variations here observed suggested that the vibration frequency, f, should appear in a more satisfactory base parameter. Moreover, the marked influence of the alternate distant wake and its tendency to adopt the Strouhal frequency suggested that the Strouhal number S should also be represented. This reasoning led to the development of a non-dimensional frequency parameter (f_s/f) which related the *actual* frequency of the vibrating cylinder to the eddy frequency which results from the interaction of the *particular* flow and (stationary) cylinder considered.

The non-dimensional frequency parameter: (a) produced a markedly improved agreement of the curves representing the response of widely differing cylinder-flow arrangements; (b) provided a simple quantitative definition of and differentiation between the two instability regions; (c) defined the flow velocity threshold of instability and could thus be helpful for avoiding vibration problems at the design stage; (d) permitted a quantitative analysis of the excitation which led to a

method for predicting the ranges and characteristics of the excitation (Chapters 6 and 9); (e) permitted a simplified theoretical model for the second instability region where for example (f_s/f) represented $(\csc\alpha)$ or $(Pe/M_{as}\omega^2 x_o)$; and (f) provided likely explanations for example for the reported absence of in-line vibration when $R_e \lesssim 10^3$.

The use of (f_s/f) rather than (V/ND) suggested moreover that R_e and other secondary factors such as turbulence, surface roughness, etc., affected the excitation only through changes in S. The results of the Immingham full-scale experiments however, suggested that in-line vibration was not affected by the marked increase of S reported for a stationary cylinder when $R_e \simeq 3 \times 10^5$ (see e.g. Walshe and Wootton), but it appeared that for a vibrating cylinder S has an approximately constant value independent of R_e. In this context moreover, the experiments with the splitter plate showed a sharp fall of the (a/D) vs (f_s/f) curve at which point the wake narrowed slightly and became fully turbulent; this behaviour which resembled that of a stationary cylinder and its wake when $R_e \simeq 3 \times 10^5$, occurred at a fixed value of (f_s/f) for given k_s and independently of R_e.

It thus appeared that for $R_e \gtrsim 10^3$ the excitation is not significantly affected by R_e but rather by the *fluctuating* inertial and viscous flow forces; these forces seemed to be strongly influenced by the ratios of the fluctuating velocities and accelerations of the flow with respect to those of the cylinder, and such ratios are determined by (a/D) and (f_s/f), rather than R_e ~~(see e.g. Appendix VIII).~~

Some novel characteristics of in-line vibration were observed which, in addition to (f_s/f) contributed to the definition of and distinction between the instability regions. For examples: (a) the new type of wake (Plates 8a and 8b) observed in the second instability region or in the double harmonic excitation section of the first, was different from the Von Kàrmàn form (Plate 6a) previously thought to prevail in those circumstances; the Von Kàrmàn form however was observed to prevail in the wake of the lock-in section (Plate 7a) or in the distance wake of the rearrangement section (Plate 6b) of the first instability region; (b) the marked increases observed in C_{DA}/C_{DO} (previously assumed = 1.0) associated with the transverse flow excitation mechanism; (c) an observed increase of f/N (was larger than any

previously reported)starting from 1.0 at the onset of both instability regions and reaching (N_v/N) in the second; (d) a relationship between f and f_e has been identified which showed "frequency lock-in" in two sections of the first instability region and throughout the second; and (e) the non-sinusoidal vibration observed at the onset of the first instability region, the analysis of which led to the association of the corresponding peak of the (a/D) vs (f_s/f) curve with a "double harmonic excitation".

10.2 Density and Damping

From an analysis of density and damping it was concluded that they affected the cylinder behaviour independently and in different ways: ρ_r determined the frequency response and k_s the amplitude response, while for given values of (f_s/f), ρ_r did not affect (a/D) nor did k_s affect (f/N).

The ranges of flow velocity where instability could occur however were determined by both ρ_r and k_s. The stability parameter k_s was found to determine the instability ranges in terms of (f_s/f) (Fig. 49), but the same ranges in terms of flow velocity [say in terms of (V/ND) = (f_s/f)(f/N)/2S] were also affected by (f/N) and consequently by ρ_r; the density, ρ_r, thus determines the relationship between the instability ranges in terms of (f_s/f) and the same ranges in terms of the flow velocity.

The different and independent rôles played by density and damping thus indicate that in contrast to aerodynamic practice, where they are often considered together and where frequency variations are negligible, for flow-induced, in-line vibration in *water*, density and damping should be considered separately.

Consideration of the most common parameters used to represent damping led to a redefinition of the stability parameter, k_s, in terms of c and f rather than δ and N; the newly defined k_s was independent of ρ_r, and was therefore suited to represent the independent influence of external damping on the excitation.

In contrast with previous research reports where external and hydrodynamic damping have been considered together and extrapolated from still water measurements, only *external* damping (mainly structural)

was here considered for the determination of k_s; this was done because it was felt that *hydrodynamic* damping formed an integral part of the total hydrodynamic forces and so should be dealt with separately.

The clearer definition of density and external damping, and of their independent influence on the excitation, thus led to correlations (the first for in-line vibration to the knowledge of the author) between (i) ρ_r and (f/N); (ii) k_s and (a/D); and (iii) k_s and the ranges of (f_s/f) where instability can occur. These correlations and a knowledge of f_s/f, ρ_r and k_s provided a technique for predicting whether in-line vibration could occur, and if so, for predicting the ranges and characteristics of the motion for two-dimensional cylinder-flow arrangements.

Novel characteristics were identified in connection with the frequency response of the cylinder. For example: (a) the frequency in the second instability region tended to the value of the natural frequency in air (or in vacuo N_v); (b) (f/N) varied approximately linearly with (f_s/f) and the slope of the curve was a function of ρ_r alone; (c) the high (f/N) values corresponded to (V/ND) values larger than 6.

In association with (a/D), the following was observed: (a) there existed a unique value of (a/D) for every value of k_s independently of (f_s/f) over most of the second instability region; (b) in the first instability region different values of (a/D) corresponded to each (f_s/f) when k_s remained constant, although all the (a/D) vs k_s curves had similar shapes; (c) the damped (a/D) relative to its undamped value for the same (f_s/f) in the first instability region however, was found to generate a unique relationship with k_s for all values of (f_s/f) (Fig. 46).

The empirical correlations mentioned above were applicable to two-dimensional stituations only. To improve the understanding of this type of vibration and to widen the applicability of the results of this research, hydrodynamic forces were then considered. Hydrodynamic parameters were sought which should be independent of cylinder characteristics such as ρ_r and k_s, for purposes of developing a theoretical model which would incorporate the hydrodynamic characteristics of the excitation.

10.3 Hydrodynamic Forces

To facilitate its analysis the measurable total hydrodynamic force was divided into components: added mass, hydrodynamic damping and excitation forces.

A variable mass coefficient which would be responsible for the frequency variations was considered and rejected because it was difficult to explain : (a) the absence of intertial forces when $f = N_v$, and (b) the constancy of the phase angle of the excitation force.

A constant mass coefficient was adopted because (a) it permitted the attribution of frequency variation to the fluctuating drag forces and their phase relationships; (b) a value of $C_M = 1.0$ was confirmed for $(f_s/f) < 0.5$; (c) a constant mass coeffficient allowed for a variable phase angle which was suggested by the difference between the characteristic frequencies f_s and N;and (d) it facilitated further analysis of the excitation leading to the simplification of the theoretical model for the second instability region.

It was argued that hydrodynamic damping could not be extrapolated from measurements in still water because (a) it was observed to vary with (f_s/f) and (a/D) ,for $(f_s/f) < 0.5$; (b) the flow patterns appeared very different in the two situations; and (c) in still water the damping was mainly viscous while in flowing water it was mainly due to pressure forces associated with separated flow.

Hydrodynamic damping was thus expressed in terms of the mean drag force which included both pressure and friction forces.

To represent the excitation forces, the total drag force was expressed in terms of a force coefficient, consisting of a mean and a fluctuating part; to generate the frequency variations a variable phase angle between the fluctuating force coefficient and the cylinder motion was introduced, and to reproduce the behaviour of $\bar{x}$, the mean part was also allowed to vary.

The resulting model (Eqns. 7.23 and 7.24) represents the excitation in terms of (a) flow parameters; (b) cylinder motion and geometry; and (c) force coefficients and a phase angle which are independent of cylinder characteristics such as ρ_r and k_s.

For the second instability region, the flat top of the (a/D) vs (f_s/f) diagram permitted a significant simplification of the theoretical model for two-dimensional cases. For this simplified model: (a) the total damping force is equal in magnitude to the inertial force of the added mass; (b) the excitation force, P_e, is equal to the inertial force of the added mass multiplied by (f_s/f); (c) the cosecant of the phase angle, α, is equal to (f_s/f); (d) the product $[(\overline{C}_F/C_{DO})(f_s/f)]$ is a function of (a/D) only, and (e) the coefficient C_F' is directly proportional to V_r ($C_F' \simeq 4V_r$).

The hydrodynamic forces and their phase relationship in the second instability region are thus determined by $M_{as}\omega^2 x_o$ and (f_s/f) only, which further confirmed the usefulness of the adoption of (f_s/f) and of ($C_M = 1$). The force coefficients and the phase angle on the other hand were found to be independent of ρ_r and k_s and this confirmed the validity of the theoretical model to represent the excitation.

The model also resulted in equation 8.9 which gives C_I as a function of (f_s/f) only and which permits a more accurate and theoretically more sound prediction of the frequency response in the second instability region. Although the amplitude response could also be predicted, the accuracy obtained was not good enough to improve the empirical relations of Chapter 6.

When any one of the conditions: (a) $N < f < N_v$; (b) $1 < (f_s/f) < \sqrt{2}$ or (c) $90^o < \alpha < 135^o$, was given, the model predicted the other two, although the model itself did not predict the limits of the excitation. It was thought that these limits may arise mainly from the sensitivity of the wake to variations in the magnitude, frequency and timing of its power (or vorticity) supply.

The complex excitation mechanisms of the first instability region did not allow either a simplification of the theoretical model or any accurate prediction of cylinder response. The behaviour of the hydrodynamic forces as predicted by the model however, permitted a qualitative analysis which improved the understanding of the excitation.

From the experiments conducted with the splitter plate, it was concluded that for the "pairs mechanism" the variation of the drag force depended on: (a) V_r through its influence on the magnitude and time distribution of the vorticity supply to the wake (and hence eddy-strength);

(b) the motion of the separation points and the fluctuating width of the wake, which were themselves determined by the acceleration ratio $(a/D)(f_s/f)^{-2}$; (c) the energy extracted from the stream per vibration cycle, which is approximately proportional to (f_s/f); and d) the distance between consecutively shed eddies which is proportional to (f_s/f). The phase angle, α, appeared to be determined by the distance between consecutively shed eddies and hence by (f_s/f).

The results of these experiments however did not provide precise correlations except for the angle, α, which appeared to be a function of (f_s/f) alone.

Similar trends could be observed without the splitter plate in the rearrangement and lock-in sections of the first instability region, although in these latter cases the interaction between excitation mechanisms influenced the behaviour of $\overline{C}_F$, C_F' and α as follows: (a) two slightly different α vs (f_s/f) trends appeared before and after the abrupt fall of the corresponding (a/D) vs (f_s/f) curves; (b) different C_F' vs (a/D) curves, showing two distinctive trends each, corresponded to every (f_s/f) value, although all the curves had similar shape (Fig. 76); (c) in general $\overline{C}_F$ increased when the transverse flow mechanism was most effective, i.e. with low (a/D) values in the rearrangement section or with high (a/D) values in the lock-in section (Fig. 60).

The transition between these two sections of the first instability region occurred consistently when $(f_s/f) \simeq 0.85$. In contrast to this the sharp fall of (a/D) occurred earlier in terms of (f_s/f) the smaller the (a/D); this was attributed to the lower V_r values due to low (a/D), which resulted in a more uniform (less organized) vorticity supply to the wake; in consequence the wake itself became more turbulent. Since (a/D) reductions were caused by increased k_s, the above argument explained the reduction of the instability regions with increasing k_s.

The small local peak of the (a/D) vs (f_s/f) curve at the beginning of the first instability region was here attributed to the excitation of the two harmonic components of a non-sinusoidal motion. These components of excitation were supplied by the "pairs" and the "transverse flow" excitation mechanisms as was evident from: (a) the observation of both pairs and transverse flow in the near wake; (b) marked increases of C_{DA} which occurred elsewhere in association with

the transverse flow mechanism; (c) the coincidence of the frequency of pairs of eddies with the main vibration frequency of the cylinder; and (d) the coincidence of the frequency of single eddies in the distant wake with the frequency of increase of (a/D) in alternate vibration cycles.

The 2:1 frequency ratio here observed suggested a 4:1 ratio between the frequency of the main, in-line motion and the frequency of a fluctuating cross flow force associated with the transverse flow mechanism; this explained the lisajous figures representing the motion of the full scale Immingham piles for $(f_s/f) \simeq 0.5$, which exhibited the same frequency ratio.

10.4 Practical Applications and Conclusion

Analysis of the results of the experiments here conducted showed that these were only slightly affected by three-dimensional and other secondary factors. Consideration of such factors moreover, reinforced the assumptions made and the conclusions arrived at in the analytical work; for example consideration of boundary layers and blockage provided a reasonable explanation for the differences between predicted and recorded values of f/N (and consequently of V/ND). The correlations and models obtained here can thus be considered to represent the excitation in two-dimensional cylinder-flow arrangements.

The characteristics of the excitation observed in the two-dimensional arrangements moreover, appeared to be common to all situations; this was illustrated by the improved agreement between the amplitude response curves of different two and three-dimensional arrangements when plotted against (f_s/f) rather than (V/ND); by the predicted frequency response of the Immingham piles; or by the resemblance of the (a/D) vs k_s curves here obtained to those obtained by Wootton for three-dimensional model stacks.

The arguments and prediction procedures of Chapters 6 and 9 have further shown that full scale, three-dimensional vibration problems can be represented and predicted by the two-dimensional models here developed, if the appropriate values of (f_s/f), ρ_r and k_s, and the specific three-dimensional and secondary factors are considered.

It can thus be concluded that the outcome of this research:

(a) Provides a designer attempting to avoid vibration with a more accurate and reliable flow velocity threshold-value than has hitherto been available.

(b) Provides designers and engineers with the means to make preliminary predictions of amplitude and frequency response, mean deflections and the flow velocity ranges where instability can occur, in any case of flow-induced in-line vibration of circular cylinders.

(c) Allows engineers faced with existing vibration problems to make a better interpretation of an observed vibration than was hitherto possible, for example by expecting (f/N) and (C_{DA}/C_{DO}) to vary rather than to remain constant, or by having additional ways to define more precisely the type of the observed instability, etc.

(d) Allows a researcher or engineer dealing with two-dimensional cylinder-flow arrangements to predict fully the in-line excitation.

(e) Correlates the observations of previous researches and thus increases their usefulness.

(f) Increases the reliability, flexibility and usefulness of modelling techniques in this field by showing that quantitative similarity does exist between two-dimensional laboratory models and three-dimensional prototypes, and by improving the similarity criteria, e.g.: (f_s/f) rather than (V/ND) and R_e, or ρ_r *and* k_s rather than ($2M\delta/\rho_f D^2 L$).

(g) Permits a clearer definition and an improved understanding of the characteristics and limits in general of this type of excitation.

Finally, the present work has indicated areas for further study: (a) the interaction of excitation mechanism in the first instability region; (b) a more precise investigation of the influence of three-dimensional and secondary factors on the excitation; (c) the development of a similar theoretical model for cross-flow vibration; (d) studies of the wake in the second instability region and the wake of a cylinder with a splitter plate; and (e) interactions between in-line and cross-flow excitation.

APPENDIX I

APPARATUS AND EQUIPMENT DETAILS

(a) Flow velocity measurements

(1) Propeller meter: KENT-LEA, Miniflo-probe 265-3, Low speed.

(2) Pulse counters: Novar, Stream Flow. Kent, Mini-Flowmeter Dekatron Counter unit, type 176-2.

(3) Range: 4 cm/s to 150 cm/s.

(b) Vibration amplitude and frequency measurements

(1) Strain gauges: four wire, Post Yield, gauges, type YL-10 (Tokio Sokki Kenkyujo Co. Ltd.).

(2) Transducer-amplifier: Peekel, Strain gauge instrument type 581 DNH.

(3) Recorder: S.E., Oscillograph 3006;and U.V. Recorder Type 1185, Mark 2, (New Electronic product Ltd.).

(4) Ranges: Amplitude magnification factors greater than 500 available; trace paper speeds up to 25 cm/s, with up to 10 reference marks per second.

(c) Wake frequency measurements

(1) Dye: Potasium permanganate.

(2) Cronometer: Jonghans 0.1 sec/Smiths 0.2 sec.

(3) Range: up to 3 eddies/second could be reliably measured.

(d) Gaps measurement

(1) Moore & Wright, Feeler gauge 492.

(2) Range: 0.004 cm to 0.2 cm.

(e) Viscous damping

(1) Solution of Lyle's Golden Syrup in water.

(2) Range: K'_{so} values of up to 5 were obtained.

APPENDIX II

EXPERIMENTAL DATA

The tests of the first set were conducted with the larger cylinder (D = 3.38 cm, L = 33 cm); the damping mechanism was not used in these tests; the depth of water was kept greater than 30 cm; the gaps between the ends of the cylinder and the end plates were of approximately 0.5-2 mm. The most important data of these tests are given in Table II-1.

The tests of the second set were conducted with the smaller cylinder (D = 2.5 cm, L = 33 cm); the water depth was kept above 33.5 cm; the distance from the cylinder to the channel's bottom, z , was kept constant at 13 cm; in general the gaps between the ends of the cylinder and the end plates were smaller than one millimeter. For the second set of tests a constant head tank was installed at the entrance of the channel (Fig. 7); the variations of the resulting flow velocity profiles did not exceed ±3% of the average anywhere in the cross section of the flume at the cylinder's location, except at the boundary layers (10 sec averages considered). The most important data of these tests are given in Table II-2.

Besides calibration of the transducer measurements were made of ρ_c, N_{air}, c, M_a, ρ_r and N before and after every test. Each test comprised measurements of V, f, a, $\bar{x}$ and f_e for 20 to 70 different values of V. The flow was allowed to settle for 3-15 min; V was measured over 1 to 15 min; f was obtained from records lasting 50-100 sec and (a/D) and $\bar{x}$ from records lasting 1 to 3 minutes; f_e was obtained from several counts each lasting about one minute.

Run No.	(a) ℓ (cm)	cylinder filling	(b) ρ_r	k'_{so}	(b) δ_w	(b) N_{air} (Hertz)	(b) N (Hertz)	(c) z (cm)	splitter plate
18	8.0	air	0.495	0.025	0.163	5.20	2.80	17.3	No
22	12.0	air	0.495	0.016	0.150	3.95	2.15	13.1	No
30	16.0	air	0.492	0.013	0.190	3.31	1.80	17.3	No
34	8.0	water	1.049	-	0.120	3.45	2.40	17.0	No
36	12.0	water	1.084	-	0.106	2.76	1.91	13.2	No
39	9.9	water	1.046	-	0.110	3.09	2.13	15.2	No
44	16.0	water	1.042	-	0.140	2.33	1.57	15.0	No
49	9.0	sand	1.460	0.015	0.087	2.84	2.10	16.1	No
58	9.0	sand	1.529	-	-	2.78	2.08	16.0	Yes
60	12.0	air	0.529	-	0.170	3.80	2.13	13.0	Yes

Table II-1 Experimental data for the first set of tests (D = 3.38cm)

Notes: (a) ℓ = free length of cantilevered springs

(b) measured with splitter plate when applicable

(c) z = distance from cylinder's centre-line to channel's bottom

Run No.	(a) ℓ (cm)	cylinder filling	(b) ρ_r	(d) c_{air} gr-s/cm	(c) c_o gr-s/cm	k'_{so}	(c) δ_w	(b) N_{air} Hertz	(b) N Hertz	splitter plate
73*	12.80	air	0.634	0.0239	0.0285	0.0557	0.1565	4.148	2.429	No
77*	9.70	glass bids	1.805	0.0388	0.0492	0.1030	0.1098	2.945	2.272	No
80*	6.35	iron scrap	4.224	0.1127	0.1235	0.2749	0.0780	2.417	2.139	No
84*			4.398	0.1156	0.1500	0.3378	0.0860	2.387	2.112	Yes
85+			4.455	0.5879	0.5987	1.3316	0.2030	2.418	2.138	No
86			4.372	0.2035	0.2143	0.4768	0.1018	2.416	2.140	No
87			4.423	0.2298	0.2406	0.5350	0.1082	2.419	2.140	No
88			4.432	0.2643	0.2752	0.6118	0.1183	2.419	2.140	No
89			4.467	0.1896	0.2240	0.5007	0.1055	2.405	2.128	Yes
90			4.429	0.3037	0.3381	0.7550	0.1345	2.405	2.130	Yes
91			4.457	0.1610	0.1954	0.4361	0.0969	2.399	2.131	Yes
92+			4.462	2.3710	2.4050	5.3510	0.7150	2.414	2.138	Yes
99*	12.5	plastic scrap	1.222	0.0214	0.0292	0.0632	0.1284	3.118	2.193	No
101			1.229	0.1281	0.1359	0.2945	0.1930	3.129	2.196	No
102			1.209	0.2246	0.2324	0.5024	0.2509	3.122	2.199	No
103+			1.224	0.7070	0.7179	1.5574	0.5710	3.116	2.192	No
104			1.213	0.2659	0.2737	0.5906	0.2738	3.125	2.202	No
105			1.207	0.3217	0.3294	0.7104	0.3070	3.127	2.206	No
107			1.279	0.3230	0.3544	0.7754	0.3190	3.055	2.174	Yes
108			1.249	0.2328	0.2642	0.5780	0.2745	3.061	2.174	Yes
109+			1.253	0.5389	0.5703	1.2470	0.4580	3.065	2.175	Yes
110*			1.253	0.0239	0.0553	0.1207	0.1369	3.065	2.179	Yes
111			1.253	0.0721	0.1035	0.2264	0.1667	3.053	2.174	Yes
112			1.253	0.1637	0.1951	0.4274	0.2217	3.057	2.171	Yes

Table II-2 Experimental data for the second set of tests (D = 2.5 cm)

Notes: (a) ℓ = free length of cantilevered springs

(b) measured with splitter plate and additional damping if any

(c) for f = N; (a/D) = 0.055; includes the hydrodynamic damping of the splitter plate if any

(d) includes additional damping if any but excludes hydrodynamic damping of the splitter plate

* no additional external damping

\+ (a/D) < 0.05

APPENDIX III

ADDED MASS, DENSITY AND STIFFNESS

Before and after each test the cylinder was made to oscillate in air, on its own and with known weights added, as well as in still water. This permitted calculation of added mass, equivalent density and equivalent stiffness as outlined below.

If the subscript (1) indicates cylinder on its own and the subscript (2) indicates cylinder with additional masses, ΔM:

$$2\pi N_1 = \sqrt{\frac{k_1}{M_{c_1}}} \quad \text{and} \quad 2\pi N_2 = \sqrt{\frac{k_2}{M_{c_2}}} \tag{III-1}$$

where

$$k_2 = k_1 + \Delta k \tag{III-2}$$

$$M_{c_2} = M_{c_1} + \Delta M \tag{III-3}$$

Δk is the increment of k due to gravitational forces, and can be calculated from the formula of the natural frequency of a pendulum, N_p, i.e. (see e.g. Den Hartog)

$$N_p = \frac{1}{2\pi} \sqrt{\frac{g}{R}}$$

where g is the acceleration of gravity and R is the length of the pendulum. This formula can also be expressed as:

$$N_p = \frac{1}{2\pi} \sqrt{\frac{k_p}{M_p}}$$

where M_p is the pendulum mass and k_p is the equivalent "stiffness" of the pendulum, given by

$$k_p = \frac{g}{R} M_p$$

Thus an increment of M corresponds to a proportional increment of k, since g and R are constants; therefore

$$\Delta k = \frac{g}{R} \Delta M$$

From equations III-1/2/3:

$$M_{c_1} + \Delta M = \frac{k_1 \frac{M_{c_1}}{M_{c_1}} + \frac{g}{R} \Delta M}{(2\pi N_2)^2}$$

dividing by ΔM and introducing $(2\pi N_1)$ from equation(III-1):

$$\frac{M_{c_1}}{\Delta M} + 1 = \frac{(2\pi N_1)^2 \frac{M_{c_1}}{\Delta M} + \frac{g}{R}}{(2\pi N_2)^2}$$

solving for M_{c_1}:

$$M_{c_1} = \Delta M \left[\frac{1 - \frac{g}{(2\pi N_2)^2 R}}{(N_1/N_2)^2 - 1} \right] \qquad \text{(III-4)}$$

The value of R can be estimated approximately by assuming the deflection curve of the spring to be given by:

$$Y = Y_o(1 - \cos \frac{\pi}{2\ell} Z)$$

i.e. a quarter sinusoid where Y indicates deflections; Y_o is the maximum deflection (at the tip); Z is the distance from the clamp along the undeflected cantilever; and ℓ is the total cantilever's length.

It can be assumed that the radius of curvature of the oscillation path of the canitlever's tip, is given by $(\ell - b)$; where b is the Z axis intercept of the tangent at $Z = \ell$; the tangent of the angle, θ, at $Z = \ell$ is

$$\tan\theta = \frac{dY}{dZ} = Y_o \frac{\pi}{2\ell} \sin \frac{\pi}{2\ell} Z$$

$$(\tan\theta)_{z=\ell} = Y_o \frac{\pi}{2\ell}$$

hence

$$(\ell - b) = \frac{Y_o}{(\tan\theta)_{z=\ell}} = \frac{2\ell}{\pi}$$

The equivalent pendulum length of the cylinder, R, is then given by

$$R = d + \frac{2\ell}{\pi} \qquad \text{(III-5)}$$

where d is the length of the stiff portion of the supporting arms (see Fig. 5).

Equation(III-4) above cannot be used to calculate the equivalent density of the cylinder because this density should also include the additional added mass of the supporting arms and of the end gaps, which cannot be included in M_{as} if $C_M = 1$.

If N_2 in equation (III-4) is replaced by the natural frequency in still water N, and the additional mass, ΔM, by the total added mass, M_{aT}, equation (III-4) can be written thus:

$$M_{aT} = M_{c_1} \left[\frac{(N_1/N)^2 - 1}{1 + \frac{g}{(2\pi N)^2 R}} \right] \qquad \text{(III-6)}$$

Values of M_{aT} obtained from this equation resulted about 4% higher than the product of ρ_f and the volume of the cylinder alone; this applied both to still water and slowly flowing water in the range $0 < (f_s/f) < 0.4$.

To investigate the influence of the supporting arms, end gaps, free water surface and channel's bottom on M_{aT}, the cylinder was allowed to oscillate in still water at different depths and with different water levels, end gaps and frequencies which covered the ranges of the flow-induced vibration tests.

In general M_{aT} was observed to decrease as the cylinder approached the free water surface and to increase as the cylinder approached the channel's bottom. No variations of M_{as} greater than ±2% were observed (a) when the cylinder was more than 2.5 diameters above the channel's bottom and more than 4.5 diameters below the water surface, or (b) when the end gaps were varied between 0.01 cm and 0.5 cm.

Although these experiments showed all these influences to be small within the ranges of the main tests, their results did not suggest any values for the contributions to M_{aT} of the arms and of the end gaps.

It was decided to assume $C_M = 1$ in order to facilitate further calculations, and thus to attribute the slight increases of M_{aT} above $(\pi D^2 L \rho_f/4)$ to the added mass of the arms and of the end gaps.

The density ratio ρ_r could then be calculated from:

$$\rho_r + 1 = \frac{M_c + M_{aT}}{\frac{\pi}{4} D^2 L \rho_f} \qquad \text{(III-7)}$$

where $M_c + M_{aT} = M_{TS}$. If $C_M = 1$, $M_{TS} = M_c + M_{as}$ where $M_{as} = \frac{\pi}{4} D^2 L \rho_f$ and $M_c = M_{as}\rho_r$.

The stiffness could then be calculated from:

$$k = M_{TS}(2\pi N)^2 \qquad \text{(III-8)}$$

The values of k obtained through this dynamic approach were compared with direct static measurements made by pulling the cylinder horizontally with a string, which after passing around a pulley, held known weights. The displacement of the cylinder was measured with either a travelling microscope or from the traces of the U.V. recorder. The travelling microscope readings showed a wide scatter with an average value of k about 10% higher than the one obtained from equation III-8. The U.V. recorder readings were less scattered and showed k values about 2% higher than those of equation (III-8). As these methods were static however, it was felt that the dynamic method of equation (III/8) was more representative of the vibrating conditions and was therefore adopted.

APPENDIX IV

MEASUREMENT OF S AND C_{DO}

Auxillary experiments covering the entire V range of the main tests, were conducted to investigate the behaviour of S and C_{DO} when the cylinder remained stationary. For this purpose the cylinder was heavily damped ($k_s > 1.0$) so as to avoid vibration but to allow the displacement, $\bar{x}$, due to the drag forces.

Knowedge of $\bar{x}$ and of k and V led to the values of C_{DO}, while the values of S were obtained from a count of the eddies in the wake in a given period of time. The resulting values of S and C_{DO} are shown in Figs 33 and 86.

It should be noted that these values of C_{DO} are affected by the additional drag of the supporting arms (see Appendix V) and by the reduced drag in the boundary layers (see 9.1) and that both S and C_{DO} are affected by blockage effects, surface roughness, flow velocity measurement technique, etc. (see Chapters 5 and 9 and Appendix VI).

For the larger cylinder (D = 3.38 cm), C_{DO} could not be measured because the damping mechanism was not yet devised when these tests were conducted; values of S were obtained by reducing to zero the gaps at the ends of the cylinder so as to avoid its motion.

APPENDIX V

DAMPING

The values of the external damping parameter k_s to be used in flowing water, were obtained from the records of transients in air (see 6.2.3d); consequently the following sources of damping had to be considered: (1) structural, (2) viscous damping mechanism, (3) aerodynamic, (4) gaps between the ends of the cylinder and the end plates, (5) supporting arms, and (6) splitter plates.

Each one of these is considered below separately and leading to a corresponding value of c (calculated with data from run 99). The contributions of all these sources to the total damping are considered in V-7.

V-1 Structural Damping

For every fixed length of the cantilevered springs of the cylinder's supports, the cylinder was made to oscillate in air with different weights added to it, so as to vary its frequency over the entire range predicted for flow induced vibration. The values of c_{air} were obtained from the logarithmic decrement δ_{air} of the recorded transients and from the formula:

$$c_{air} = 2\delta_{air} N_{air}(M_c + \Delta M)$$

where M_c was obtained as indicated in Appendix III; ΔM is the additional mass, and N_{air} is the natural frequency in air of the cylinder with the additional mass if any. Care was taken to place the additive masses at the same height as the centre line of the cylinder. Additional experiments with heavy masses placed near the springs (about 1/3 of the distance from the clamp of the springs to the cylinder) showed no significant difference in the behaviour of c_{air} with respect to (a/D) or (f/N).

These experiments resulted in the relationships of Figs. 87 and 88 which are applicable to Runs 73 to 111 (see Table II-1) and where the values of c_{air} include aerodynamic damping (see V-3 and V-7).

Figure 87 which presents c_{air} variations with (a/D), was obtained from measurements of δ_a at different amplitudes but for constant frequency; corrections were made to allow for noise in the recorded signal. Figure 88 which presents c_{air} variations with (f/N), was obtained from measurements of δ_a at the same amplitude of vibration but for different frequencies. The approximate inverse relation between c_{air} and (f/N) (Fig. 87) suggested hysteretic damping; a better approximation to $(c\omega/k)$ = constant was obtained when the gravitational effects were excluded from k. These gravitational effects however, together with the variations of c_{air} with (a/D) and especially the viscous damping of the mechanism made the term $(c\omega/k)$ irrelevant for the present research.

V-2 Damping Mechanism

Experiments were also conducted to investigate the behaviour of the viscous damping parameter, c_v, which represented the contribution of the damping mechanism. No significant variations of c_v with either (a/D) or (f/N) were observed; in addition c_v was approximately constant for up to 16 hours.

V-3 Aerodynamic Damping

Bramley has shown that for small "size numbers" (ND^2/ν) the fluid dynamic damping force on a cylinder oscillating in a still fluid can be give by:

$$c_{aero}\ \omega\ x_o$$

where:

$$c_{aero} = (M_a)_{aero}\ 2\pi N_{air} K'$$

and:

$$K' = 2\sqrt{\frac{4}{\pi \frac{N_{air} D^2}{\nu_{air}}} + \frac{4}{\pi \frac{N_{air} D^2}{\nu_{air}}}}$$

Assuming: $\nu_{air} \doteq 0.15\ cm^2/s$ and $\rho_{air} \doteq 1.23 \times 10^{-6} gr\text{-}s^2/cm^4$

$D = 2.5$ cm; and $N_{air} \doteq 3.123$ c.p.s. (Run 99):

$$c_{aero} = 0.0008 \text{ gr/cm/s.}$$

V-4 End Gaps

To estimate the damping in still water due to the gaps between the cylinder and the end plates, viscous friction drag forces can be estimated from a consideration of the flow, between two parallel flat plates, due to the motion of the plates as follows (see Schlichting):

The flow velocity in the direction of the cylinder motion can be represented by:

$$U = U_o A \sin(\omega t + \xi)$$

where: $U_o = \omega x_o$

$$A = (B/C)^{\frac{1}{2}}$$

$$B = \cosh(2Ky) - \cos(2Ky)$$

$$C = \cosh(2Kh) - \cos(2Kh)$$

y is the coordinate perpendicular to the end plates; h is the width of the gap and

$$K = (\omega/2\nu)^{\frac{1}{2}}$$

$(\omega t + \xi)$ is not a function of y (see Schlichting), therefore:

$$\frac{\partial U}{\partial y} = U_o \frac{\partial A}{\partial y} \sin(\omega t + \xi)$$

$$\frac{\partial A}{\partial y} = \tfrac{1}{2}(BC)^{-\frac{1}{2}} \frac{\partial B}{\partial y}$$

$$\frac{\partial B}{\partial y} = 2K[\sinh(2Ky)] + 2K[\sin(2Ky)]$$

hence: $$\frac{\partial U}{\partial y} = 2KU_o \frac{\sinh(2Ky) + \sin(2Ky)}{2\sqrt{BC}} \sin(\omega t + \phi)$$

At the surface of the cylinder end, y = h, and B = C; assuming $\sin(\omega t + \xi) = 1$, the maximum gradient is:

$$\left| \left(\frac{\partial U}{\partial y}\right)_{y=h} \right|_{max} = K\omega x_o \left[\frac{\sinh(2Kh) + \sin(2Kh)}{\cosh(2Kh) - \cos(2Kh)}\right] = K\omega x_o \lambda$$

the drag force then results

$$\text{Drag} = \mu \times \text{Area} \times \frac{\partial U}{\partial y} = \frac{\pi}{4} D^2 \rho_f \nu K \omega x_o \lambda$$

and the damping constant results

$$c_{gap} = \frac{\text{Drag}}{\omega x_o} = \frac{\pi}{4} D^2 \rho_f \nu K \lambda$$

for gaps larger than 0.03 cm in water $\lambda \simeq 1$; the value of c_{gaps} for two gaps in water results:

$$c_{gaps} \simeq 0.28 \times 10^{-3} D^2 \sqrt{f} \qquad (gr/cm/s)$$

Assuming D = 2.5 cm and f = 2.2 c.p.s. (Run 99):

$$c_{gaps} \simeq 0.0026 \qquad (gr/cm/s)$$

An analysis of the recorded transients of the cylinder oscillating in still water, with various sizes of gaps ranging between 0.02 cm and 0.5 cm, revealed no significant differences in the logarithmic decrement for frequencies above 2 c.p.s. In flowing water and for fixed values of (f_s/f), ρ_r and k_s, no significant variations of (a/D) were observed when the gaps were varied.

V-5 Supporting Arms

The damping arising from the additional drag forces exerted by the flow on the supporting arms of the cylinder was not included in external damping because these forces (a) were part of the actual drag force, (b) contributed to the mean displacement, $\bar{x}$, (c) varied

approximately as the mean drag force of the cylinder (proportionally to V^2) rather than as the other external damping forces (proportionally to ωx_o), (d) were difficult to calculate precisely, and (e) compensated part of the loss of drag due to boundary layers, uncorrelated flow patterns, etc., which was not deducted from the values of C_{DO} and C_{DA}. It was thus felt more important to know the actual value of the total drag force which could be measured and to consider the drag of the supports together with three-dimensional factors separately.

For flowing water these drag forces were calculated by assuming a drag coefficient for the arms of $C_D = 1.5$ (and their area presented to the flow); the forces were reduced by a third becuase their resultant was applied at a distance from the clamped end of the supports, approximately equal to two thirds of the total length of the arms. Assuming an average value of $C_{DA} = 1.5$:

$$\frac{(\text{Drag})_{\text{arms}}}{(\text{Drag})_{\text{cyl.}}} = \frac{(\frac{1}{2}\rho_f V^2) \times 2 \times (20 \times 0.1) \times 1.5}{(\frac{1}{2}\rho_f V^2) \times (33 \times 2.5) \times 1.5} \times \frac{2}{3} \simeq 1.5\%$$

To calculate the damping forces due to the arms in still water, a similar argument to that of V-4 leads to:

$$\text{Drag} = \rho_f \nu \times \text{Area} \times K\omega x_\ell \lambda$$

where $\lambda = 1$; and x_ℓ is the displacement of the cylinder at a distance, ℓ, along the arms from the clamp. The area of the tapered arms used for the 2.5 cm cylinder is given by:

$$\text{Area} = b\ell \simeq \ell(3 - 0.06\ell)$$

and the displacement of the arms in the direction of motion at a distance, ℓ, from the clamp is given by:

$$x_\ell \simeq \frac{x_o}{40} \ell$$

where 40 is the distance in cm from the clamp to the cylinder. The moments at the clamp due to the drag forces are

$$M = \text{Drag} \times \ell$$

and

$$dM \simeq [\rho_f \nu K \frac{\omega x_o}{40}]\, d[\ell^3(3 - 0.06\ell)]$$

therefore:

$$M \simeq [\rho_f \nu K \frac{\omega x_o}{40}] \int_{20}^{40} (9\ell^2 - 0.24\ell^3)d\ell$$

i.e. only 20 cm of the arms are immersed in water; M then results.

$$M \simeq [\rho_f \nu K \frac{\omega x_o}{40}]\, 24 \times 10^3$$

The damping constant, c_{arms}, for the two sides of the two arms, is given by

$$c_{arms} \simeq \frac{4M}{40\omega x_o}$$

Assuming K ≃ 26 (Run 99) and $\nu = 0.01 cm^2/s$,

$$c_{arms} \simeq 0.0159 \quad (gr/cm/s)$$

V-6 Splitter Plate

The same formula used in V-4 for the gaps at the cylinder's ends can be used to estimate the damping due to the splitter plate; assuming the gap between the two plates (Fig. 6) to be greater than 0.04 cm, $\lambda \simeq 1$; hence:

$$c_{spl.pl.} = 2bL\rho_f \nu K\lambda$$

$$c_{spl.pl.} \simeq 0.0245 \quad (gr/cm/s)$$

This value can be compared with c = 0.0237 obtained from the difference between c values calculated from the recorded behaviour of the cylinder in still water, with and without a splitter plate; this last method was adopted to measure a fixed value of $C_{spl.pl.}$ which was then added to external damping (see V-7).

V-7 Total Damping

To calculate the total external damping of the cylinder, it should be noted that the aerodynamic damping (which should be subtracted from c_{air}) is small relative to the structural damping, but of the same order of magnitude as the hydrodynamic damping due to the gaps (which should be added to c_{air}). It was thus decided to neglect these two sources of damping on the assumption that their effects, which were in any event small, tended to cancel each other.

The total external damping could be calculated by (i) measuring structural damping in air (see V-1) without the damping mechanism, (ii) connecting the damping mechanism and measuring the difference for the same (a/D) and (f/N) and (iii) calculating the total damping from the c vs (f/N) and c vs (a/D) relationships obtained in (i) above, in addition to the constant values of c due to the damping mechanism (ii above) and the splitter plate if needed (V-6).

To calculate external damping from transients in still water (see 6.3.3), hydrodynamic damping must be subtracted from the total. For the samll size numbers and vibration amplitudes involved in the present research the expressions given in V-3 can be used to calculate hydrodynamic damping (see Bramley). With $\nu = 0.01$ cm /s; $\rho_f = 0.00102$ gr-s^2/cm^4; D = 2.5 cm and N = 2.2 c.p.s. (Runs 99 to 105), thus:

$$c_{hyd} = 0.141 \quad \text{gr/cm/s}$$

The total value of c_{sw} in still water should result from the addition of

$$c_{air} - c_{aero.} + c_{arms} + c_{gaps} + c_{hyd.}$$

This results in $c_{sw} = 0.18$ gr/cm/s, which is smaller than the measured $c_{sw} = 0.207$ gr/cm/s. The difference is perhaps due mainly to an underestimation of $c_{hyd.}$, which results from applying Stokes method for (a/D) > 0.05 (see Bramley).

It should be noted that c_{sw} leads to $k_{sw} = 0.459$ which is significantly larger than the corresponding $k'_{so} = 0.0632$ here used.

APPENDIX VI

BLOCKAGE EFFECTS

When the transverse or "shadow area", A_s, that the cylinder presents to the oncoming flow is a significant proportion of the cross sectional area of the flow channel, A_f, there is an increase in the local flow velocities over those that would occur in an infinitely large channel (blockage effects).

Semiempirical methods mainly from wind tunnel experience (e.g. Maskell) are available for the correction of measured flow velocities to account for blockage effects, although their validity and accuracy is difficult to assess when dealing with vibrating bodies (and fluctuating wakes) immersed in a stream of water with a free surface.

In the present research the flow velocity measurements were not affected by blockage because they were made outside the area of influence of the cylinder (Fig. 5); consequently the measured values of V (and the calculated R_e) are underestimated with respect to the more relevant flow velocities at the cylinder location, which were affected by blockage.

As explained in Chapter 4, S and C_{DO} were not obtained from published data intended for cylinders in an infinite stream, but they were calculated from direct measurements of f_s, $\bar{x}$ and V; in the case of a stationary cylinder this procedure avoided the need to consider the effects of blockage, turbulence, surface roughness, etc. Assuming that blockage effects were the same for a stationary and a vibrating cylinder, the values of S and C_{DO} were included in other non-dimensional groups to avoid the need for blockage corrections, for example ($f_s/f = SV/fD$) instead of (V/fD), or (C_{DA}/C_{DO}) instead of C_{DA}, etc.

As mentioned in Chapter 9 however, it appeared that blockage effects increased (i.e. more underestimated) when the cylinder vibrated; consequently any force coefficient for the vibrating cylinder will be somewhat overestimated, even when expressed in the form (C_F/C_{DO}).

In what follows the subindex, b, will indicate corrected for

blockage effects, while the subindex, m, will indicate as measured or calculated from the measured values of V.

The correction for the flow velocity can be given by:

$$\beta = \left[\frac{V_b}{V_m} - 1\right] > 0 \qquad \text{(VI-1)}$$

if β is small moreover:

$$(1 + \beta)^n \simeq 1 + n\beta$$

(a) $\overline{C}_F$ and P_d

From equation 7.31, approximately 90% of the value of $\overline{C}_F$ is determined by C_{DA} and 10% by $(C_F' V_r \sin\alpha)$; moreover,

$$\frac{(C_{DA})_m}{(C_{DA})_b} = \frac{V_m^{-2}}{V_b^{-2}} = (1 + \beta)^2 \simeq 1 + 2\beta$$

and (see section (d) below)

$$\frac{(V_r C_F' \sin\alpha)_m}{(V_r C_F' \sin\alpha)_b} \simeq \frac{V_m^{-5}}{V_b^{-5}} \simeq 1 + 5\beta$$

hence:

$$\frac{(\overline{C}_F)_m}{(\overline{C}_F)_b} \simeq 0.9(1 + 2\beta) + 0.1(1 + 5\beta) \simeq 1 + 2.3\beta \qquad \text{(VI-2)}$$

From equations 8.1 & 8.2 $(P_d/M_{as}\omega^2 x_o)$ is approximately proportional to the product $(\overline{C}_F\, V/fD)$; hence from equation VI-2:

$$\frac{(P_d)_m}{(P_d)_b} = \frac{(\bar{C}_F \frac{V}{fD})_m}{(\bar{C}_F \frac{V}{fD})_b} = \frac{(\bar{C}_F)_m}{(\bar{C}_F)_b} \frac{V_b}{V_m} \simeq 1 + 1.3\beta \qquad \text{(VI-3)}$$

since $M_{as}\omega^2 x_o$ is not affected by blockage.

To correct the product $\frac{\bar{C}_F}{C_{DO}} \frac{f_s}{f}$, it should be noted that:

$$C_{DO} \propto \frac{\bar{x}}{V^2}$$

where $\bar{x}$ was measured from the stationary cylinder, and is consequently proportional to the square of the velocity, V_s, which was affected by the blockage of the stationary cylinder, hence:

$$\frac{(C_{DO})_m}{(C_{DO})_b} \propto \frac{V_b^2}{V_s^2} = \frac{V_b^2}{V_m^2} \frac{V_m^2}{V_s^2} \qquad \text{(VI-4)}$$

$$\frac{(C_{DO})_m}{(C_{DO})_b} = (1 + \beta)^2(1 - \beta_o)^2 = 1 + 2(\beta - \beta_o)$$

where $\beta_o = (V_s/V_m) - 1$. By a similar argument and assuming S unaffected by blockage:

$$\frac{(f_s)_m}{(f_s)_b} = 1 - \beta + \beta_o \qquad \text{(VI-5)}$$

hence from equations VI-2/4/5:

$$\frac{\left[\frac{\bar{C}_F}{C_{DO}} \frac{f_s}{f}\right]_m}{\left[\frac{\bar{C}_F}{C_{DO}} \frac{f_s}{f}\right]_b} = \frac{(1 + 2.3\beta)(1 - \beta + \beta_o)}{1 + 2(\beta - \beta_o)} \simeq 1 - .7\beta + 3\beta_o$$

and the calculated values of this product will be overestimated by

between 3% and 7% depending on the value of $\overline{C}_F$ (see equation VI-6 below).

(b) A blockage correction

The simplest blockage correction assumes that the increase of V is solely due to the constriction of the area of the flow channel, made by the cylinder, i.e.:

$$\frac{V_m}{V_b} = 1 - \frac{D}{d}$$

where d is the depth of water. If increments of $\overline{C}_F$ are assumed to be equivalent to an increase of the cylinder diameter, an equivalent expression is obtained, i.e.

$$\frac{V_m}{V_b} = 1 - (\overline{C}_F \times \text{const.})$$

If $(\overline{C}_F \times \text{const.})$ is small the last expression can be written as:

$$\frac{V_b}{V_m} \simeq 1 + (\overline{C}_F \times \text{const.})$$

or introducting β:

$$\beta = \overline{C}_F \times \text{const.}$$

It was observed (Chapter 9) that the ratio of Eqn. VI-3 increased by 0.03 as $\overline{C}_F$ increased from 1.4 to 2.0; consequently and assuming no blockage effects when $\overline{C}_F = 0$ (see Fig. 89)

$$1.3\beta = \frac{0.03}{0.6} \overline{C}_F$$

hence

$$\beta = \frac{\overline{C}_F}{26} \qquad \text{(VI-6)}$$

(c) C_F' and P_e

From equations 7.32 and VI-3, and considering the 1.5% increase of $\bar{C}_F$ due to the drag of the supporting arms:

$$C_F' \propto V^{-2}\sqrt{(C_I-1)^2+ \text{const.} \times (V^{-1.3} \times 1.015)^2}$$

The first term inside the radical is independent of blockage and varies between 0 and 1 as (f_s/f) varies between 1 and $\sqrt{2}$; the second term is approximately equal to 1 (Eqn. 8.1) and represents between 50% and 100% of the value of the radical; hence:

$$\frac{(C_F')_m}{(C_F')_b} \simeq (1 + 2\beta)\sqrt{\left(1 + \frac{1.3\beta + 0.015}{(2) \text{ to } (1)}\right)^2}$$

therefore:

$$1 + 2.65\beta + 0.0075 < \frac{(C_F')_m}{(C_F')_b} < 1 + 3.3\beta + 0.015 \qquad \text{(VI-7)}$$

corresponds to $\sqrt{2} > (f_s/f) > 1$. When $(f_s/f) = \sqrt{2}$, moreover:

$$\frac{(C_F')_m}{(C_F')_b} \simeq 1 + 3\beta \qquad \text{(VI-8)}$$

From equation 7.30:

$$\frac{P_e}{M_{as}\omega^2 x_o} \propto V^2 C_F'$$

and from equation VI-7 for $(f_s/f) = \sqrt{2}$ and $\bar{C}_F \simeq 1.4$:

$$\frac{(P_e)_m}{(P_e)_b} = (1 - 2\beta)(1 + 2.65\beta) + 0.0075$$

i.e.

$$\frac{(P_e)_m}{(P_e)_b} \simeq 1.045$$

(d) α and $(V_r C_F' \sin\alpha)$

From equation 8.8

$$\sin\alpha = \frac{f}{f_s} \propto \frac{1}{V}$$

hence:

$$\frac{(\sin\alpha)_m}{(\sin\alpha)_b} \simeq 1 + \beta$$

For $(f_s/f) = \sqrt{2}$, from this equation and equation VI-8:

$$\frac{(V_r C_F' \sin\alpha)_m}{(V_r C_F' \sin\alpha)_b} \simeq (1 + \beta)(1 + 3\beta)(1 + \beta)$$

$$\frac{(V_r C_F' \sin\alpha)_m}{(V_r C_F' \sin\alpha)_b} \simeq 1 + 5\beta \qquad \text{(VI-9)}$$

APPENDIX VII

DEDUCTION OF EQUATIONS

Deduction or expansion of some of the equations presented in the text is given in more detail in this appendix, as indicated in the table below:

Appendix Address	Equation Numbers	Text Address	
		Chpt./Sect.	Page
VII - 1	7.4 & 7.5	7.1	82
VII - 2	7.15a	7.2.2	86
VII - 3	7.16 & 7.17	7.2.3	88
VII - 4	7.26/7/8	7.4.1	91
VII - 5	7.31/2/3/4	7.4.1	92
VII - 6	7.39/40/41	7.4.3	96
VII - 7	8.2	8.1.2	101

VII-1 (see 7.1)

From the diagram of Fig. 51:

$$F'_{To} \cos\zeta = kx_o - M_c\omega^2 x_o$$

dividing by kx_o and from equation 7.6

$$\frac{F'_{To} \cos\zeta}{kx_o} \doteq 1 - \left(\frac{f}{N_v}\right)^2$$

similarly:

$$F'_{To} \sin\zeta = c\omega x_o$$

$$\frac{F'_{To}\sin\zeta}{kx_o} = \frac{c}{2\pi M_c N_v}\left(\frac{f}{N_v}\right)$$

solving now for F'_{To} and ζ:

$$F'_{To} = \sqrt{(F'_{To}\cos\zeta)^2 + (F'_{To}\sin\zeta)^2}$$

therefore

$$F'_{To} = kx_o\sqrt{[1 - (\frac{f}{N_v})^2]^2 + [\frac{c}{2\pi M_c N_v}(\frac{f}{N_v})]^2} \quad (7.4)$$

and:

$$\tan\phi = \frac{F'_{To}\sin\zeta}{F'_{To}\cos\zeta}$$

therefore

$$\tan\phi = \frac{\frac{c}{2\pi M_c N_v}\left(\frac{f}{N_v}\right)}{1 - \left(\frac{f}{N_v}\right)^2} \quad (7.5)$$

VII-2 (see 7.2.2)

$$\frac{kx_o - M_c\omega^2 x_o}{M_{as}\omega^2 x_o} = \frac{\frac{k}{M_{TS}} - \frac{M_c\omega^2}{M_{TS}}}{\frac{M_{as}\omega^2}{M_{TS}}}$$

where:

$$M_{TS} = M_c + M_{as} = M_{as}(\rho_r + 1)$$

and

$$\frac{k}{M_{TS}} = (2\pi N)^2$$

hence:

$$\frac{kx_o - M_c\omega^2 x_o}{M_{as}\omega^2 x_o} = \frac{(2\pi N)^2 - \frac{\rho_r}{\rho_r+1}\omega^2}{\frac{\omega^2}{\rho_r + 1}}$$

and

$$\frac{kx_o - M_c\omega^2 x_o}{M_{as}\omega^2 x_o} = \left(\frac{N}{f}\right)^2(\rho_r + 1) - \rho_r \qquad (7.15a)$$

VII-3 (see 7.2.3)

From the diagram of Fig. 52b

$$F_o' \cos\phi = kx_o - M_c\omega^2 x_o - M_{as}\omega^2 x_o$$

since cos ϕ is negative; dividing by $M_{as}\omega^2 x_o$, and from equation 7.15a:

$$\frac{F_o' \cos\phi}{M_{as}\omega^2 x_o} = C_I - 1$$

also from Fig. 52b

$$F_o' \sin\phi = c\omega x_o$$

dividing by $M_{as}\omega^2 x_o$ and from the definition of k_s given in 6.2.3.d:

$$\frac{F_o' \sin\phi}{M_{as}\omega^2 x_o} = \frac{2}{\pi^2} k_s$$

hence:

$$F_o' = M_{as}\omega^2 x_o \sqrt{(C_I - 1)^2 + \left(\frac{2}{\pi^2} k_s\right)^2} \qquad (7.16)$$

and

$$\tan\phi = \frac{F_o' \sin\phi}{F_o' \cos\phi} = \frac{2k_s}{\pi^2(C_I - 1)} \qquad (7.17)$$

From equations 7.25 and 7.10, F can be given by:

$$F = \overline{F} + F_o' \sin\phi \cos\omega t + F_o' \cos\phi \sin\omega t$$

Expanding now the right hand side of equation 7.24 and replacing all squared and cubed trigonometric functions with the respective functions of twice and three times the argument:

$$\begin{aligned}
\frac{F}{\frac{1}{2}\rho_f D L V^2 \overline{C}_F} = {} & \left[1 + \frac{1}{2}V_r^2 - V_r \frac{C_F'}{\overline{C}_F} \sin\alpha\right] + \\
& + \left[\frac{C_F'}{\overline{C}_F}\cos\alpha + \frac{1}{4}V_r^2 \frac{C_F'}{\overline{C}_F}\cos\alpha\right]\sin\omega t + \\
& + \left[\frac{C_F'}{\overline{C}_F}\sin\alpha + \frac{3}{4}V_r^2 \frac{C_F'}{\overline{C}_F}\sin\alpha - 2V_r\right]\cos\omega t + \\
& + \left[\frac{1}{2}V_r^2 - V_r \frac{C_F'}{\overline{C}_F}\sin\alpha\right]\cos 2\omega t - \\
& - \left[V_r \frac{C_F'}{\overline{C}_F}\cos\alpha\right]\sin 2\omega t + \\
& + \left[\frac{1}{4}V_r^2 \frac{C_F'}{\overline{C}_F}\cos\alpha\right]\sin 3\omega t + \\
& + \left[\frac{1}{4}V_r^2 \frac{C_F'}{\overline{C}_F}\sin\alpha\right]\cos 3\omega t
\end{aligned}$$

It is clear from this expression that the first group of terms which is invariant, constitutes the mean force $\overline{F}$ (Eqn. 7.26); the second and third groups of terms are clearly in phase with $F_o'\cos\phi$ and $F_o'\sin\phi$ respectively (Eqns. 7.27 and 7.28), the remaining terms were neglected because they have frequencies which are multiples of ωt, and

consequently they do no work on a vibration characterized by $x = x_o \sin\omega t$; the terms in $(3\omega t)$ moreover are negligibly small.

It should be noted however, that in the double harmonic excitation section of the first instability region where the motion can be given by:

$$x = x_1 \sin\omega t + x_2 \sin(2\omega t + \gamma)$$

the terms in $(2\omega t)$ which arise from the excitation mechanism associated with the transverse flow, may contribute to increase (a/D) and to the slight decrease of (f/N) observed (see also VII-6).

VII-5 (see 7.4.1)

From equations 3.1 and 7.3a:

$$\overline{F} = k\overline{x} = \tfrac{1}{2}\rho_f DLV^2 C_{DA}$$

and from equation 7.26

$$C_{DA} = (1 + \tfrac{1}{2}V_r^2)\overline{C}_F - V_r C_F' \sin\alpha$$

hence:

$$\overline{C}_F = \frac{C_{DA} + V_r C_F' \sin\alpha}{1 + \tfrac{1}{2}V_r} \qquad (7.31)$$

From Fig. 56 and Eqns. 7.15a and 7.29:

$$P_e \cos\alpha = kx_o - (M_c + M_{as})\omega^2 x_o$$

$$\tfrac{1}{2}\rho_f DLV^2 (1 + \tfrac{1}{4}V_r^2) C_F' \cos\alpha = M_{as}\omega^2 x_o (C_I - 1)$$

hence: $$\cos\alpha = \frac{M_{as}\omega^2 x_o}{\frac{1}{2}\rho_f DLV^2} \frac{(C_I - 1)}{(1 + \frac{1}{4}V_r^2)C_F'}$$

but $$\frac{M_{as}\omega^2 x_o}{\frac{1}{2}\rho_f DLV^2} = \frac{\frac{\pi}{4}D^2 L\rho_f(2\pi f)^2 x_o}{\frac{1}{2}\rho_f DLV^2} = \pi^2 \frac{V_r}{\frac{V}{fD}}$$

hence: $$\cos\alpha = \pi^2 \frac{V_r}{\frac{V}{fD}} \frac{(C_I - 1)}{(1 + \frac{1}{4}V_r^2)C_F'} \qquad \text{(VII-5.1)}$$

From Fig. 56, from the definition of k_s (see 6.2.3d) and from equations 7.29 and 7.30:

$$P_e \sin\alpha = P_{hd} + c\omega x_o$$

$$\frac{1}{2}\rho_f DLV^2(1 + \frac{3}{4}V_r^2)C_F' \sin\alpha = \frac{1}{2}\rho_f DLV^2(2V_r\bar{C}_F) + c\omega x_o$$

hence:

$$\sin\alpha = \frac{2V_r\bar{C}_F + \left(\frac{M_{as}\omega^2 x_o}{\frac{1}{2}\rho_f DLV^2}\right)\left(\frac{c\omega x_o}{M_{as}\omega^2 x_o}\right)}{(1 + \frac{3}{4}V_r^2)C_F'}$$

$$\sin\alpha = 2\frac{V_r}{\frac{V}{fD}} \frac{\left(\frac{V}{fD}\bar{C}_F + k_s\right)}{(1 + \frac{1}{4}V_r^2)C_F'}\psi \qquad \text{(VII-5.2)}$$

where

$$\psi = \frac{1 + \frac{1}{4}V_r^2}{1 + \frac{3}{4}V_r^2} \qquad (7.34)$$

From, $\cos^2\alpha + \sin^2\alpha = 1$, and from equations VII-5.1 and VII-5.2:

$$C_F' = \frac{V_r}{\frac{V}{fD}(1 + \frac{1}{4}V_r)} \sqrt{[\pi^2(C_I - 1)]^2 + [2\psi(\bar{C}_F \frac{V}{fD} + k_s)]^2} \qquad (7.32)$$

and from $\tan\alpha = \sin\alpha/\cos\alpha$

$$\tan \alpha = \frac{2\psi(\bar{C}_F \frac{V}{fD} + k_s)}{\pi^2(C_I - 1)} \qquad (7.33)$$

VII-6 (see 7.4.3)

Substituting C_F' for $b\gamma^2/D$, and $V_r\cos\omega t$ for $\dot{x}/V$, in equation 7.38:

$$F = \tfrac{1}{2}\rho_f DLV^2 C_F'(1 - V_r\cos\omega t)^2[1 + \sin(\omega t + \alpha)]$$

expanding:

$$\begin{aligned}\frac{F}{\frac{1}{2}\rho_f DLV^2 C_F'} = {} & [1 + \tfrac{1}{2}V_r^2 - V_r\sin\alpha] \\ & + [\sin\omega t\cos\alpha + \cos\omega t\sin\alpha \\ & \quad + \tfrac{1}{4}V_r^2\sin\omega t\cos\alpha + \tfrac{3}{4}V_r^2\cos\omega t\sin\alpha] \\ & - [2V_r\cos\omega t] \\ & - V_r\sin 2\omega t\cos\alpha \\ & - V_r\cos 2\omega t\sin\alpha + \tfrac{1}{2}V_r^2\cos 2\omega t \\ & + \tfrac{1}{4}V_r^2\sin 3\omega t\cos\alpha \\ & + \tfrac{1}{4}V_r^2\cos 3\omega t\sin\alpha\end{aligned}$$

Neglecting all terms in $2\omega t$ and $3\omega t$ which do no work on a sinusoidal motion, $x = x_o\sin\omega t$:

$$\frac{F}{\frac{1}{2}\rho_f DLV^2 C_F'} = [1 + \tfrac{1}{2}V_r^2 - V_r \sin\alpha]$$

$$+ [\sin(\omega t + \alpha) + \tfrac{1}{4}V_r^2 \sin(\omega t + \alpha)]$$

$$- [2V_r \cos\omega t - \tfrac{1}{2}V_r^2 \sin\alpha\cos\omega t]$$

The three groups of terms in the R.H.S. of this equation clearly lead to equations 7.39, 7.41 and 7.40 respectively.

VII-7 (see 8.1.2)

From the diagram of Fig. 56:

$$P_{hd} + c\omega x_o = P_e \sin\alpha \qquad \text{(VII-7.1)}$$

and from equations 7.29 and 7.30

$$\tfrac{1}{2}\rho_f DLV^2 \overline{C}_F 2V_r - \tfrac{1}{2}\rho_f DLV^2 C_F' \tfrac{1}{2}V_r^2 \sin\alpha + c\omega x_o = \tfrac{1}{2}\rho_f DLV^2 (1+\tfrac{1}{4}V_r^2) C_F' \sin\alpha \qquad \text{(VII-7.2)}$$

hence:

$$\tfrac{1}{2}\rho_f DLV^2 (2V_r)\overline{C}_F + c\omega x_o = \tfrac{1}{2}\rho_f DLV^2 (1 + \tfrac{3}{4}V_r^2) C_F' \sin\alpha \qquad \text{(VII-7.3)}$$

multiplying this equation by ψ (see Eqn. 7.34), the Right Hand Side becomes $P_e \sin\alpha$ as in the R.H.S. of Eqn. (VII-7.2), therefore:

$$P_{hd} + c\omega x_o = \psi [\tfrac{1}{2}\rho_f DLV^2 (2V_r)\overline{C}_F + c\omega x_o]$$

dividing by $M_{as}\omega^2 x_o$

$$\frac{P_{hd} + c\omega x_o}{M_{as}\omega^2 x_o} = \psi \left[\frac{2}{\pi^2} k_s + \frac{\frac{1}{2}\rho_f DLV 2\omega x_o}{\frac{\pi}{4}\rho_f D^2 L\omega^2 x_o V} \overline{C}_F \right]$$

hence:

$$\frac{P_{hd} + c\omega x_o}{M_{as}\omega^2 x_o} = \psi \frac{2}{\pi^2} \left[k_s + \overline{C}_F \frac{V}{fD} \right] = 1$$

REFERENCES

1. Auger, B. "Wind induced vibrations in a space frame structure"; Proc. Sym. on Wind effects on Bldgs. and Struc., Loughborough Univ. of Techn., April 1968.

2. Bearman, P. "Investigation of the flow behind a two-dimensional model with a blunt trailing edge and fitted with splitter plates"; Jrnl. Fluid Mech., 21, pp 451, 1972.

3. Bishop, R.E.D., and Hassan, A.Y. "The lift and drag forces on a circular cylinder in a flowing fluid"; Proc. Roy. Soc. Lond. A, 277, pp.32-75, 1963.

4. Bramley, M.E. "On the hydrodynamic damping of a circular cylinder"; M.Sc. Thesis, Imperial College, Univ. of London, 1969.

5. Clark, P.B. "The flow-induced vibration of cylinders with particular reference to the phenomenon of in-line motion with the symmetrical shedding of vortices"; M.Sc. Thesis, Imperial College, Univ. of London, 1973.

6. Den Hartog, J.P. "Mechanical Vibrations"; 4th ed., McGraw-Hill, 1956.

7. Dickens, W.R. "Self-induced vibration of a cylinder-in line with a fluid flow"; Ph.D. Thesis, Univ. of London, 1976.

8. Dickens[2], W.R. "Flow induced in-line vibration of cylinders";M.Sc. Thesis, Imperial College, Univ. of London, 1972.

9. Fage, A., and Warsap, J.H. "The effect of turbulence and surface roughness on the drag of a circular cylinder"; British Aero. Res. Comm. R.& M., 1283, 1929.

10. Goldstein, S. (Editor) "Modern developments in fluid dynamics"; 2 Vol.s, Dover ed., 1965.

11. Hardwick, J.D. (Private Communication).

12. Hardwick, J.D., and Wootton, L.R. "The use of model and full-scale investigations on marine structures"; Int. Sym. on Vibration problems in industry, Keswick, England, paper 127, 1973.

13. King, R. "Vortex excited structural oscillations of a circular cylinder in flowing water"; Ph.D. Thesis, Loughborough Univ. of Techn., July 1974.

14. Lamb, " Hydrodynamics"; Cambridge Univ. Press, 6th ed., 1953.

15. Maskell, E.C. "A theory of blockage effects on bluff bodies and stalled wings in a closed wind tunnel"; R. & M., No. 3400, Nov. 1963.

16. Raudkivi, A.J., and Callender, R.A. "Advanced fluid mechanics"; Edward Arnold (Pub.), 1975.

17. Richter, A. "Effects of walls on the flow around circular cylinders"; Proc. Int. Sym. on vibration problems in industry, Keswick, England, 1973.

18. Sainsbury, R.N., and King, D. "The flow induced oscillation of marine structures"; Proc. Instn. Civ. Engrs., 49, pp.269-302, July 1971.

19. Schaefer, J.W., and Eskinazi, S. "An analysis of the vortex street generated in a viscous fluid"; Jnl. of Fluid Mech., Vol. 6, pp.241, 1959.

20. Scruton, C. "Wind effects on structures"; Proc. Instn. Mech. Engrs., Vol. 185, 23/71, 1970-71.

21. Small, A.F. "Hydroelastic excitation of cylinders"; Ph.D. Thesis, Univ. of Auckland, New Zealand, July 1971.

22. Schlichting, H. "Boundary layer theory"; Pergamon Press, 1955.

23. Toebes, G.H., and Ramamurthy, A.S. "Fluid-elastic forces on circular cylinders": Proc. Am. Soc. Civ. Engrs., 93, (No. EM6) paper 5627, Dec. 1967.

24. Vickery, B.J., and Watkins, R.D. "Flow-induced vibrations of cylindrical structures"; Proc. 1st Autralasian Conf., pp.213-241, 1962.

25. Walshe, D.E., and Wootton, L.R. "Preventing wind induced oscillations of structures of circular section"; Proc. Instn. Civ. Engrs., Vol. 47, Sept., 1970.

26. Wootton, L.R. "The oscillations of large circular stacks in wind"; Proc. Instn. Civ. Engrs., Vol. 43, paper 7188, 1969.

27. Wootton,[2] L.R. (Private Communication).

28. Wootton, L.R., Warner, M.H., and Cooper, D.H. "Some aspects of the oscillations of full-scale piles"; C.I.R.I.A., Tech. note No. 41, 1972.

29. Wootton, L.R., Warner, M.H., Sainsbury, R.N.,and Cooper, D.H.[2] "Oscillation of piles in marine structures - a description of the full-scale experiments at Immingham"; C.I.R.I.A., Techn. note No. 40, Aug., 1972.

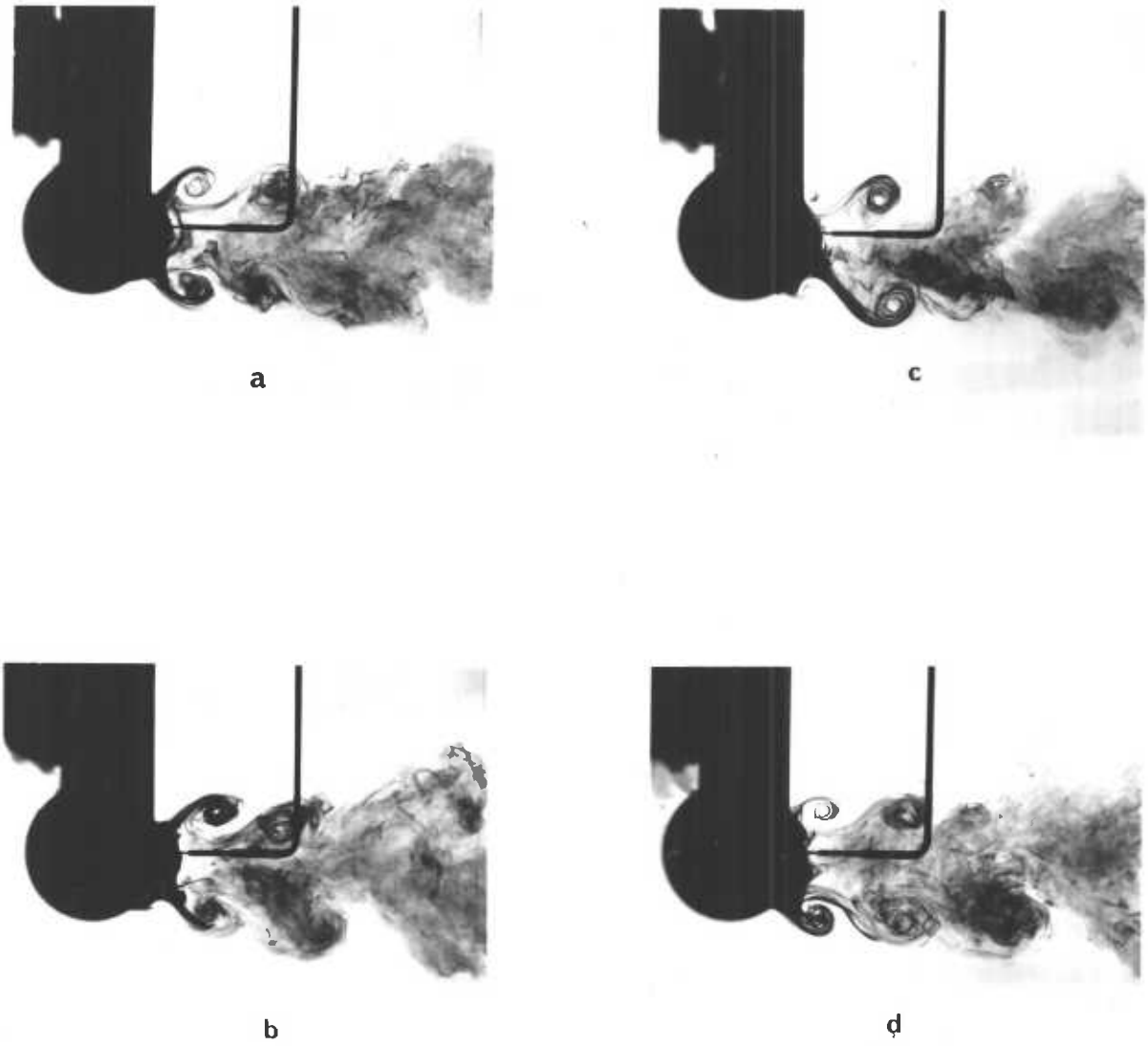

Plate 1 Shedding of pairs of simultaneous eddies in the reorganization section of the first instability region. Selection of photographs taken at random during many cycles. (a) Upstream stroke, cylinder near mean position; wake near its narrowest; (b) cylinder near the furthest upstream position; new pair of eddies begins to form; (c) downstream stroke, cylinder near mid position; eddies growing near their furthest upstream position with respect to the cylinder; wake near its widest for that value of (f_s/f); (d) cylinder near the furthest downstream position; eddies move downstream and the wake narrows. $(f_s/f) = 0.67$; $(a/D) = 0.11$; $f = 1.66$ c.p.s.; $D = 3.38$ cm.

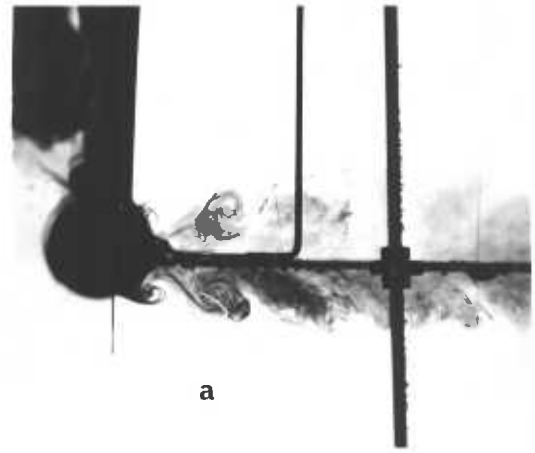

a

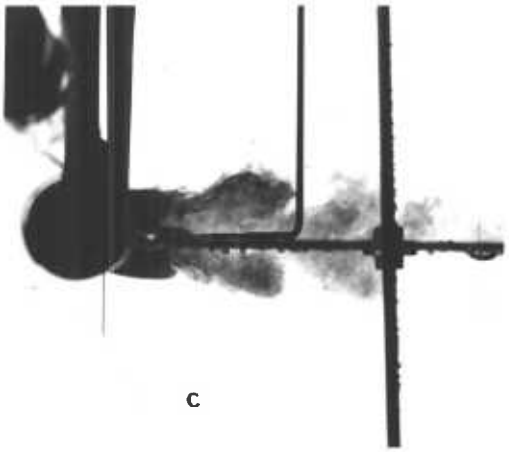

c

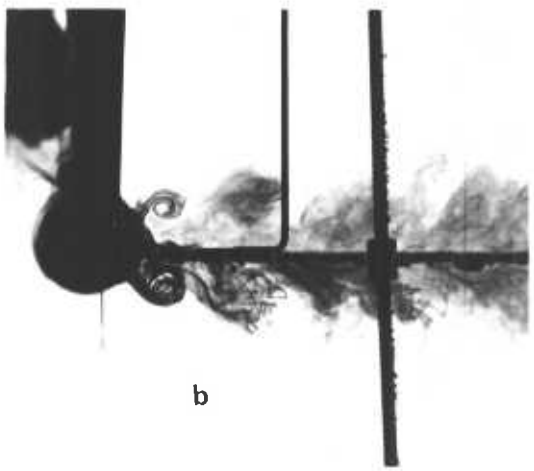

b

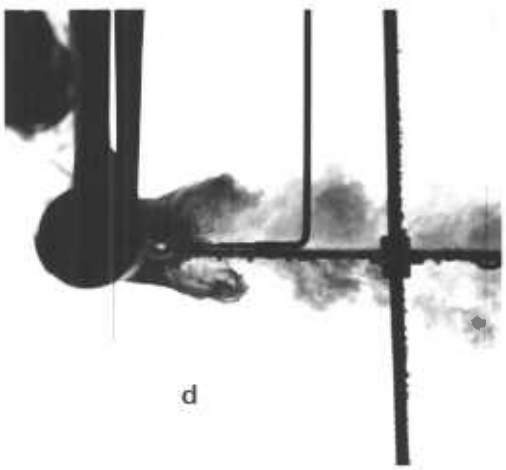

d

Plate 2 Wake behind a cylinder fitted with a splitter plate.
(a) and (b) laminar eddies; $(f_s/f) \simeq 0.96$; $(a/D) \simeq 0.18$;
D = 2.5 cm; f = 2.12 c.p.s.
(c) and (d) turbulent eddies; $(f_s/f) \simeq 1.13$; $(a/D) \simeq 0.08$
D = 2.5 cm; f ≃ 2.59 c.p.s.

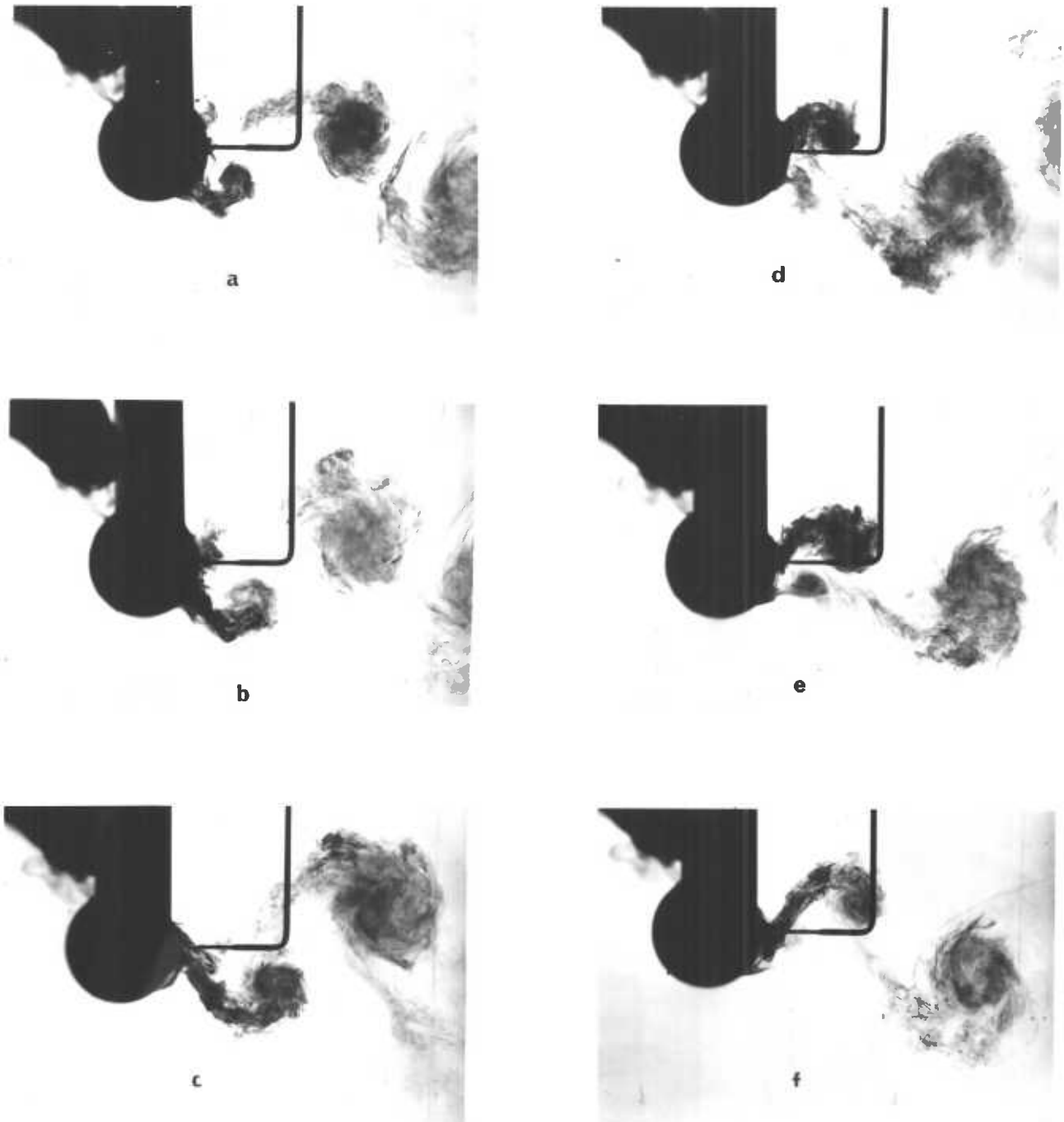

Plate 3 The near wake in the lock-in section of the first instability region. Selection of photographs taken at random during many cycles. (a) A pair of eddies is being shed; the lower (counter-clockwise) member of the pair rapidly moves downwards and downstream, near and below the lower member of the previously shed pair; (b) and (c) the two lower eddies coalesce into a larger eddy which moves downstream to take its position in the staggered wake; the downwards transverse flow associated with the kinetic field of the larger eddy, displaces the upper eddy downwards to the centreline of the wake; (d) a new pair of eddies is being shed; the upper member of the new pair coalesces with the upper eddy of (b) and (c); (e) and (f) the lower member of the new pair is swept upwards by the transverse flow; the next pair of eddies can just be seen in (f). $(f_s/f) \simeq 0.9$; $(a/D) = 0.22$; $D = 3.381$ cm; $f = 1.829$ c.p.s.; $N = 1.66$ c.p.s.

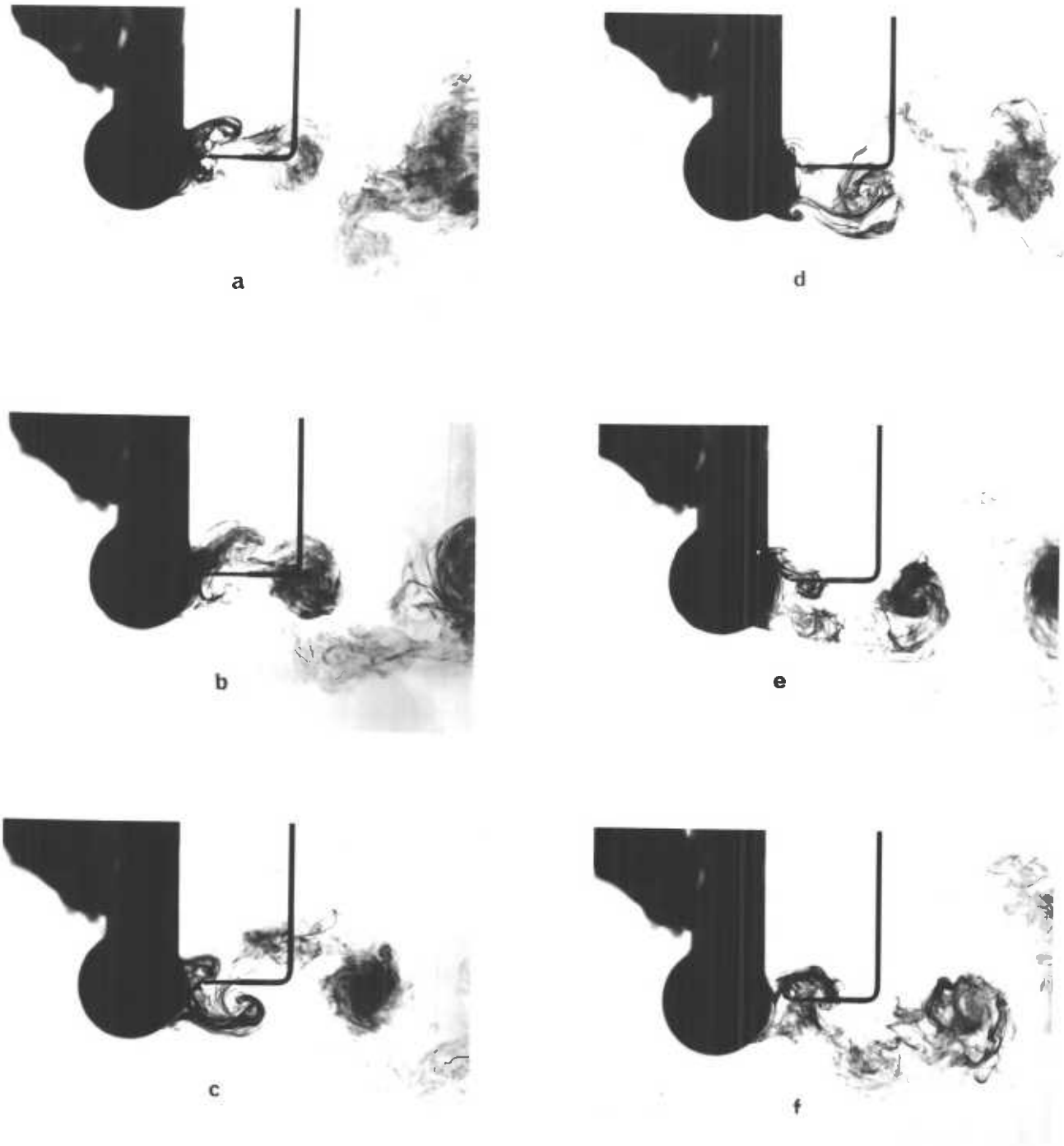

Plate 4 Developments of the near wake in the double harmonic excitation section of the first instability region. Selection of photographs taken at random during many cycles. Four consecutively shed, upper (clockwise) eddies can be seen joining to form one of the large eddies of the distant wake as follows: (a) Eddy No 4 of one such group moves rapidly away from the cylinder to join the amalgamated eddies Nos 1,2 and 3 (centre of picture); (b) eddy No 1 of the next group is only appearing and is clearly visible in (c); (d) eddy No 1 has moved downwards due to the transverse flow and is about to be joined by the newly shed eddy No 2; (e) the transverse flow has ceased; eddies 1 and 2 have joined together to form a larger eddy, and eddy No 3 is just being formed; (f) eddies Nos 1, 2 and 3 have joined to form a larger eddy and begin to move downstream. Similar developments can be seen for the lower (counter-clockwise) eddies. $(f_s/f) = 0.56$; $(a/D) = 0.056$; $D = 3.38$ cm; $f = 1.65$ c.p.s.

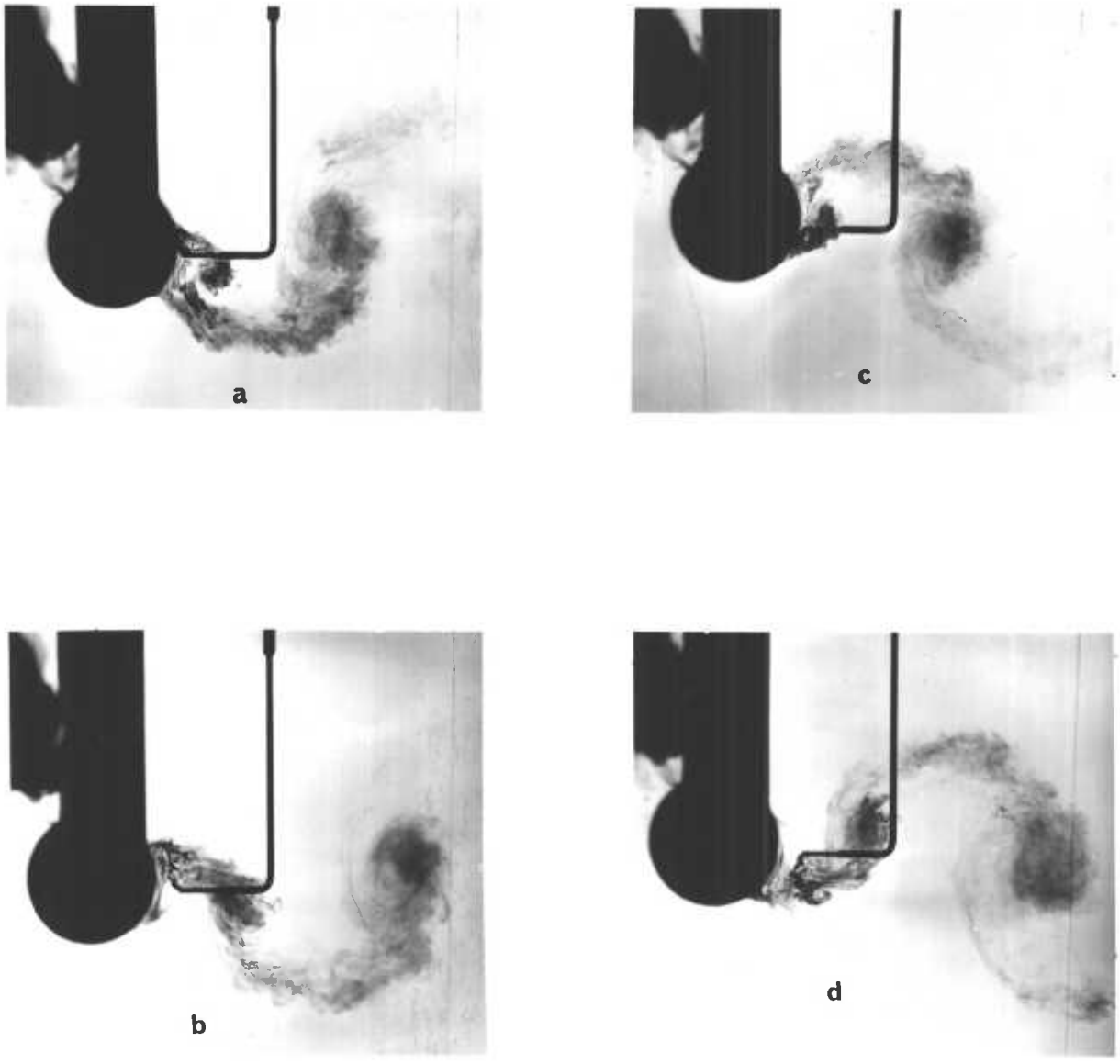

Plate 5 The near wake in the second instability region. Selection of photographs taken at random during many cycles. (a) cylinder near its downstream position; an eddy has just been shed but is still connected to the cylinder by the upper shear layer; upwards transverse flow commences; (b) cylinder approaching its upstream position; the previous (clockwise) eddy moves downstream along the wake's centre line probably still supplied of vorticity by the upper shear layer; the new (counterclockwise) eddy starts to form; transverse flow dies down; (c) and (d) approximate mirror images of (a) and (b). $(f_s/f) = 1.15$; $(a/D) = 0.17$; $D = 3.38$ cm; $f = 1.93$ c.p.s.; $N = 1.66$ c.p.s.

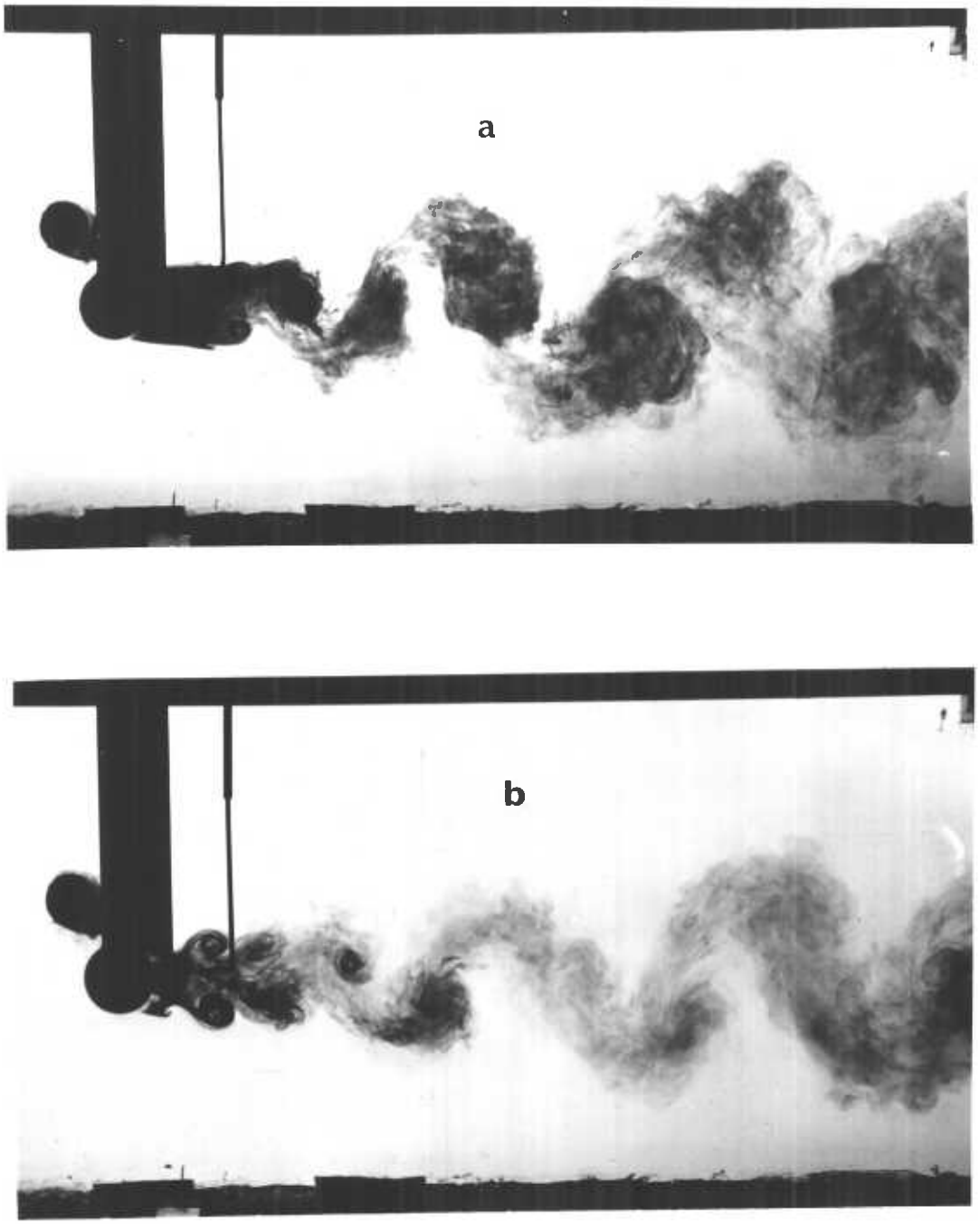

Plate 6 - a - Von Kàrmàn wake behind a stationary cylinder.
R_e = 2300; D = 3.38 cm

- b - Wake in the rearrangement section of the first instability region. (f_s/f) = 0.65; (a/D) = 0.096; D = 3.38 cm;
f ≃ N = 1.66 c.p.s.

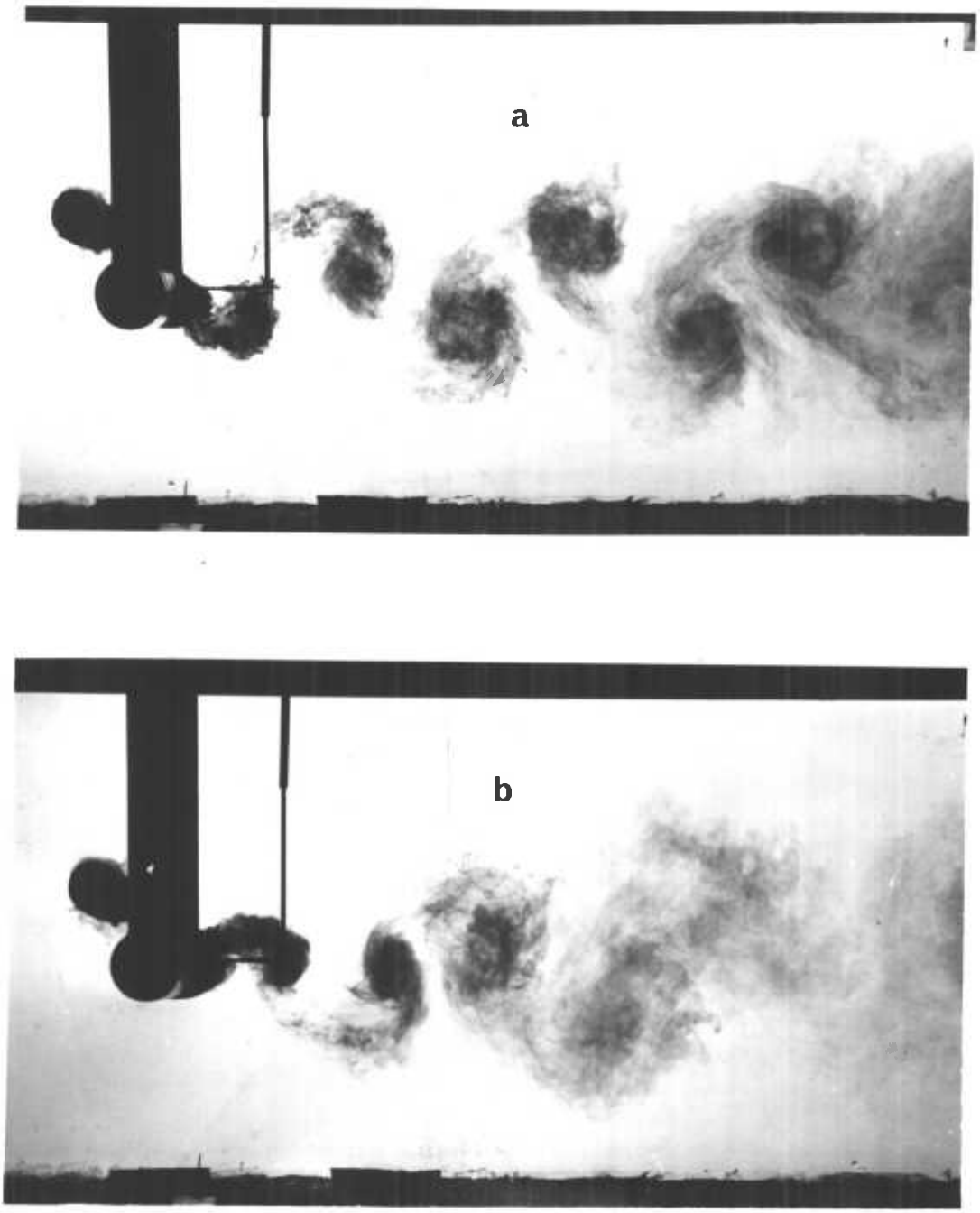

Plate 7 - a - Wake in the lock-in section of the first instability region. $(f_s/f) = 0.9$; $(a/D) = 0.202$; $D = 3.38$; $f = 1.83$ c.p.s.; $N = 1.66$ c.p.s.

- b - Undefined shape of the wake behind a cylinder oscillating between the two instability regions. $0.93 \leq (f_s/f) \leq 1.03$; $(a/D) < 0.05$; $D = 3.381$ cm; $\rho_r = 1$; 1.66 c.p.s. $< f <$ 1.83 c.p.s. $N = 1.66$ c.p.s.

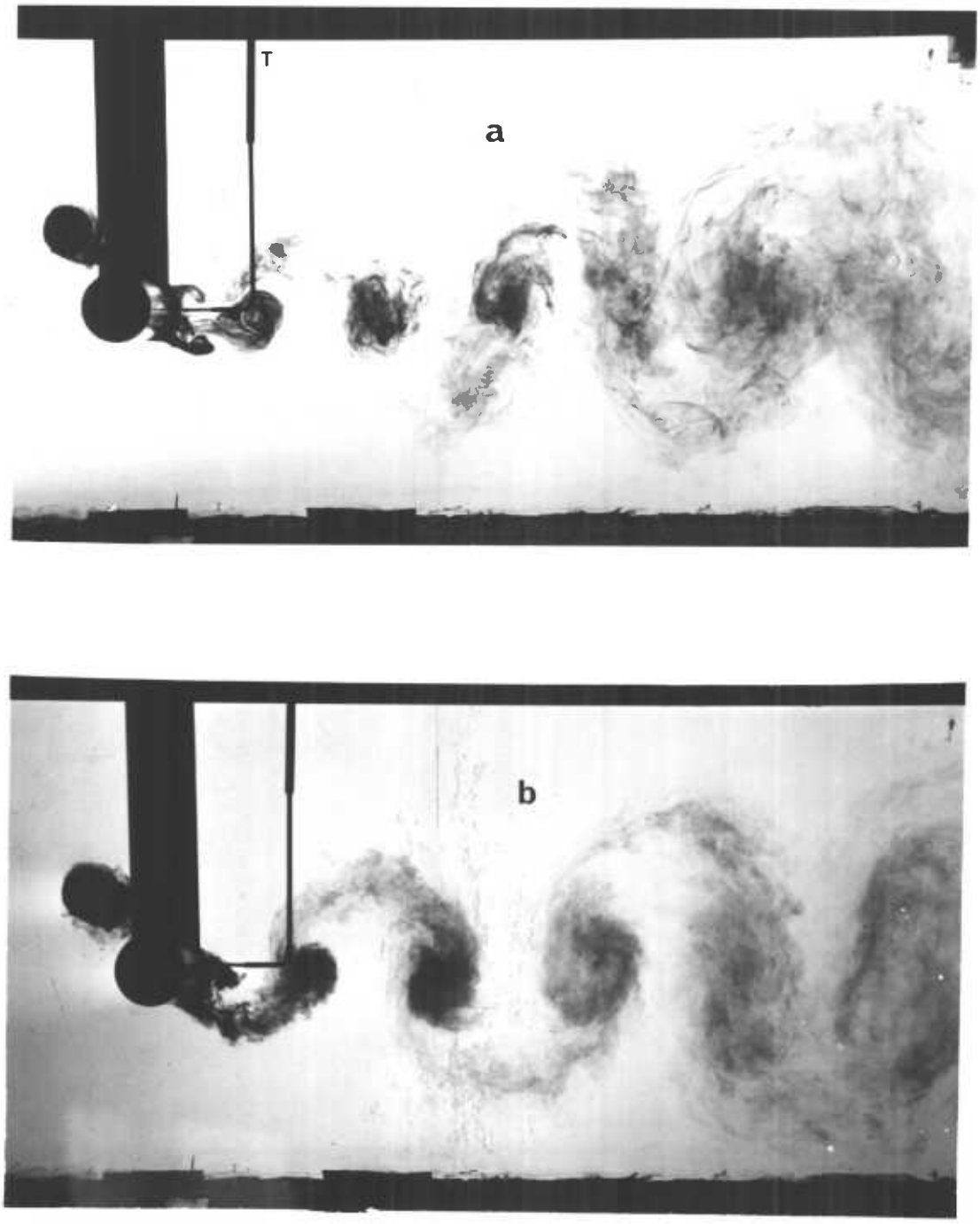

Plate 8 - a - Wake in the double harmonic excitation section of the first instability region. $(f_s/f) = 0.56$; $(a/D) = 0.05$; $D = 3.38$ cm; $\rho_r = 1$; $f \simeq N = 1.66$ c.p.s.

- b - Wake in the second instability region. $(f_s/f) \simeq 1.15$; $(a/D) = 0.173$; $D = 3.38$ cm; $f = 1.916$; $N = 1.66$.

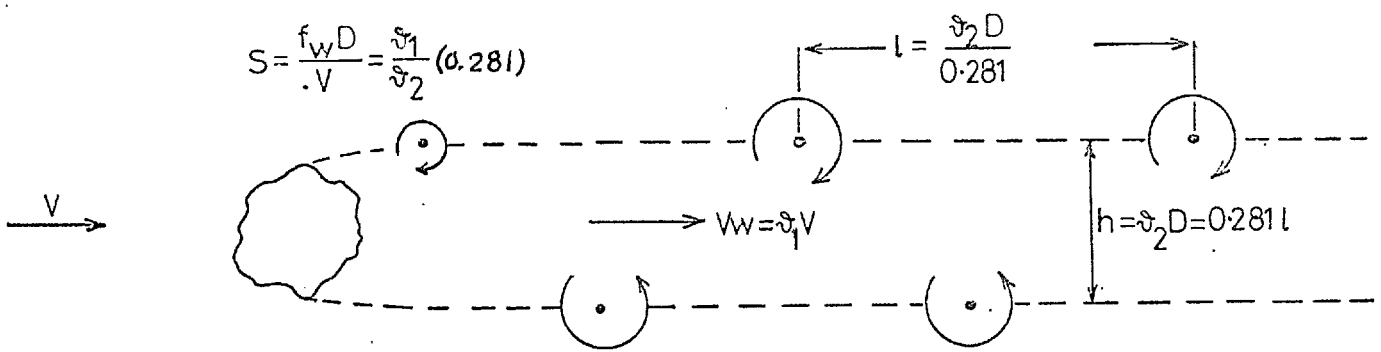

Fig. 1 Typical Von Kàrmàn wake behind a bluff body and its main characteristics (from Scruton)

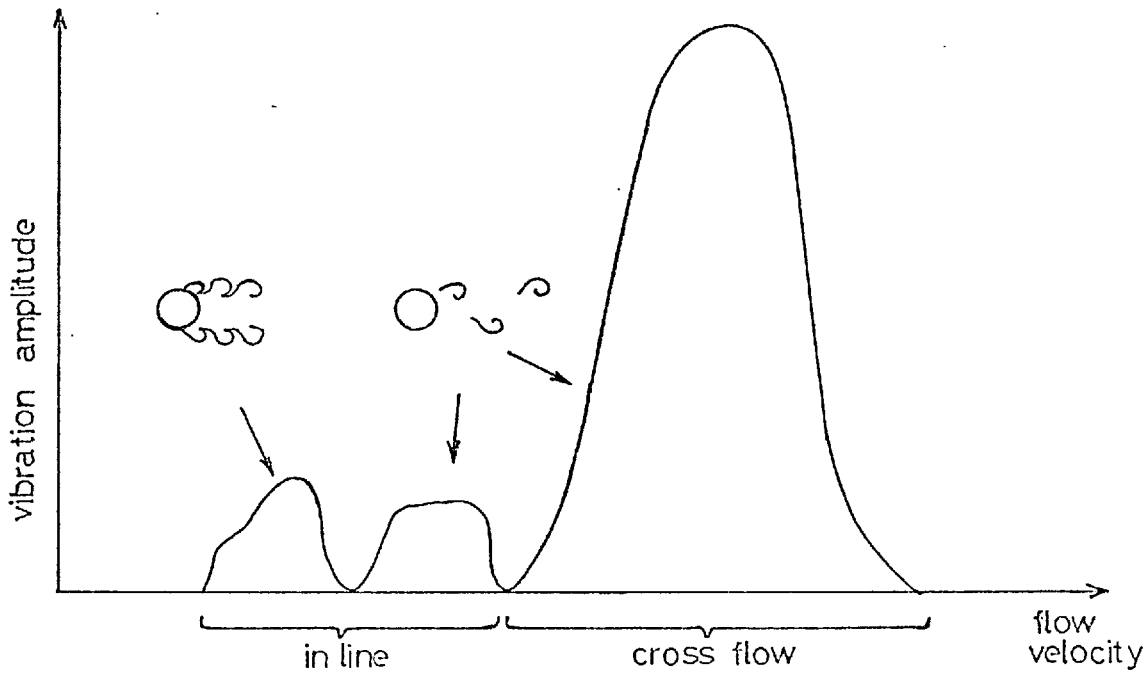

Fig. 2 Typical amplitude response curve of a lightly damped pile, with equal in-line and cross-flow natural frequencies

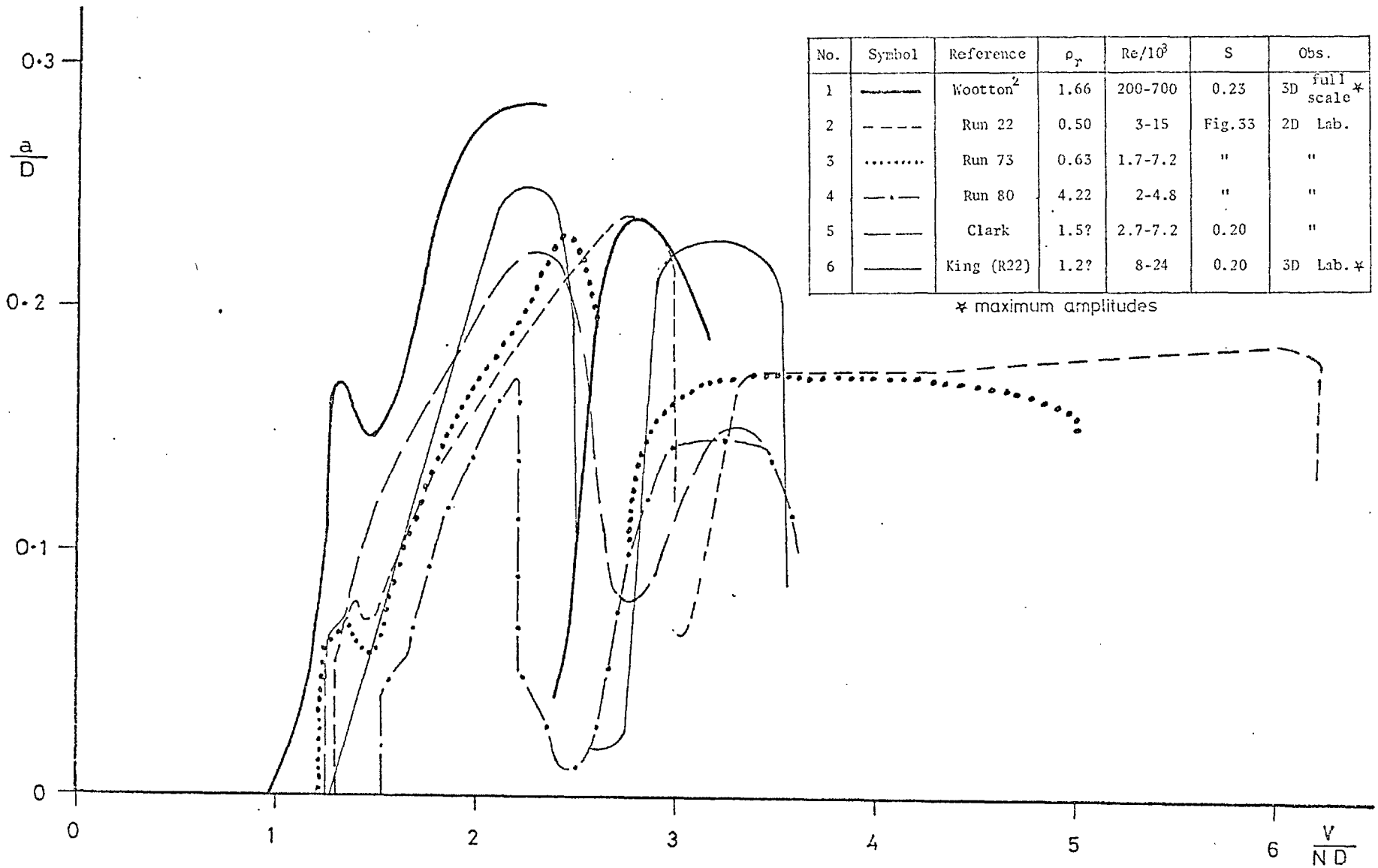

No.	Symbol	Reference	ρ_r	$Re/10^3$	S	Obs.
1	———	Wootton[2]	1.66	200-700	0.23	3D full scale *
2	– – – –	Run 22	0.50	3-15	Fig.33	2D Lab.
3	·····	Run 73	0.63	1.7-7.2	"	"
4	—·—	Run 80	4.22	2-4.8	"	"
5	— —	Clark	1.5?	2.7-7.2	0.20	"
6	———	King (R22)	1.2?	8-24	0.20	3D Lab. *

* maximum amplitudes

Fig. 3 Amplitude response of different cylinder-flow arrangements plotted against (V/ND)

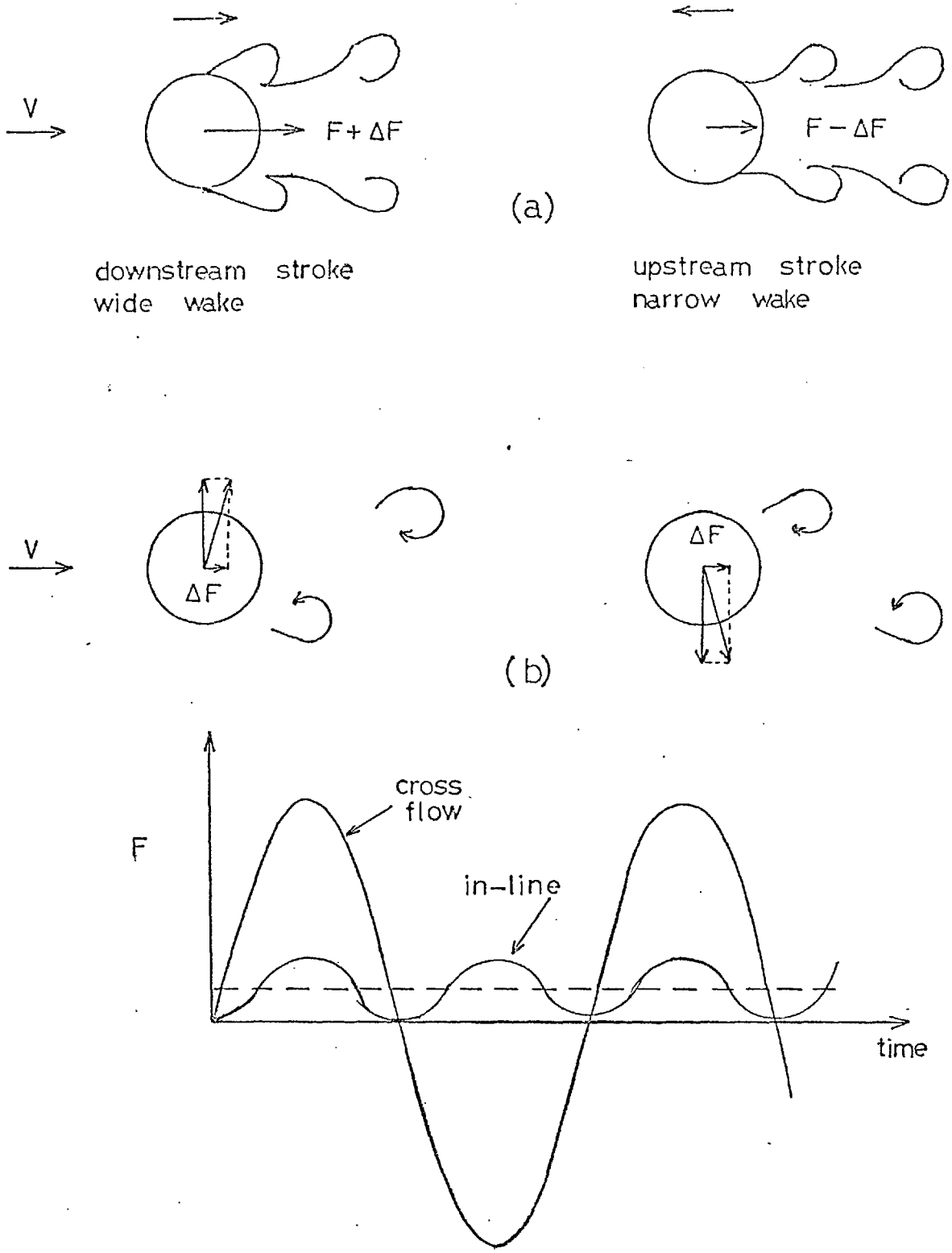

Fig. 4 Schematic representation of the basic forces and flow patterns associated with eddy shedding: (a) simultaneous shedding (pairs); (b) alternate shedding, showing frequency ratio of in-line and cross-flow forces

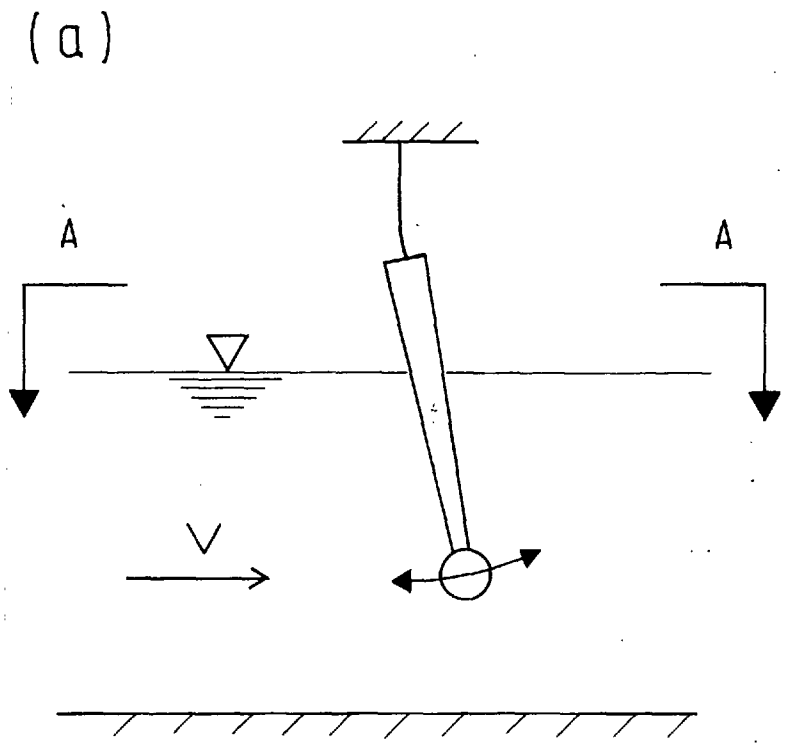

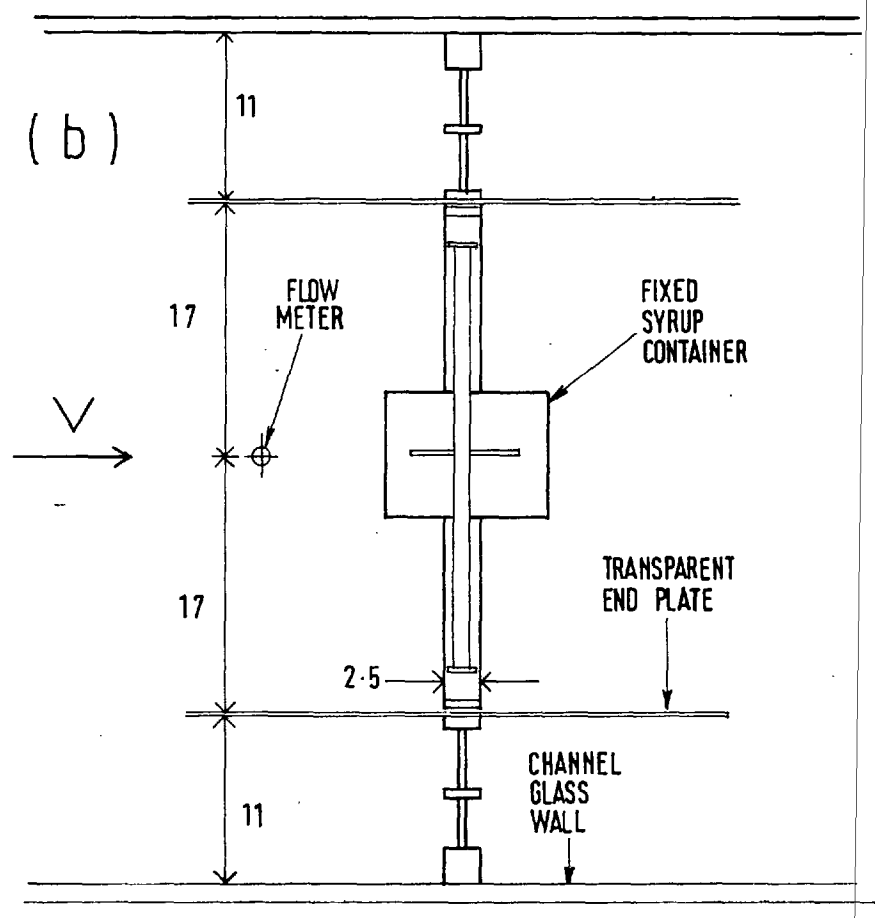

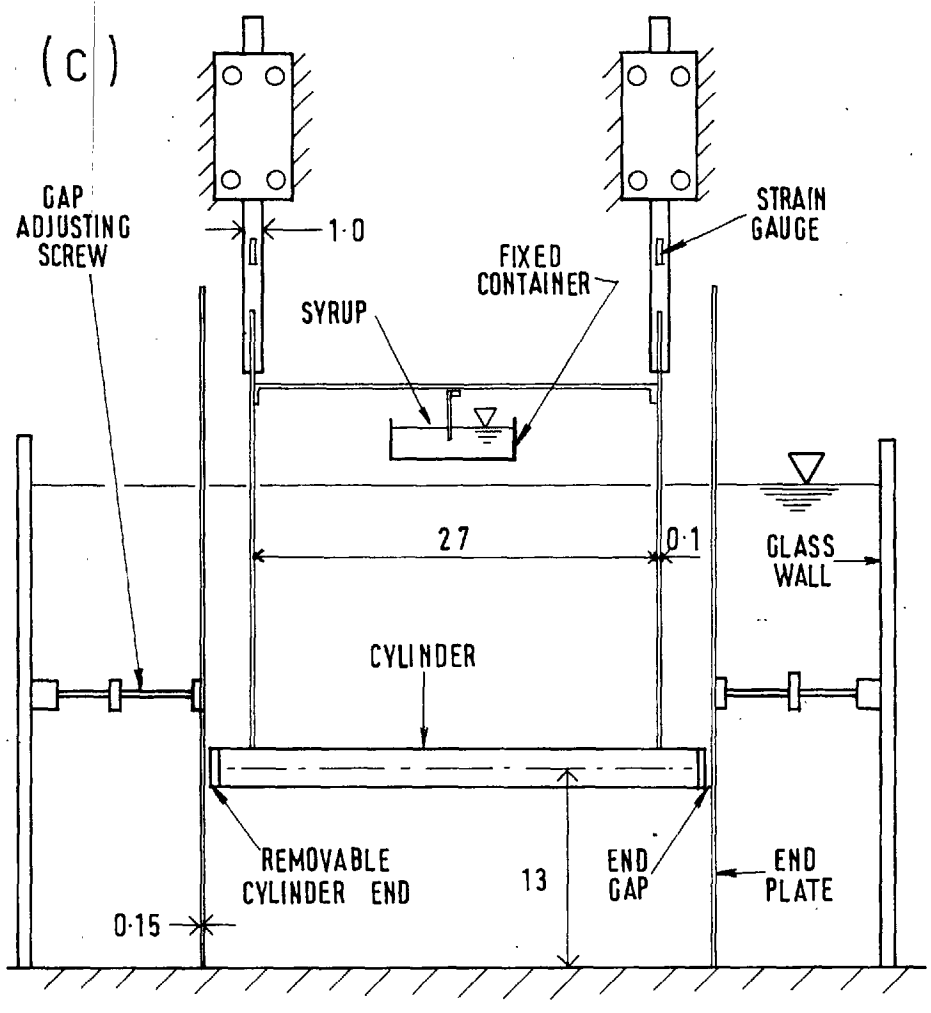

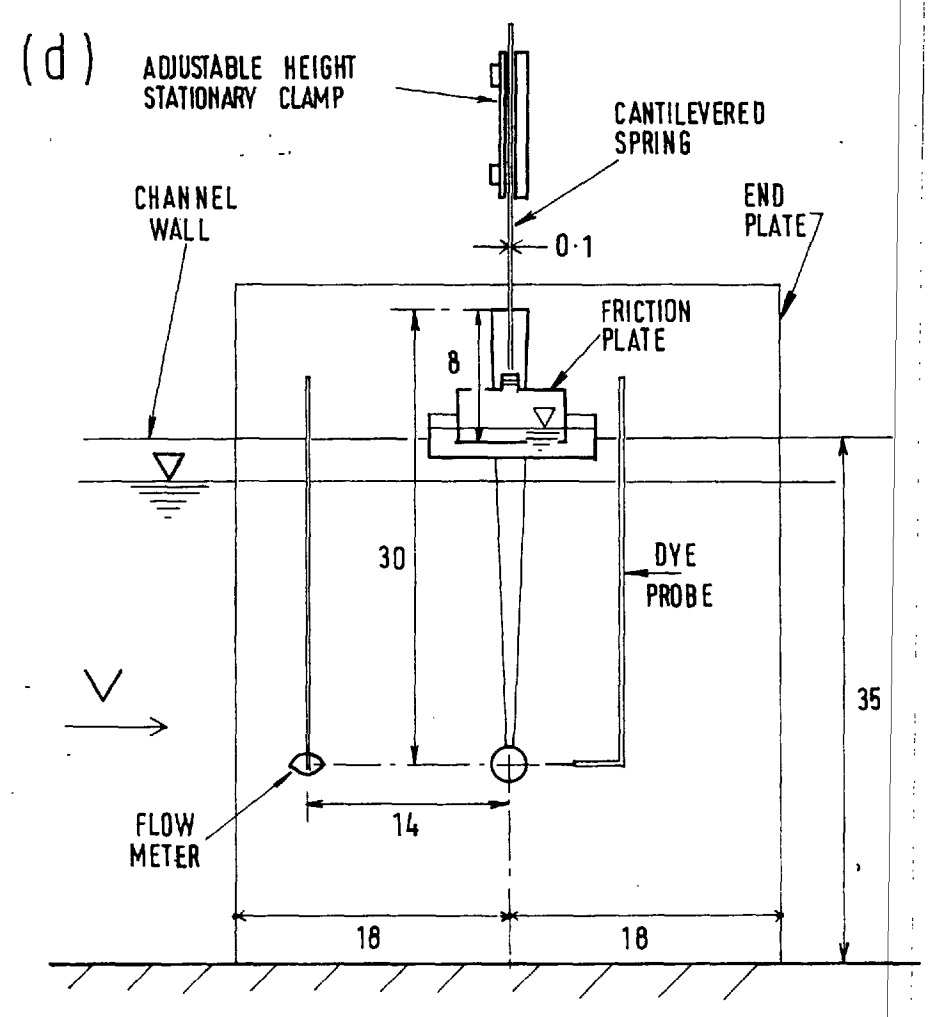

FIG. 5 - Experimental arrangement showing the 2·5 cm dia cylinder and the viscous damper. Dimensions in cm. a) Cylinder and flow motion, b) Section A-A showing flow meter, c) Frontal view, d) Side view showing flow meter and dye probe.

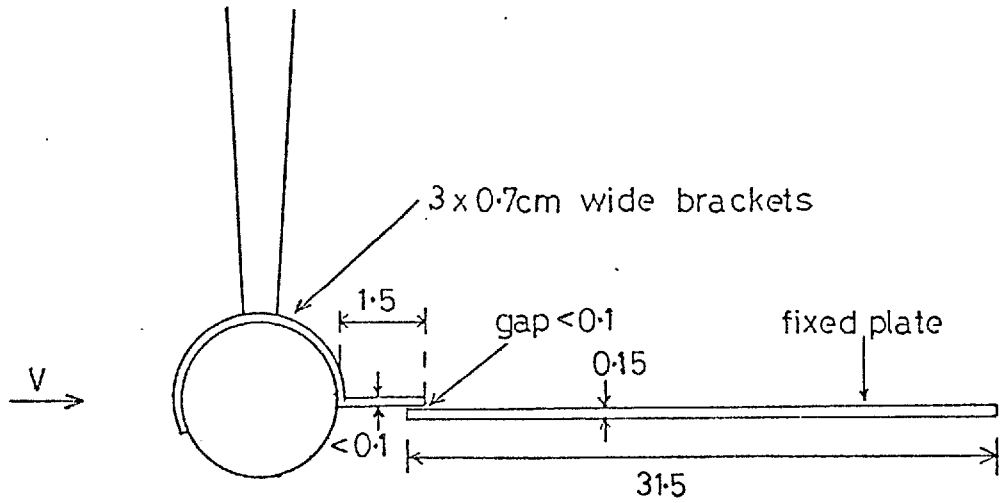

Fig. 6 The two sections of the splitter plate

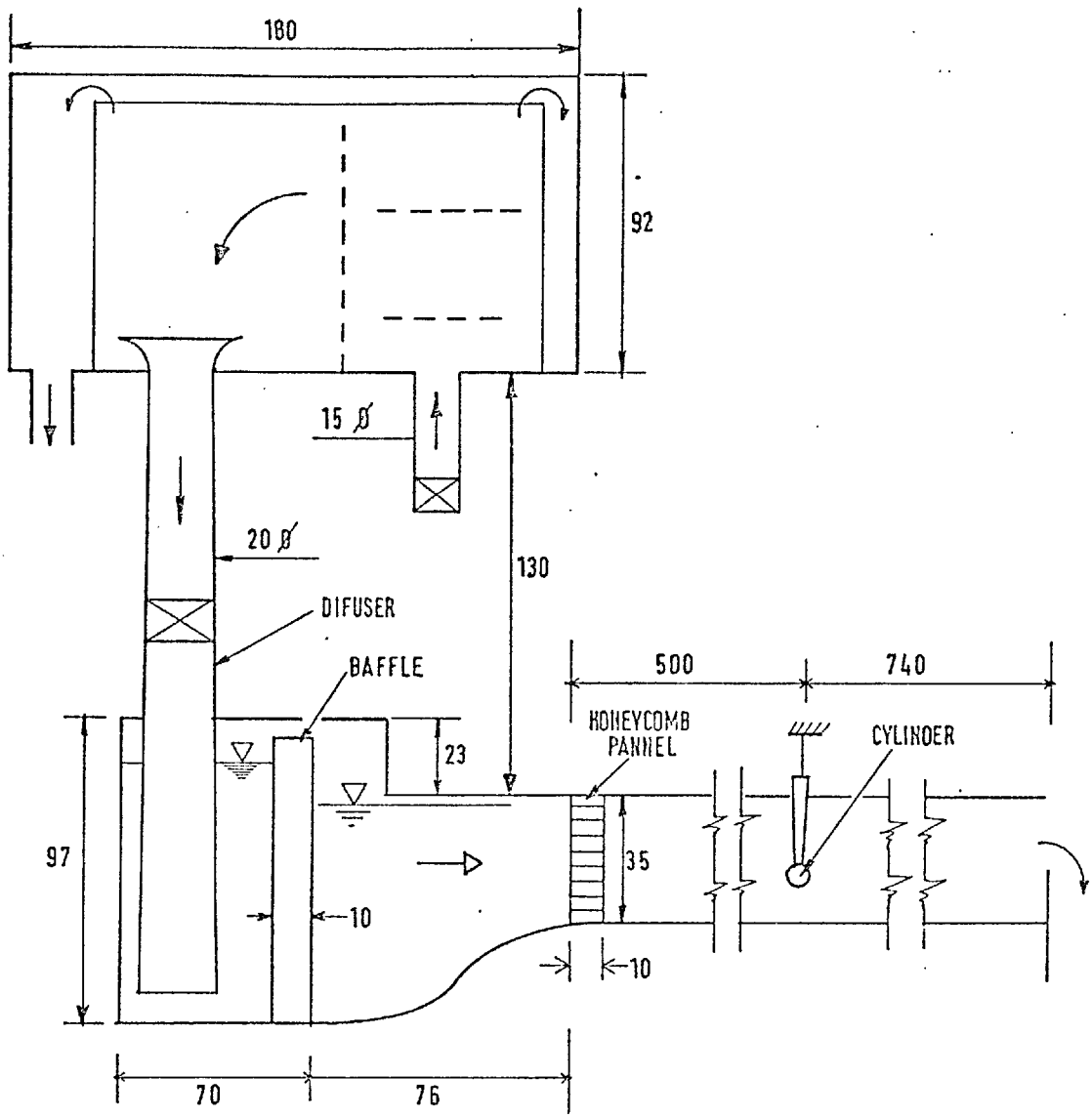

Fig. 7 Schematic side view of the flume and of the stilling tank installed for the second set of tests

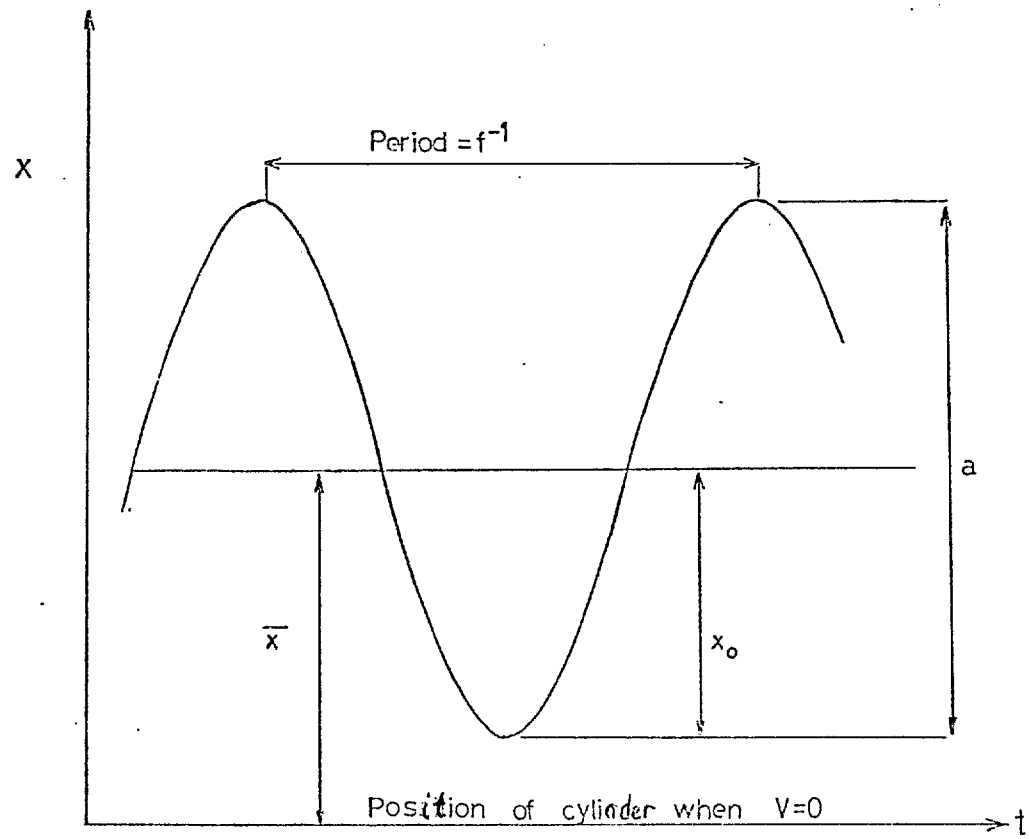

Fig. 8 Schematic (a/D) vs time trace of cylinder vibration for $V \neq 0$, showing definition of x_o, $\overline{x}$, a and f

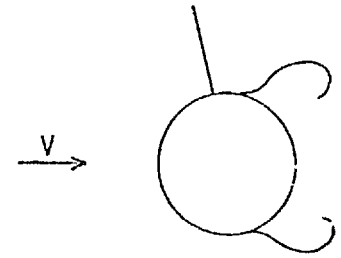

(a) down stream position - a pair of eddies has just been shed, separation points move back and f.s.l. come closer together

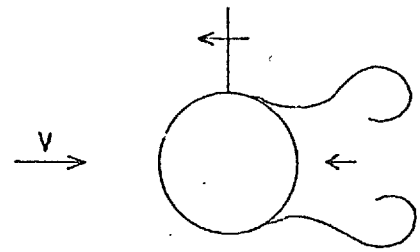

(b) mean position moving upstream - separation points at their rearmost position, f.s.l. at their closest and the wake is narrowest, flow inside the wake starts to move upstream

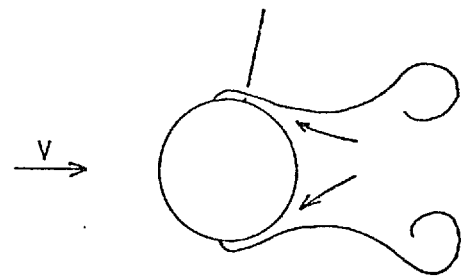

(c) upstream position - new eddies have started to grow on the sides of the cylinder at or near the separation points which are moving upstream; upstream wake flow feeds the eddies

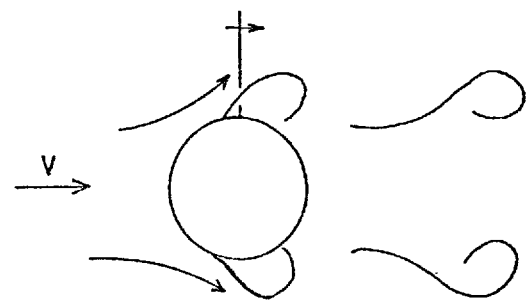

(d) mean position moving downstream - eddies are markedly grown; the main flow approaching the cylinder behaves as if it encountered a larger cylinder or a bluffer body, eddies start to move downstream

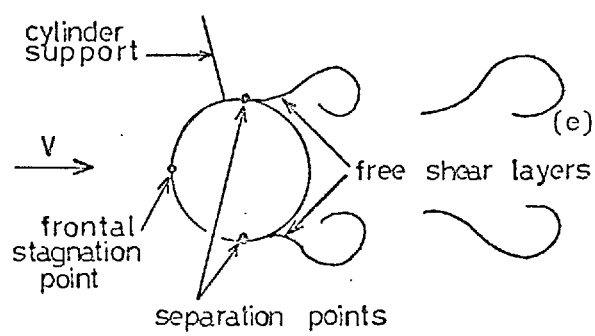

(e) as in (a)

Fir. 9 Flow patterns of the "pairs mechanism" (see also Plate 1). Note: f.s.l. = free shear layer

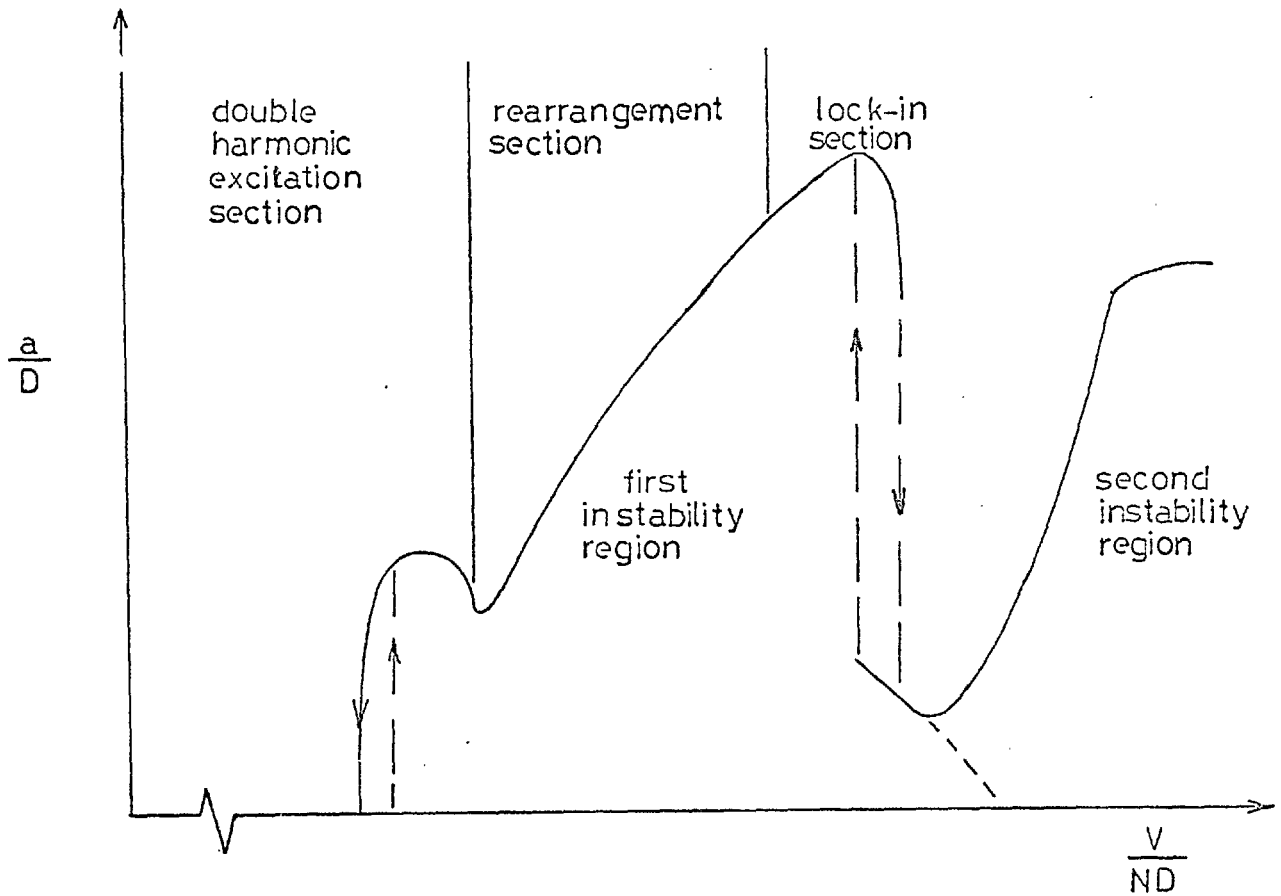

Fig. 10 Sections of the first instability region

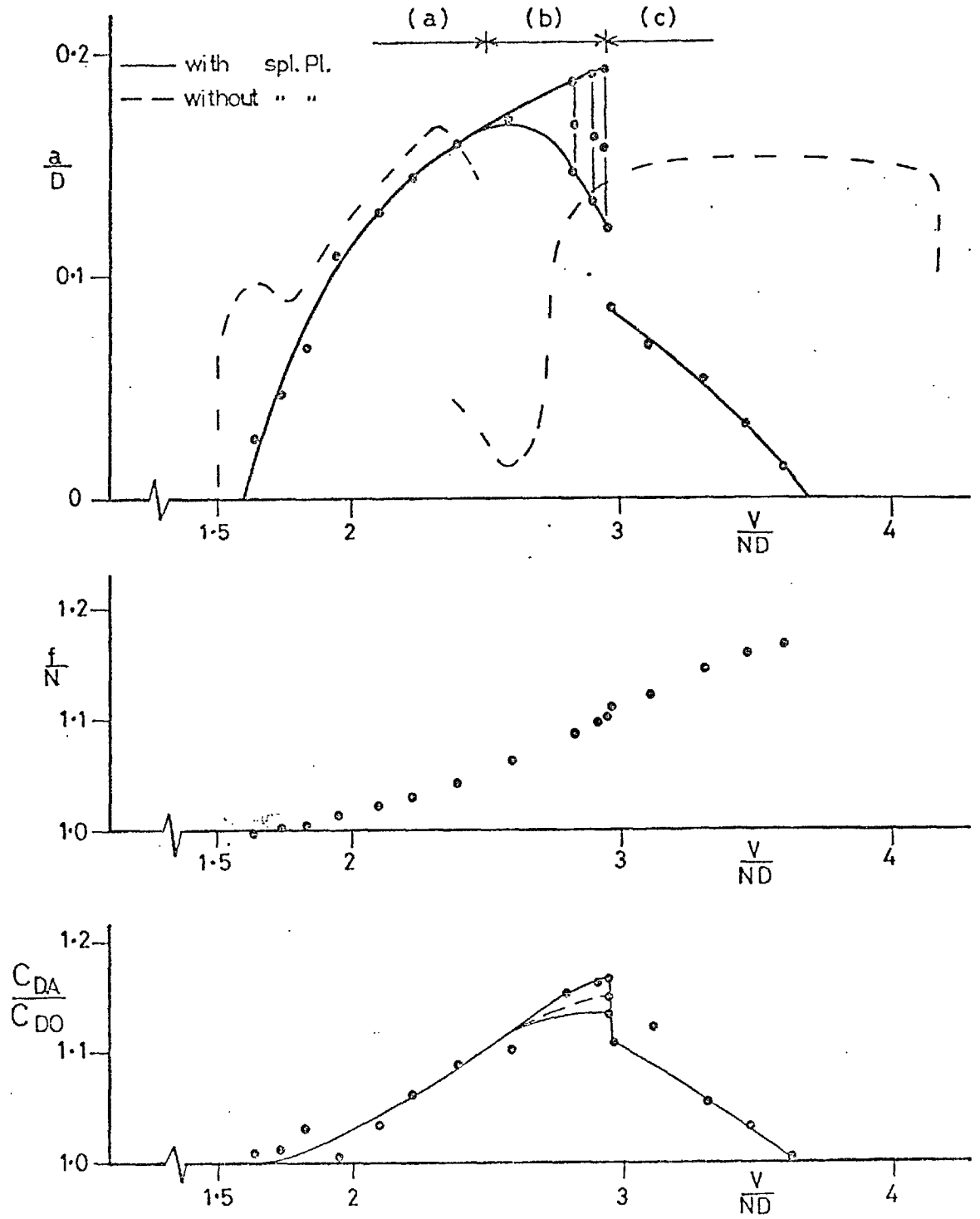

Fig. 11 Response of a cylinder fitted with a splitter plate (Run 111) and amplitude response of a bare cylinder (R 101) for comparison

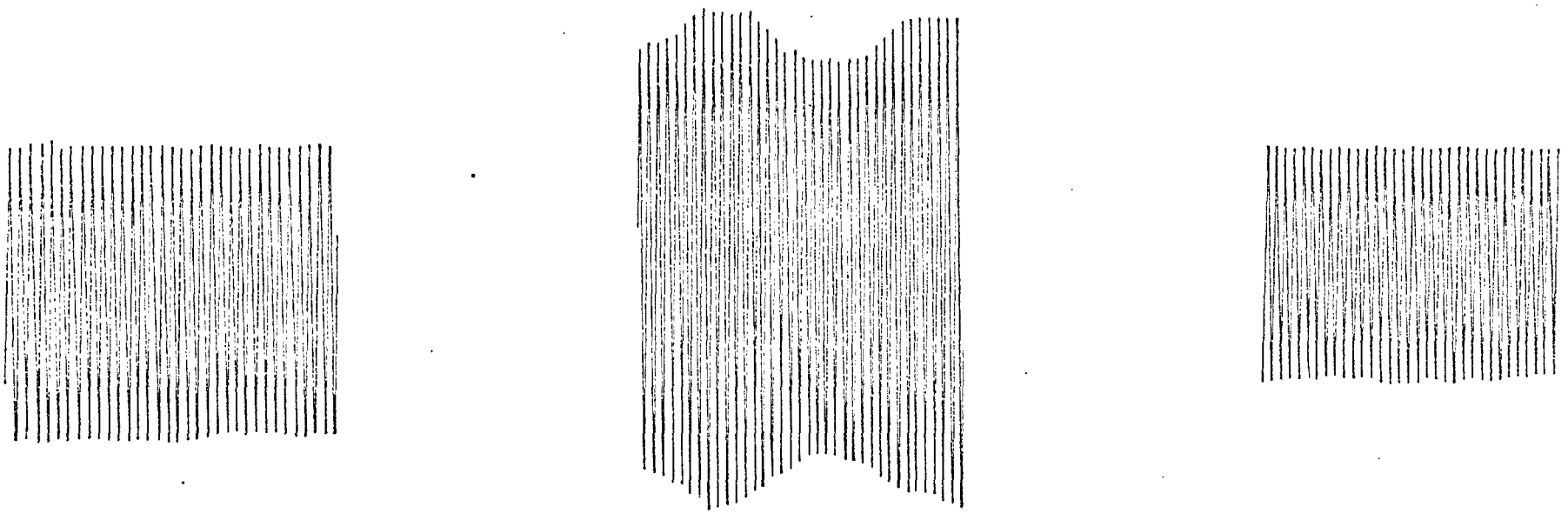

Fig. 12 Samples of (a/D) vs time traces of a cylinder fitted with a splitter plate (from Run 111)

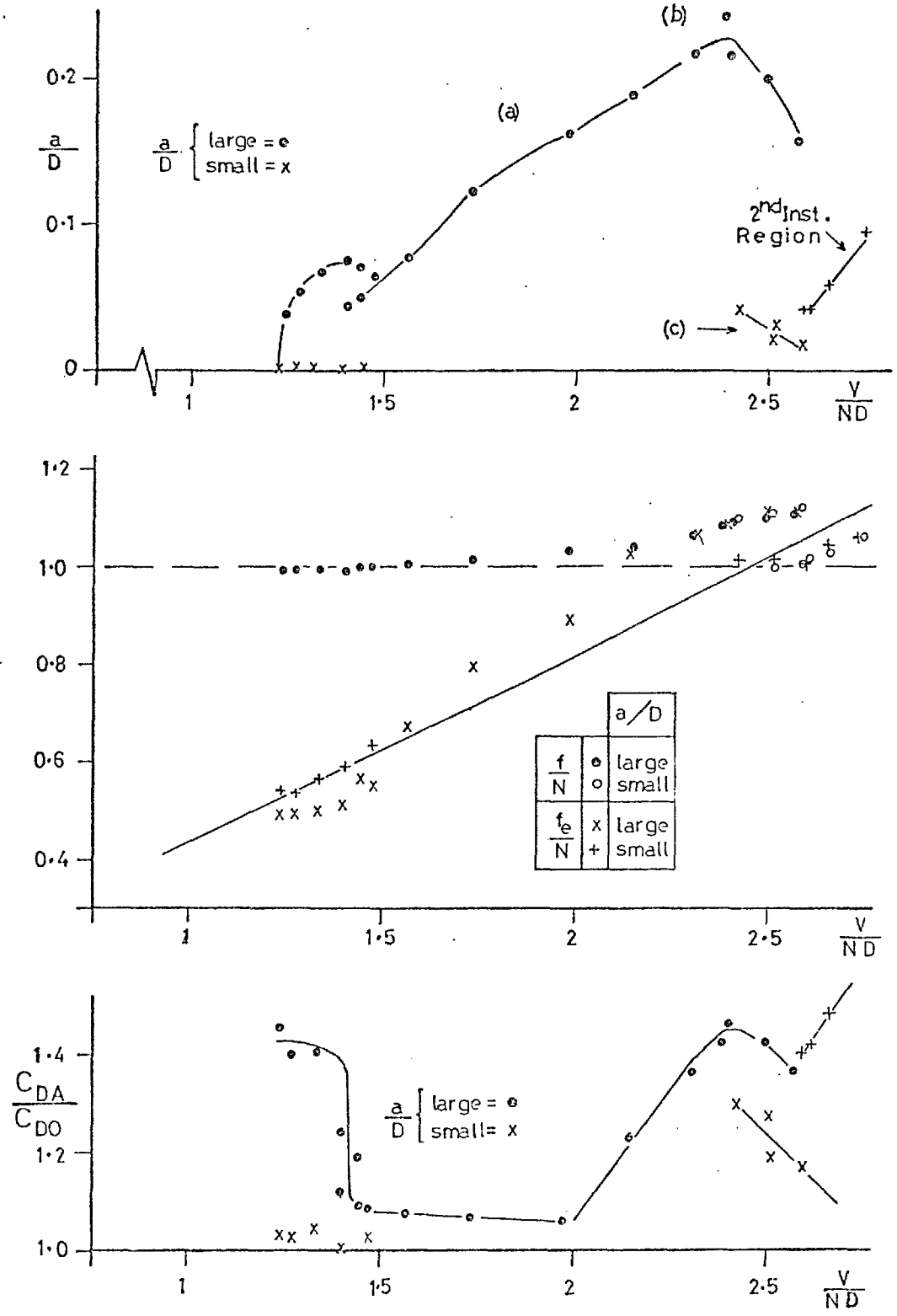

Fig. 13 Cylinder and wake behaviour in the first instability region; from Run 99

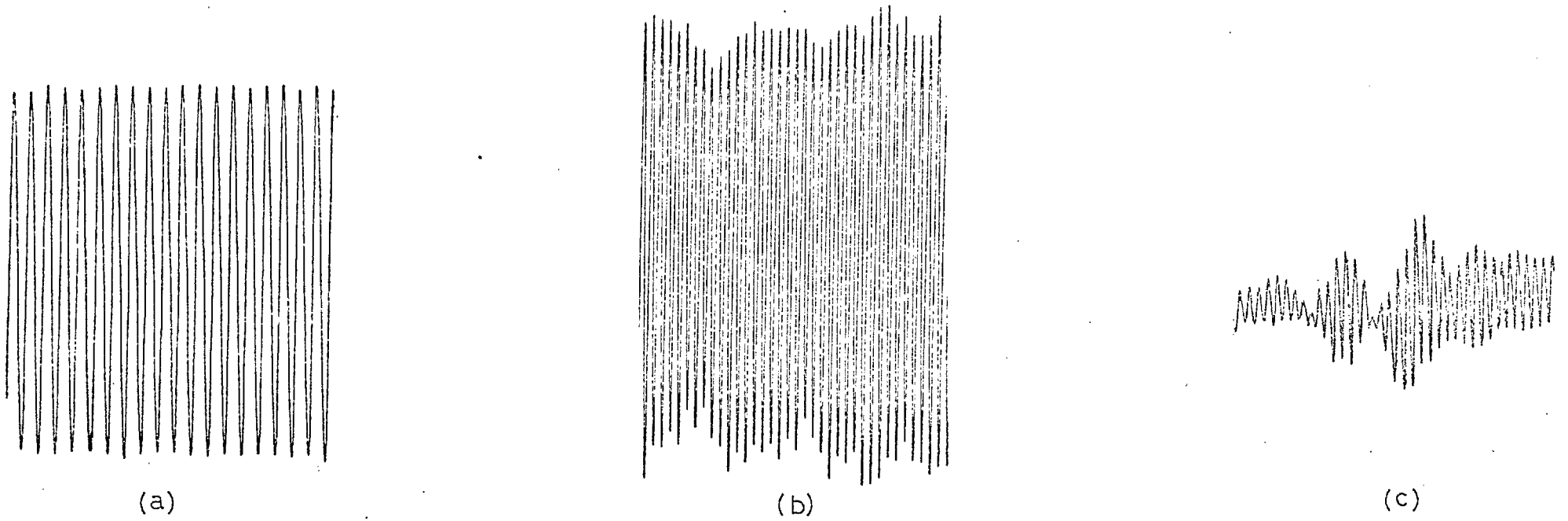

Fig. 14 (a/D) vs time traces in the first instability region, corresponding to the sections marked a, b and c in Fig. 13

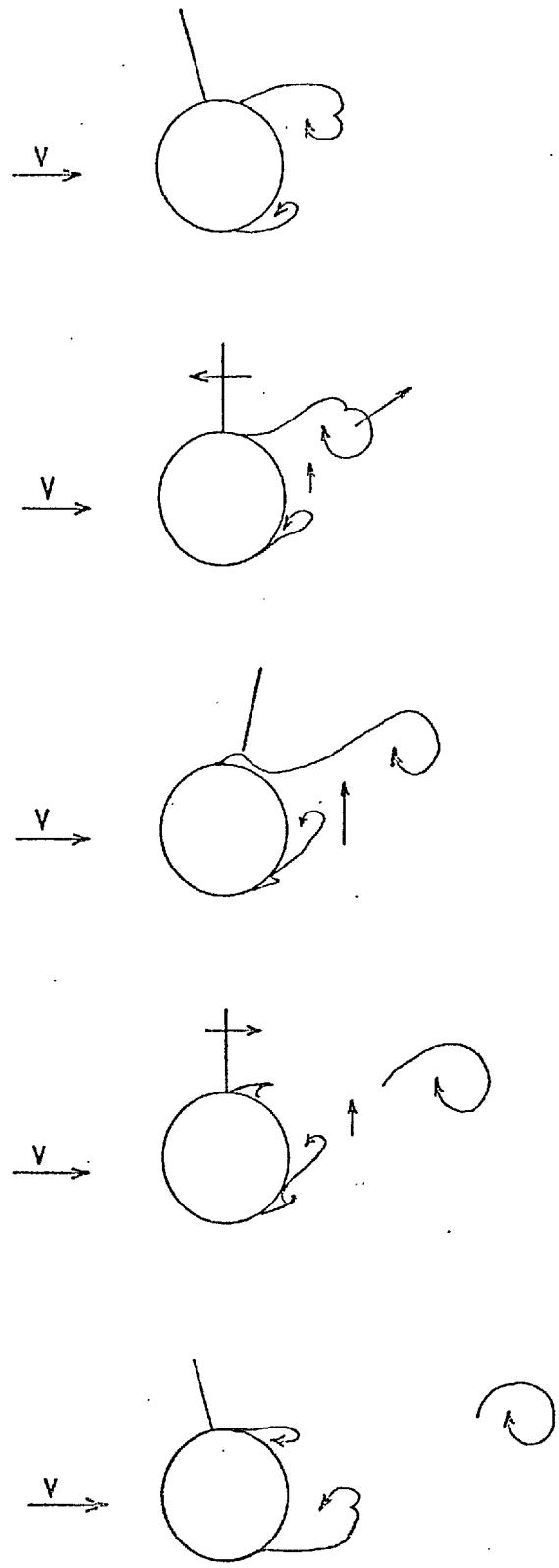

Fig. 15 Flow patterns in the lock-in section of the first instability region showing both the transverse flow and a pair of simultaneous eddies (see also Plate 3)

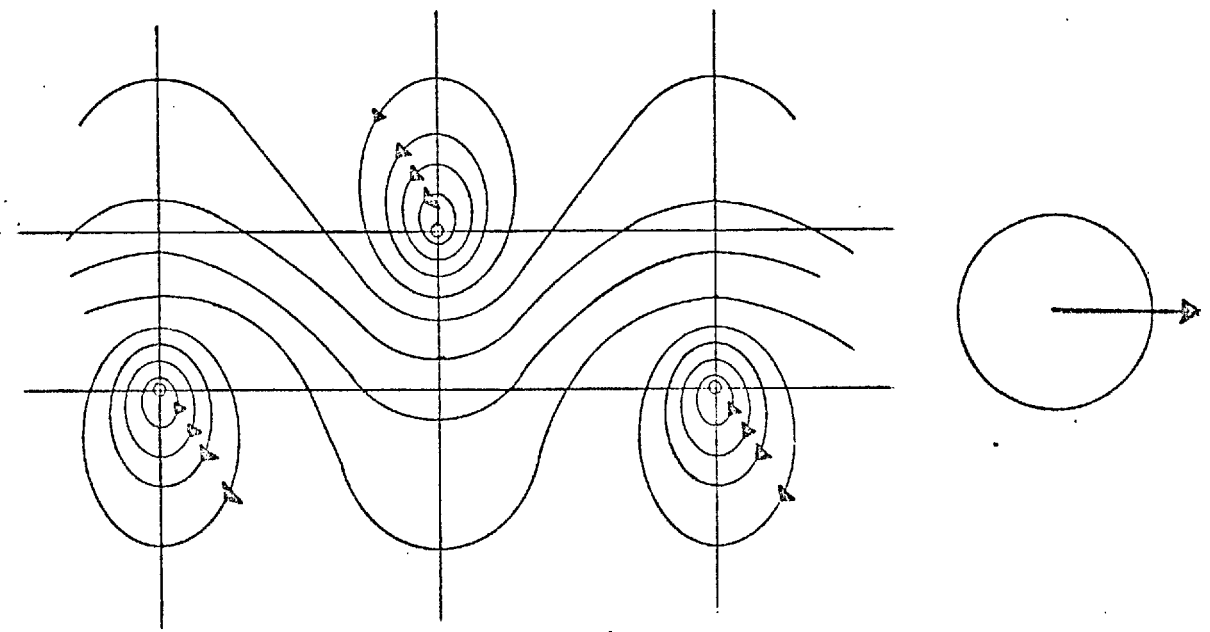

Fig. 16 Potential flow representation of a Von Kàrmàn wake

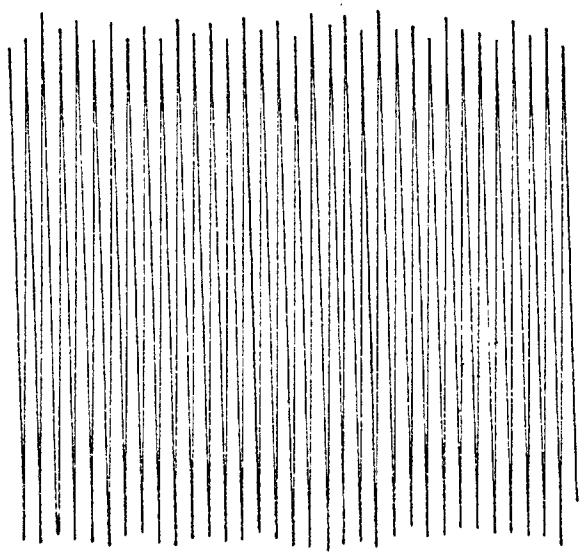

(a)

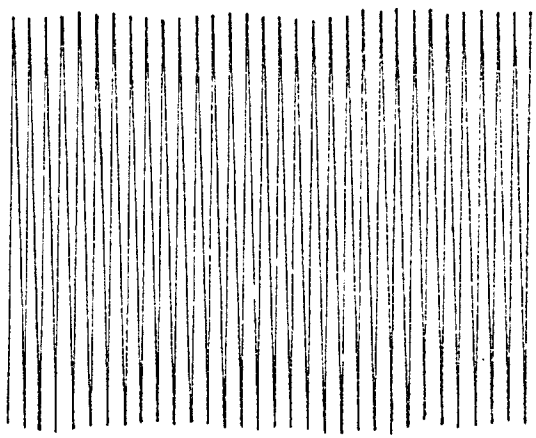

(b)

Fig. 17 a/D vs time trace at the end of the double harmonic excitation section showing (a) double harmonic excitation and (b) excitation by the "pairs mechanism" alone

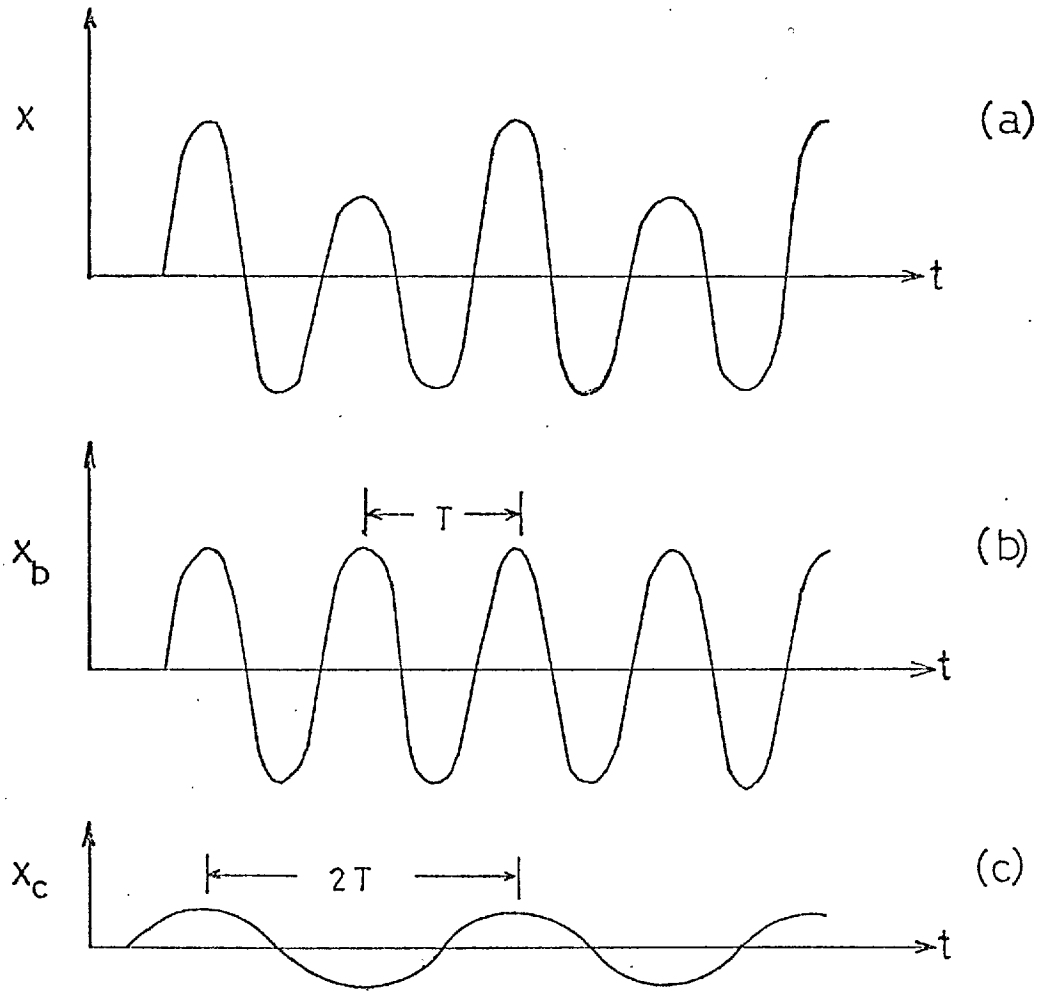

Fig. 18 Dominant harmonic components of the vibration in the "double harmonic excitation section" of the first instability region (Note: $T = f^{-1}$)

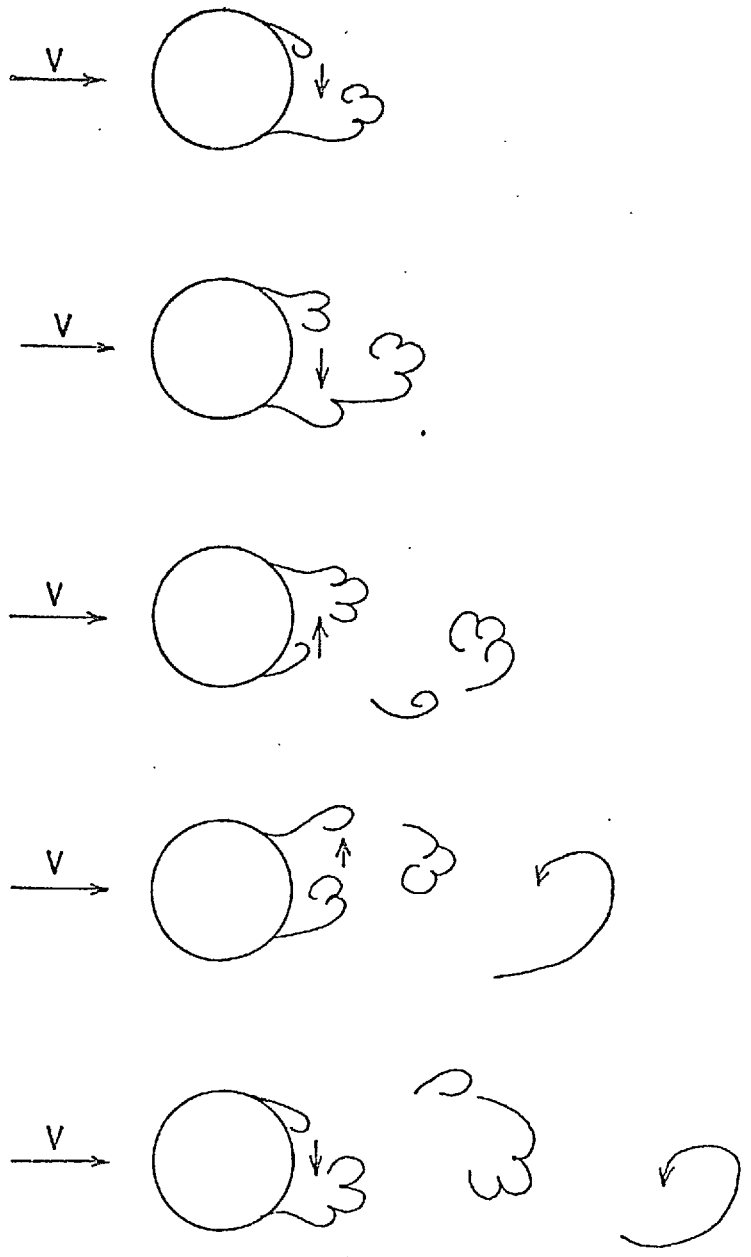

Fig. 19 Eddy organization and transverse flow direction in consecutive cycles of the near wake, in the double harmonic excitation section of the first instability region (see also Plate 4)

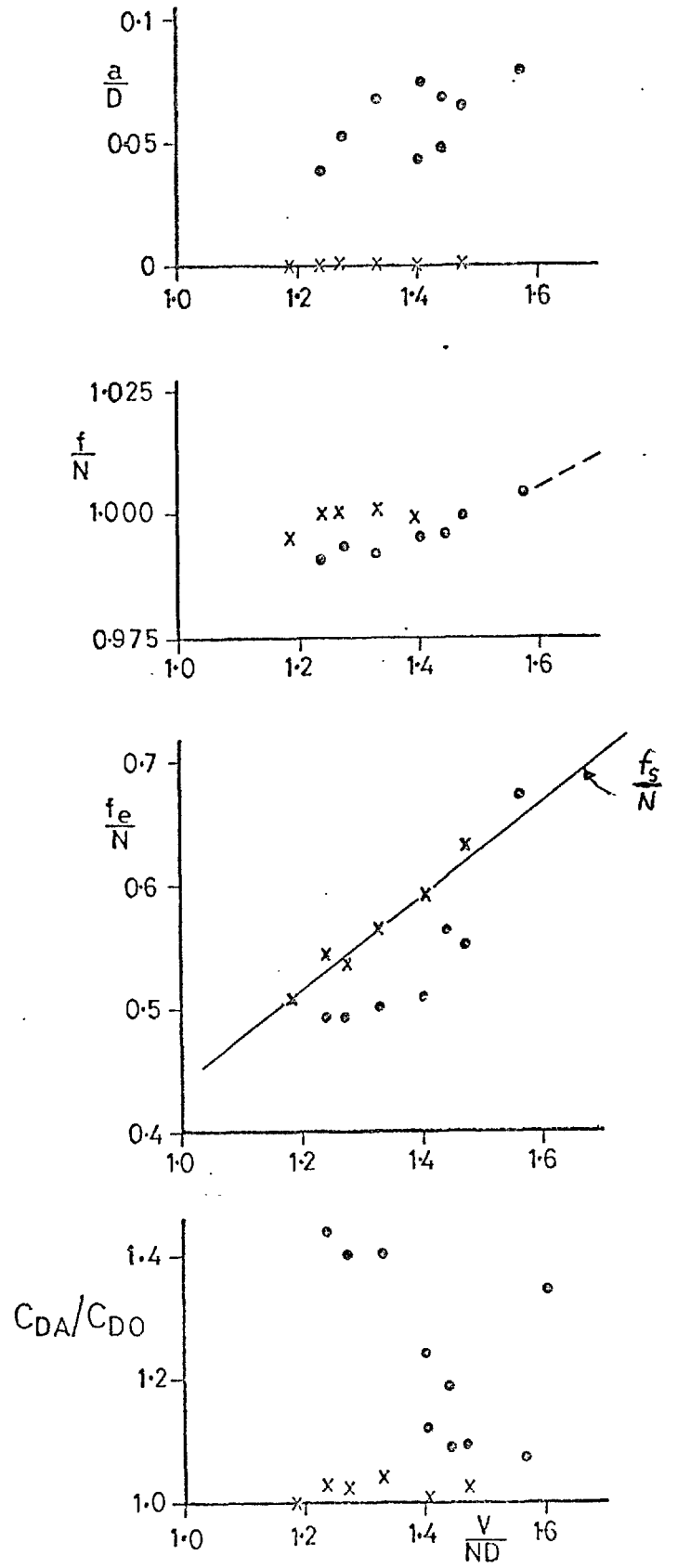

Fig. 20 Cylinder and wake behaviour in the double harmonic excitation section of the first instability region (from Run 99); (⊙) = (a/D) large; X = (a/D) small (no instability)

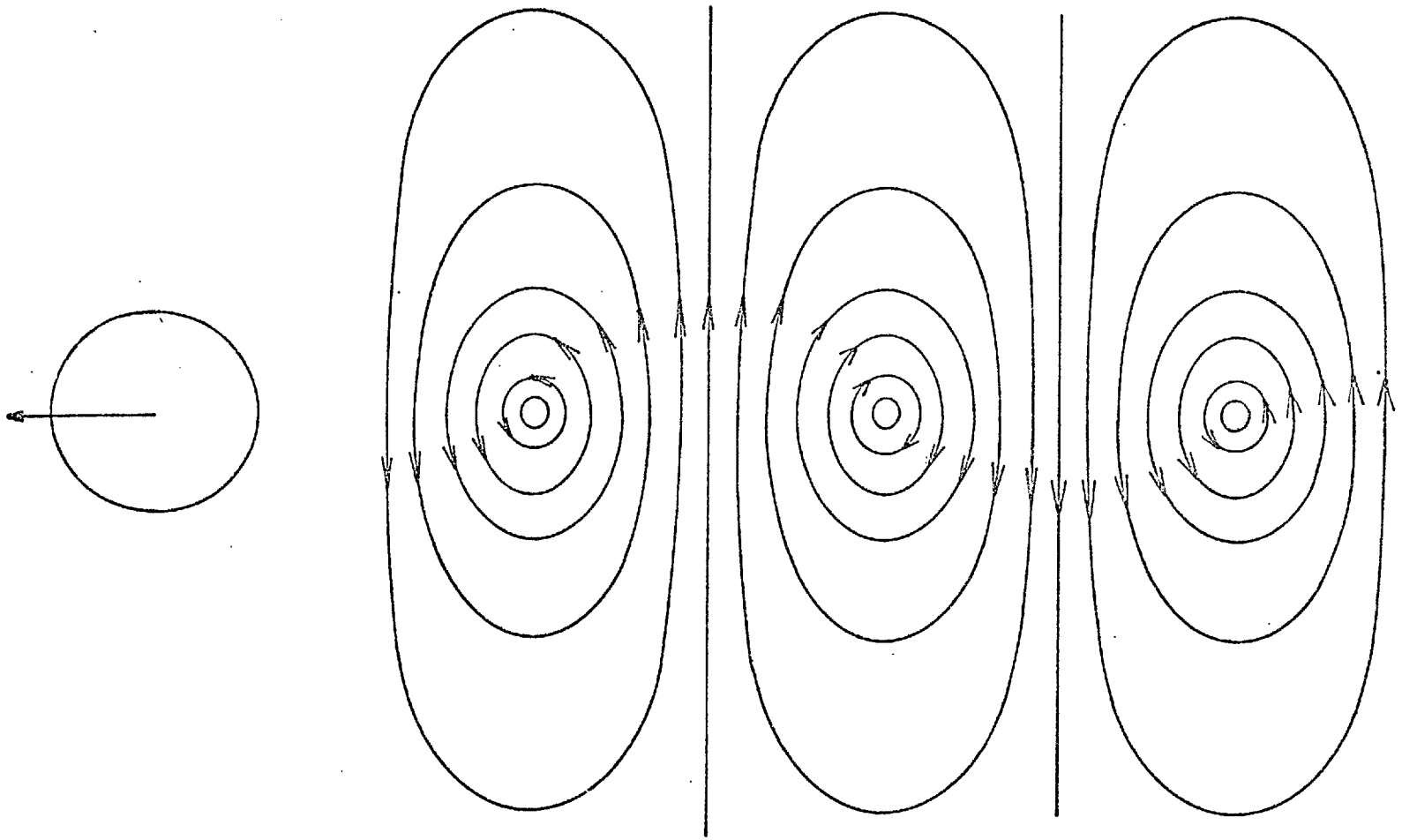

Fig. 21 Potential flow representation of the second peak wake

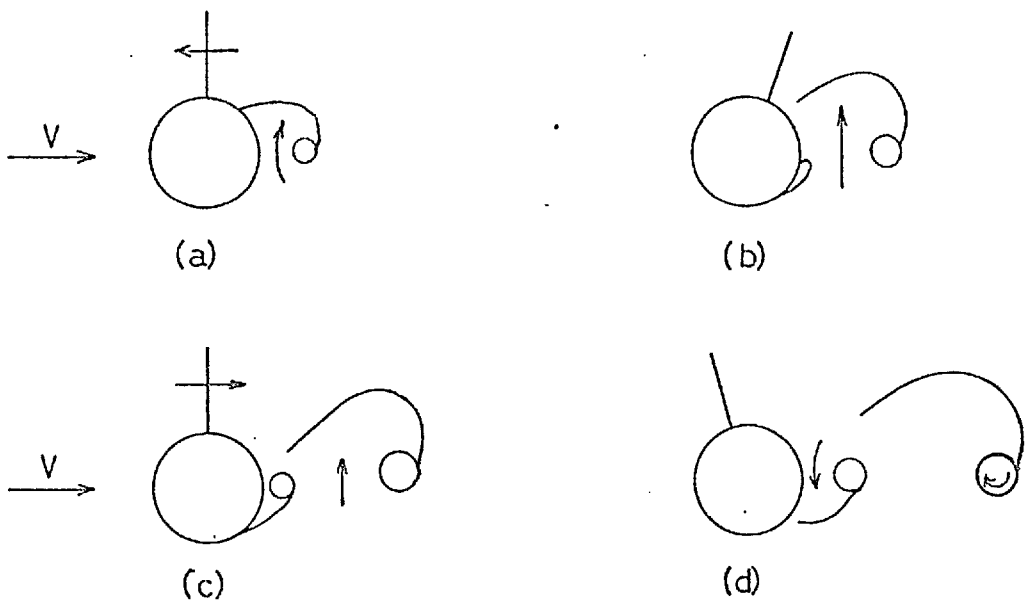

Fig. 22 Shedding process in the second instability region
(see page 37 and Plate 5)

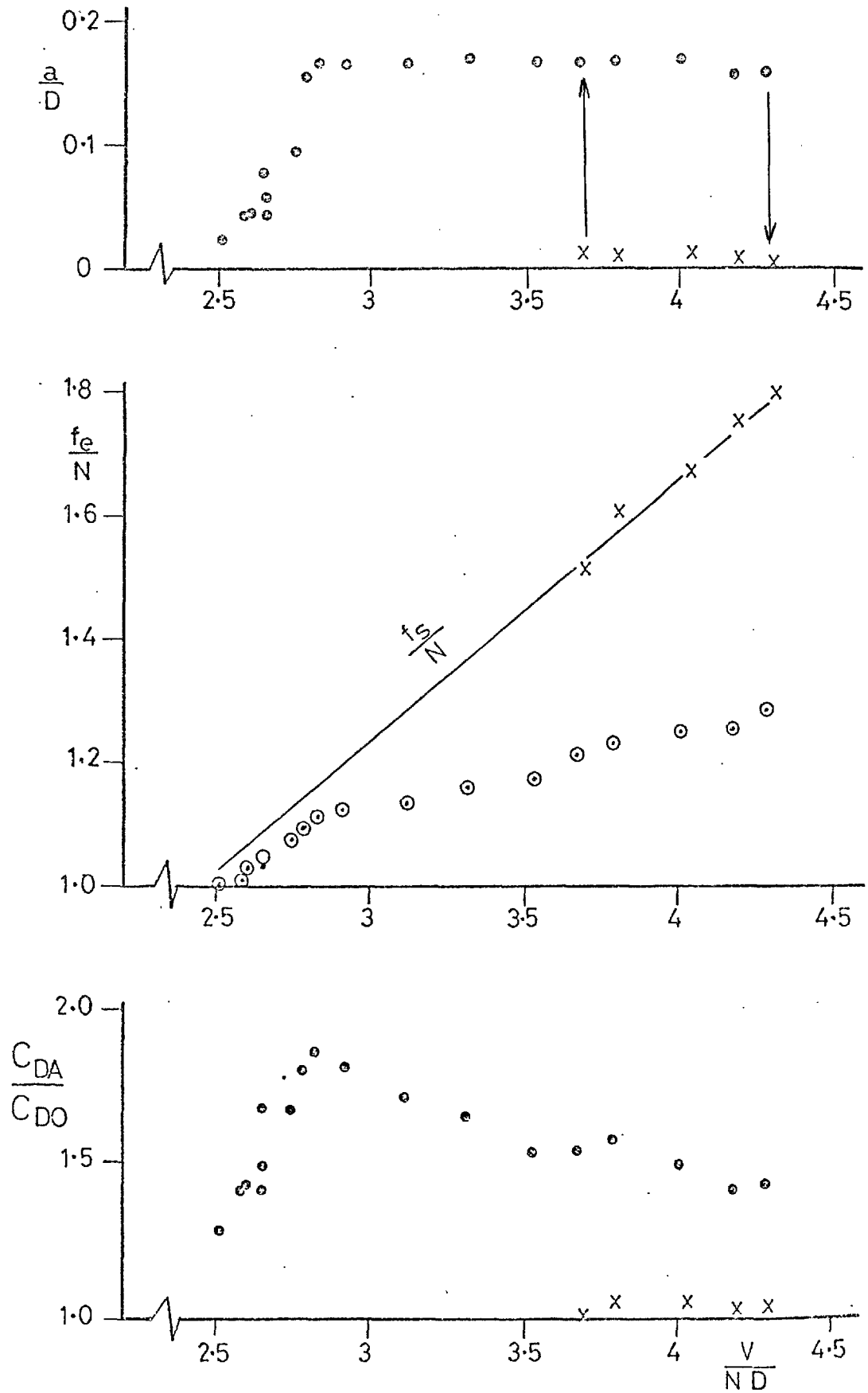

Fig. 23 Cylinder and wake behaviour in the second instability region; (⊙) = $\frac{a}{D}$ large; (X) = $\frac{a}{D}$ small; (O) = (f/N). From run 99.

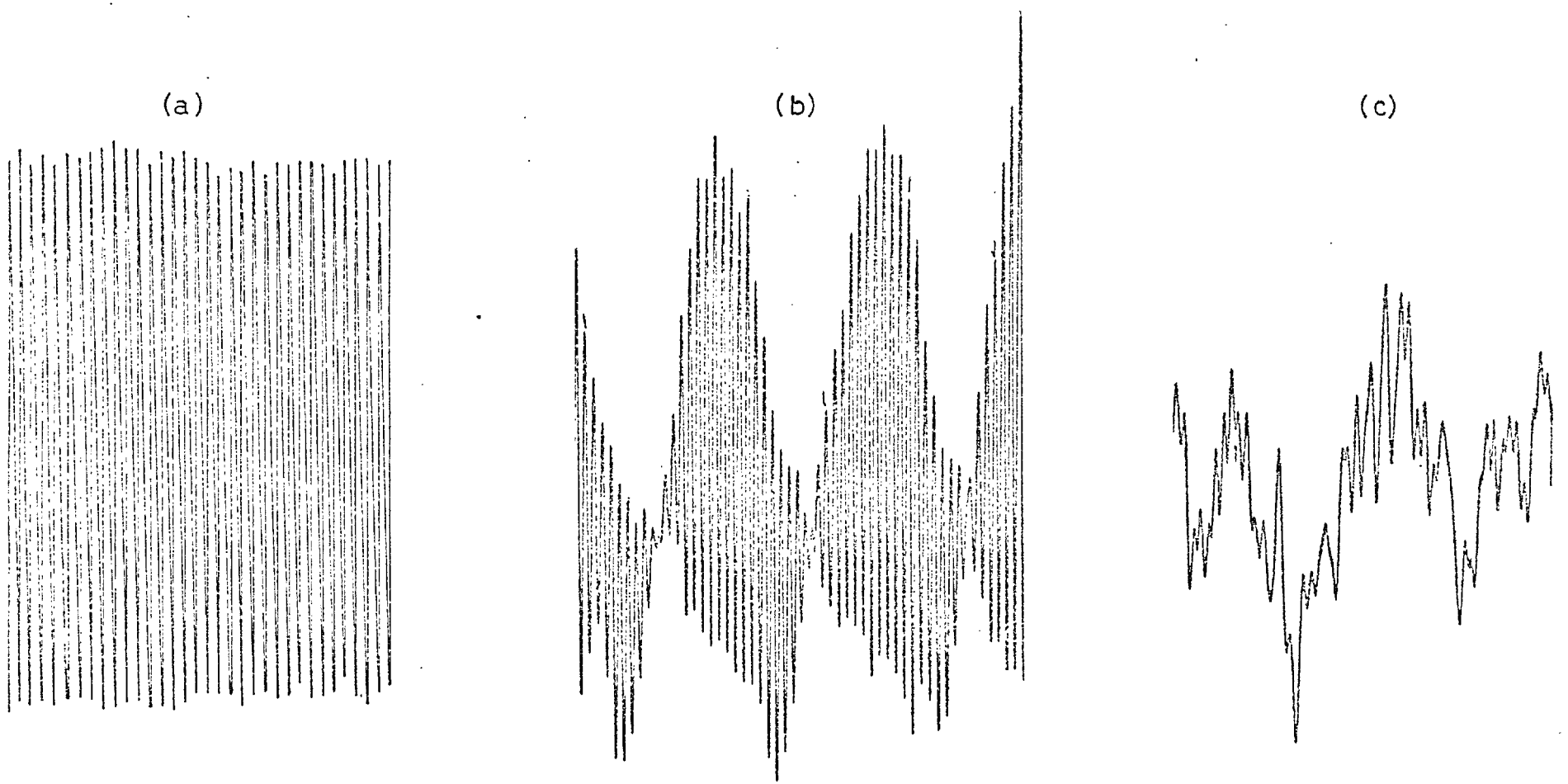

Fig. 24 (a/D) vs time traces in the second instability region: (a) main, constant-amplitude section; (b) growth section; (c) random vibration for (V/ND) values beyond the instability region

Note: traces not at the same scale

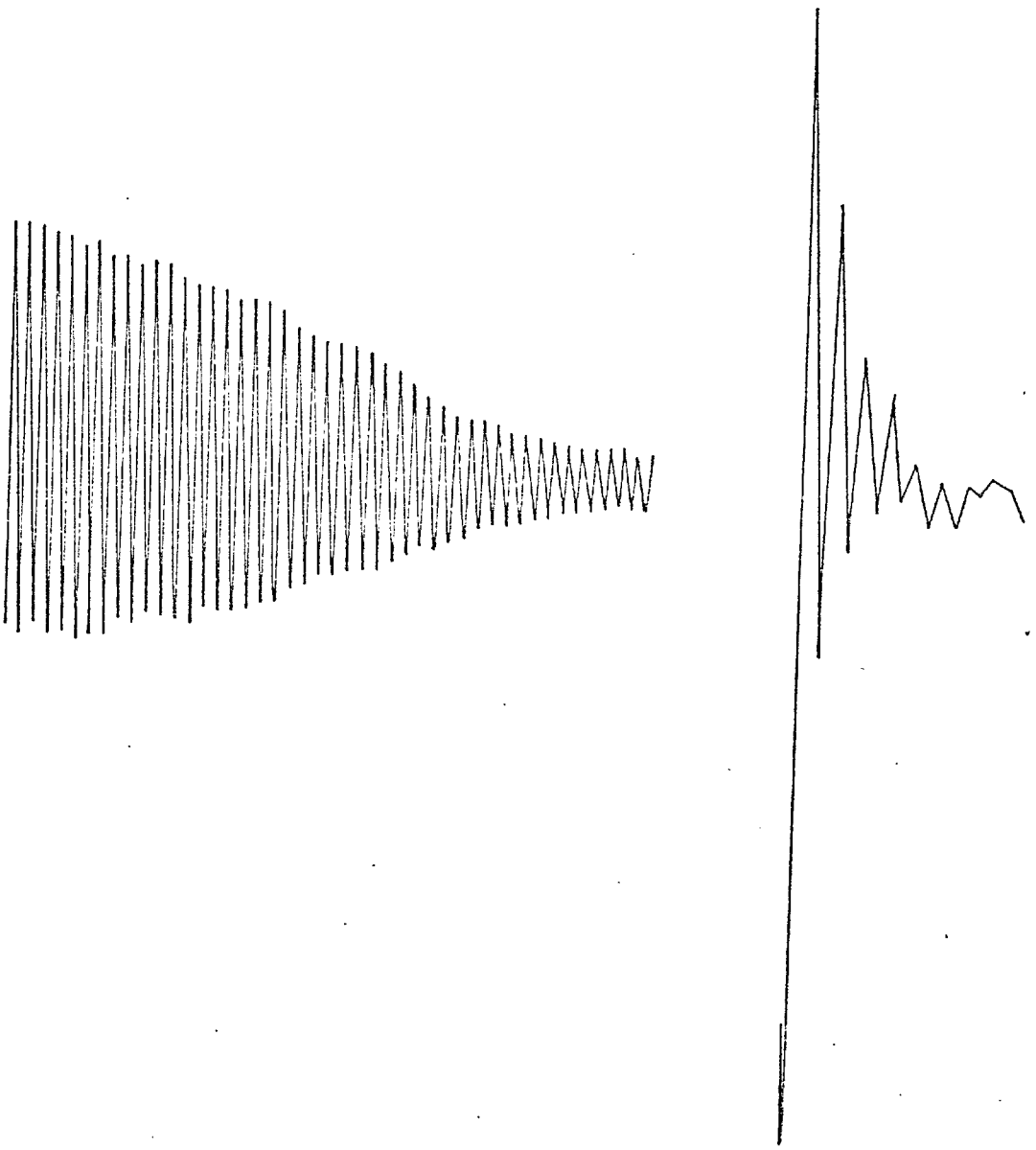

Fig. 25 Recorded transients: (a) for $(f_s/f) \lesssim \sqrt{2}$, and (b) for $(f_s/f) > \sqrt{2}$

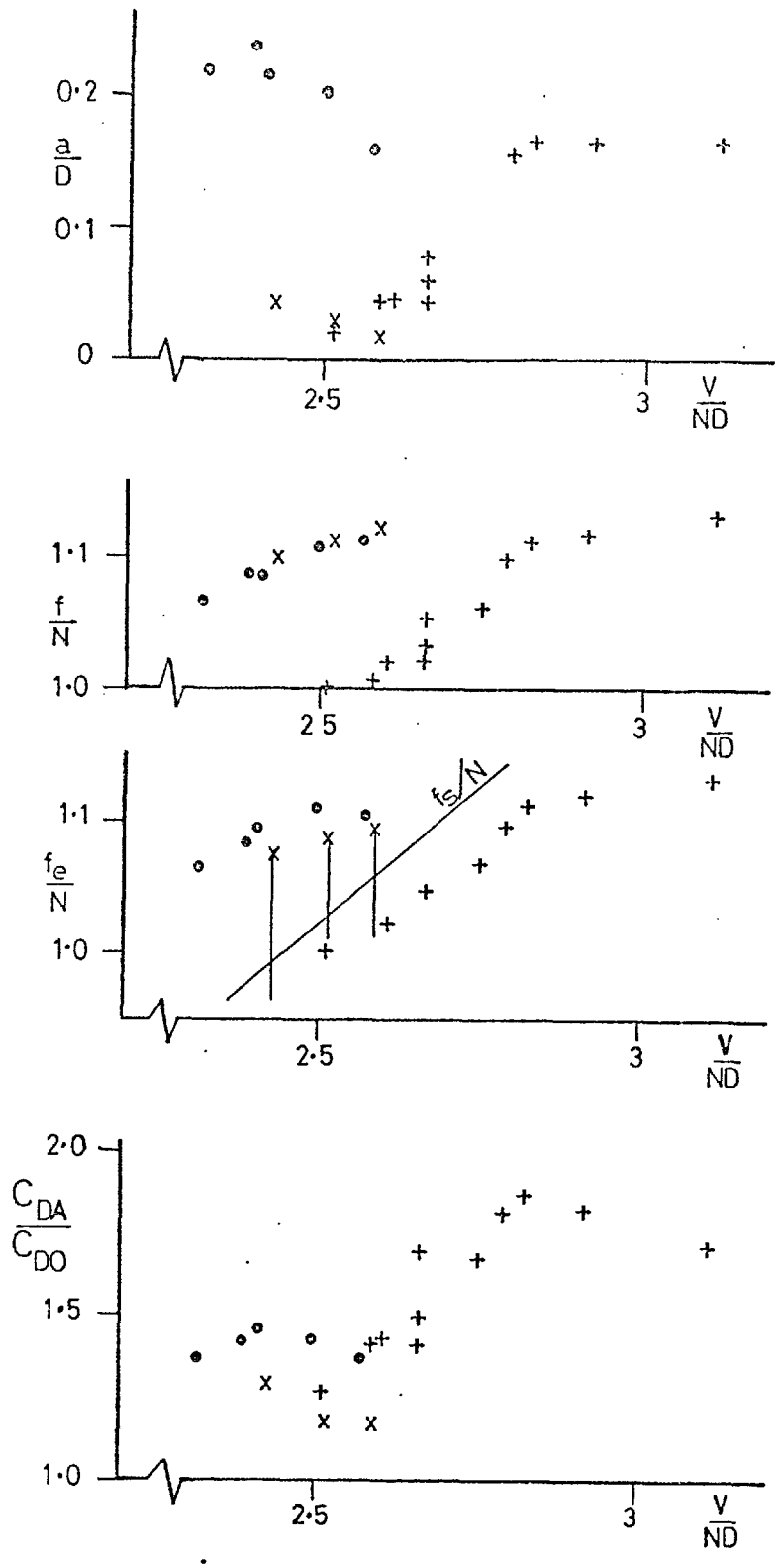

Fig. 26 Cylinder and wake behaviour in the region between instability regions: (● and X) = first; (+) = second. From run 99.

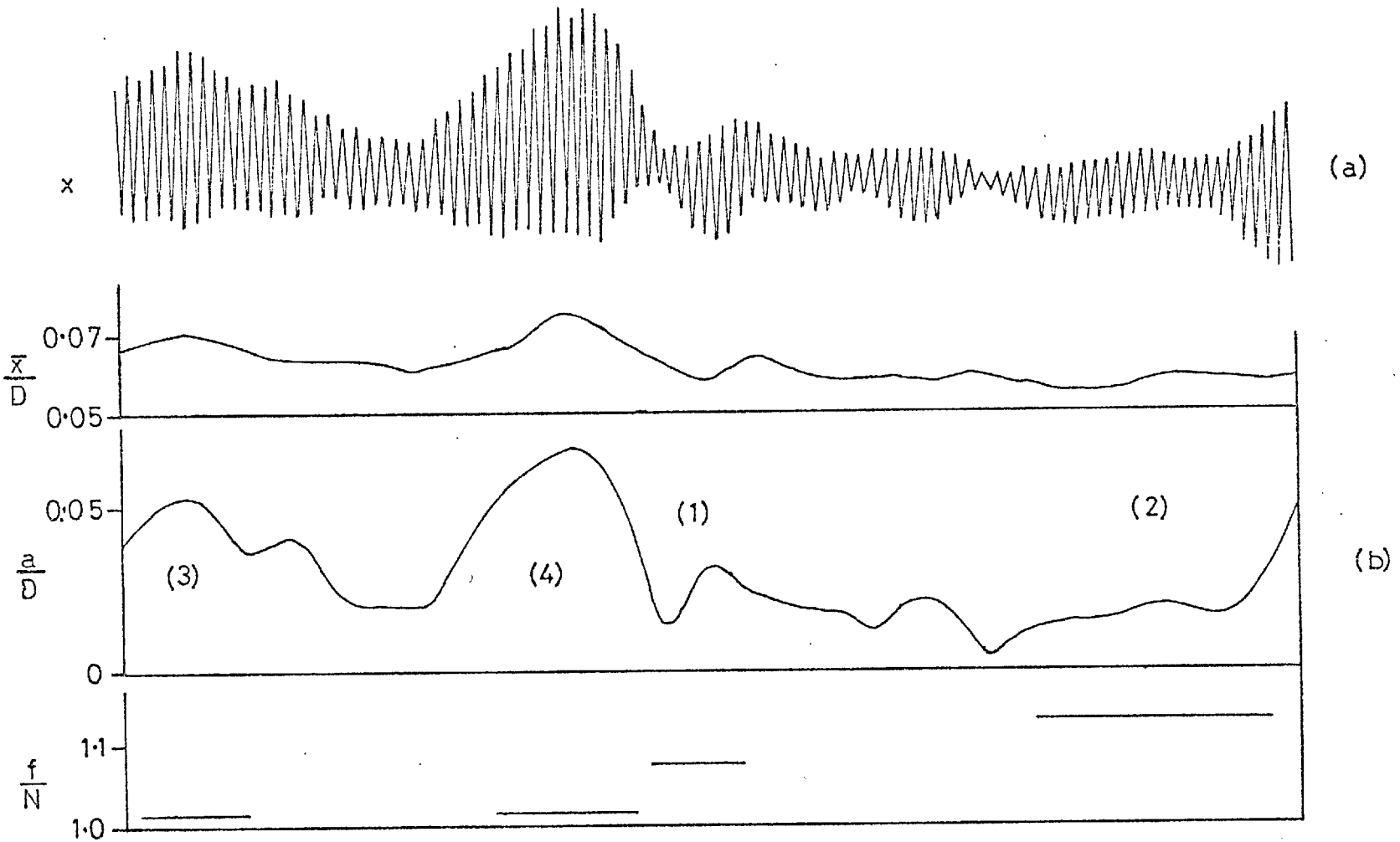

Fig. 27 Analysis of the vibration in the region between instability regions

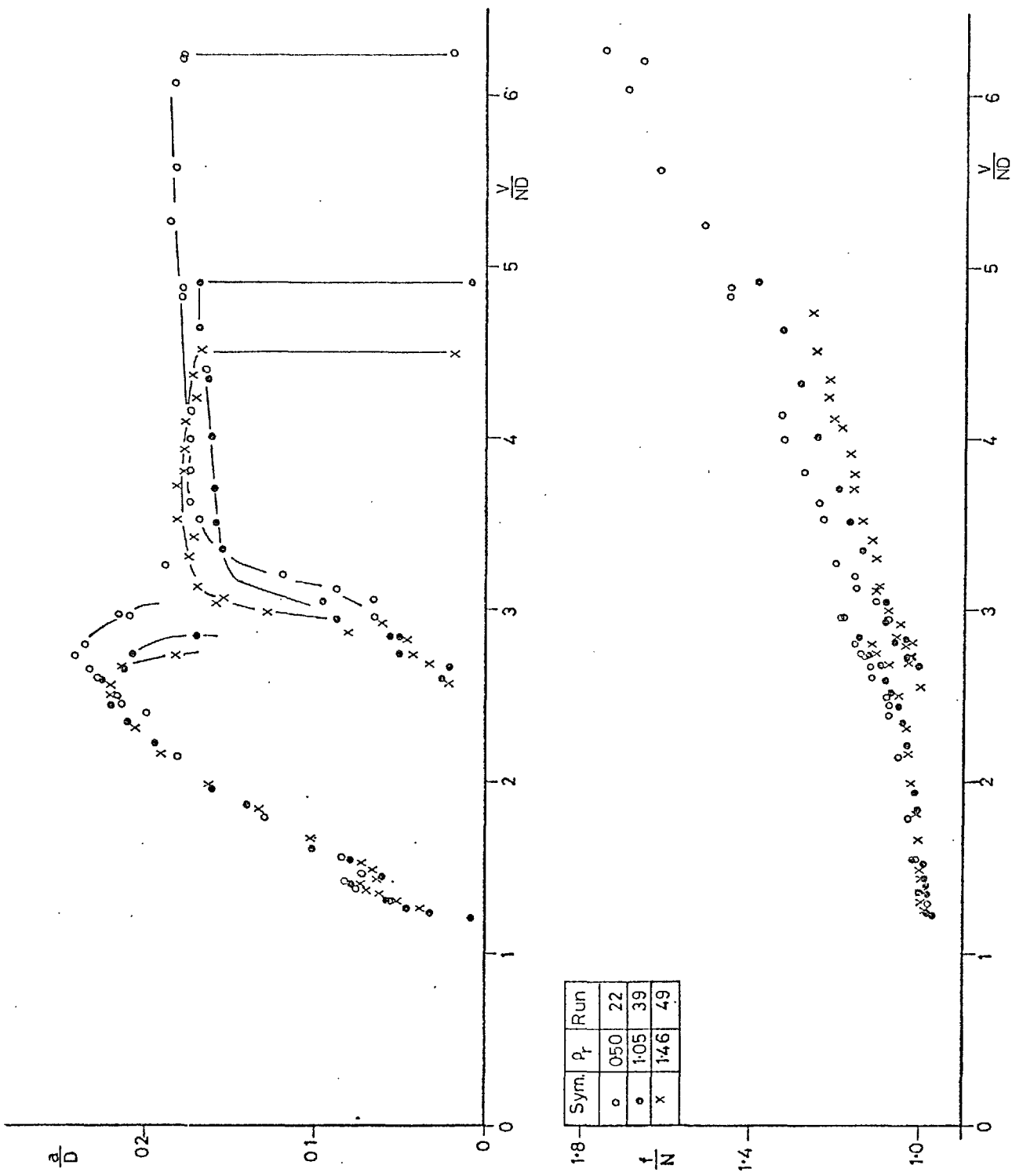

Fig. 28 Amplitude and frequency response of three cylinders with different density, plotted against (V/ND)

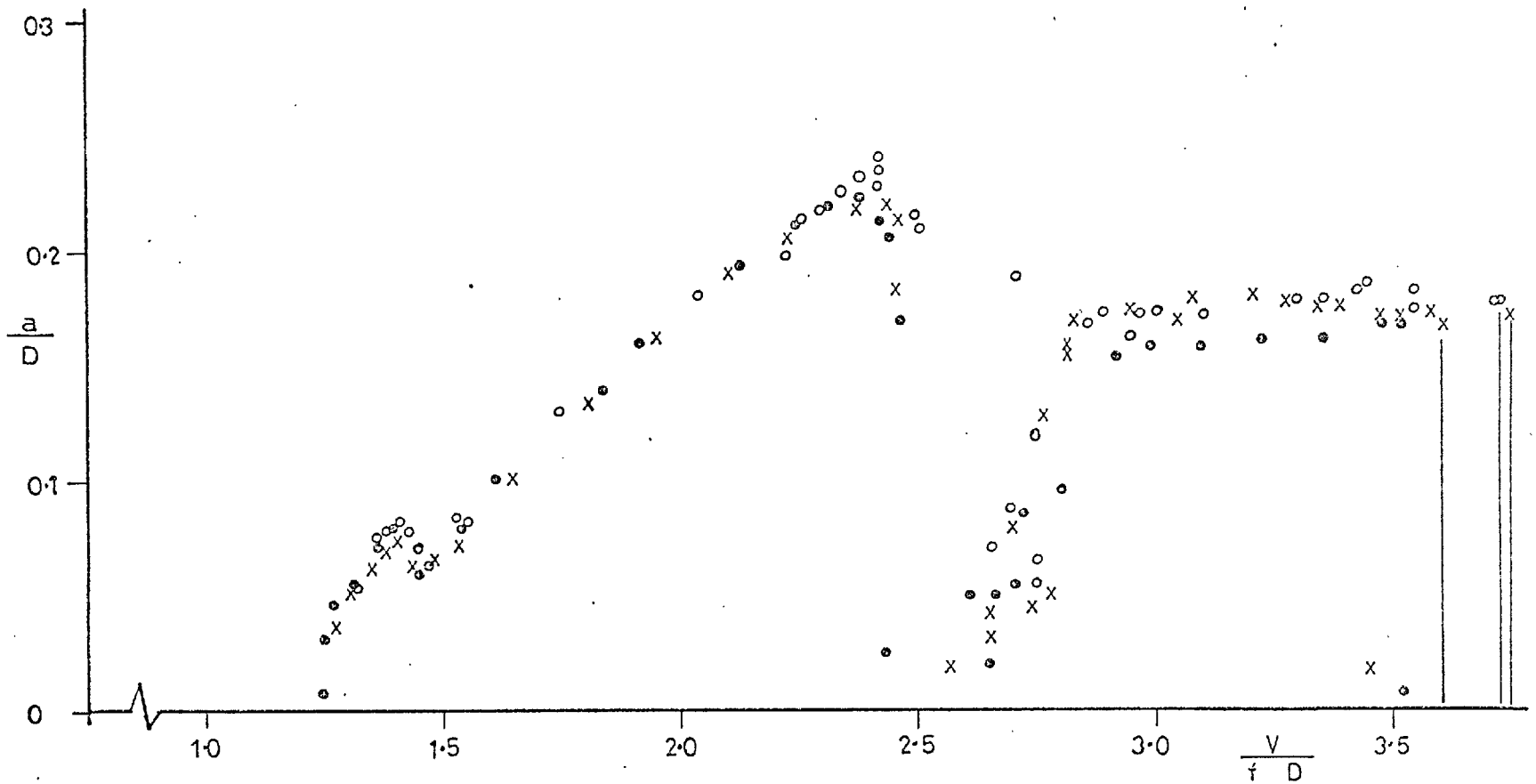

Fig. 29 Replotting the amplitude response curves of Fig. 28, against (V/fD)

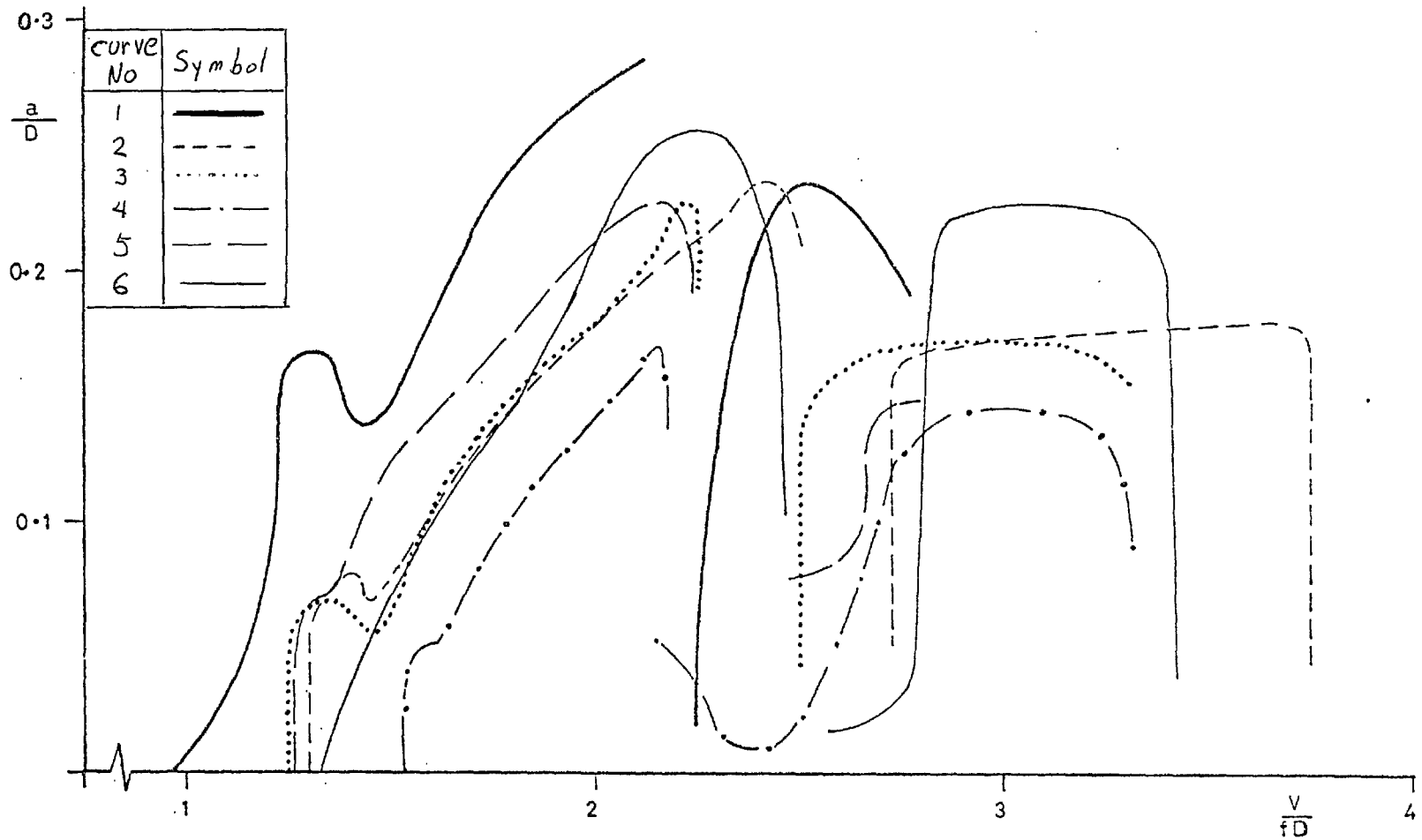

Fig. 30 Replotting the curves of Fig. 3 against (V/fD)

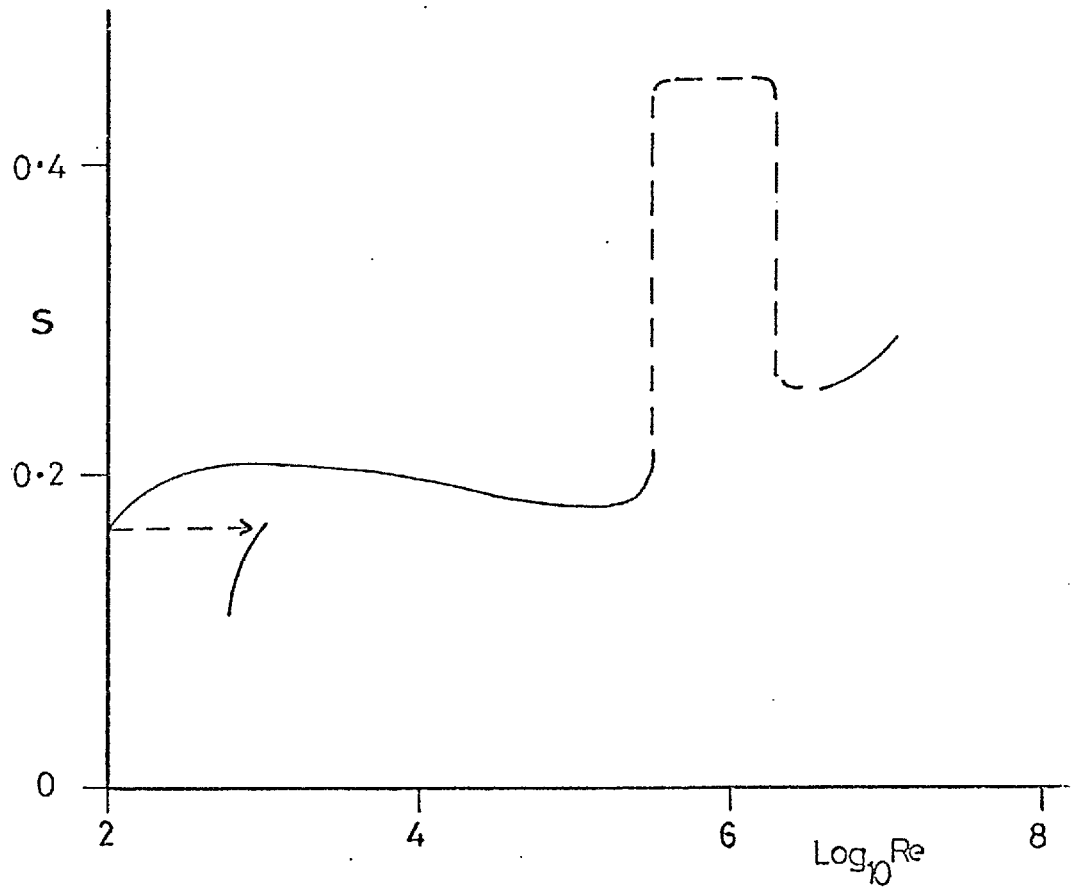

Fig. 31 Dependence of the Strouhal number for a stationary circular cylinder, on the Reynolds number (from Raudkivi and Callander)

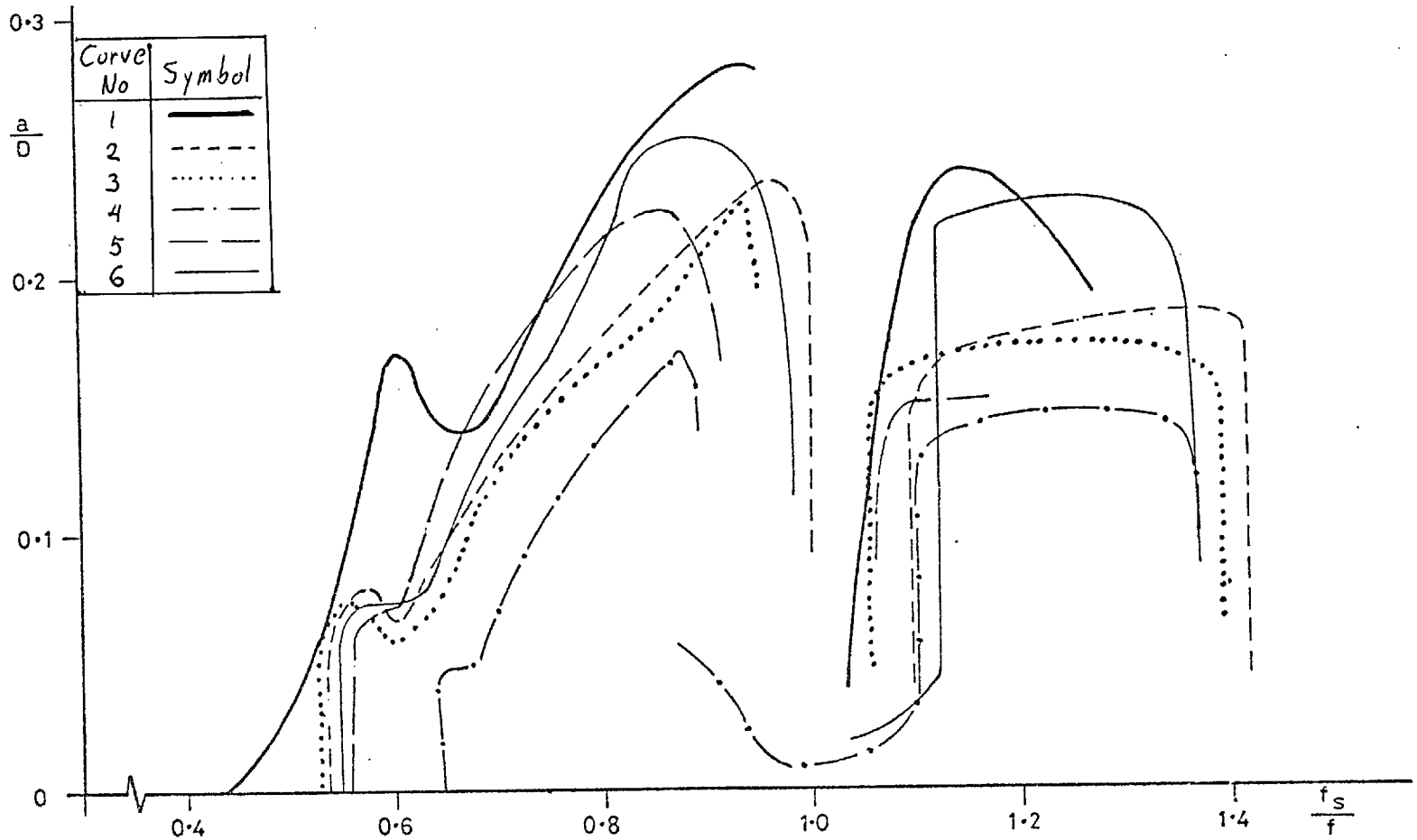

Fig. 32 Replotting the curves of Figs. 3 and 30 against (f_s/f)

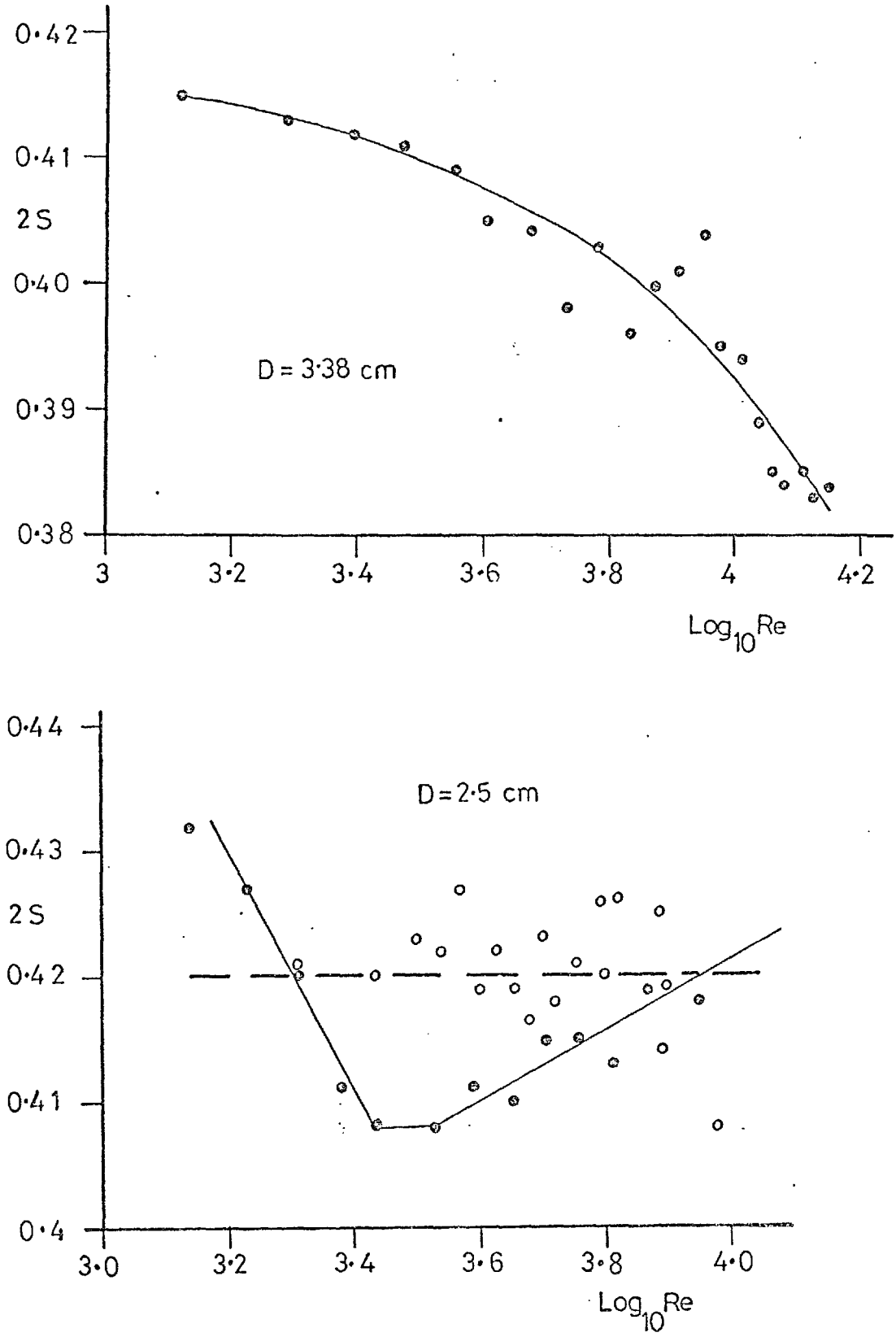

Fig. 33 Experimental values of S as a function of R_e; (—o—°—) = Runs 73 & 77 only; (—°—) = all other runs

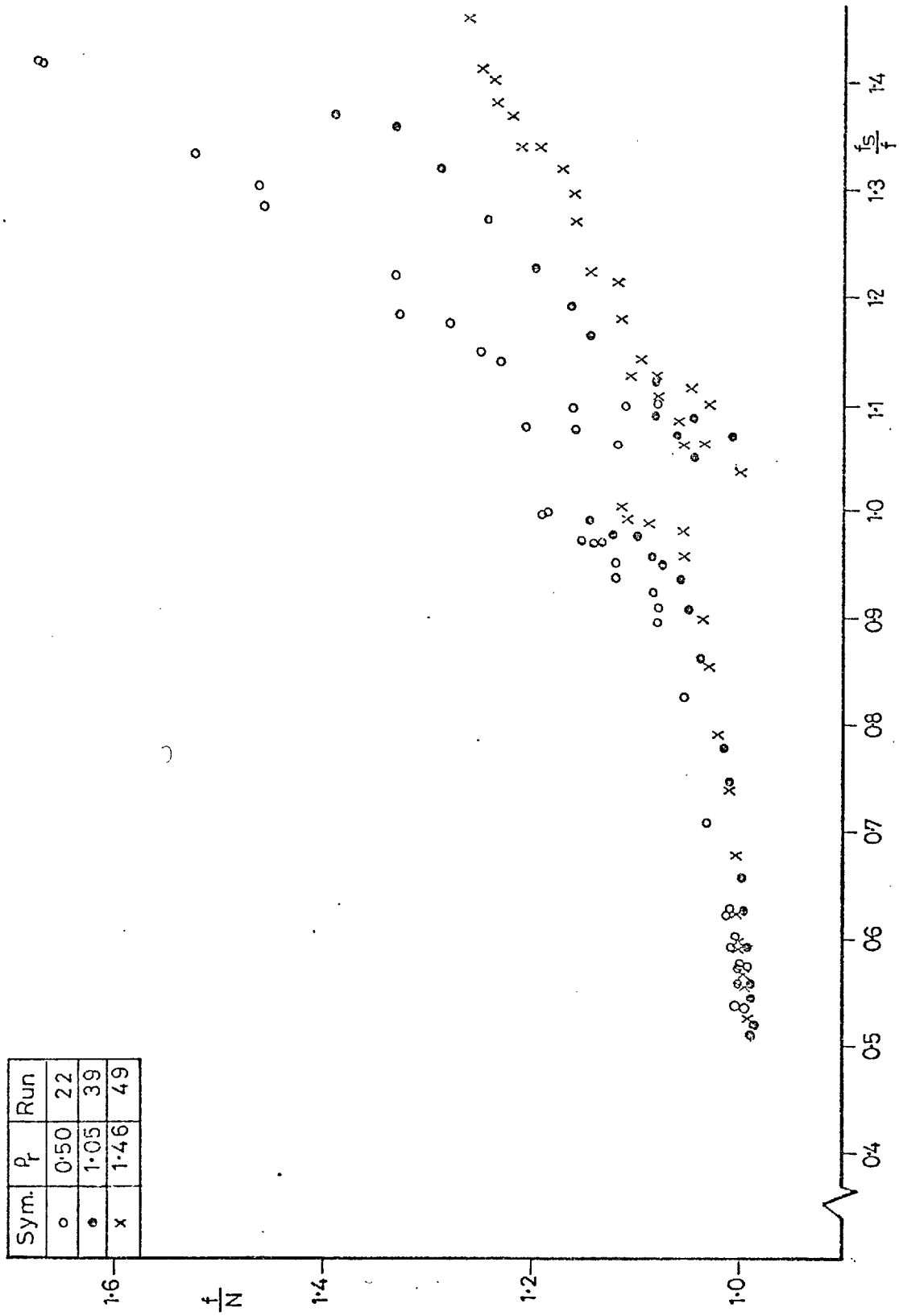

Fig. 34 Replotting the frequency response curves of Fig. 28 against (f_s/f)

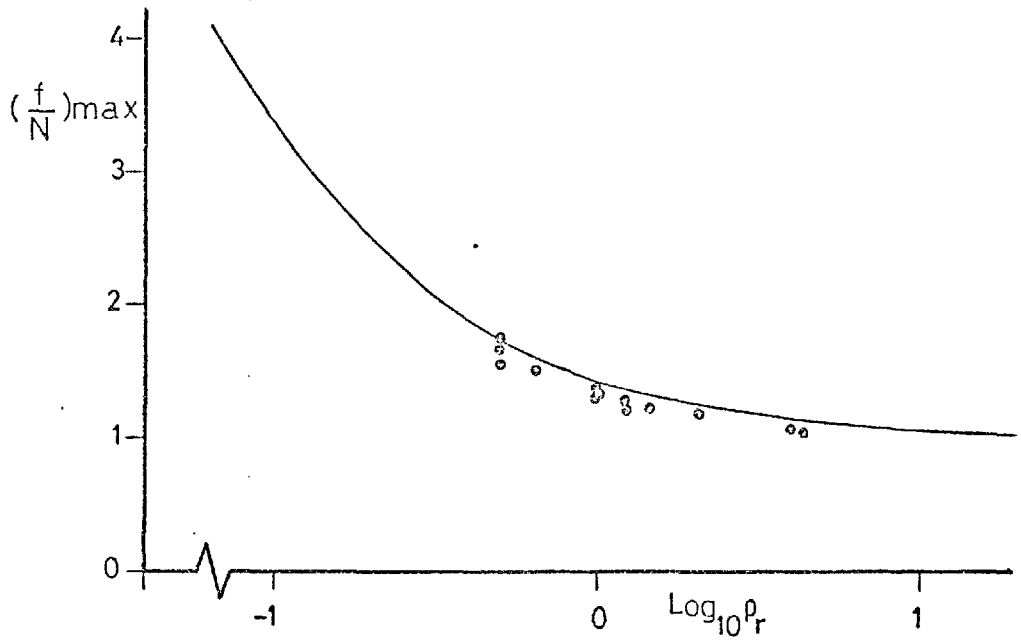

Fig. 35 Maximum values of (f/N) from all the tests, compared with equation 6.1

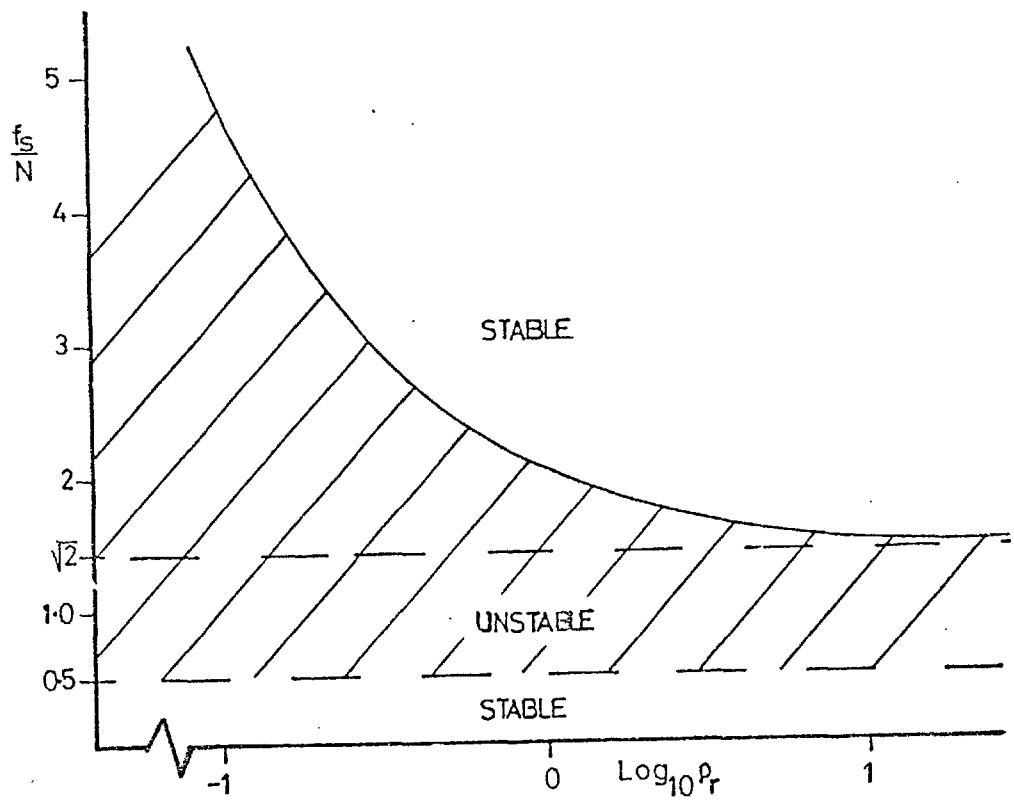

Fig. 36 Maximum ranges of $(f_s/N) = 2S(V/ND)$ where instabilities can occur

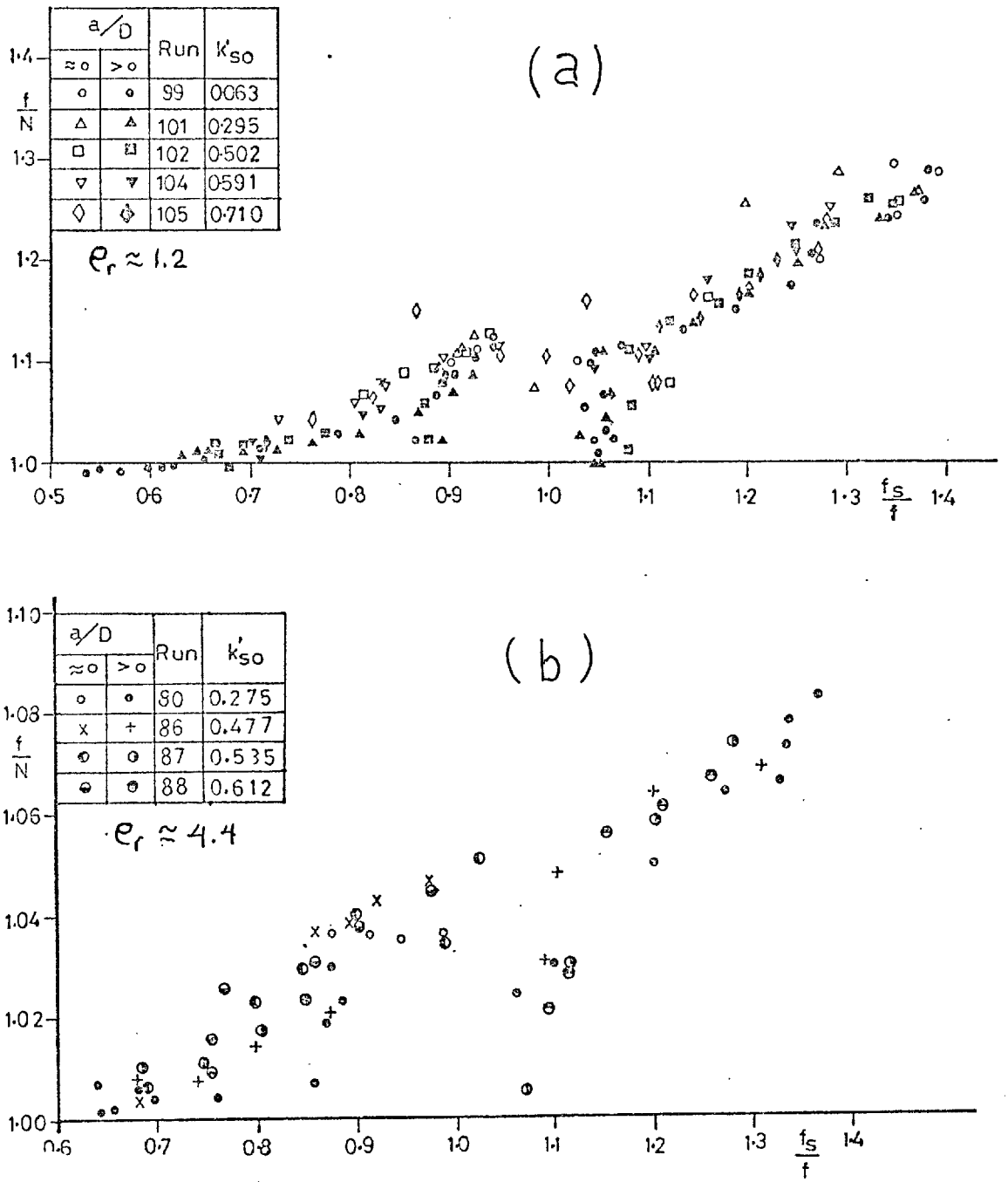

Fig. 37 Frequency response of cylinders with different values of ρ_r and k_s

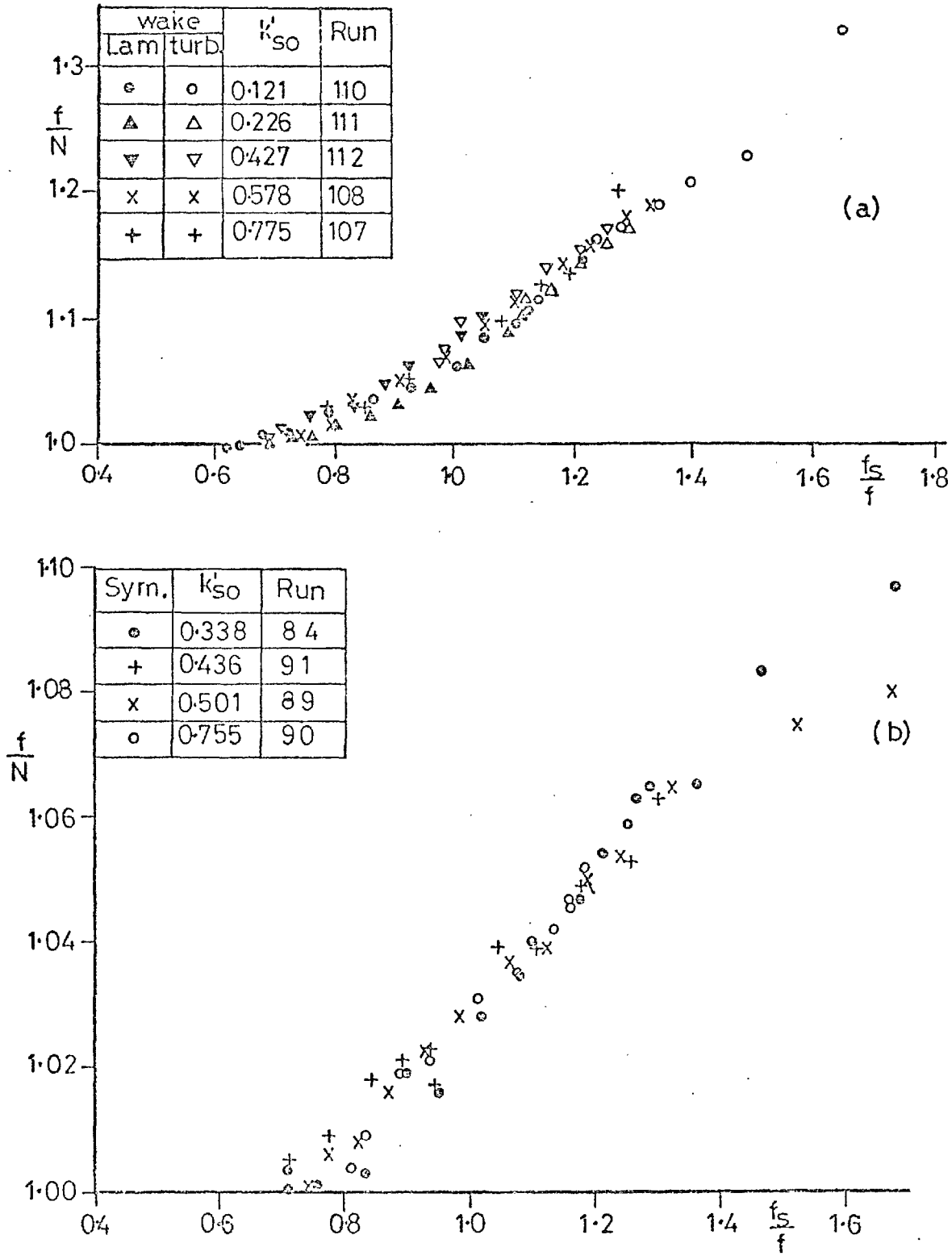

Fig. 38 Frequency response of cylinders fitted with a splitter plate: (a) $\rho_r \simeq 1.3$; (b) $\rho_r \simeq 4.4$

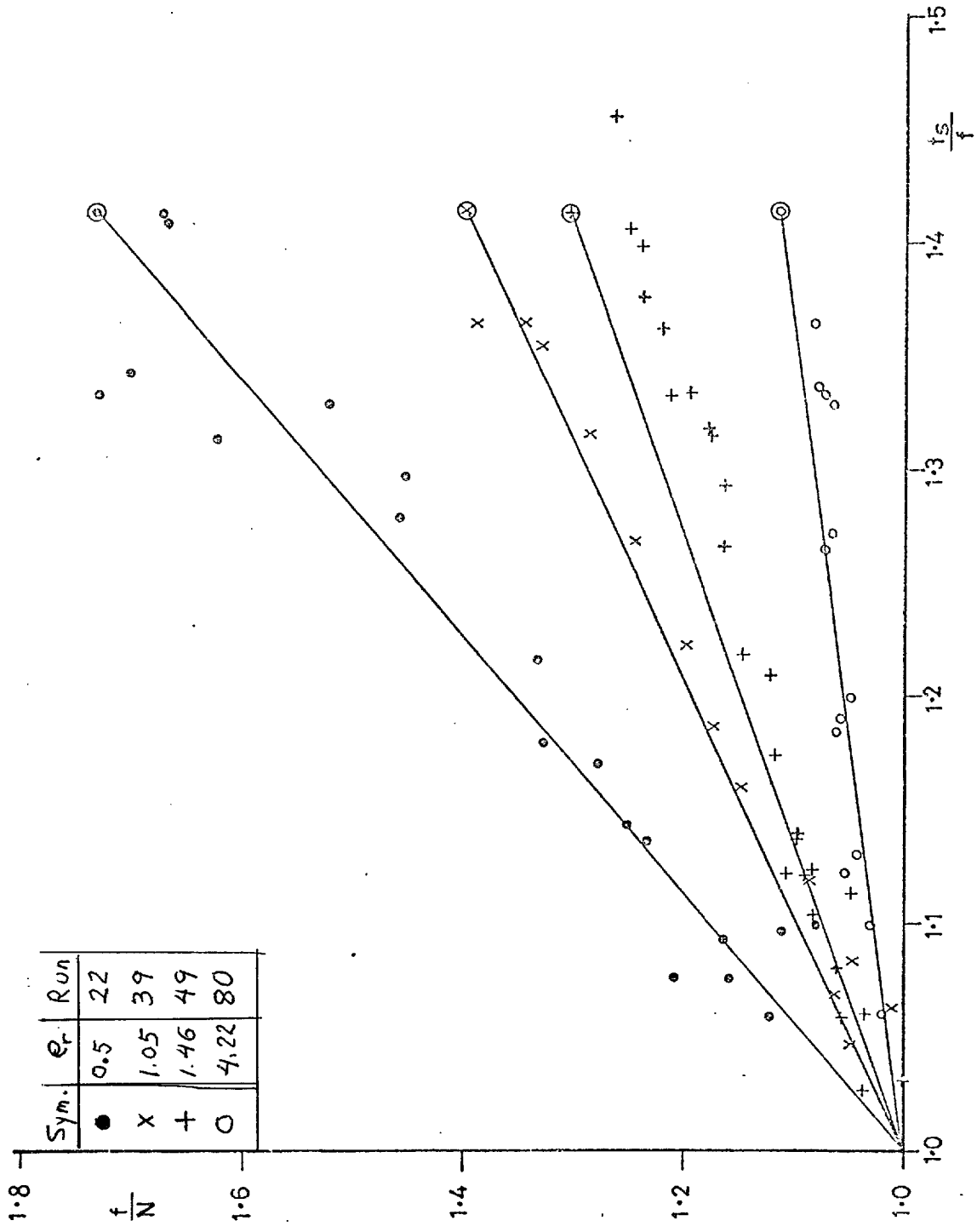

Fig. 39 Frequency response of various cylinders in the second instability region compared with equation 6.2. Note: continuous line and encircled symbols represent equations 6.1/2/3

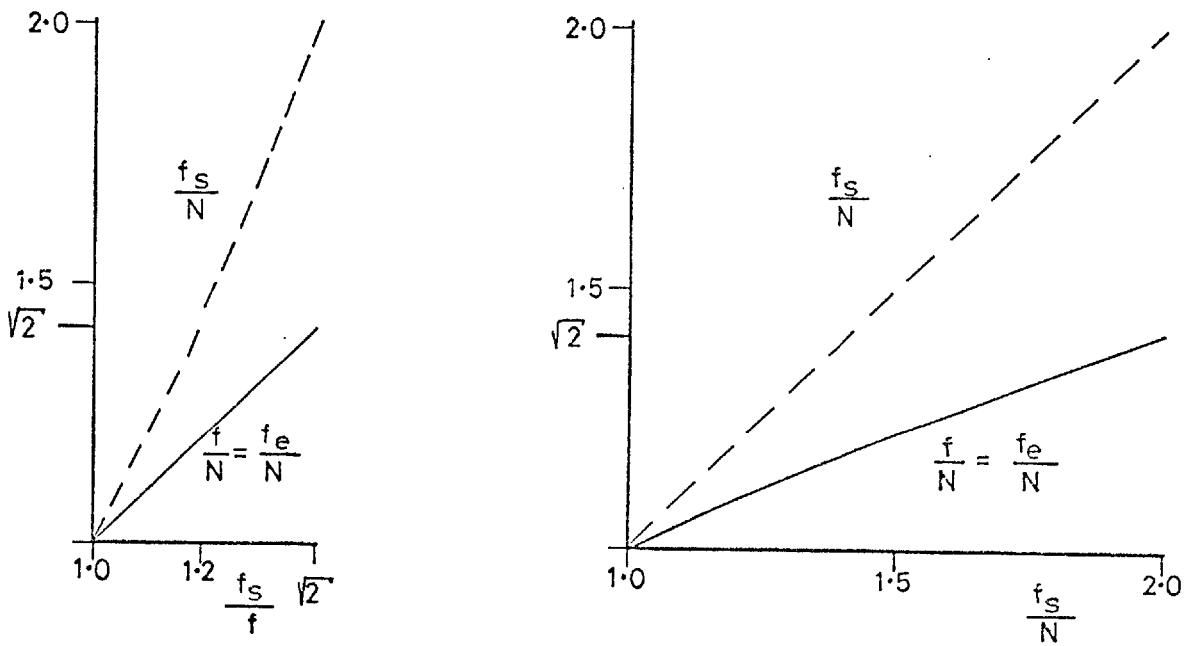

Fig. 40 Frequency relationships in the second instability region for $\rho_r = 1$; from equation 6.2

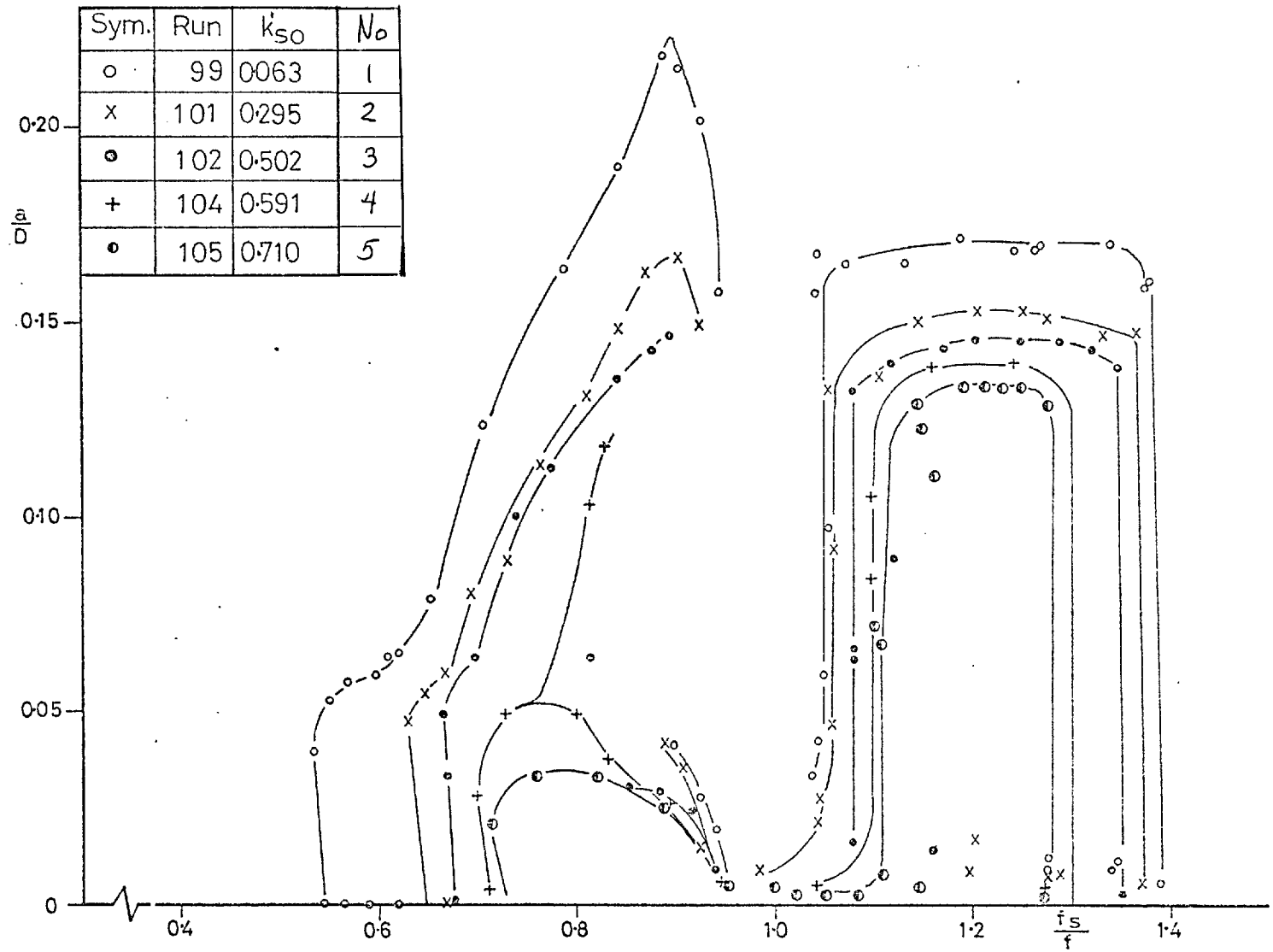

Fig. 41a Amplitude response of cylinders with $\rho_r \simeq 1.2$ (continued on next page)

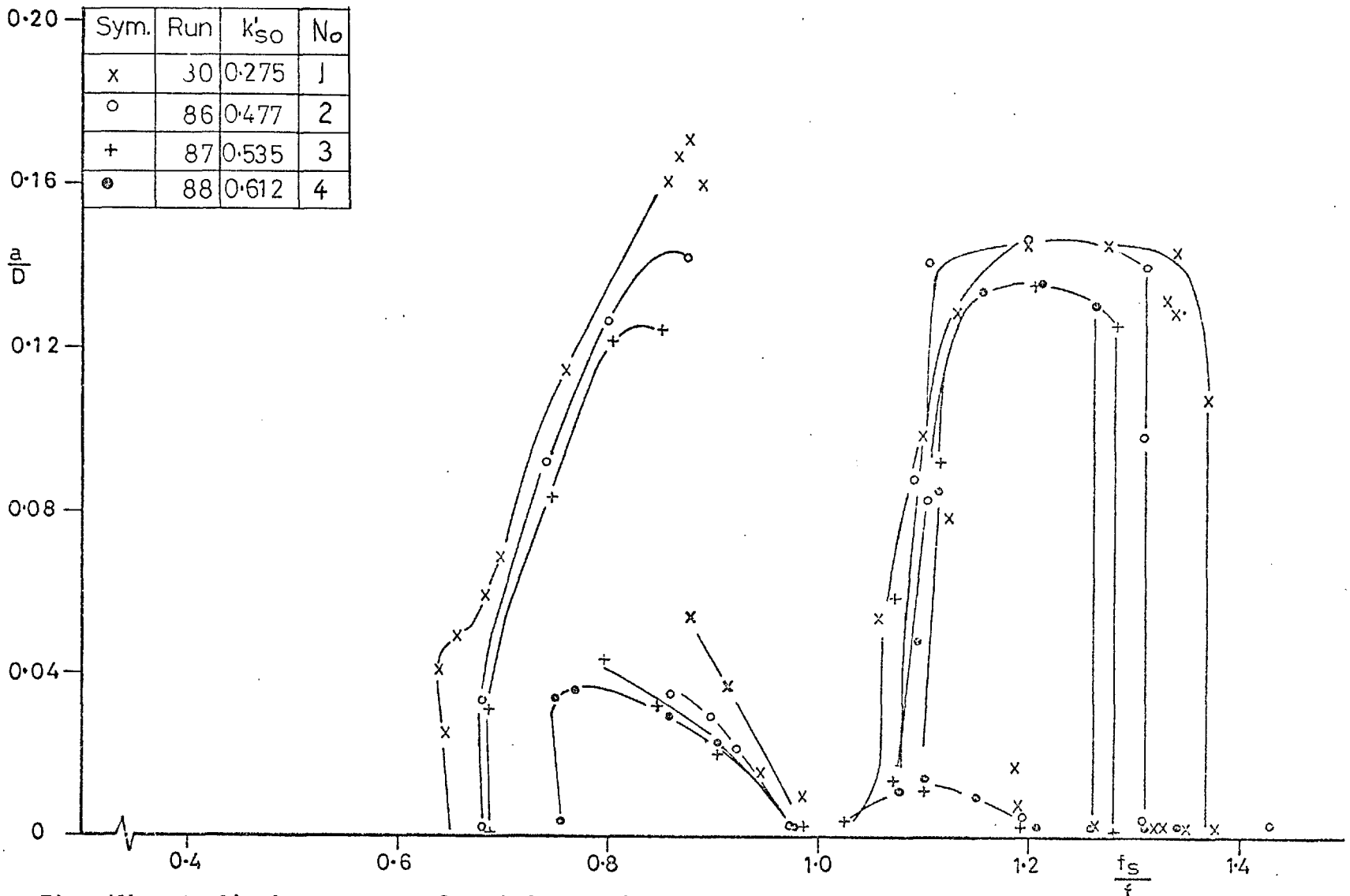

Fig. 41b Amplitude response of cylinders with $\rho_r \approx 4.3$

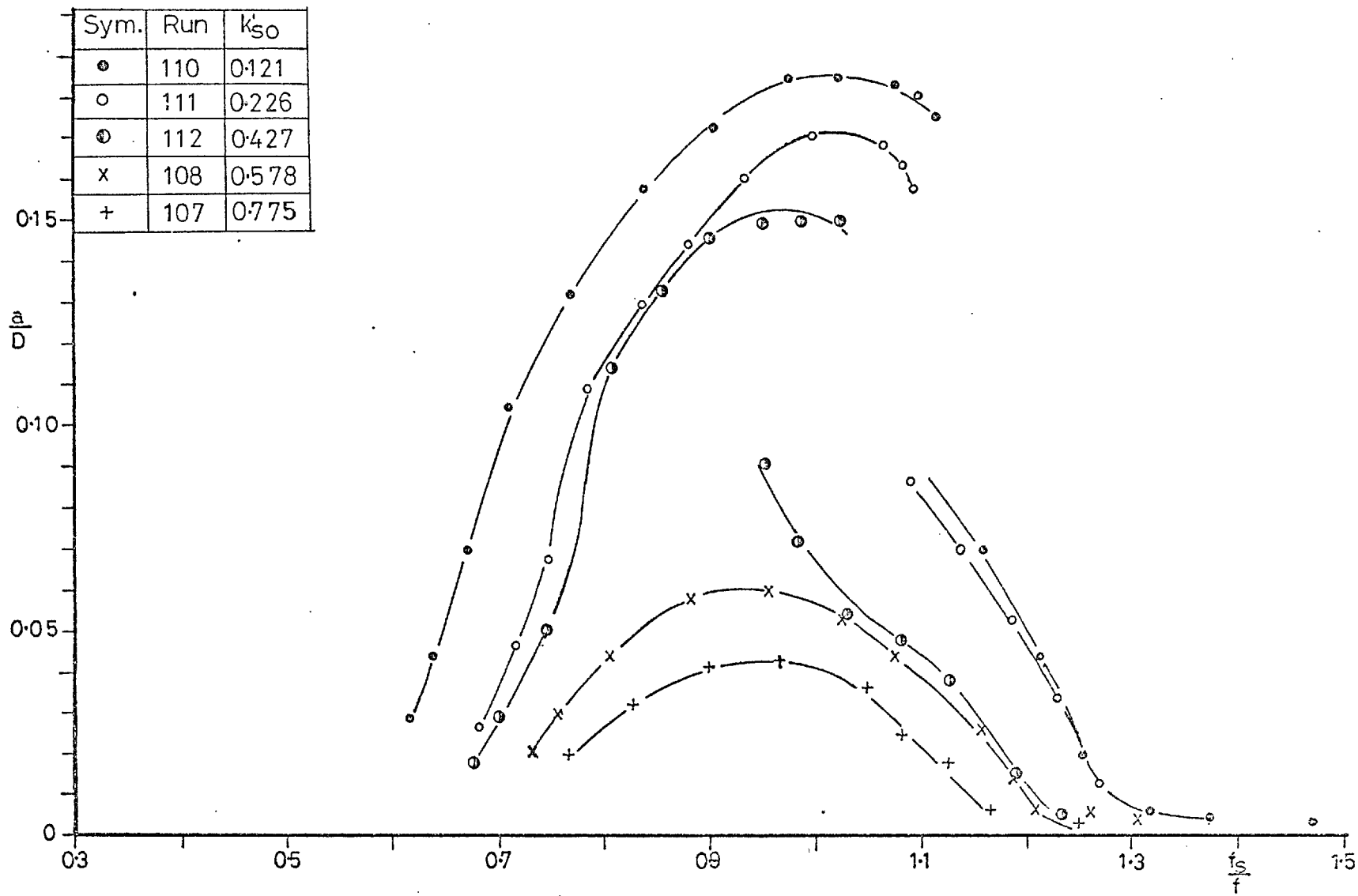

Fig. 42a Amplitude response of cylinders fitted with a splitter plate with $\rho_r \simeq 1.2$ (continued)

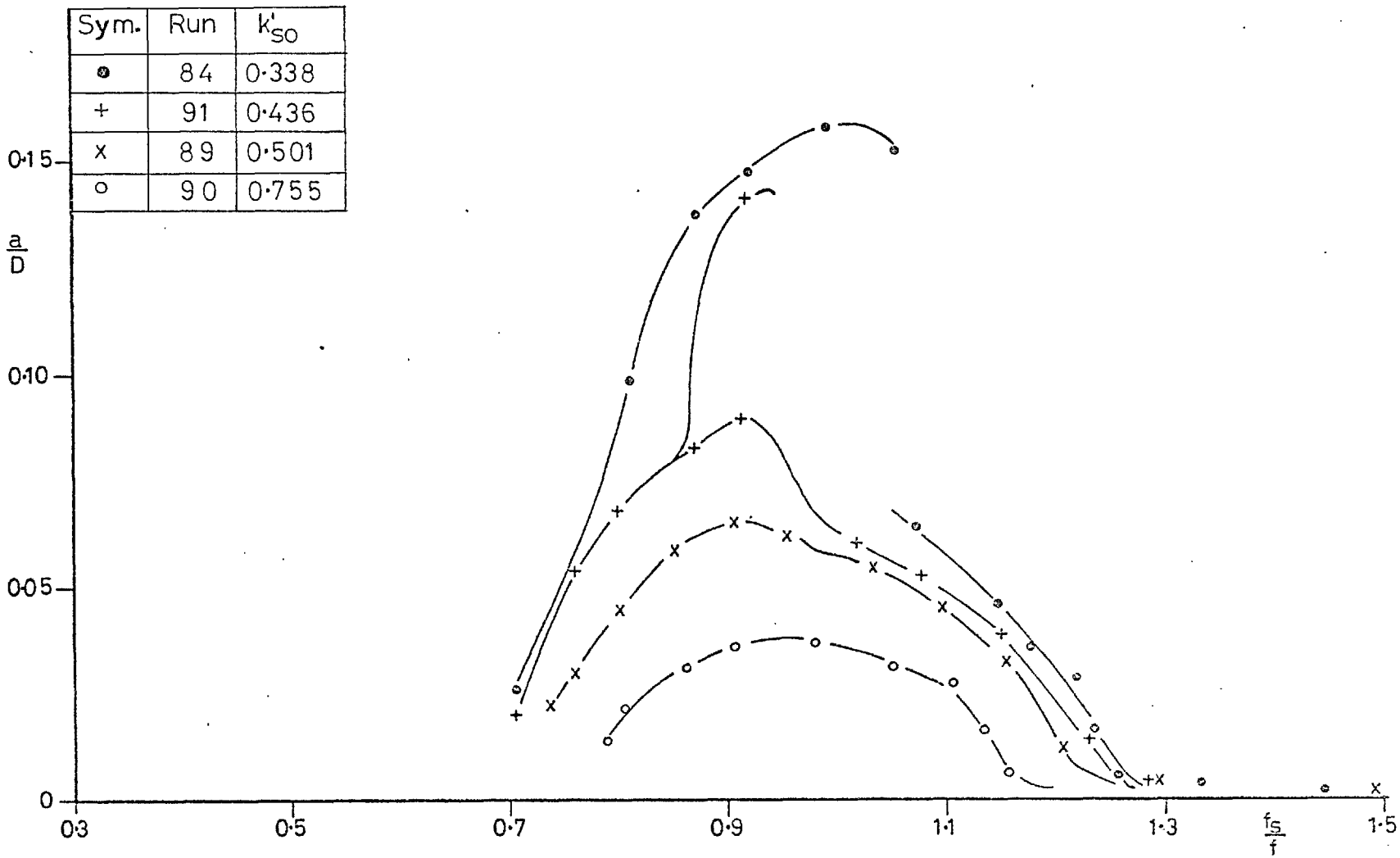

Fig. 42b Amplitude response of cylinders fitted with a splitter plate ($\rho_r \approx 4.4$)

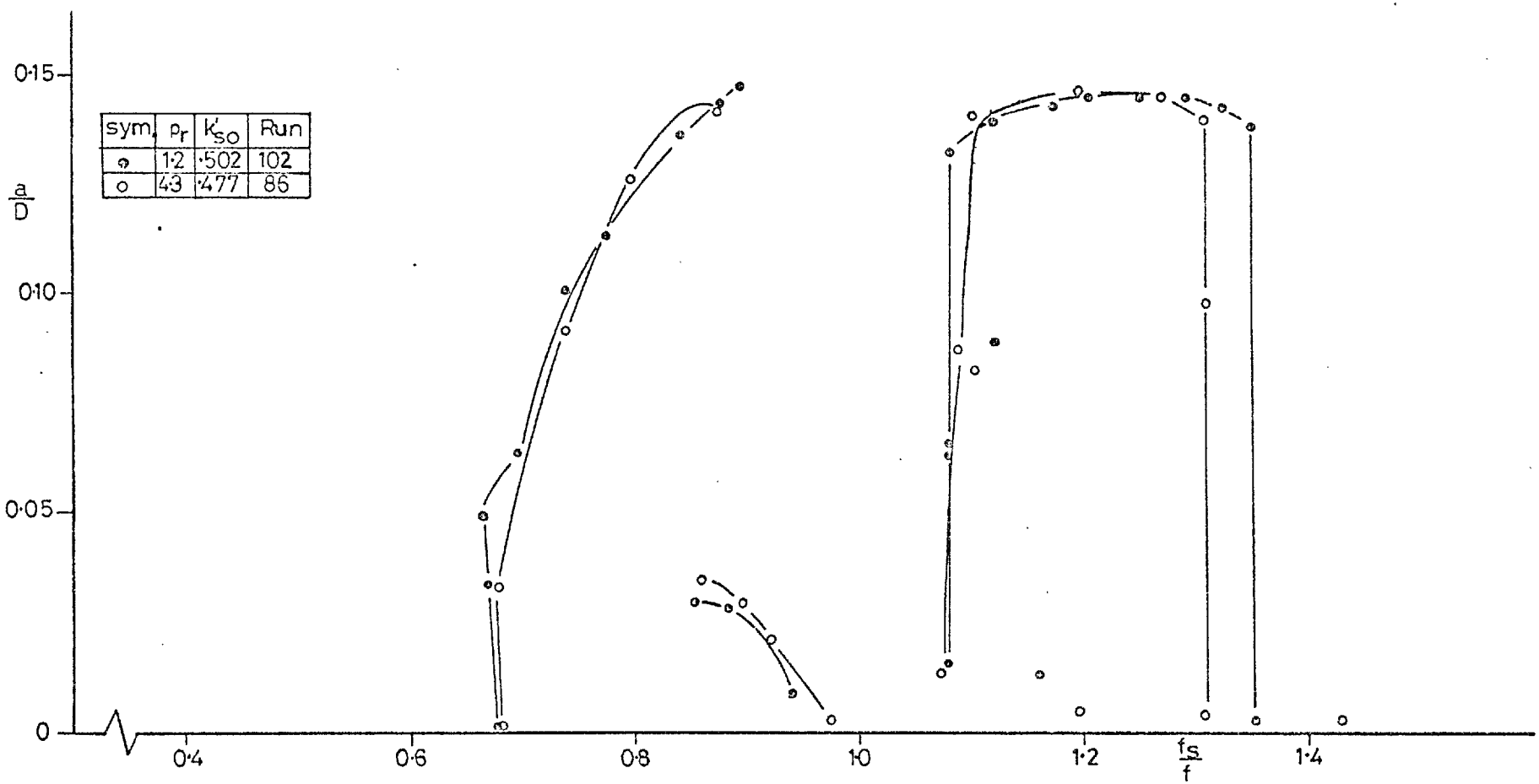

Fig. 43 Comparison of amplitude response of two cylinders

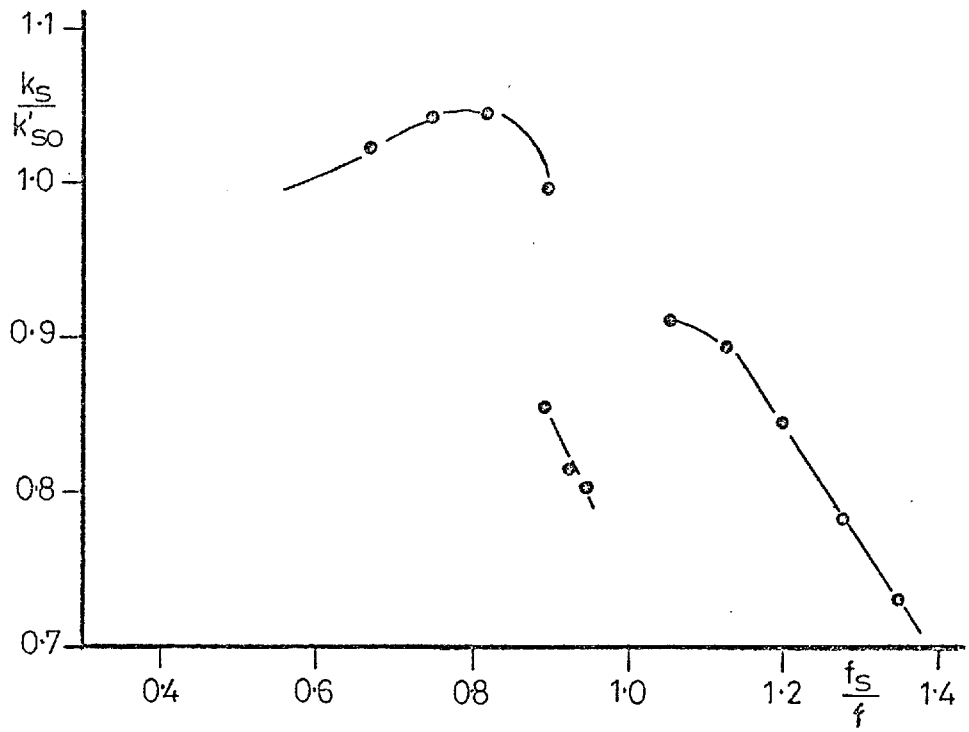

Fig. 44 Typical Variations of k_s with f_s/f; from run 99

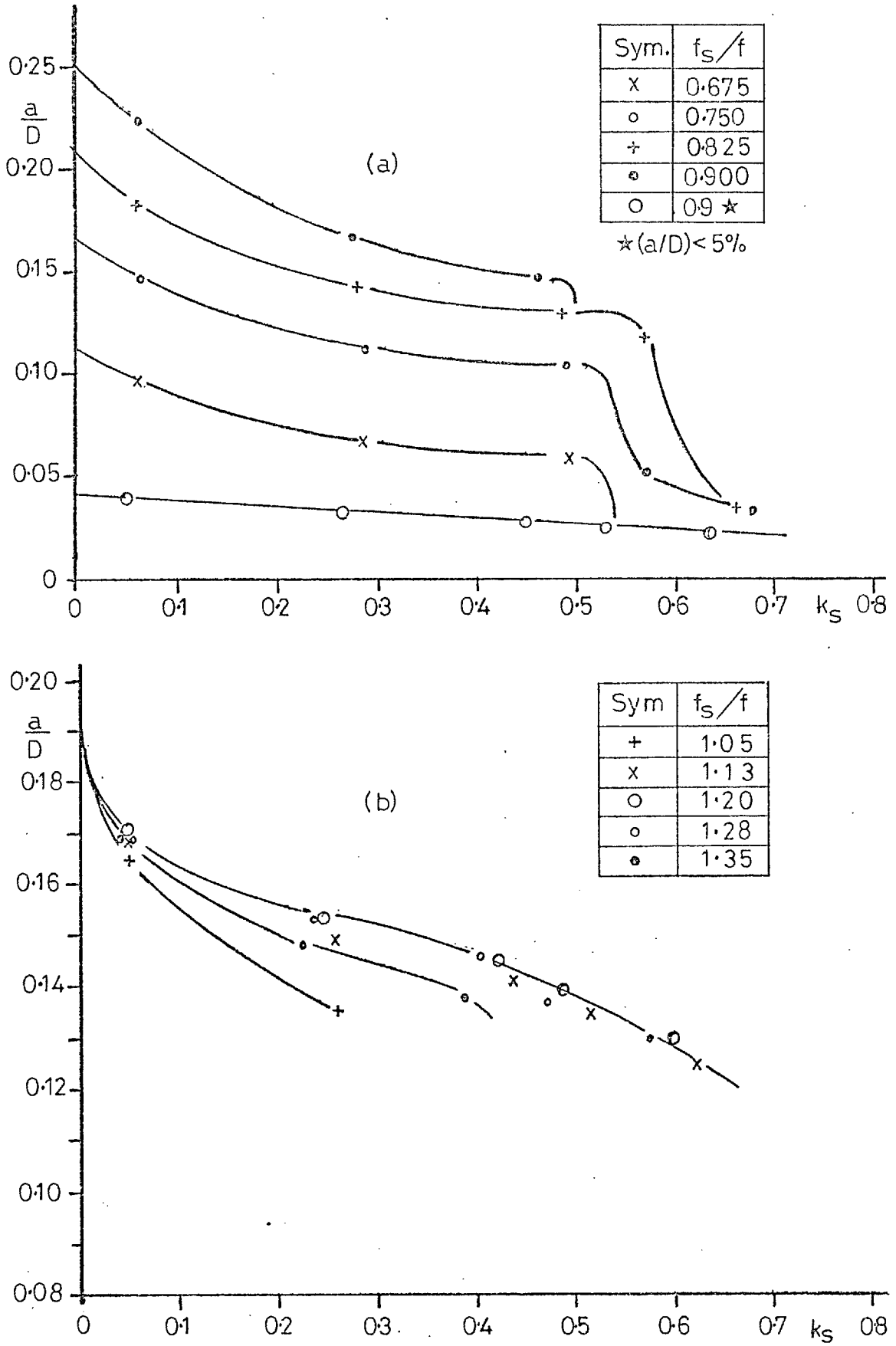

Fig. 45 Influence of damping on the amplitude response in (a) the first and (b) the second instability regions

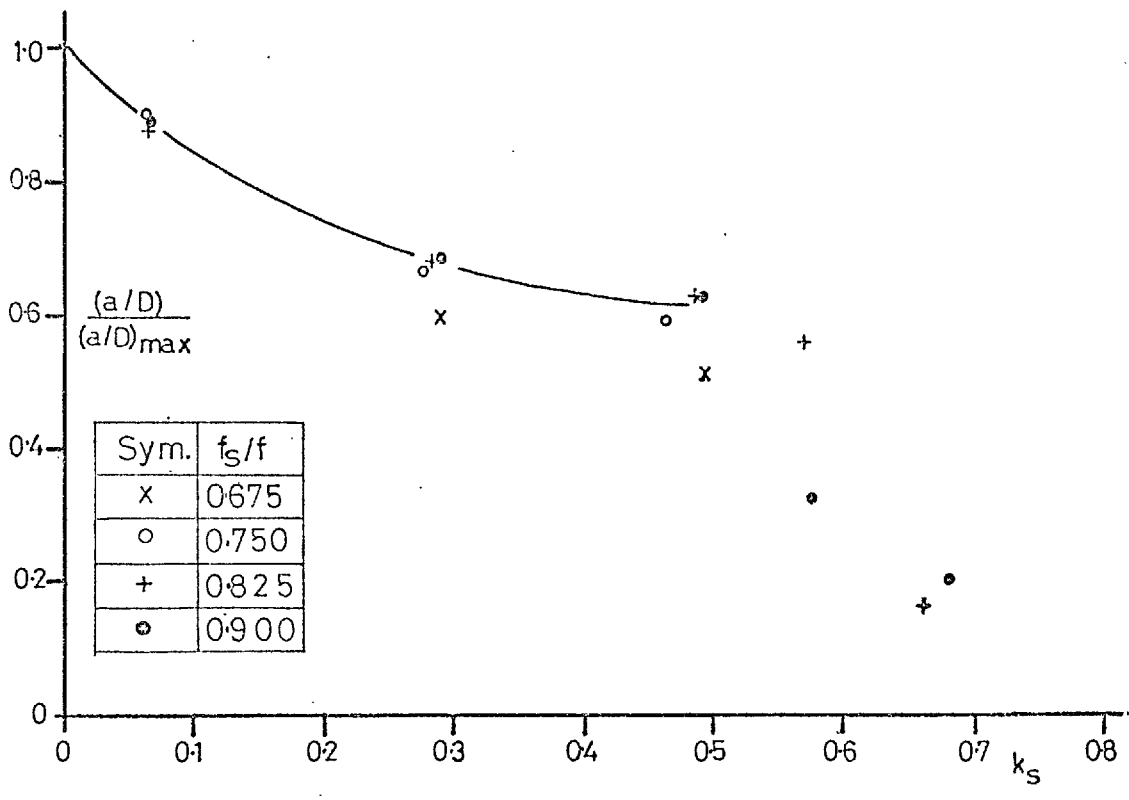

Fig. 46 Effect of damping on the variations of (a/D) with respect to their undamped value, in the first instability region

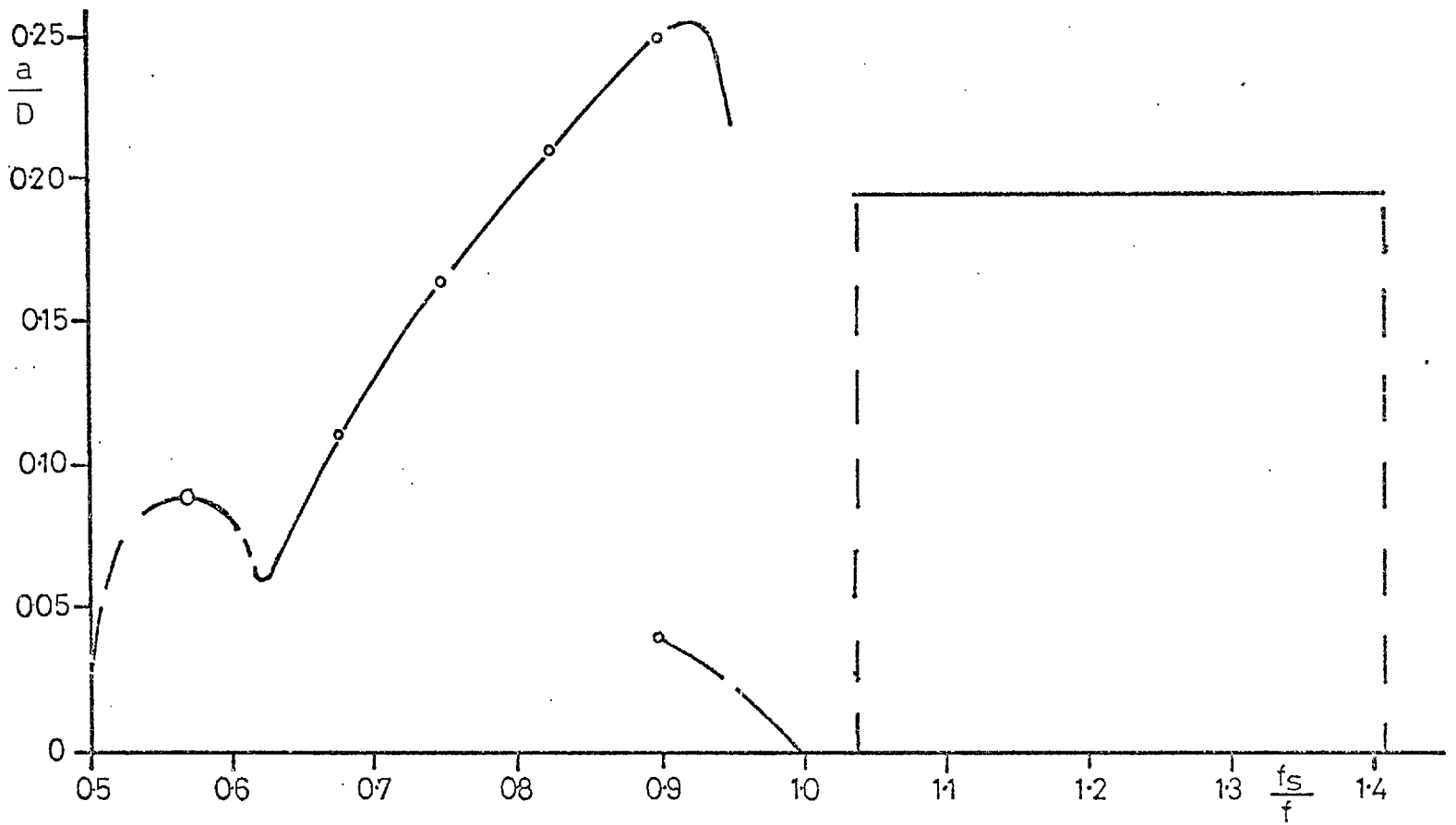

Fig. 47 Extrapolated maximum amplitude response

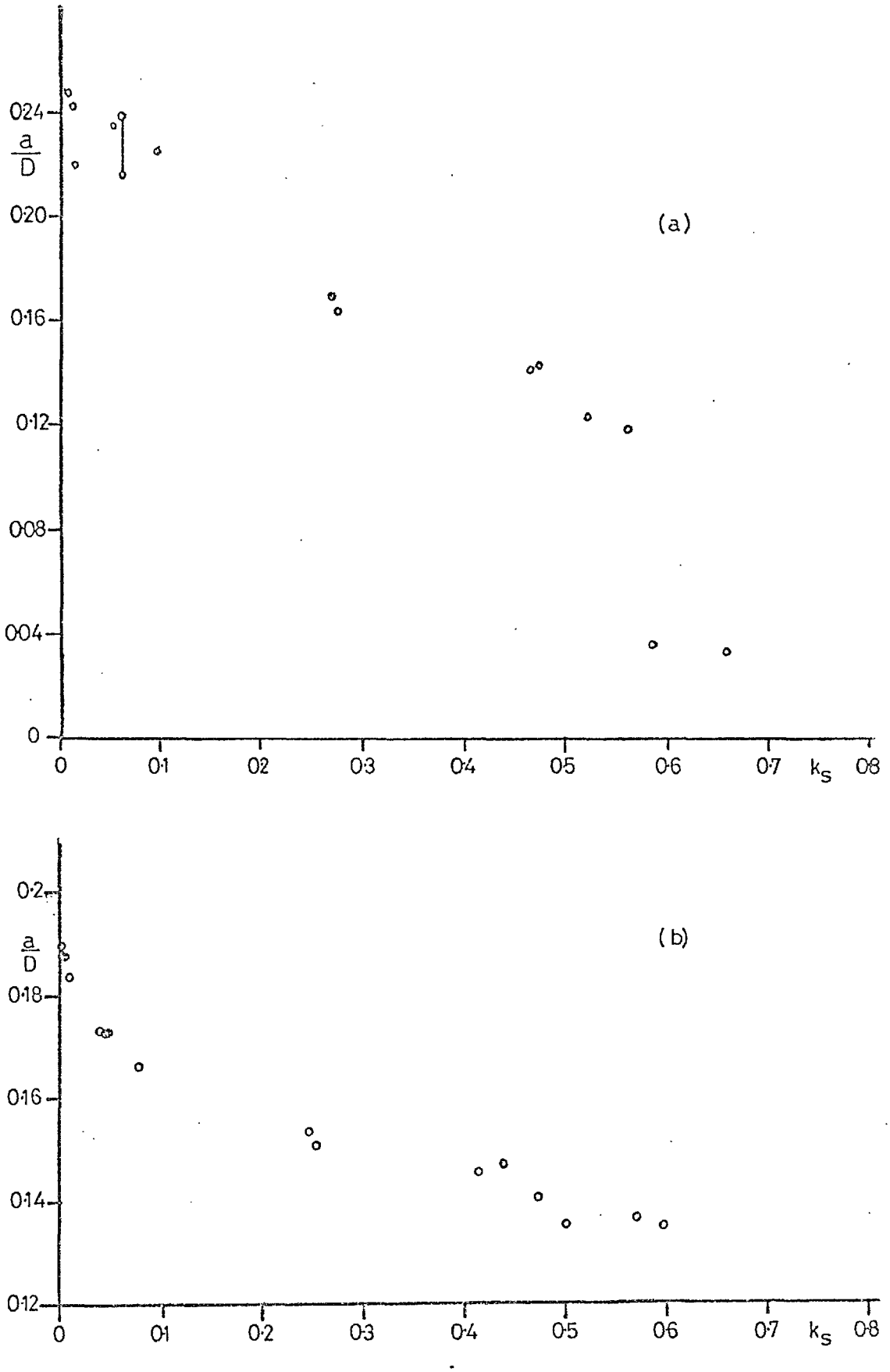

Fig. 48 Maximum recorded values of (a/D) in (a) the first and (b) the second instability regions

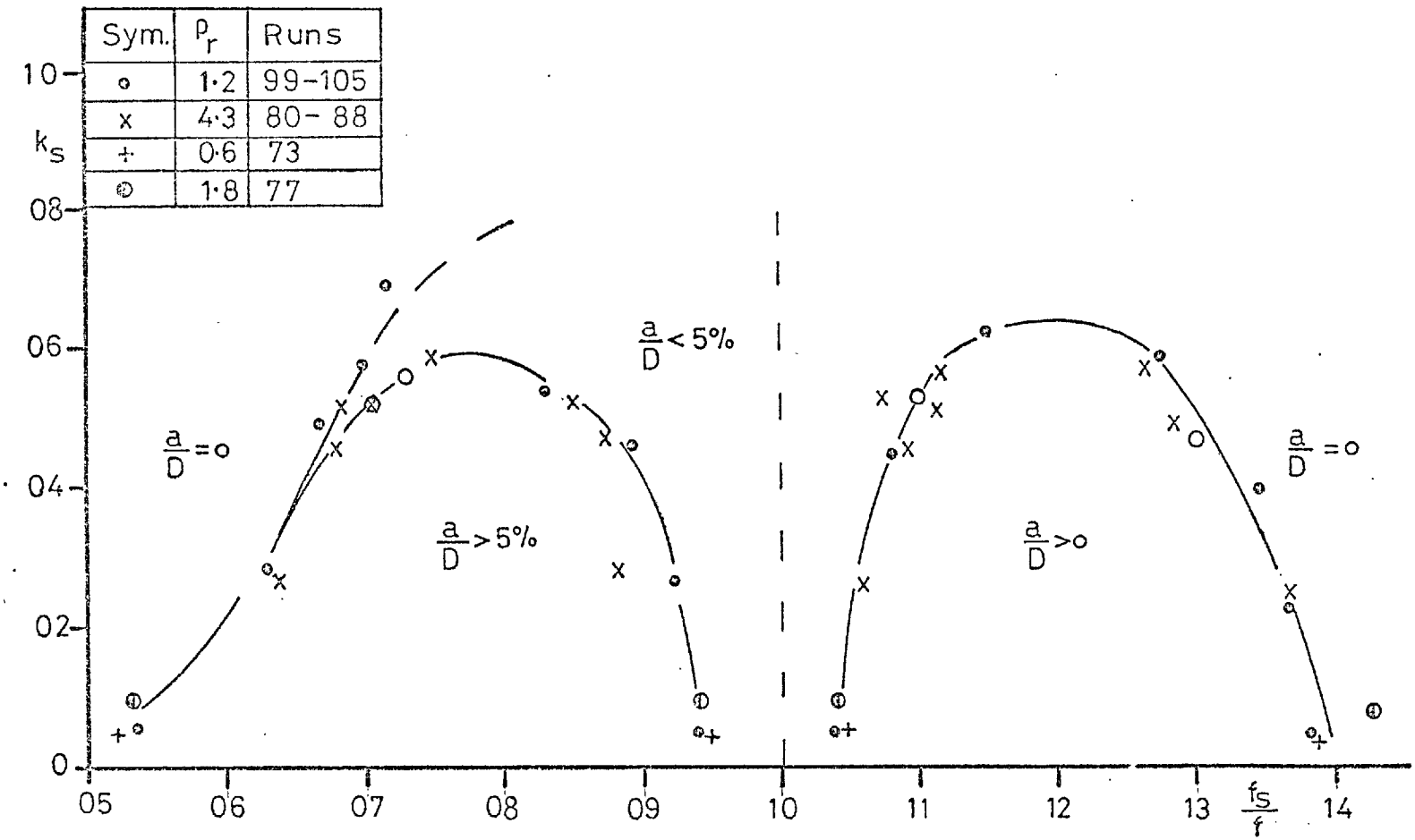

Fig. 49 Stability diagram for cylinders with different densities

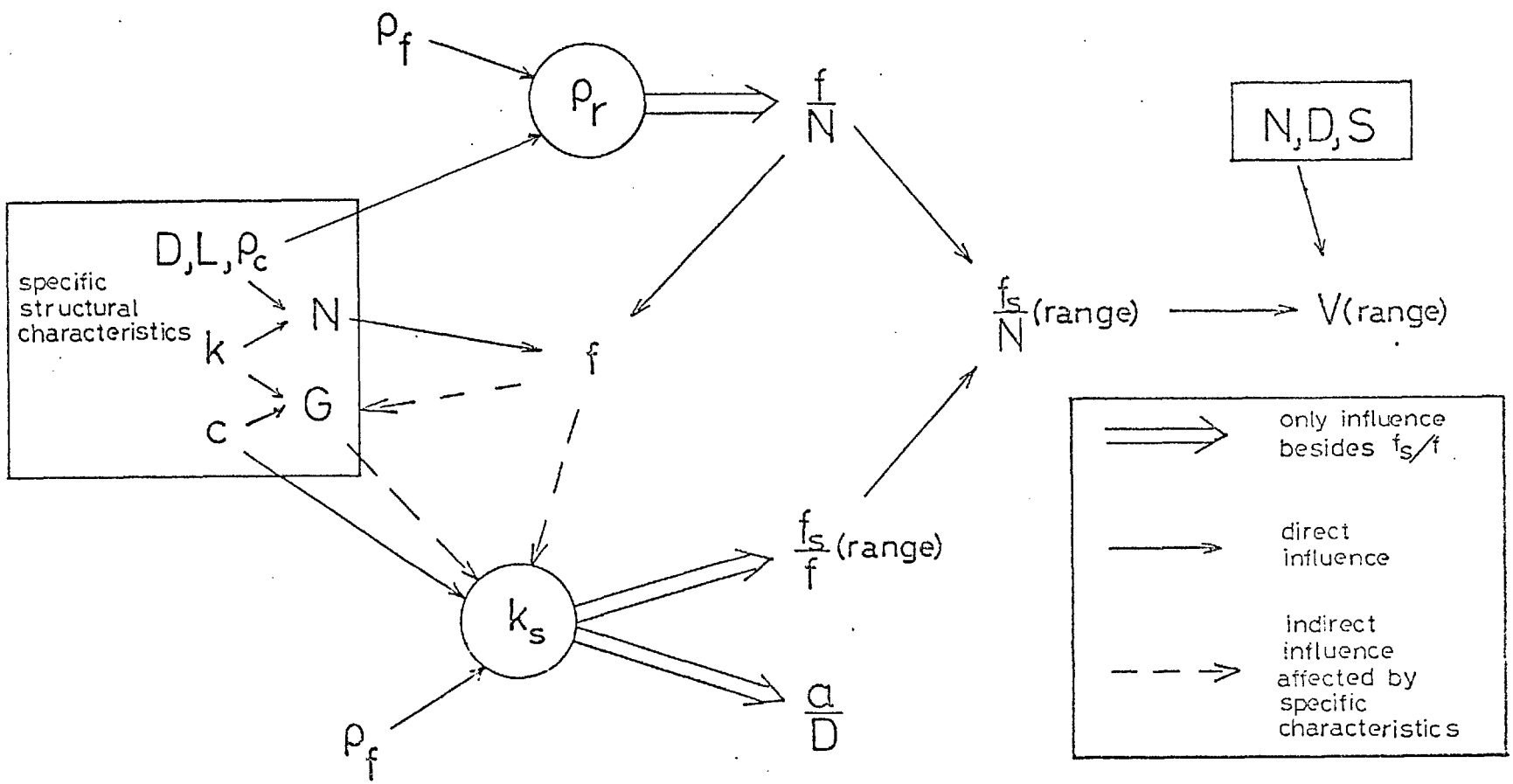

Fig. 50 Interdependence of the various parameters considered in Chapter 6

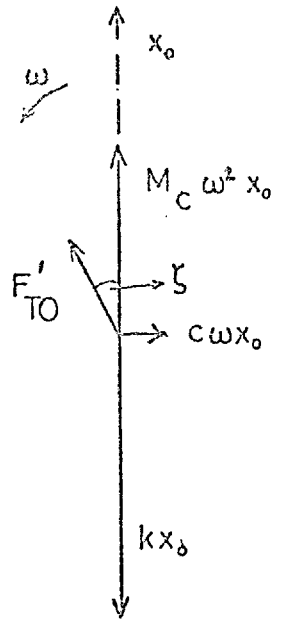

Fig. 51 Phase diagram showing the total hydrodynamic force

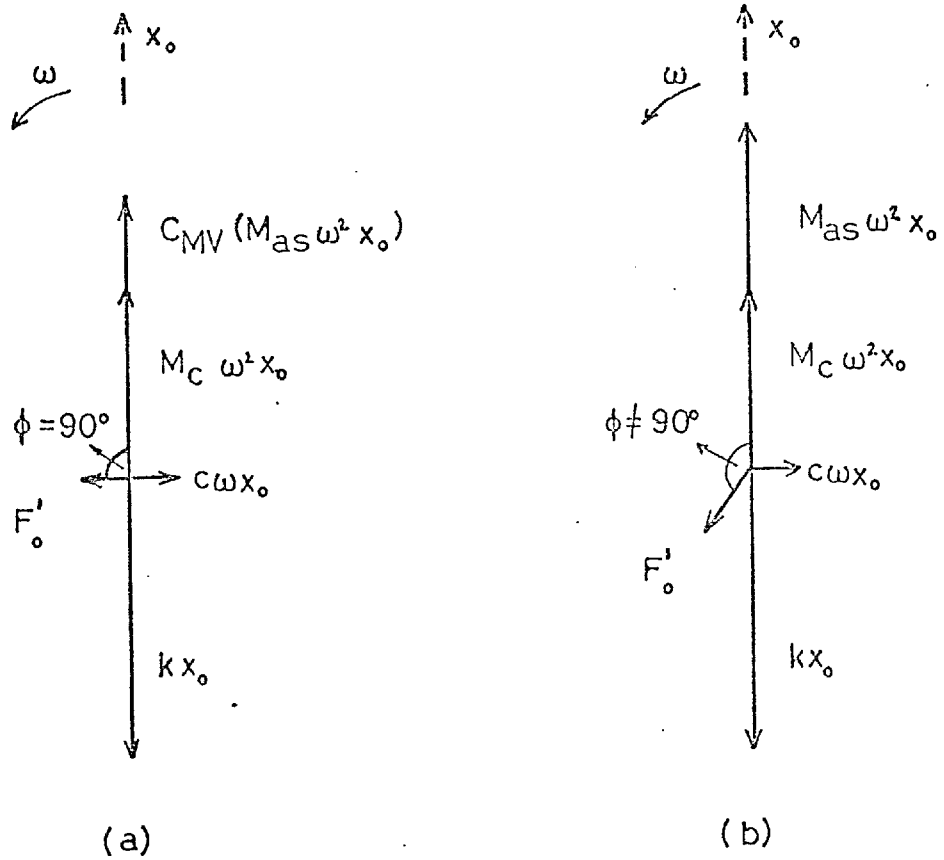

Fig. 52 Phase diagrams: (a) for $C_M = C_{MV}$; and (b) for $C_M = 1$

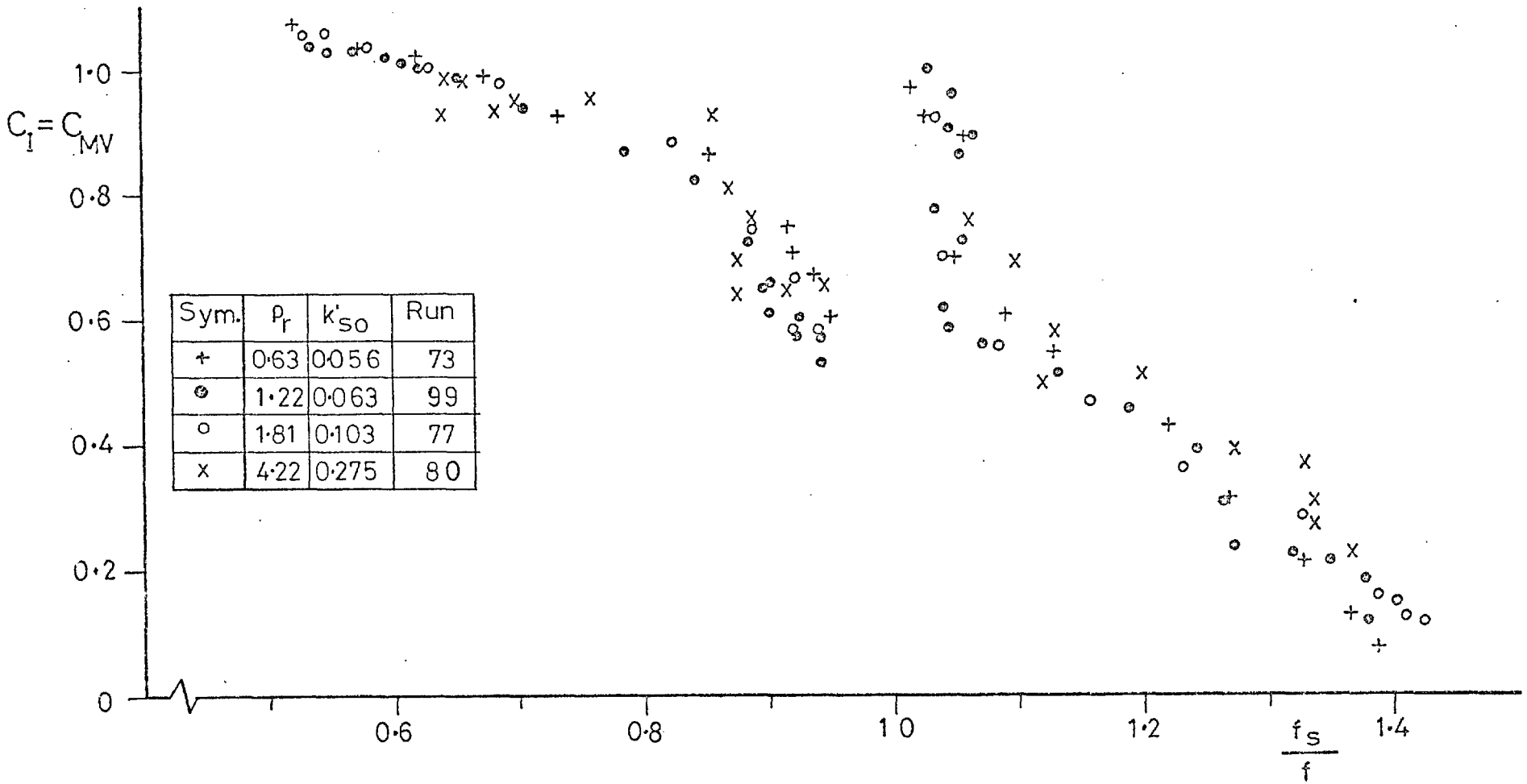

Fig. 53 Behaviour of the inertial coefficient with (f_s/f), for various values of ρ_r and k_s

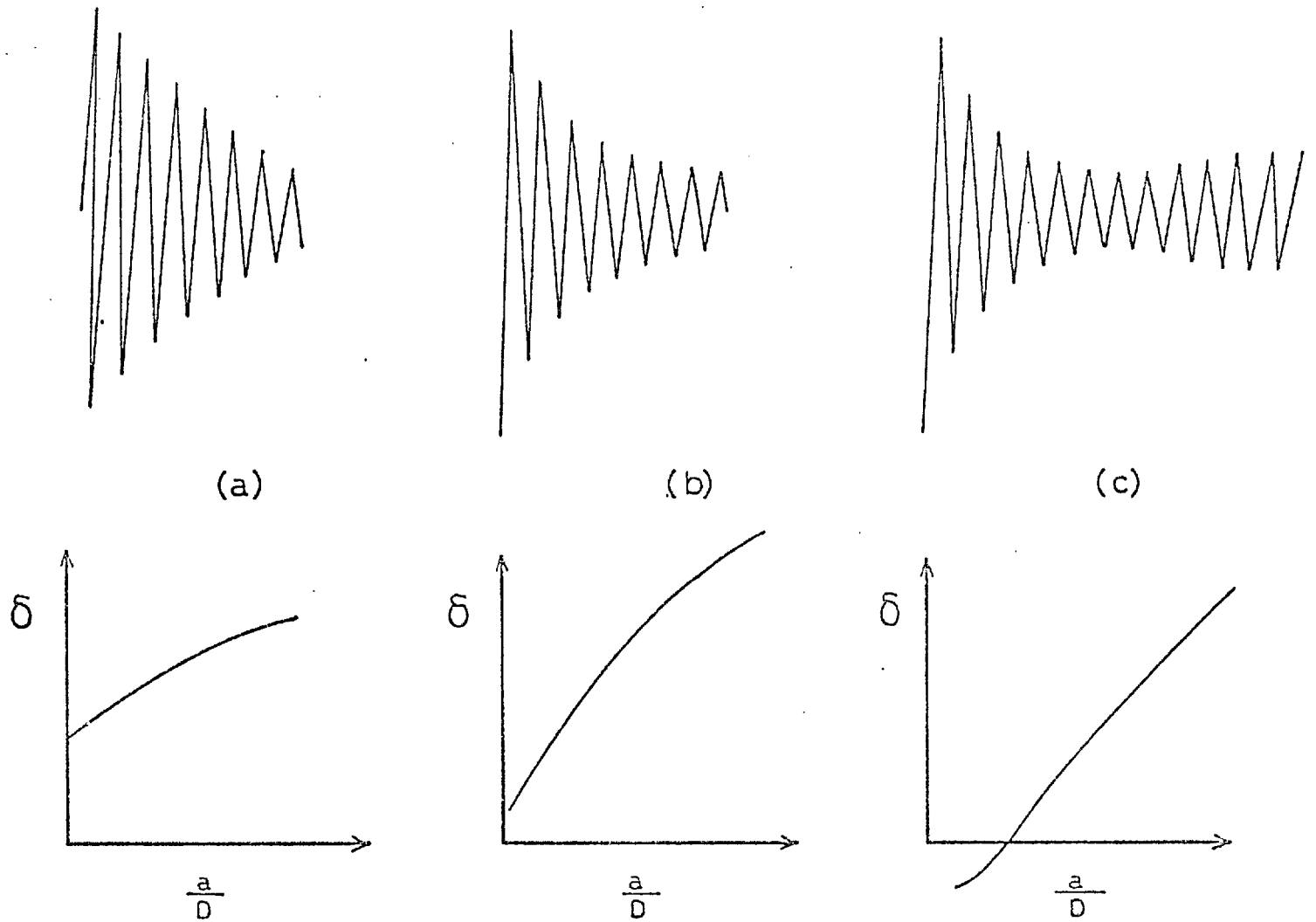

Fig. 54 Sketches of transients and their corresponding logarithmic decrements: (a) still water; (b) $f_s/f \lesssim \frac{1}{2}$; (c) $f_s/f \gtrsim \frac{1}{2}$

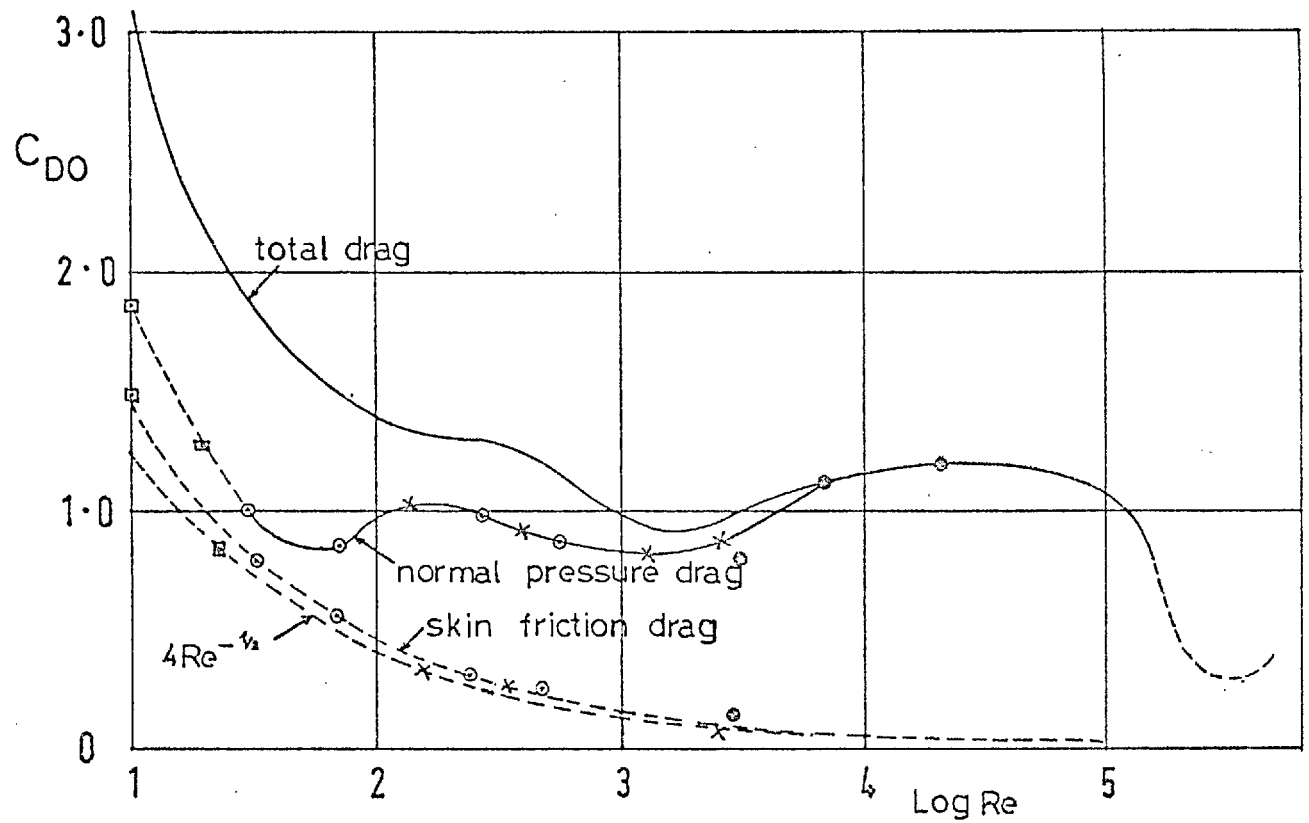

Fig. 55 Drag coefficients for a stationary circular cylinder as functions of R_e (from Goldstein)

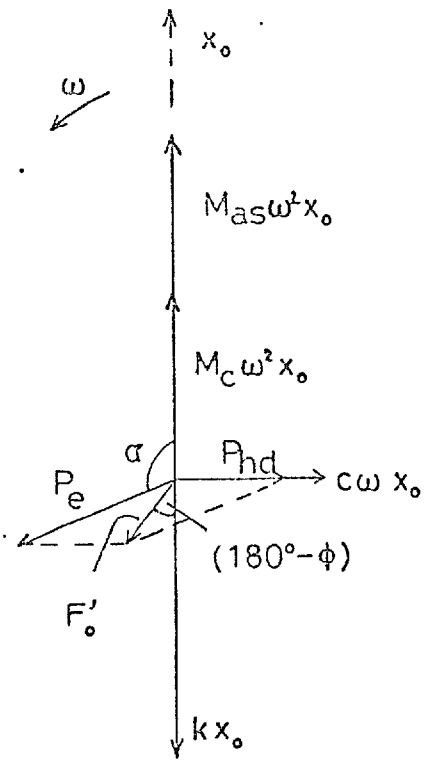

Fig. 56 Phase diagram showing the hydrodynamic forces

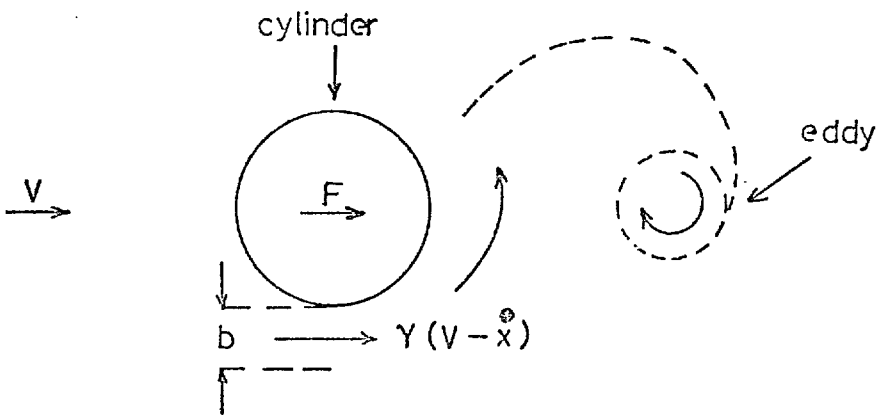

Fig. 57 Sketch showing transverse flow

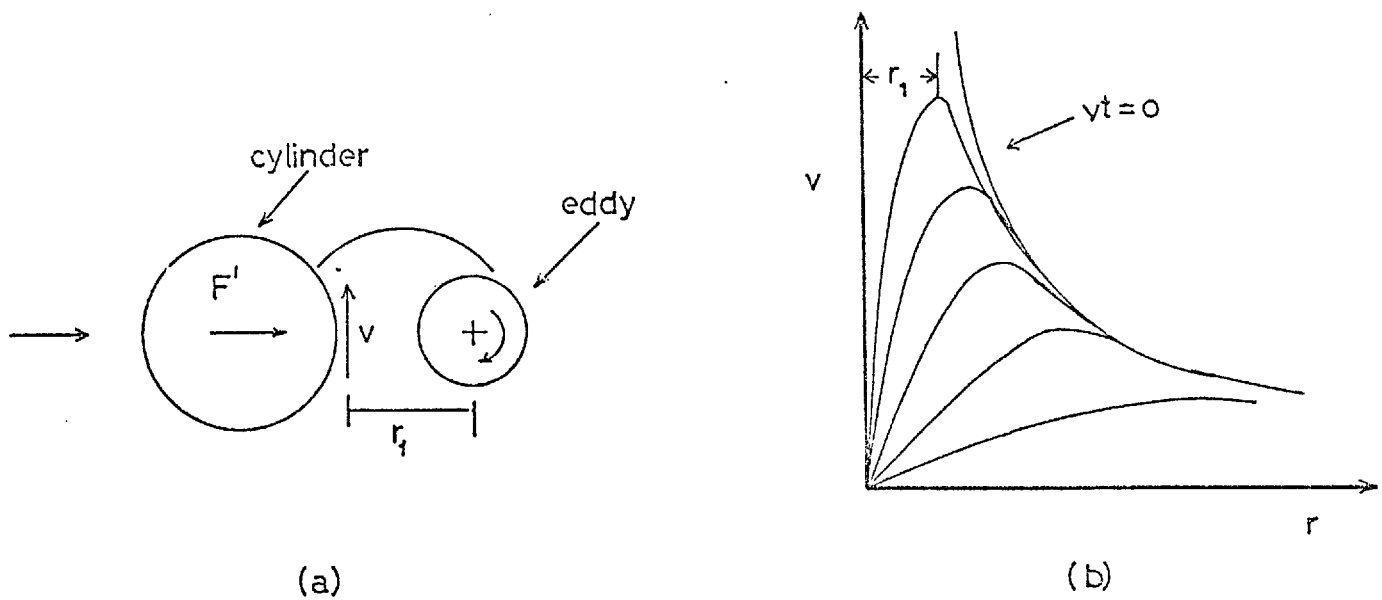

Fig. 58 Kinetic field of an eddy

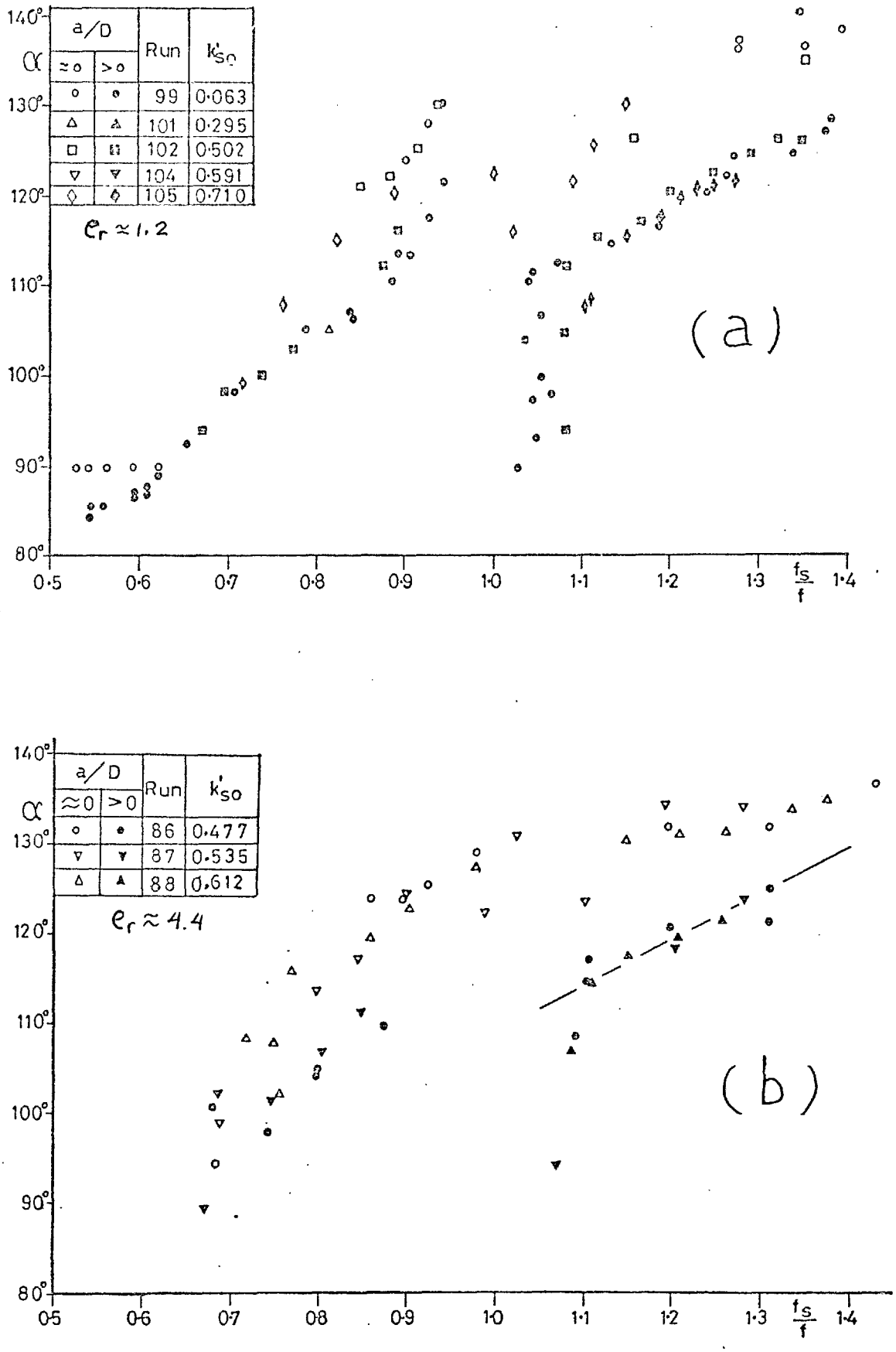

Fig. 59 Behaviour of α with (f_s/f). The line in the lower figure is an interpolation through the data of the upper figure

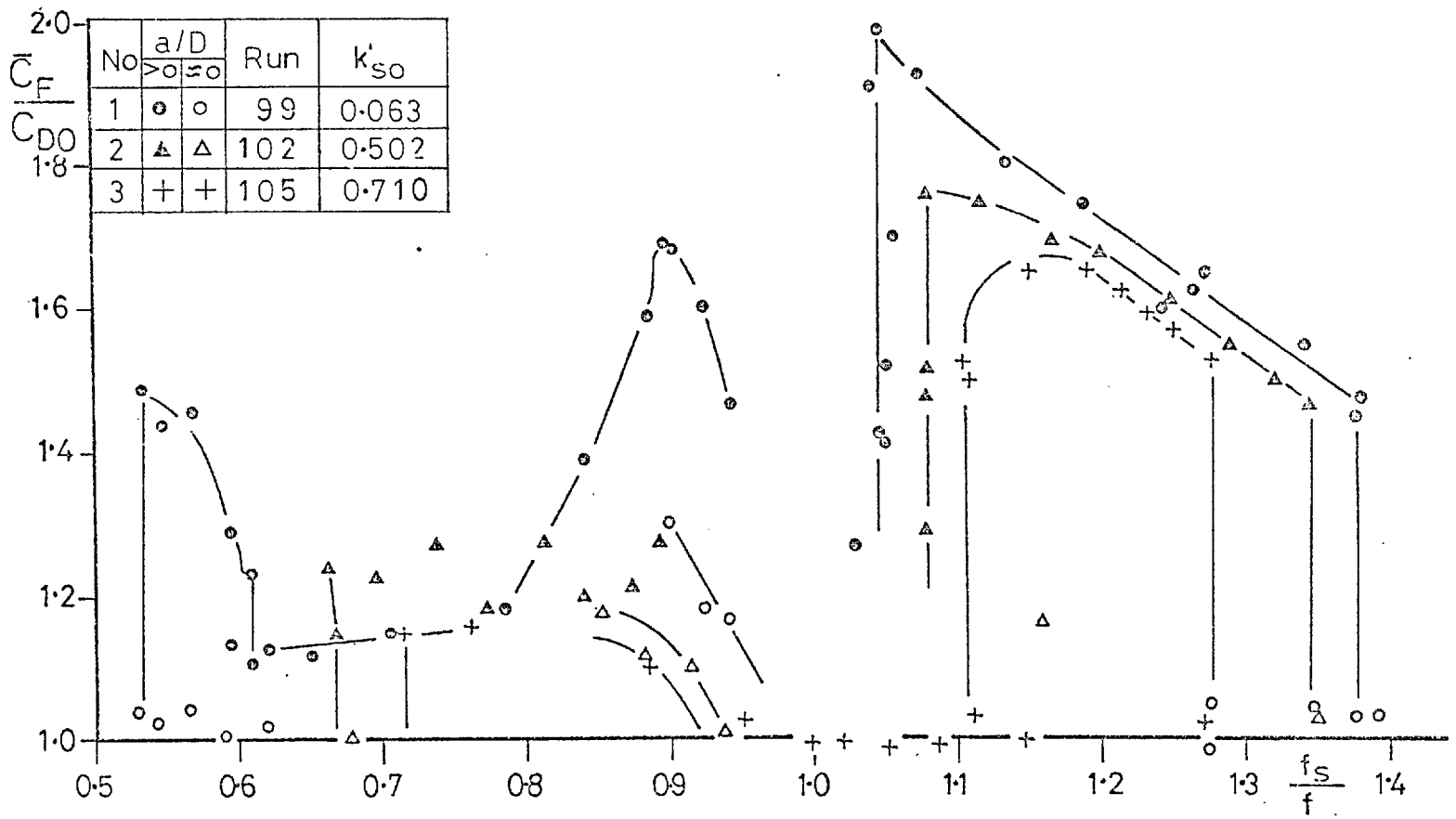

Fig. 60 Behaviour of $\bar{C}_F$ with (f_s/f)

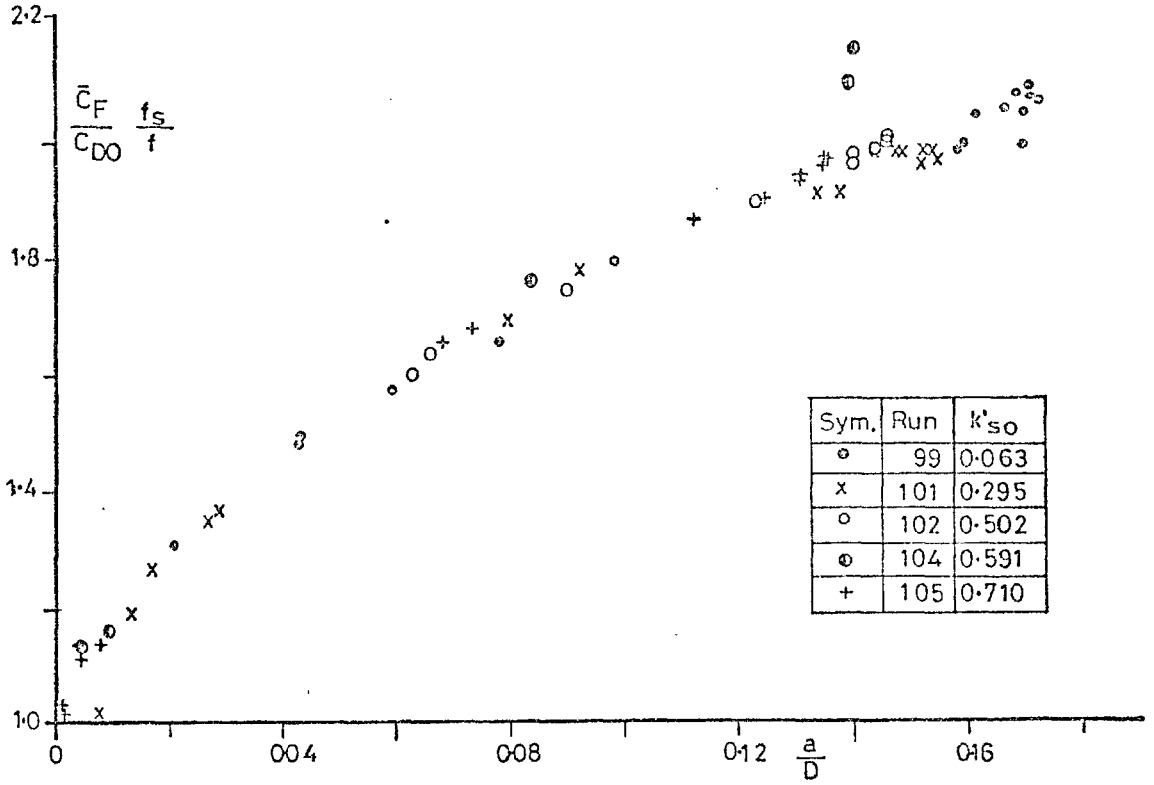

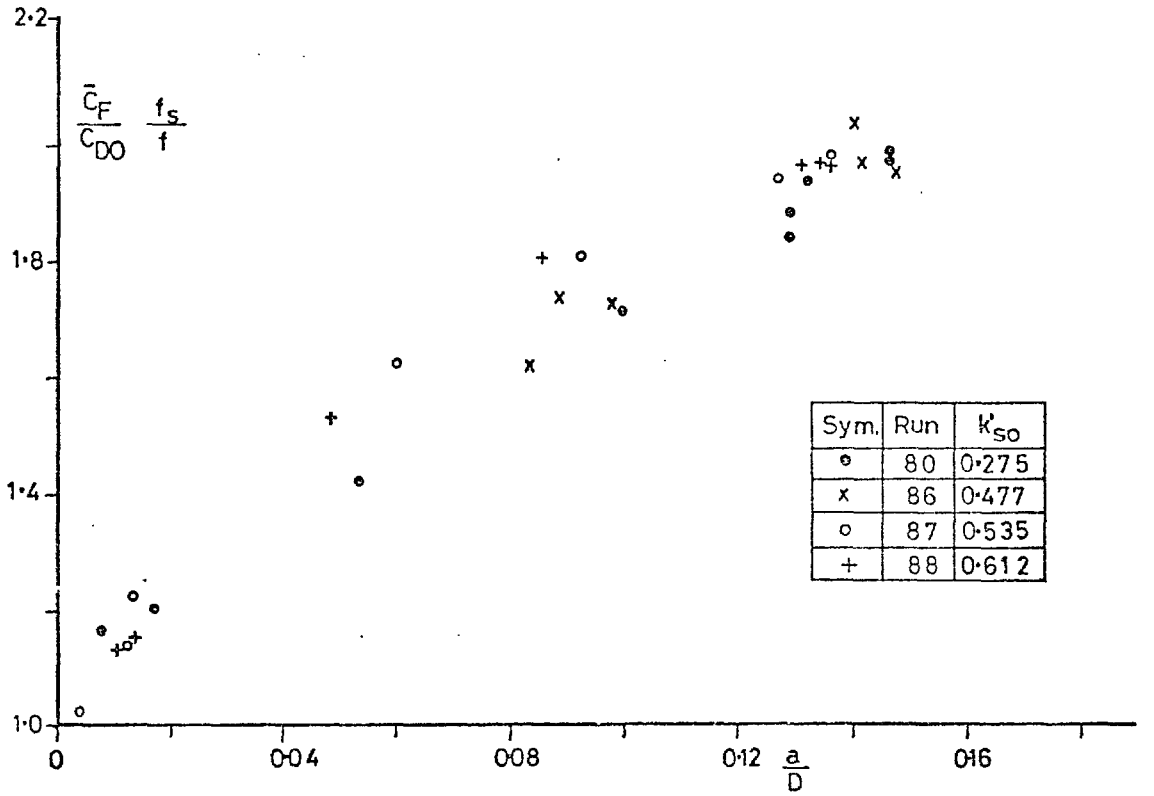

Fig. 61 $\bar{C}_F$ dependence on (a/D) in the second instability region

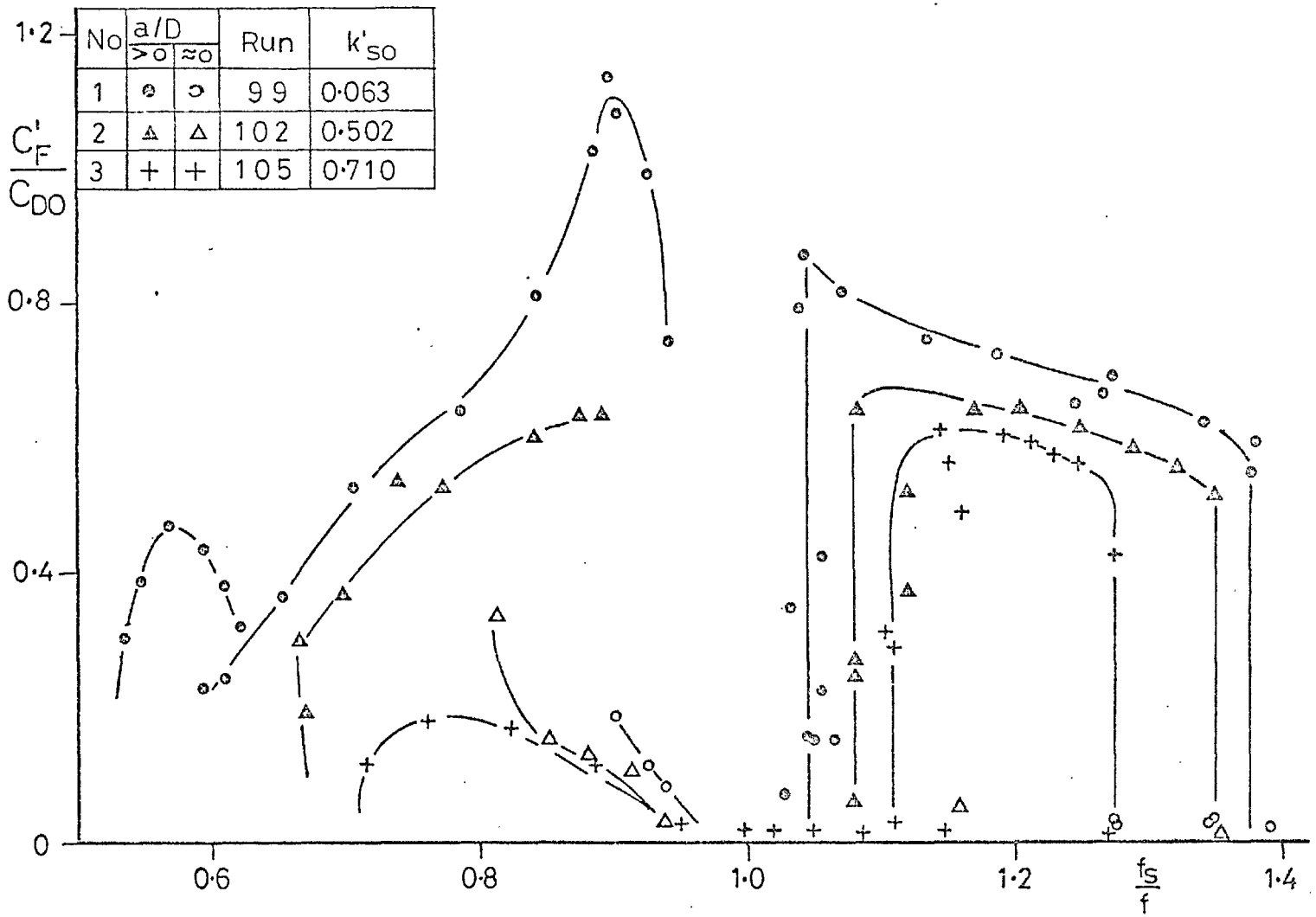

Fig. 62 Behaviour of C_F' with f_s/f

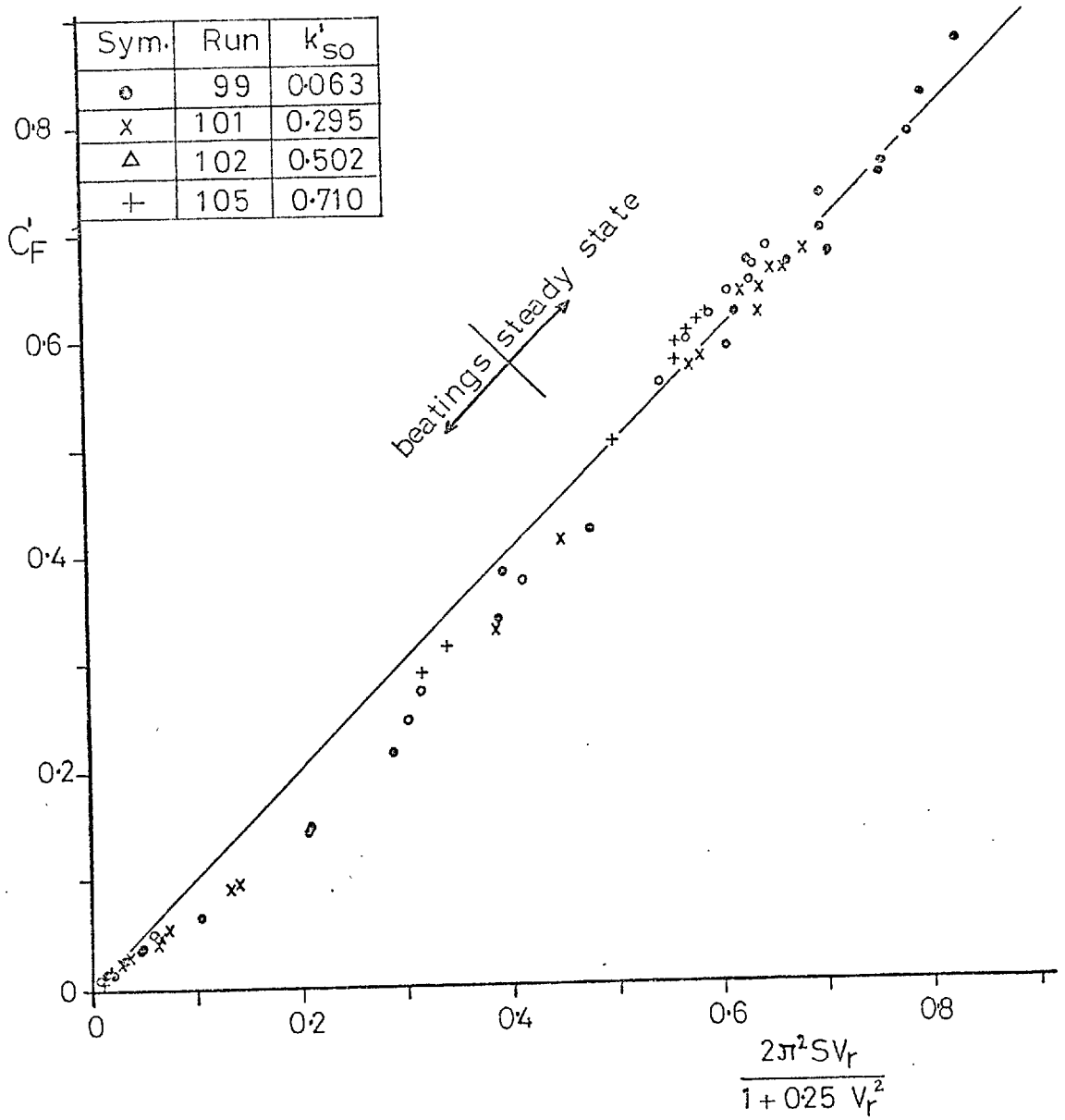

Fig. 63 Dependence of C_F on V_r in the second instability region

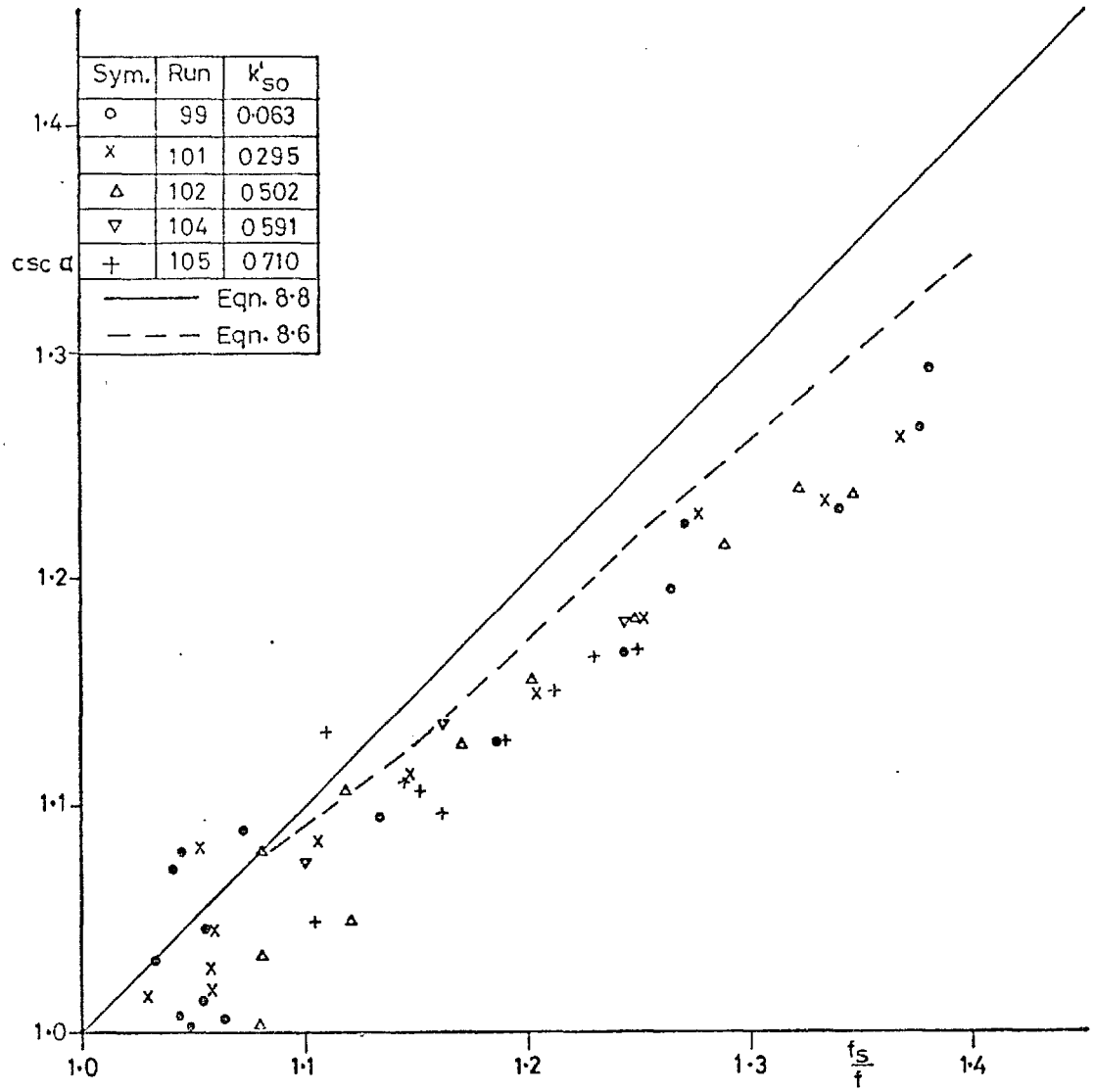

Fig. 64 The phase angle α as a function of f_s/f in the second instability region

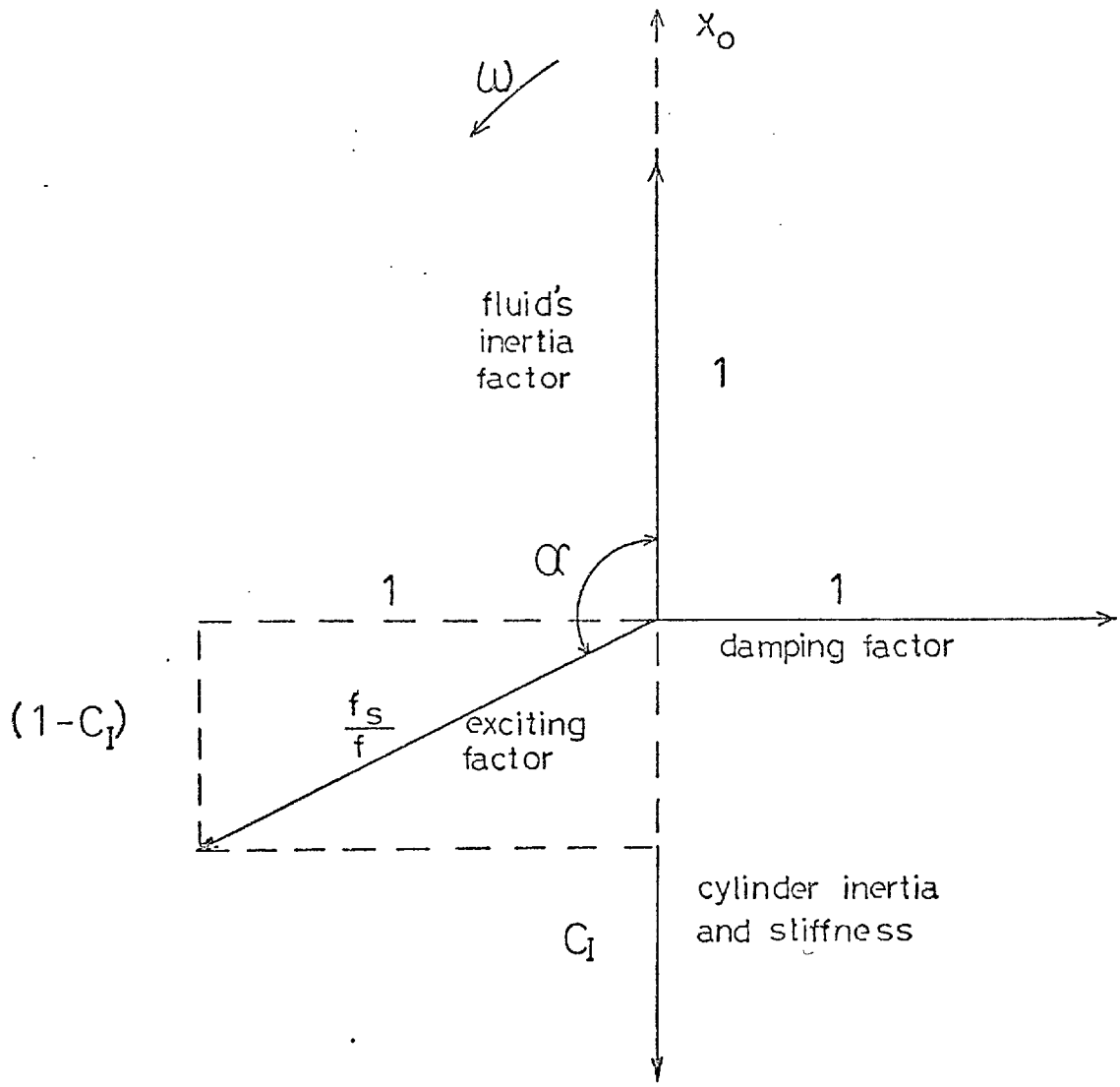

Fig. 65 Simplified phase diagram of the forces involved in the second instability region

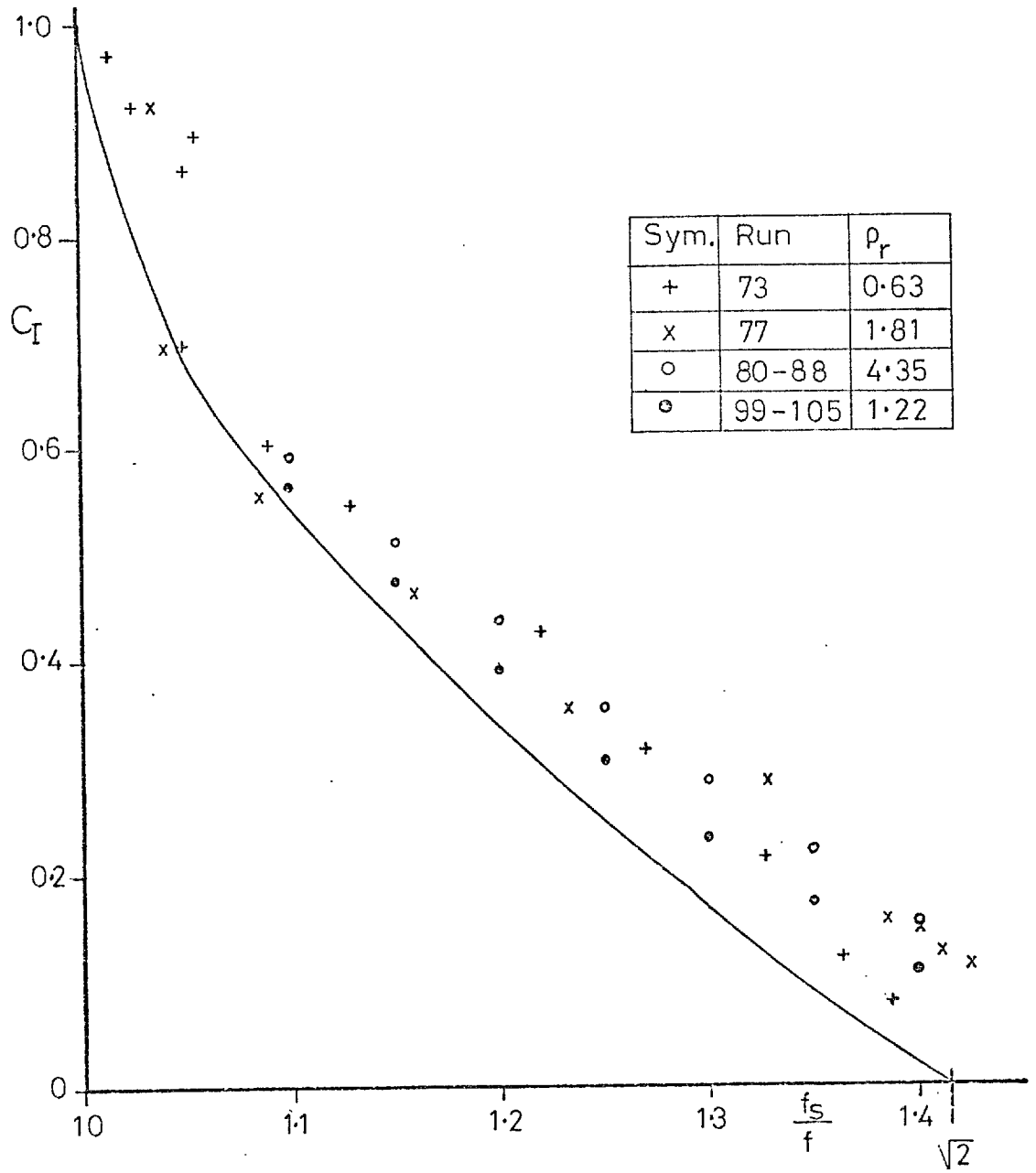

Fig. 66 Behaviour of C_I in the second instability region compared with equation 8.9

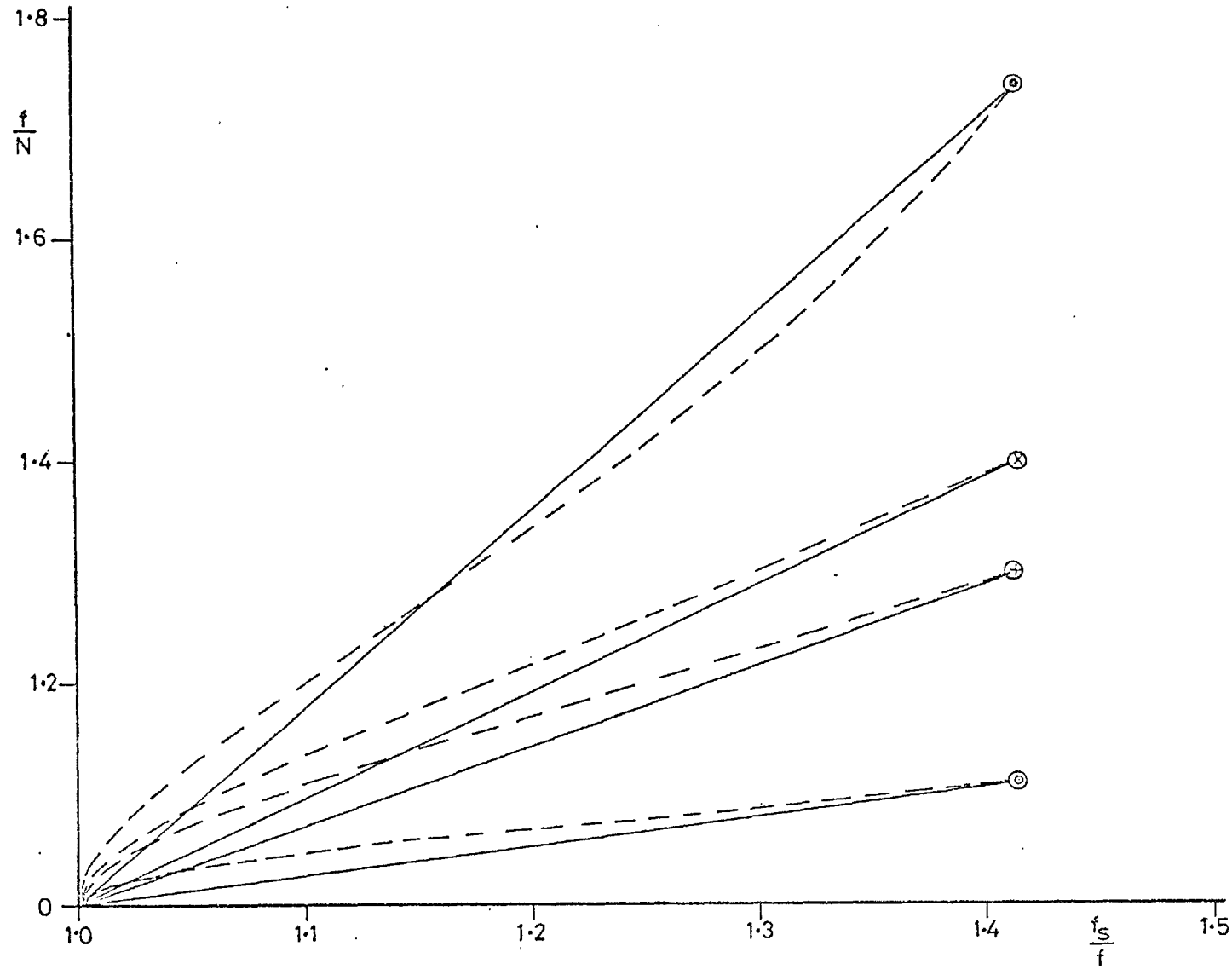

Fig. 67 Comparison of equations 6.2 (continuous line) and 8.10 (interrupted line) for: ρ_r = 0.5 (⊙); ρ_r = 1.04 (X); ρ_r = 1.43 (+); ρ_r = 4.3 (O)

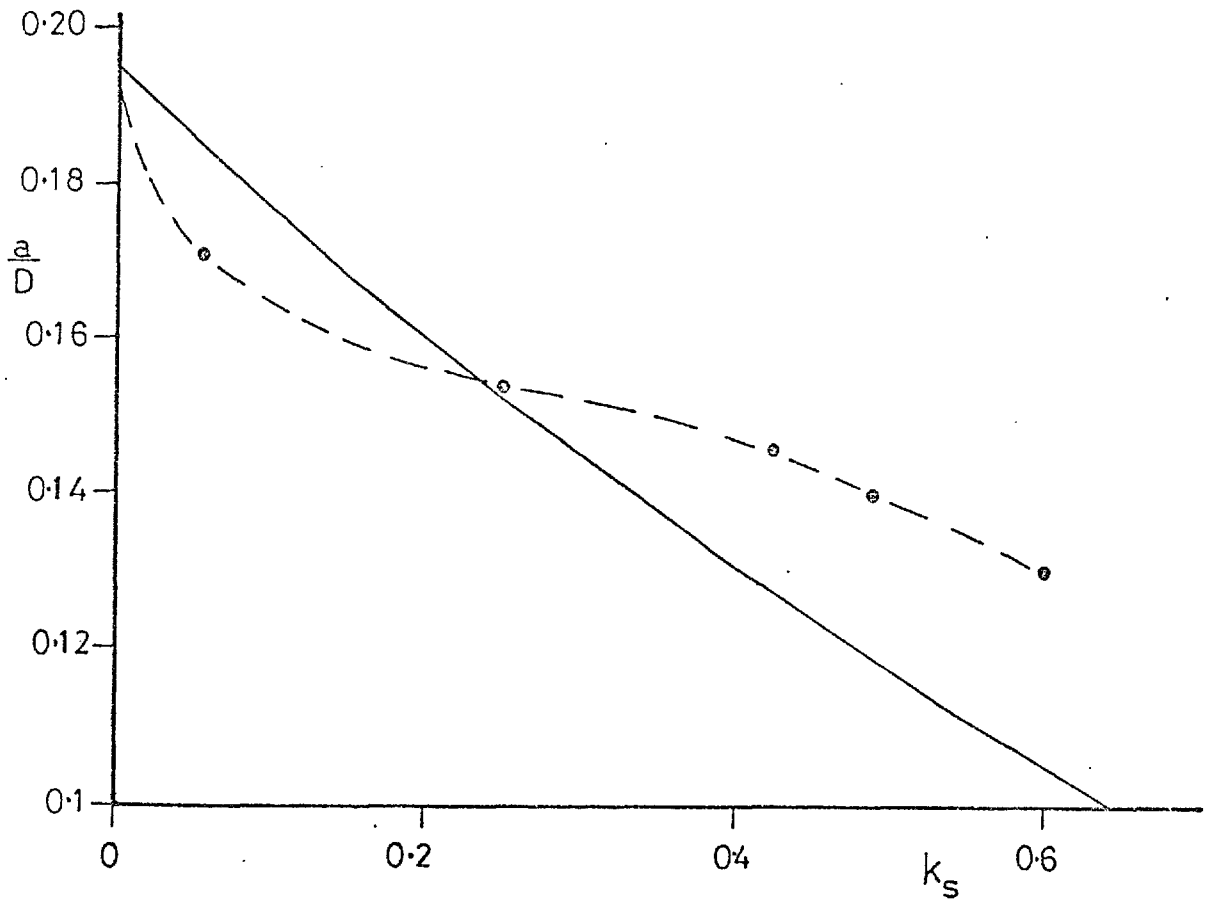

Fig. 68 Vibration amplitudes predicted from equations 8.12 and 8.13 (continuous line) compared with experimental results (ρ_r = 1.2; f_s/f = 1.2)

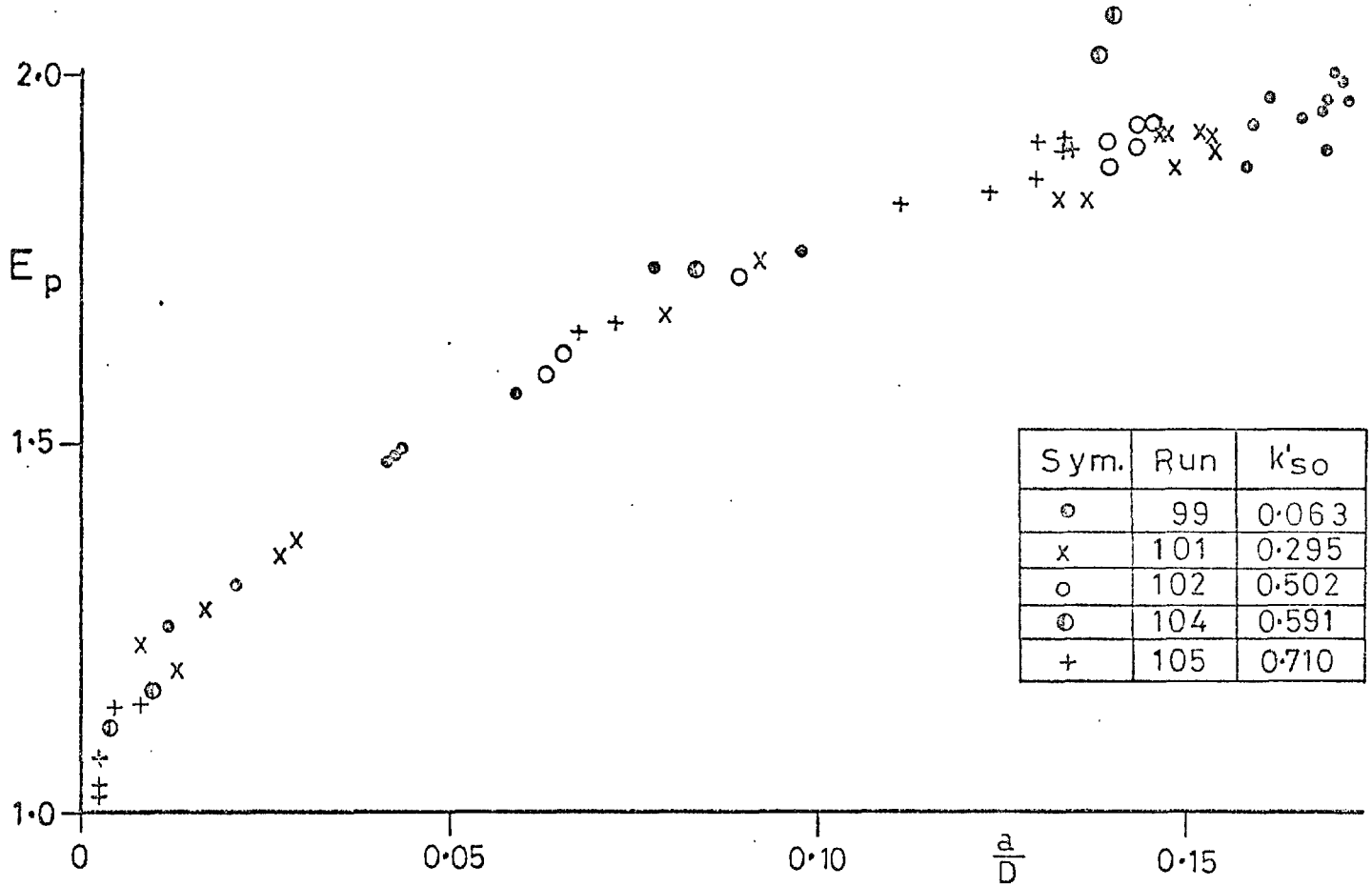

Fig. 69 Dependence of E_p on (a/D) in the second instability region

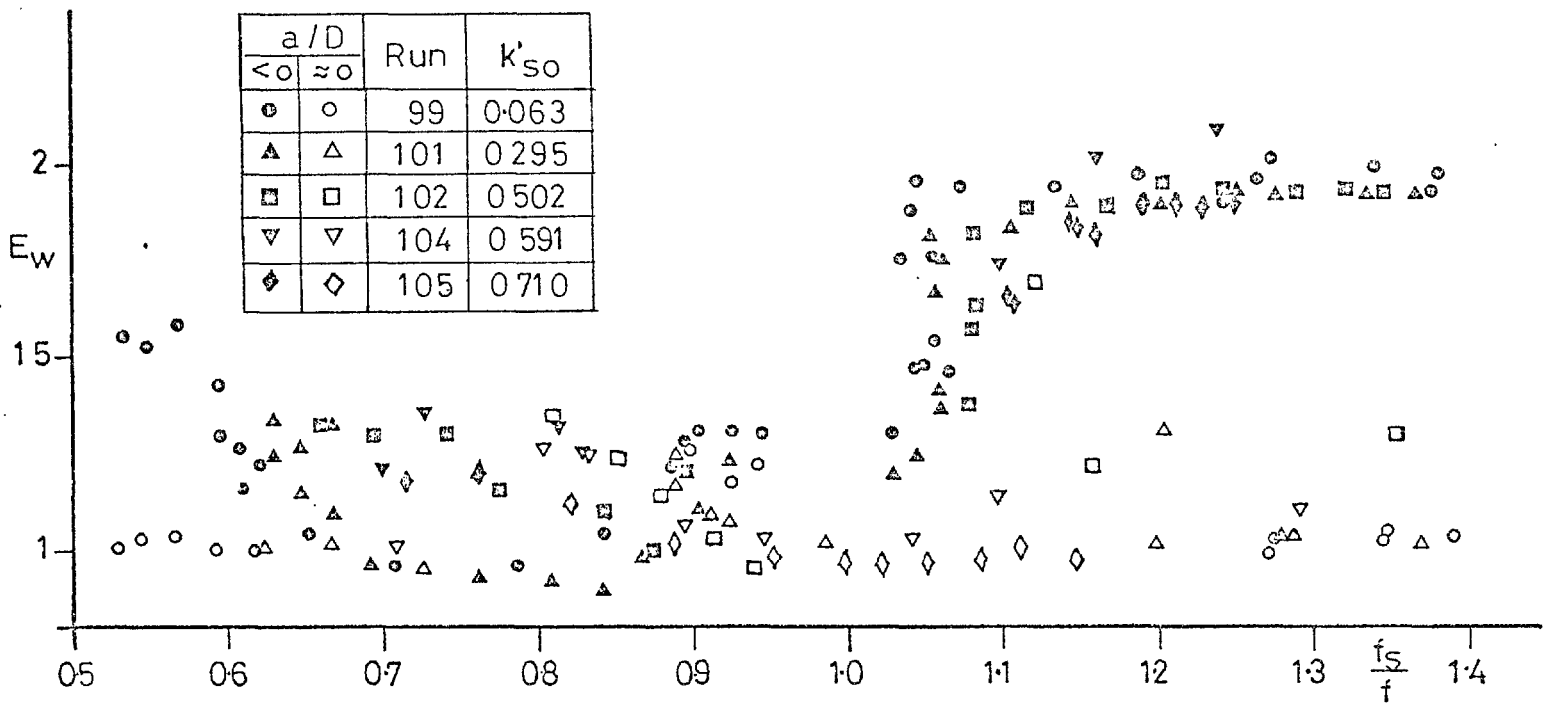

Fig. 70 Behaviour of $E_w = \frac{C_{DA}}{C_{DO}} \frac{f_s}{f_e}$ with $\frac{f_s}{f_e}$

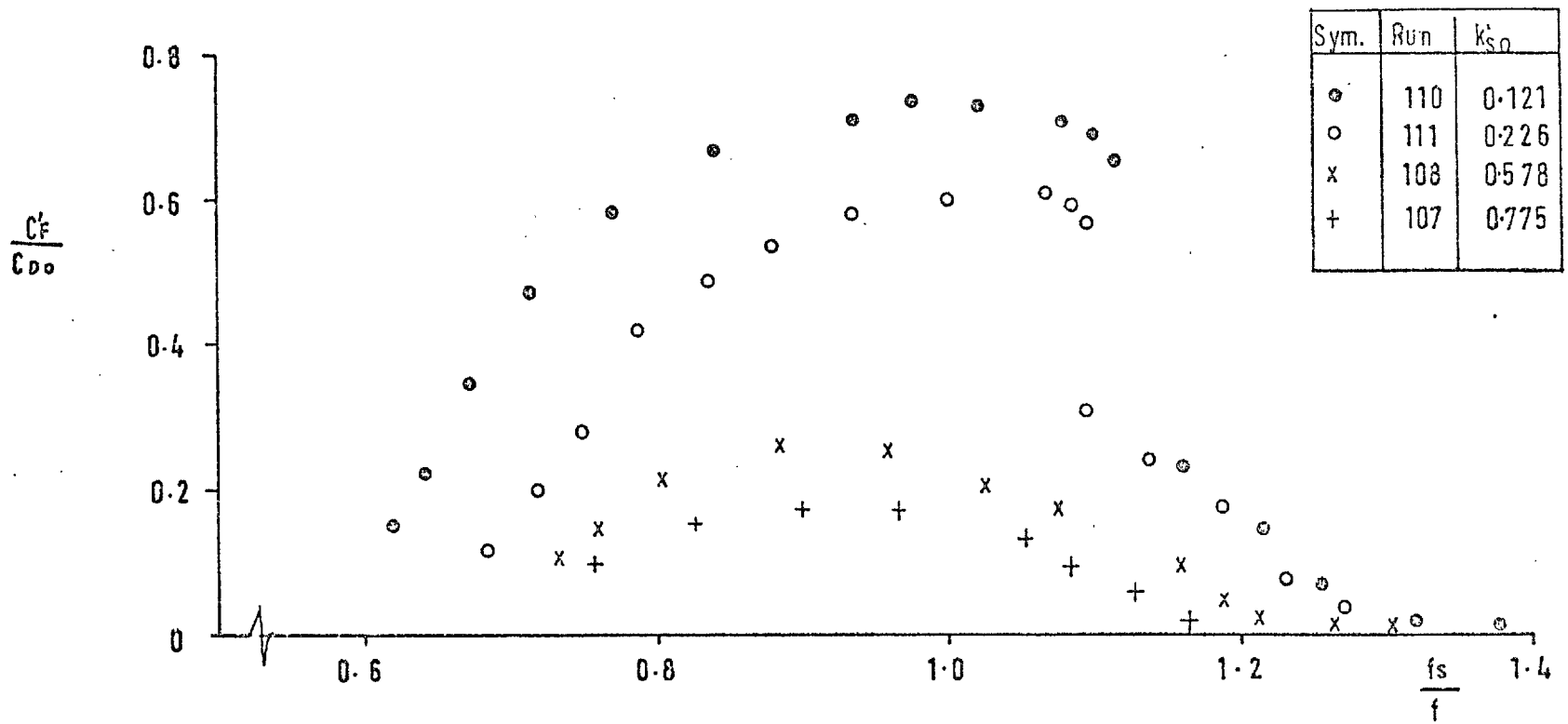

Fig. 71 Behaviour of C_F' for cylinders fitted with a splitter plate

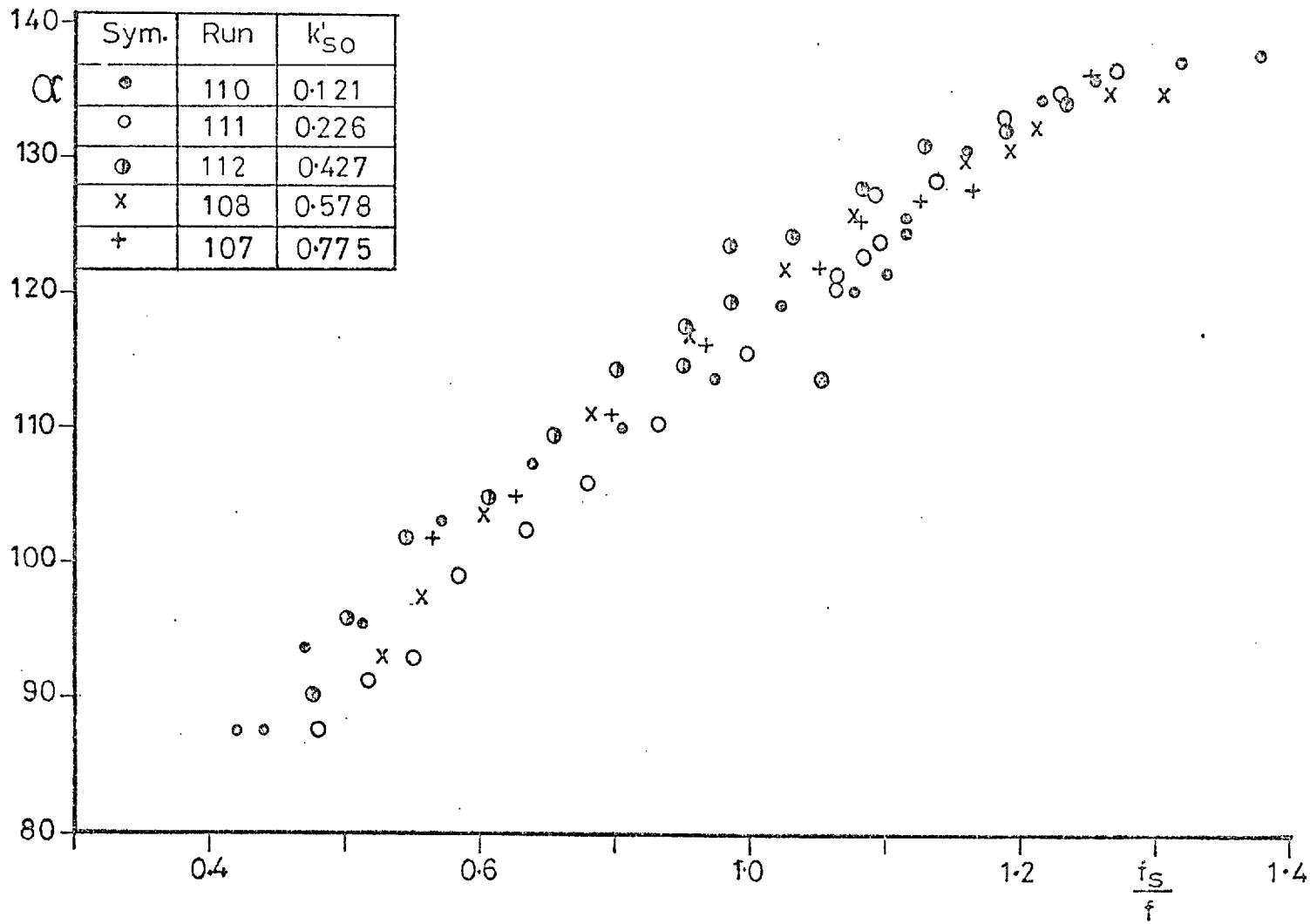

Fig. 72 Behaviour of α for cylinders fitted with a splitter plate

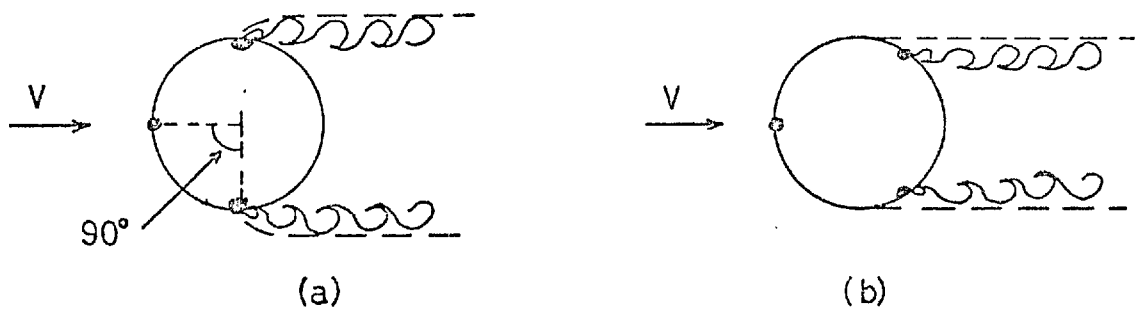

Fig. 73 Geometrical features of the "pairs mechanism"

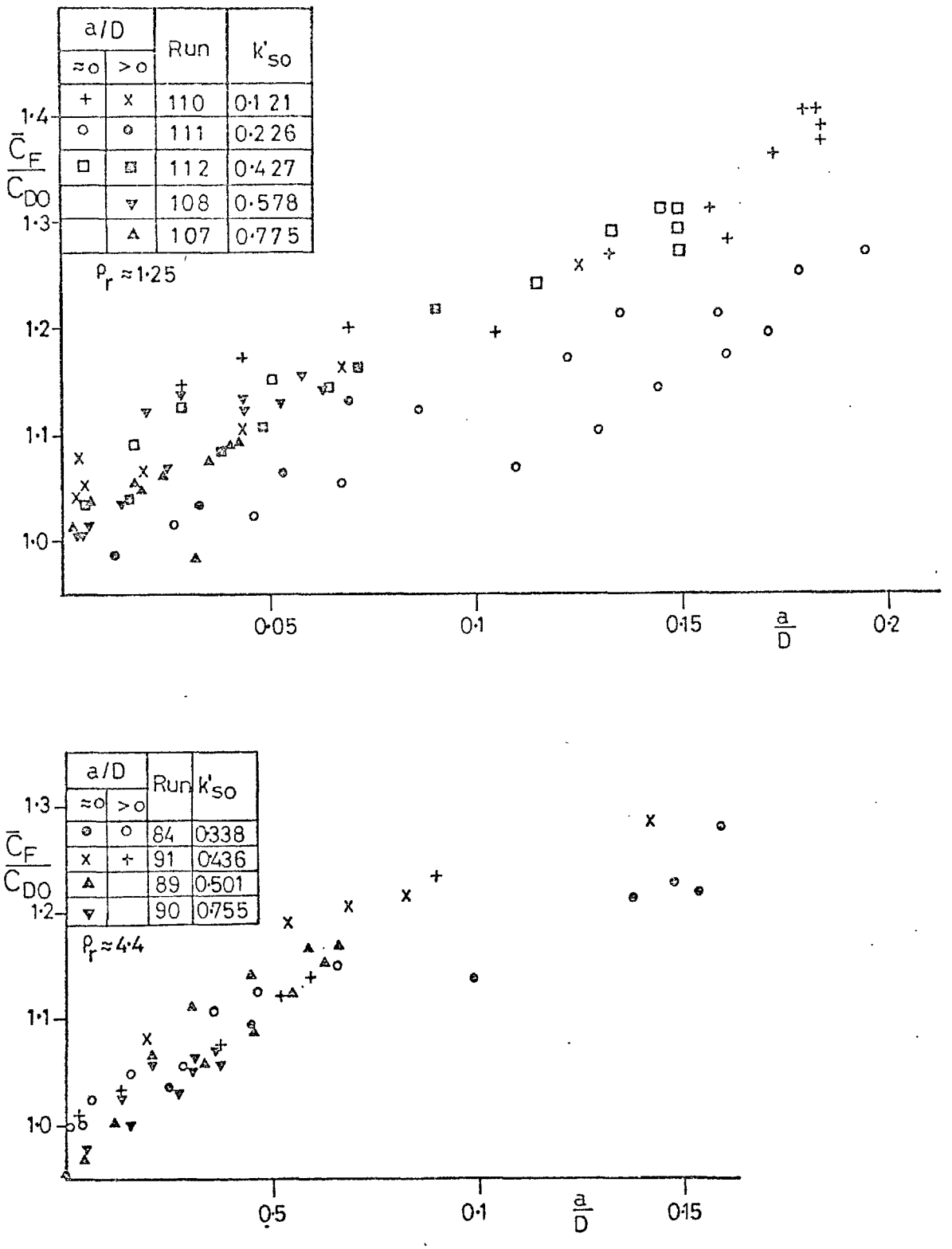

Fig. 74 Influence of (a/D) on $\bar{C}_F$ for cylinders fitted with a splitter plate

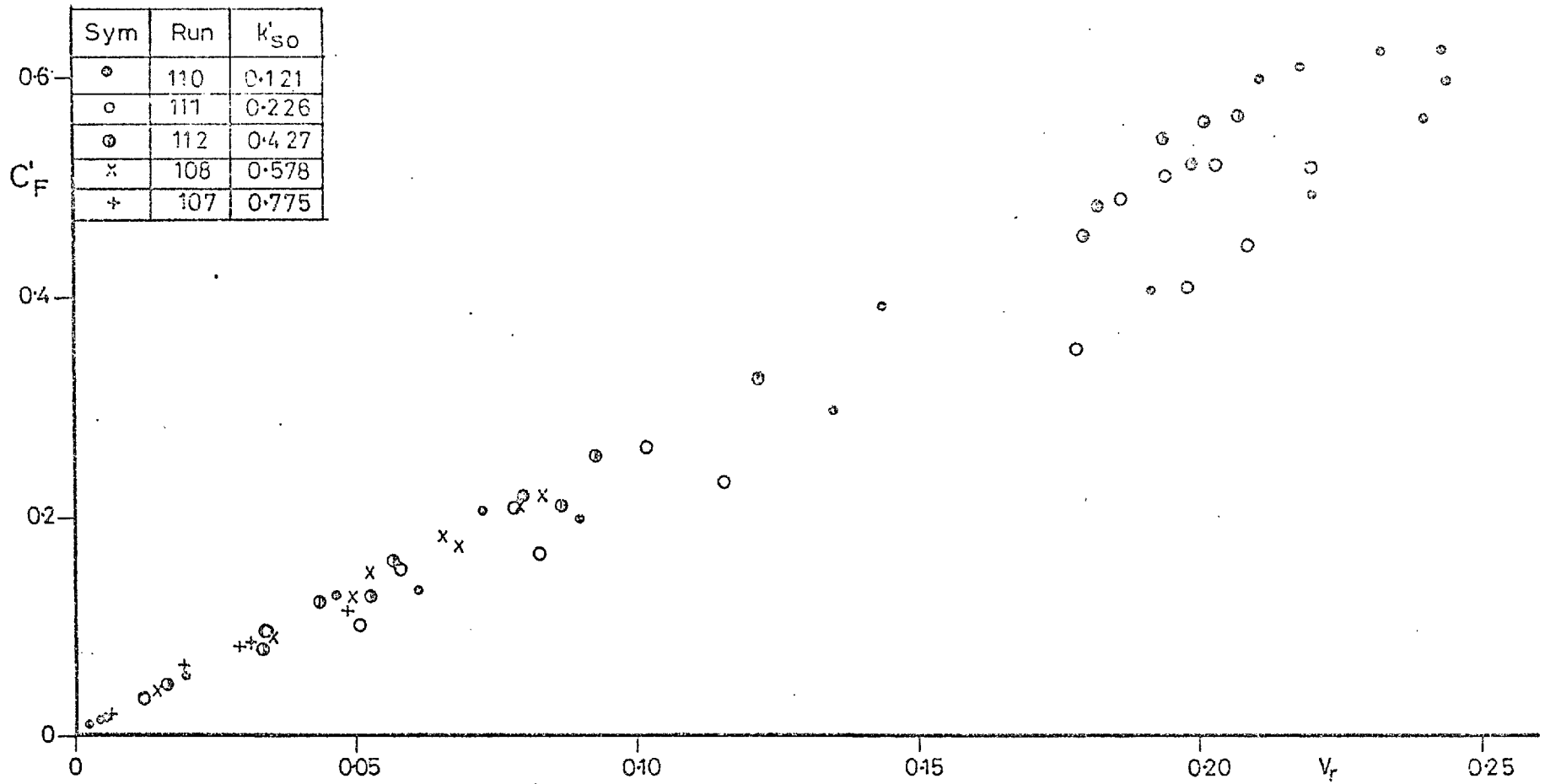

Fig. 75 Relationship between C'_F and V_r for cylinders fitted with a splitter plate

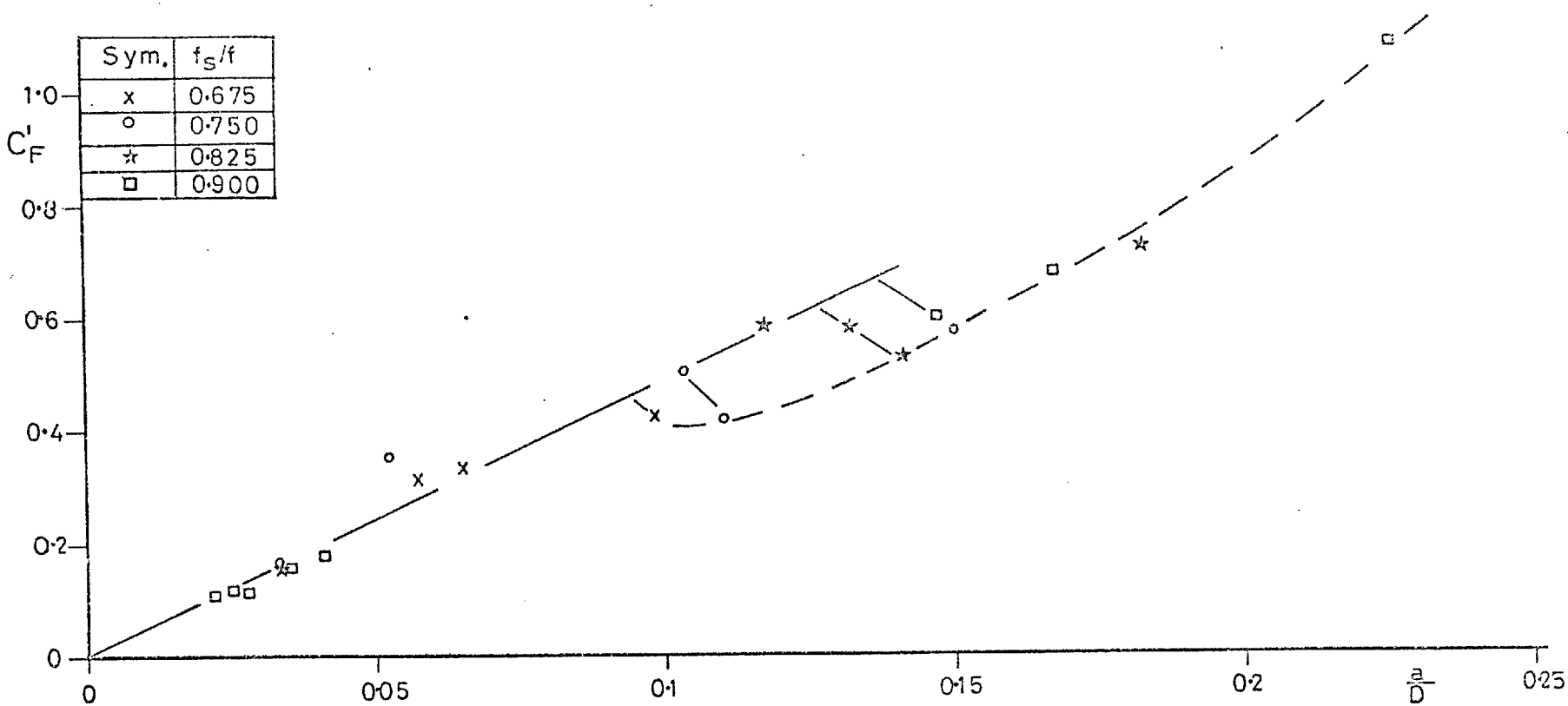

Fig. 76 Behaviour of C_F' with (a/D) for constant values of (f_s/f) in the first instability region. (Runs 99-105)

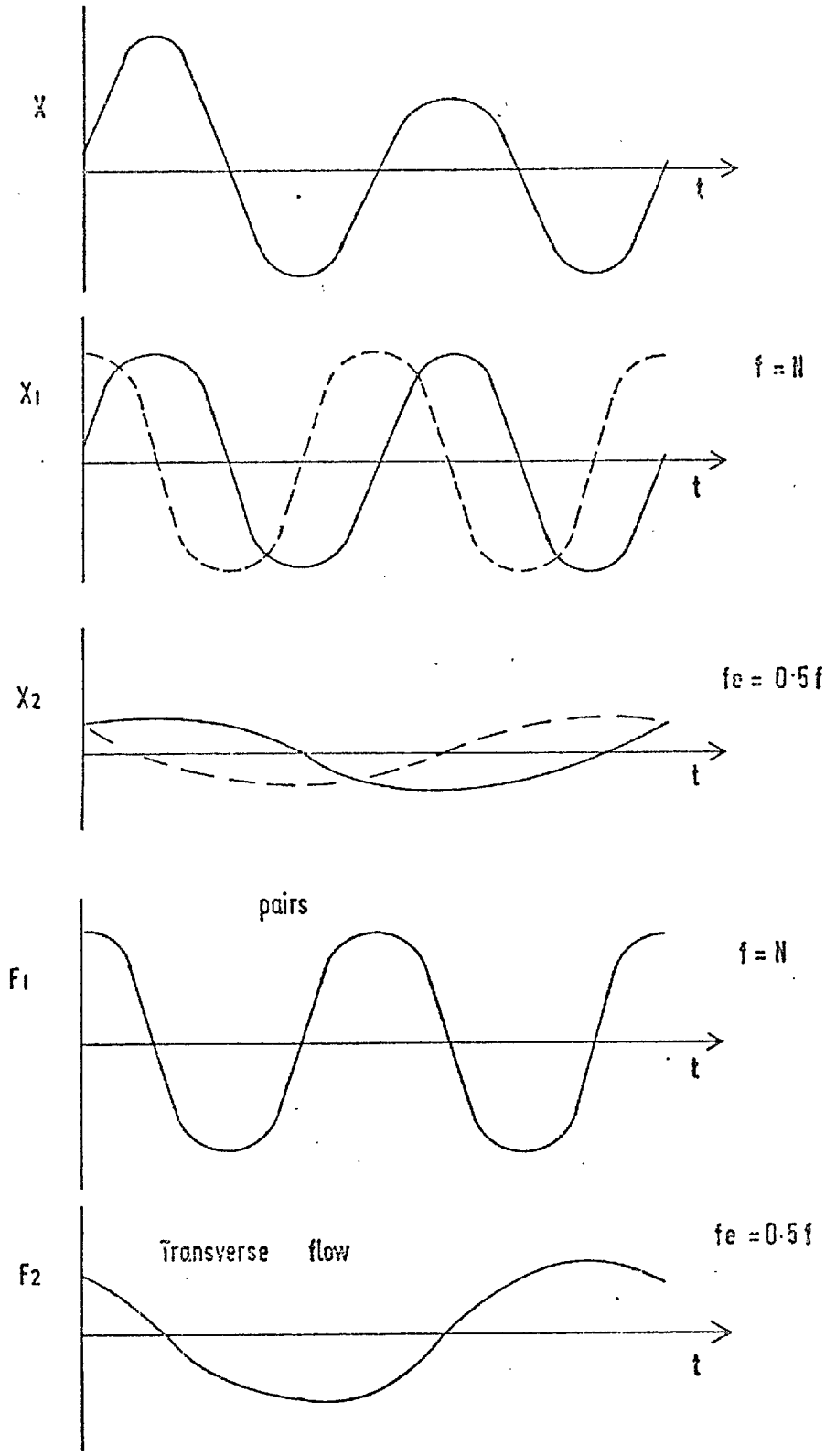

Fig. 77 One possible harmonic composition of cylinder motion and of excitation force

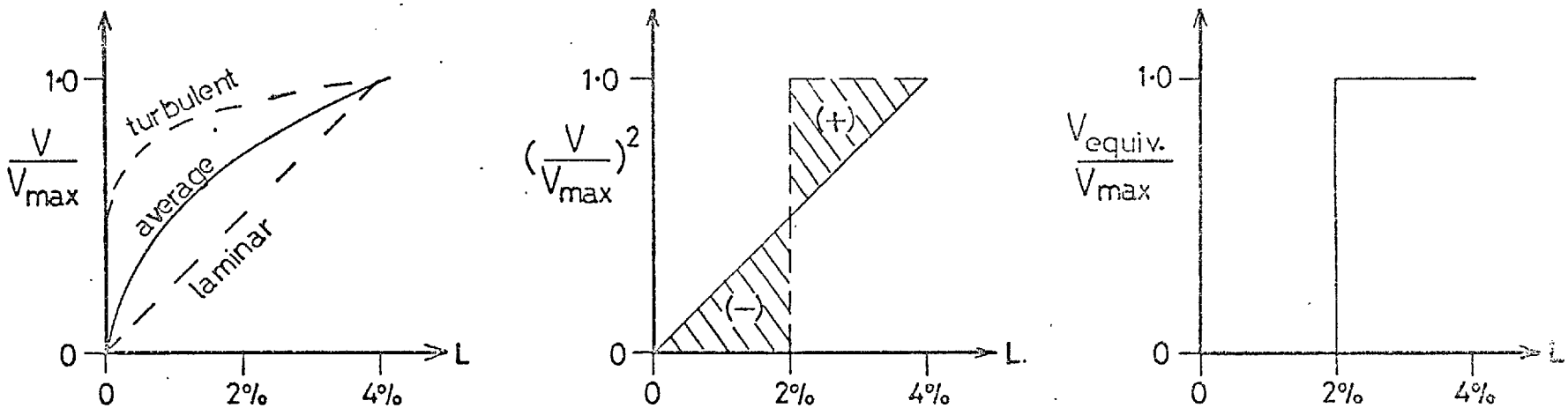

Fig. 78 Approximate and equivalent shapes of boundary layer

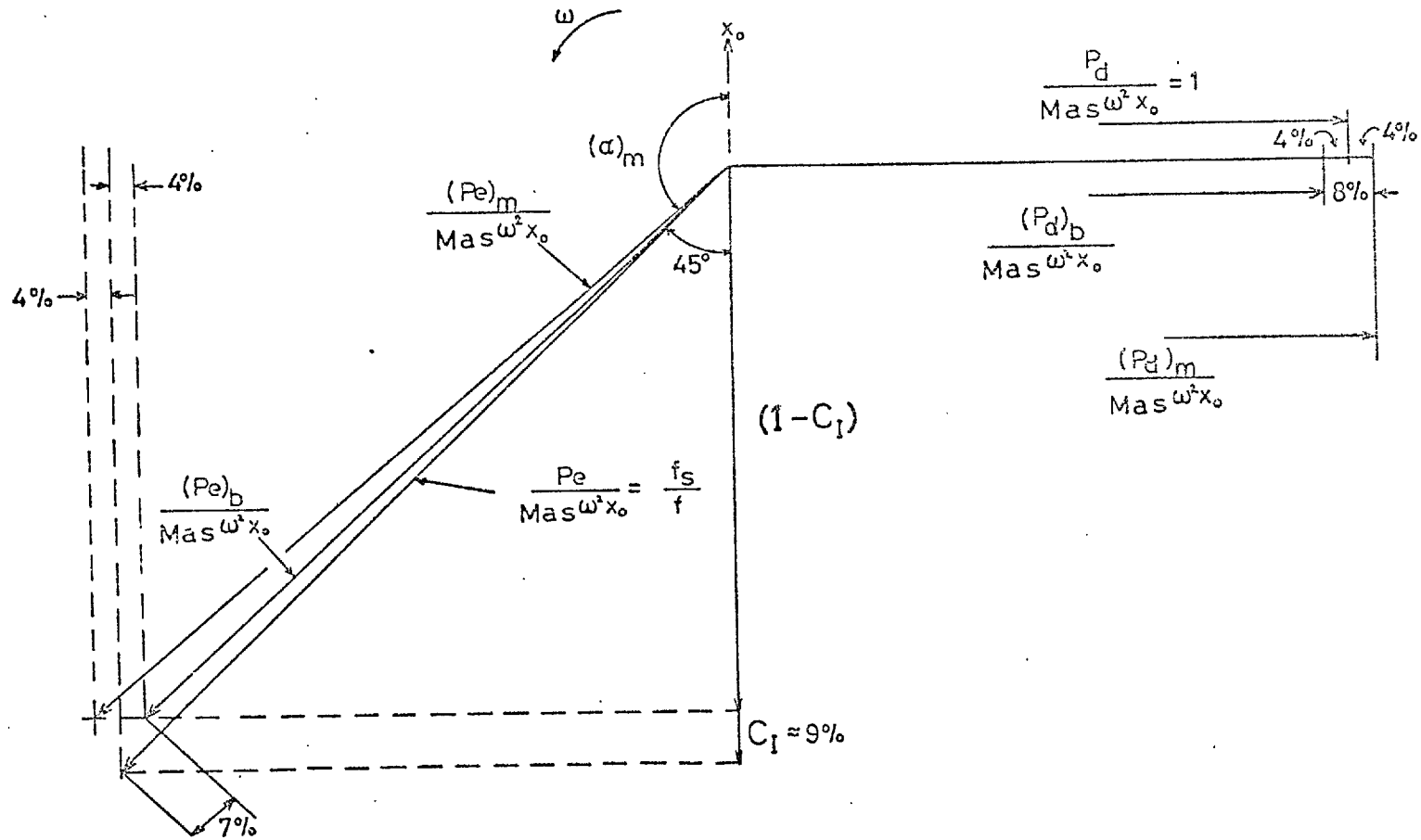

Fig. 79 Phase diagram of the hydrodynamic forces for $(f_s/f) = \sqrt{2}$

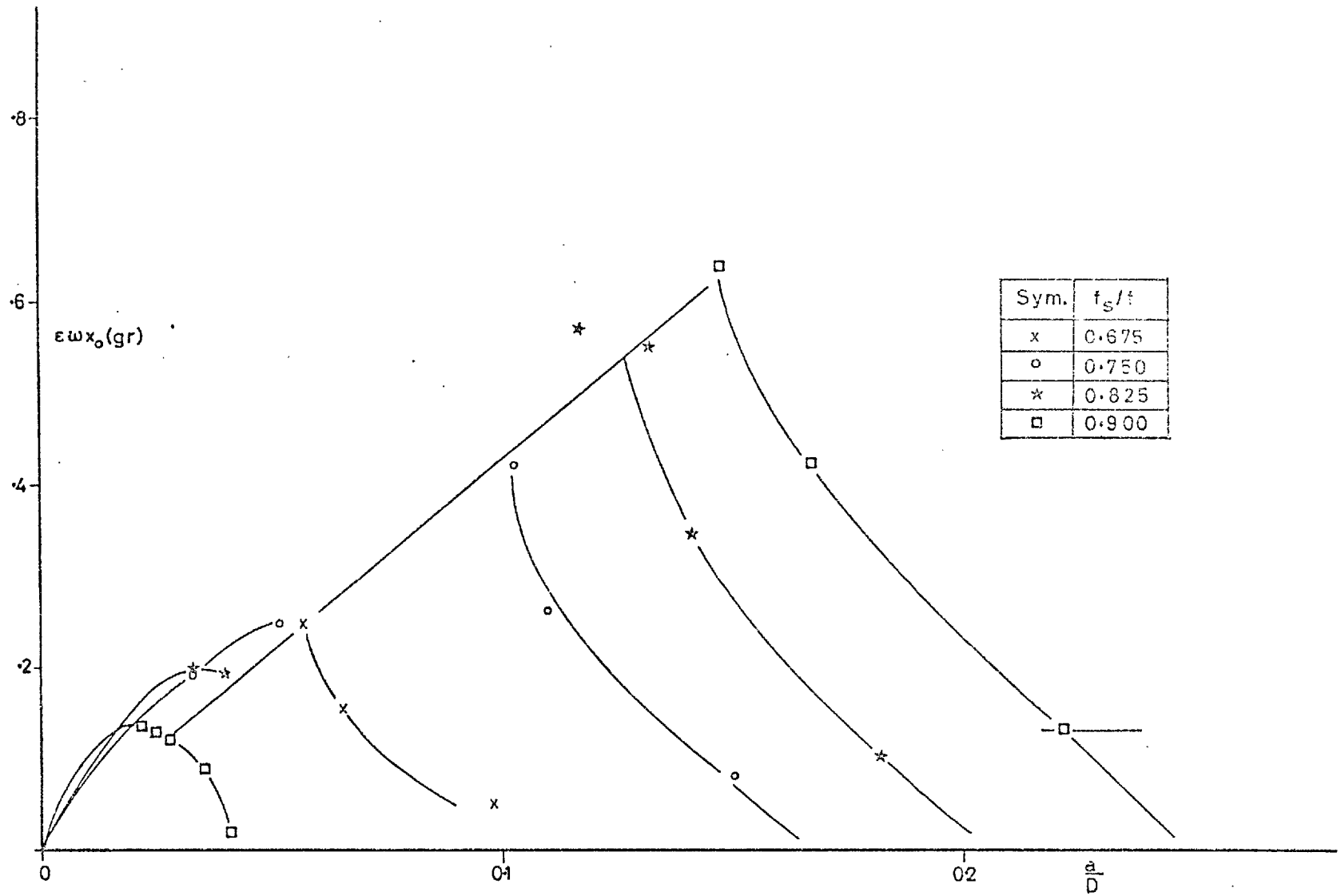

Fig. 80a The exciting force as a function of vibration amplitude in the first instability region

(continued on next page)

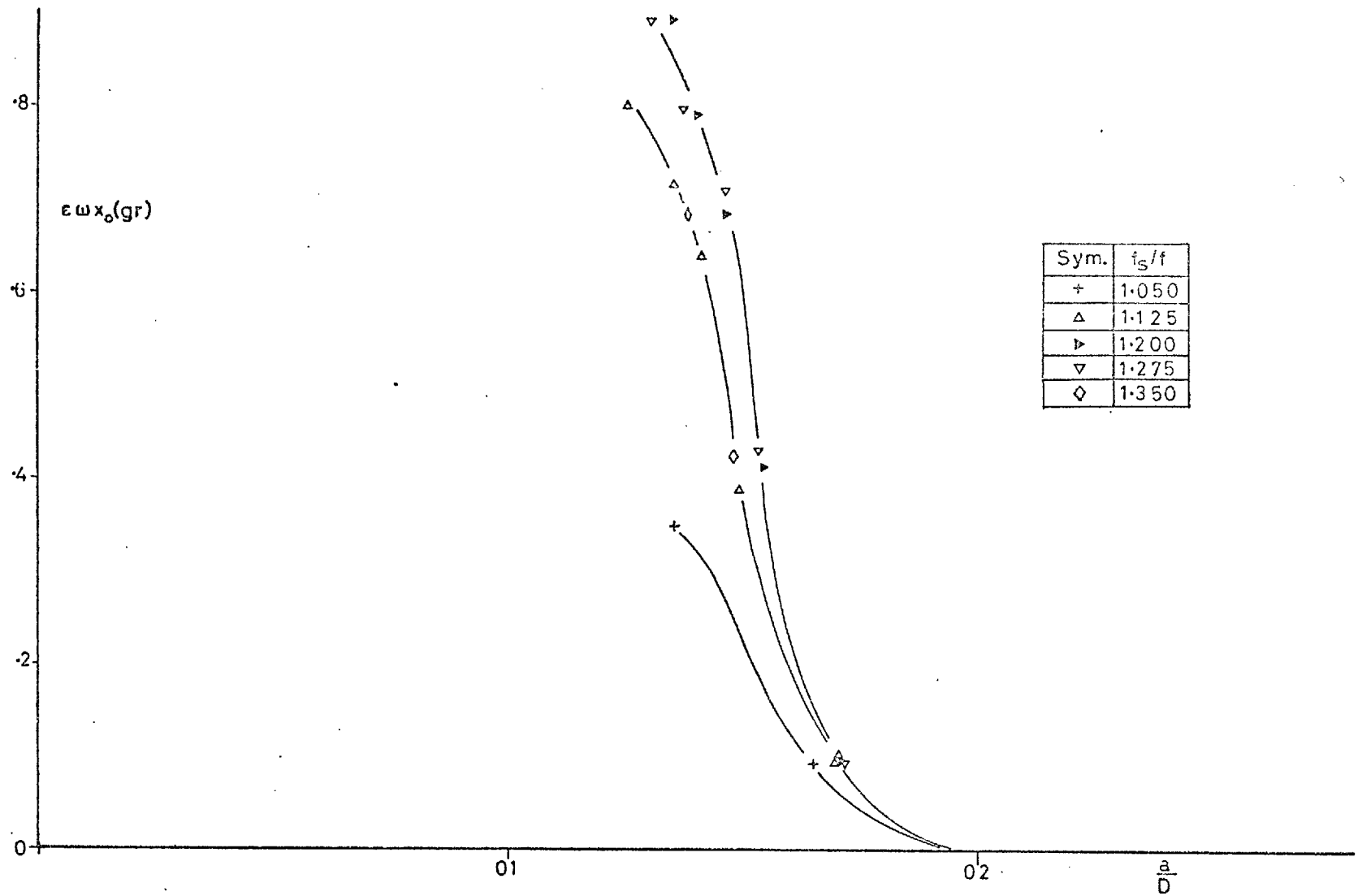

Fig. 80b The exciting force as a function of (a/D) in the second instability region

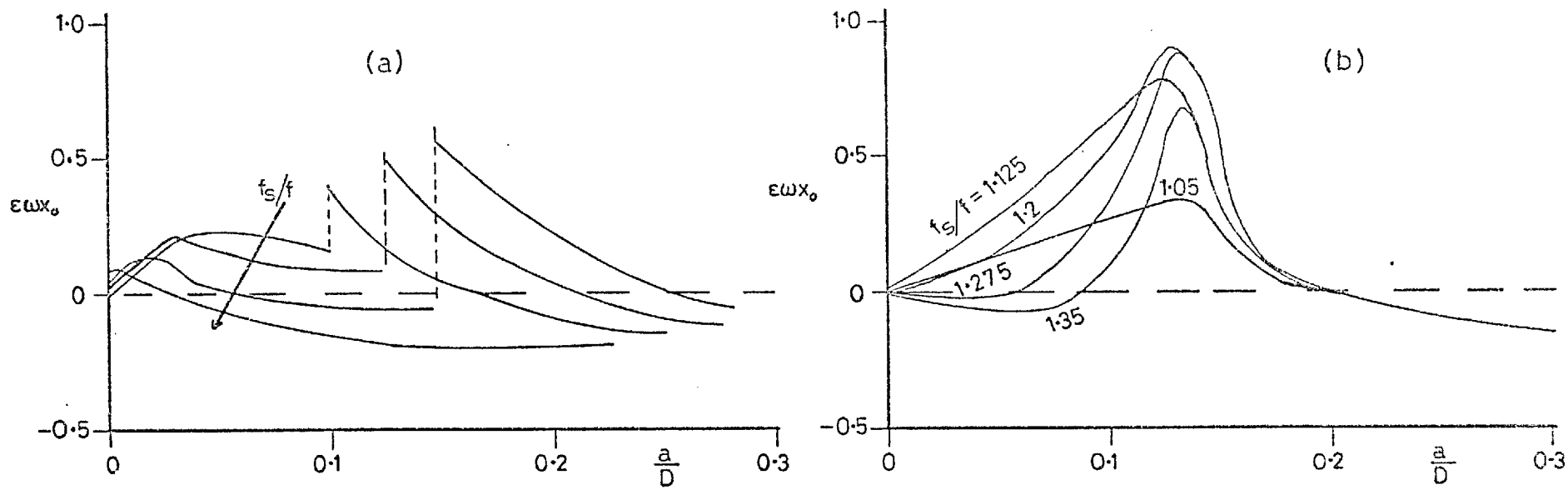

Fig. 81 Approximate shape of the full ($\varepsilon\omega x_o$) vs (a/D) curves, (a) in the first and (b) in the second instability regions

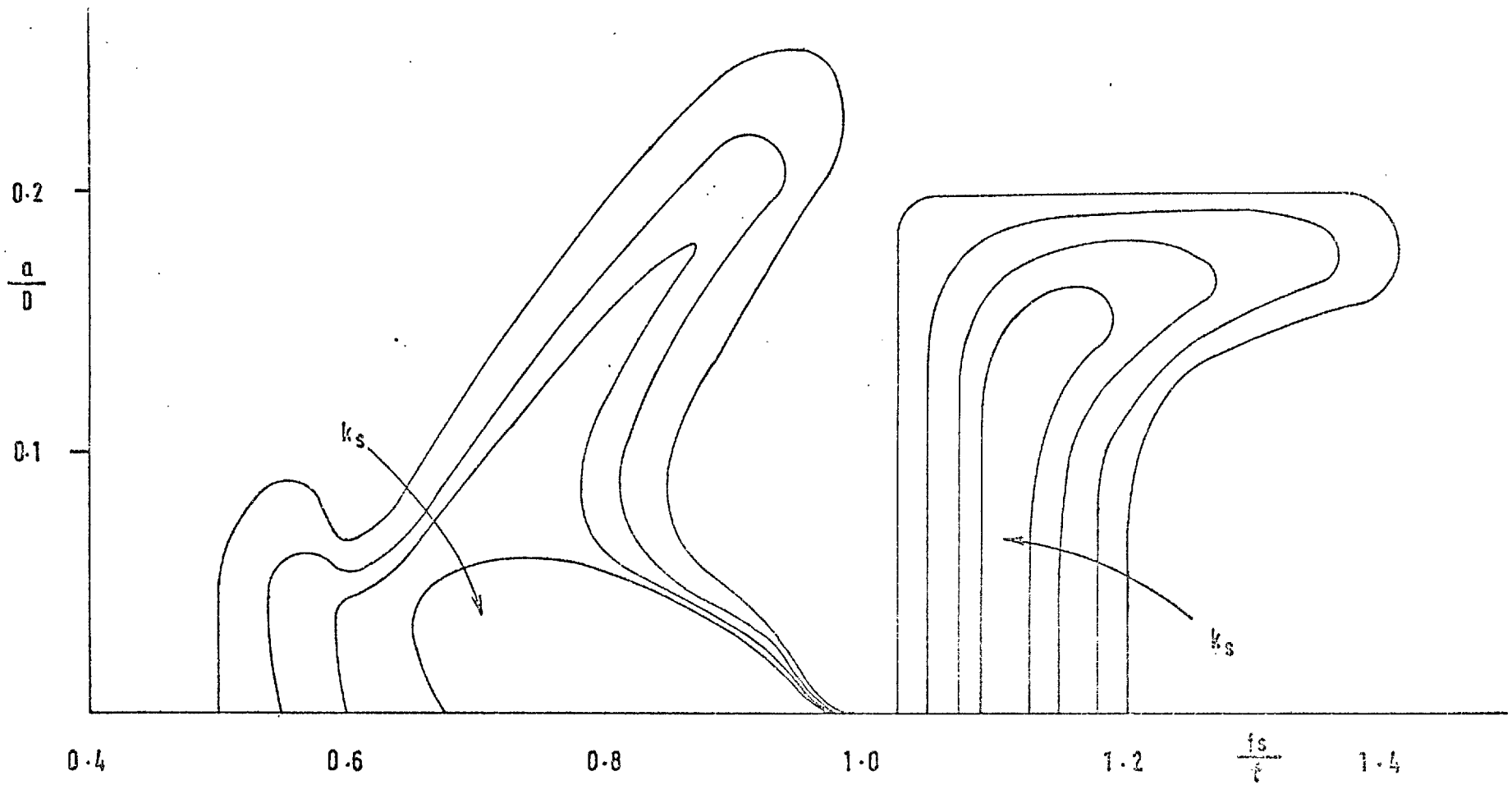

Fig. 82 Approximate amplitude response curves for varying k_s and showing hysteresis

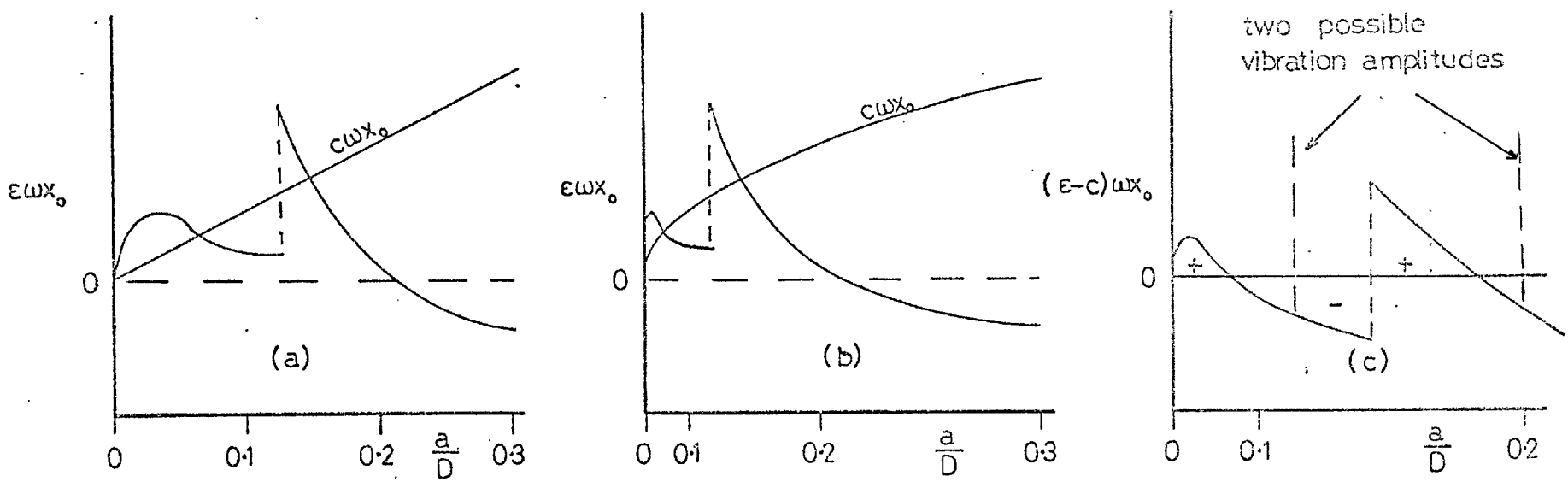

Fig. 83 Replotting one of the curves of Fig. 81, considering external damping (a), and modifying the abscissa according to the deflection curve of the pile (b), so as to predict vibration amplitudes from an energy balance (c).

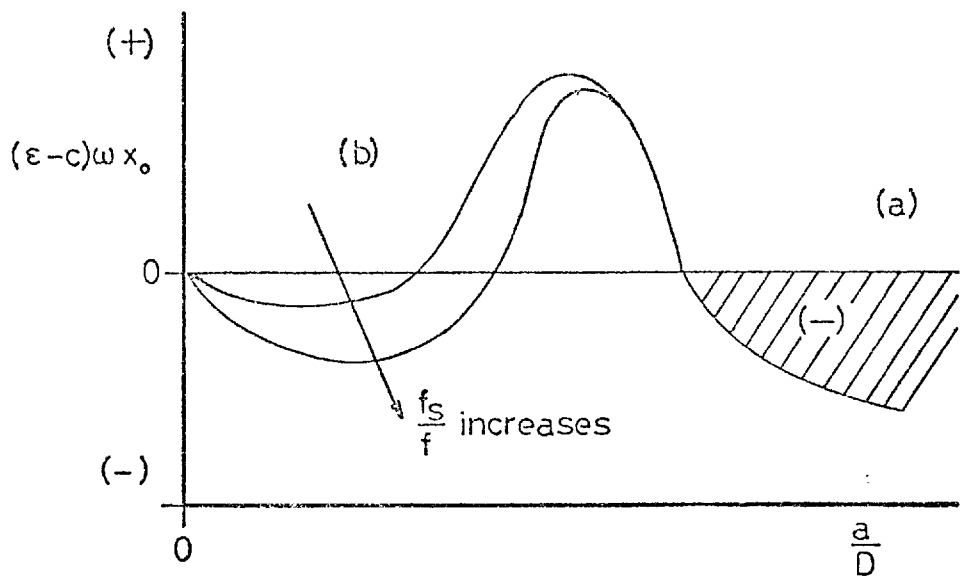

Fig. 84 Typical net exciting force curves for the second instability region

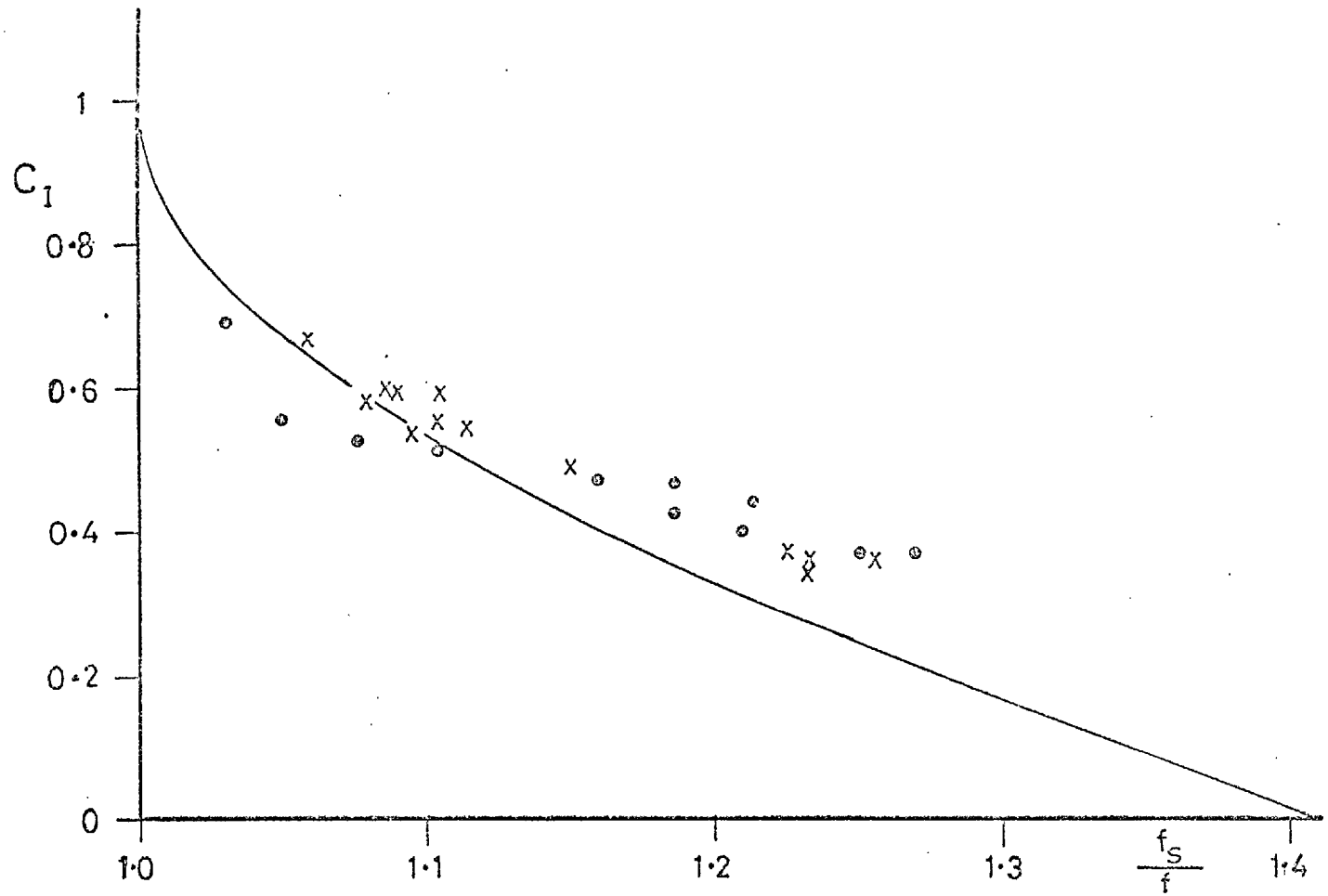

Fig. 85 Frequency response of the Immingham piles in terms of C_I (from Wootton[2] and Eqn. 7.15b) compared with equation 8.9: (⊙) V increasing, (X) V decreasing

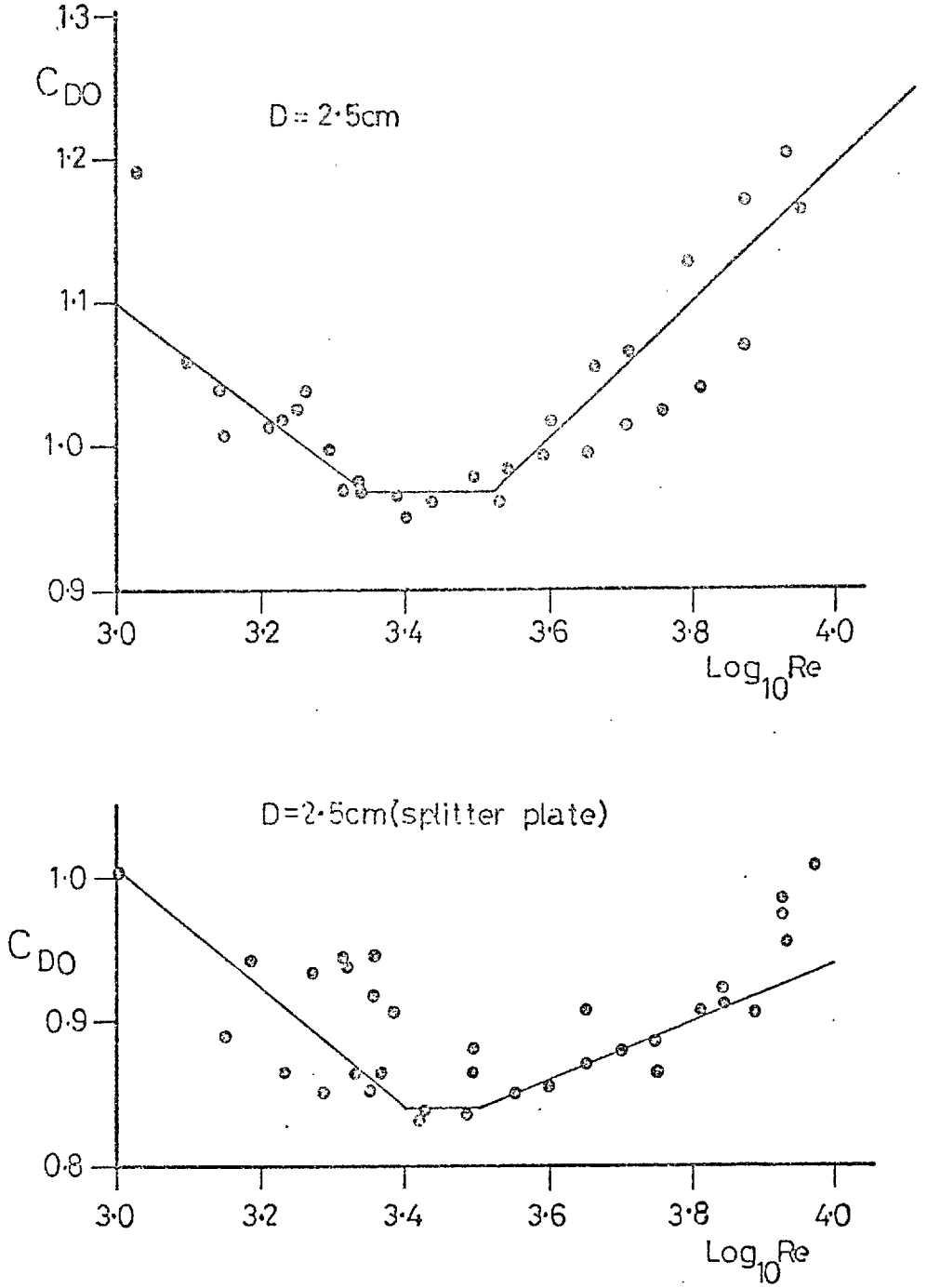

Fig. 86 The drag coefficient of the stationary cylinders as a function of R_e

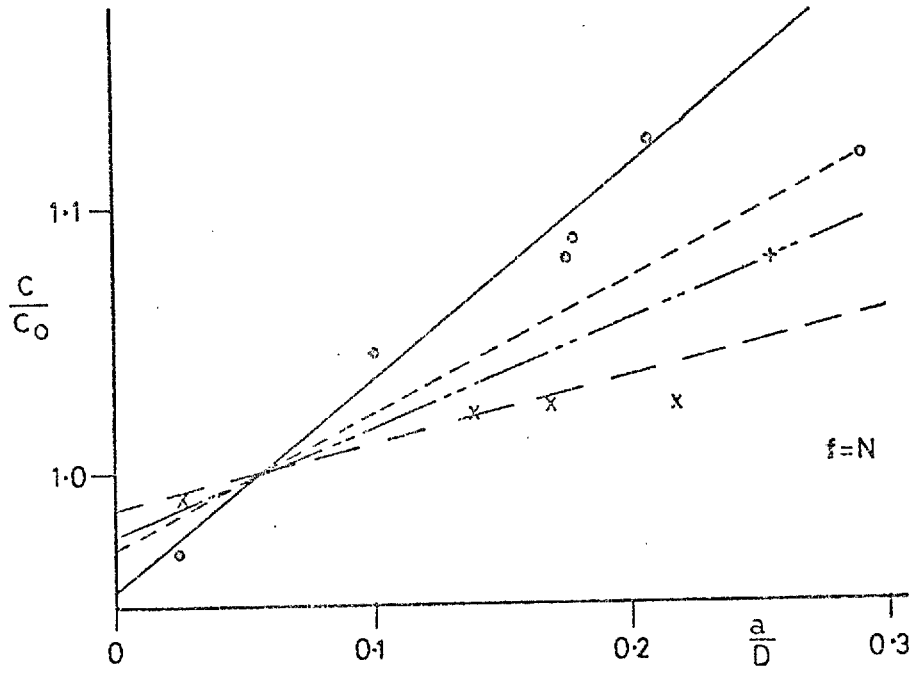

Fig. 87 Variation of "c" with vibration amplitude (see Fig. 88)

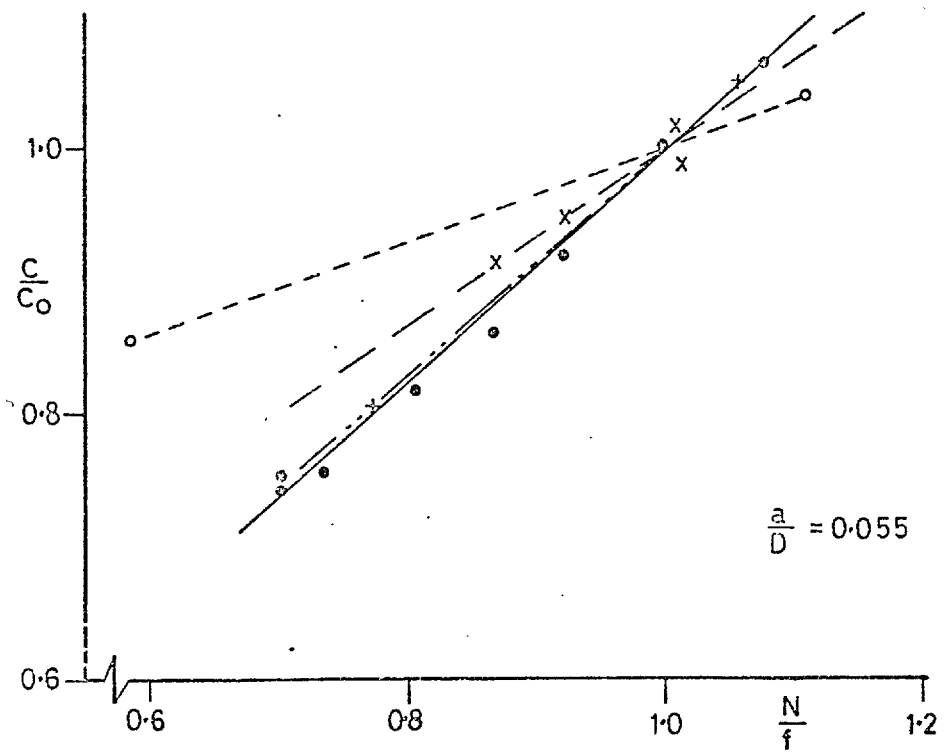

Fig. 88 Variation of "c" with frequency for runs: 73 (o); 77 (+); 80-92 (x); 99-113 (⊙). Note: c_o = c when f = N and (a/D) = 0.055

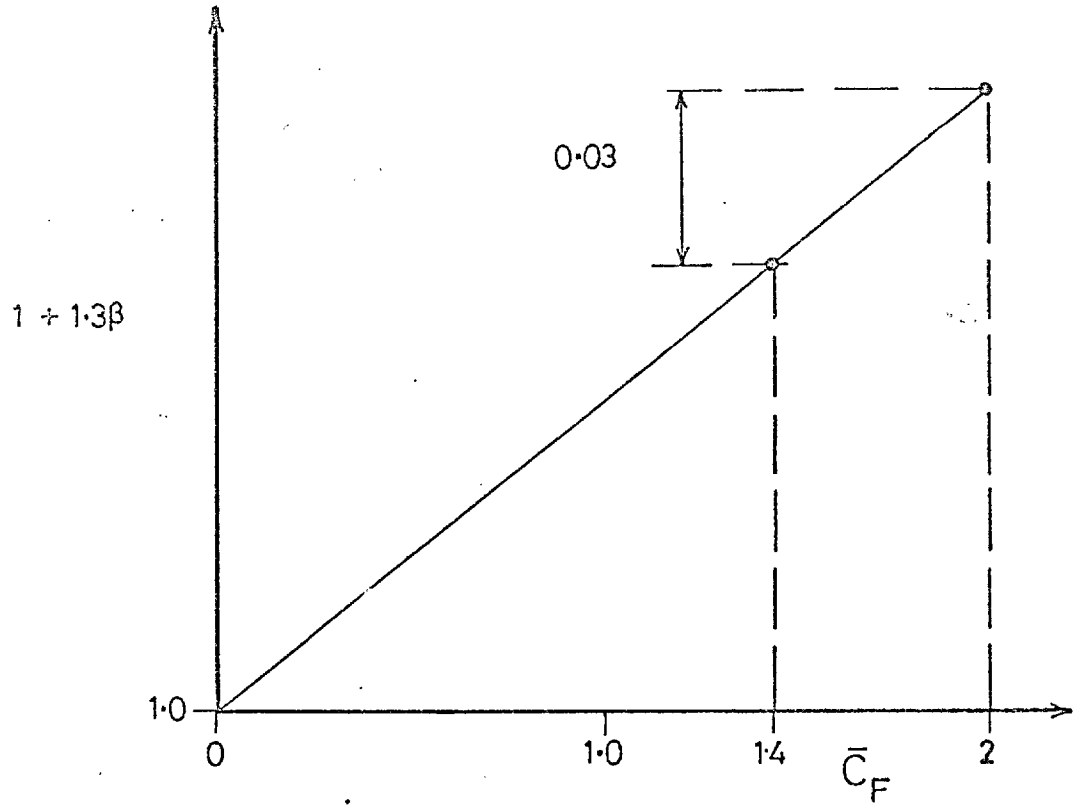

Fig. 89 Simplified blockage correction